[ur] DIMENSIONS

The Journal of Undergraduate Research in Natural Sciences and Mathematics
Volume **18** | Spring **2016**

Marks of a CSUF Graduate from the College of Natural Sciences and Mathematics

Graduates from the College of Natural Sciences and Mathematics:

Understand the basic concepts and principles of science and mathematics.

Are experienced in working collectively and collaborating to solve problems.

Communicate both orally and in writing with clarity, precision and confidence.

Are adept at using computers to do word processing, prepare spreadsheets and graphs, and use presentation software.

Possess skills in information retrieval using library resources and the Internet.

Have extensive laboratory, workshop, and field experience where they utilize the scientific method to ask questions, formulate hypotheses, design and conduct experiments, and analyze data.

Appreciate diverse cultures as a result of working side by side with many people in collaborative efforts in the classroom, laboratory and on research projects.

Have had the opportunity to work individually with faculty members in conducting research and independent projects, often leading to the generation of original data and contributing to the research knowledge base.

Are capable of working with modern equipment, instrumentation, and techniques.

DIMENSIONS

DIMENSIONS: The Journal of Undergraduate Research in Natural Sciences and Mathematics is an official publication of California State University, Fullerton. DIMENSIONS is published annually by CSUF, 800 N. St. College Blvd., Fullerton, CA 92834.

About the Cover

The paper airplane symbolizes the beginning of an idea. The orbits around the paper airplane represent an atom. The stars in the background represent space, which is boundless and infinite. This journal is about how big ideas start off with small beginnings and how exploration and creativity create innovation and discovery.

DIMENSIONS Editorial Staff and Thanks

Editor-In-Chief
Phillipe Diego Rodriguez - *Physics*

Editors
Saumya Jani - *Biological Science*
Lauren Michelle - *Chemistry & Biochemistry*
Nancy Chen - *Geological Sciences*
Lisa Mueller - *Mathematics*
Jessica Duron - *Physics*

Advisors
Dr. Colleen McDonough - *Assistant Dean for Student Affairs*
Jennifer Palermo - *Graduate Assistant*

Graphic Design
Niv Ginat - *Layout Editor*
Sophia Shimamura - *Cover Designer*

College of Natural Sciences & Mathematics
Dr. David Bowman - *Interim Dean*
Dr. Mark Filowitz - *Associate Dean*
Dr. Sean E. Walker - *Chair, Department of Biological Science*
Dr. Peter de Lijser - *Chair, Department of Chemistry and Biochemistry*
Dr. Phillip Armstrong - *Chair, Department of Geological Sciences*
Dr. Stephen W. Goode - *Chair, Department of Mathematics*
Dr. James M. Feagin - *Chair, Department of Physics*

College of the Arts
Mr. Dale Merrill - *Dean*
Dr. Arnold Holland - *Interim Associate Dean*
Ms. Maricela Alvarado - *Assistant Dean for Student Affairs*

Special Thanks To
The CNSM administrative staff for their support, the faculty for advising students and providing them with valuable research opportunities, and Dr. Colleen McDonough who helped make DIMENSIONS a reality.

Table of Contents

Biological Science

Chemistry & Biochemistry

Geological Sciences

Mathematics

Physics

Credits

Correlation of Egg Lipid Content with Early Spider Development in the Western Black Widow Spider, *Latrodectus hesperus*, and the Brown Widow Spider, *Latrodectus geometricus*

Jake R. Bergara and Gloria J. Camacho
Advisor: Dr. Merri L. Casem

Department of Biological Science, California State University, Fullerton

Abstract

Latrodectus hesperus is the native cobweb weaving black widow spider in the western United States. In recent years, the non-native cobweb weaver, Latrodectus geometricus or brown widow spider, has increased in population density; appearing to replace the native black widow populations. The apparent success of the brown widow may be due to several factors. In this paper, the potential role of reproduction was explored, specifically the lipid content of eggs. Comparison of the two Latrodectus species reveal that while Latrodectus geometricus produces clutches with fewer and smaller eggs, the per egg lipid content is significantly greater than that of Latrodectus hesperus. Furthermore, there is a significantly different rate of metabolic activity of the developing spider embryos, as inferred from the change in egg case weight over time, between the two widow species. Surprisingly, the lipid-poor species, Latrodectus hesperus demonstrated the faster rate. Despite the difference in metabolic rate, the ultimate emergence of the first instar spiderlings from the egg case occurred after approximately the same amount of time. The differences in lipid content in L. hesperus may reflect variation in the metabolic pathways used to generate energy or an unequal distribution of yolk across the clutch of eggs.

Introduction

Spider eggs are produced in the ovaries of female spiders. The eggs progress through several stages of maturation or *vitellogenesis* during which time they increase in size as they accumulate yolk, a combination of vitellogenin proteins and lipids [Trabalon, Pourie & Hartmann 1998]. Yolk supports the development of the spiderling, eventually becoming enclosed in the abdomen of the embryo [Foelix 2011] where it will continue to support the growth of the spiderling through its larval and early instar stages until the spider begins to feed independently [Foelix 2011].

Spiders are capable of producing multiple clutches of eggs from a single mating. During copulation, a male spider will deposit his sperm on an external object (usually web) where it is transferred into his pedipalps. Following this, the male spider will use his pedipalps to deposit the sperm packet into the female's genital opening located just inferior to the book lung slits

[Foelix 2011]. The sperm is stored in the seminal receptacle near the oviduct. The mature eggs are fertilized as they move out of the female during the process of oviposition. The fertilized eggs are deposited into a silken egg case that will serve to protect the developing embryos. While still within the egg case, the larval spiders (spiderlings) hatch from their eggs, shed their embryonic cuticle, and complete one molt of their exoskeleton (first instar). Only then will the spiderlings emerge from the egg case.

Spiders in the genus *Latrodectus* are cob weaving, "widow" spiders that are commonly found in urban environments. In southern California, the native *Latrodectus* species is the black widow spider, *Latrodectus hesperus*. Populations of the non-native brown widow spider, *Latrodectus geometricus*, have become increasingly prevalent, seeming to replace the native black widow spider. Differences in the reproductive properties of these two spiders could provide a possible explanation for the apparent change in the population density of black versus brown widow spiders.

Methods

Spider Collection and Maintenance

Black and brown widow spiders were collected from neighborhoods in Orange and Riverside counties during the summer months of 2014 and 2015. Spiders were housed individually in plastic containers and maintained in a growth chamber with a 14:10 day: night cycle at a temperature of 27°C. Spiders were fed a diet of mealworms (juvenile *Tenebrio molitor*) every 14 days. Spiders that had mated prior to capture were able to produce multiple egg cases, each containing a mass of developing embryos, under laboratory conditions. Egg cases were removed from the female spider's web and processed for analysis as described below.

Egg Number and Volume

Developing embryos (eggs) were removed from the egg case by gently tearing open the silken wall of the case using fine forceps. The eggs were allowed to fall into a small petri dish where they were photographed. The total number of eggs within an egg case was determined from the photograph. The diameter of the eggs was measured using Photoshop and the volume was calculated using the average radius assuming the egg to be a sphere.

Egg Case Weight Variation

Latrodectus hesperus and *Latrodectus geometricus* egg cases were individually separated into labeled petri dishes and maintained in the laboratory at room temperature. Individual petri dishes held one egg case and were labeled with the day in which the mother spider was collected and the lay date of her eggs. Using an electronic balance, the weights of each egg case were recorded daily until spiderlings emerged from the egg sac. Egg sacs were collected and weighed until the date of spiderling emergence, a process which took around one month depending on the widow species. Weight trends for opposing species were then analyzed upon collection of data. Spiderlings along with the eggs were left alone and frozen for subsequent analysis of lipid content.

Quantitation of Lipid Content

For some experiments, developing spider embryos (eggs) were removed from their egg case and, photographed as described above. The eggs were transferred to a glass vial and frozen at -20°C. In other experiments the spiderlings were allowed to complete their development, hatch from the egg and emerged from the egg case. The spiderlings were frozen then placed in a petri dish to be photographed before being transferred to a glass vial. Lipid content was determined following the protocol of Salomon, Mayntz, and Lubin (2008). Egg or spiderling samples were desiccated by incubation in an oven at 85°C for a total of 48 hours. Samples were then removed from the oven and weighed to obtain a post desiccation weight. Once this weight was taken, the samples were subject to ethyl ether washes to extract lipid. Using the same vials they were previously placed in, they were soaked in ethyl ether (enough so that all the specimens were submerged) a total of four times, fifteen minutes each (one hour total). Following ethyl ether washes, they were weighed once again. This weight was then subtracted from the post desiccation weight to obtain the "post-lipid extraction" weight. Lastly, the difference was then divided by the total number of spiderlings or eggs within the original egg case to obtain weight per individual. When specimens were desiccated and not in the oven, they were being stored at room temperature.

Individual spiders produced numerous egg cases and the lipid content was measured for each successive egg case to observe if there was any change. The main goal for this was to see if these spiders lose the ability to provide successive offspring with the same amount of nutrients required to sustain life. Again, the environment as well as the clutch size plays important roles in data variation.

Results

Egg Case Production

Spiders in the genus *Latrodectus* were capable of reproducing under laboratory conditions. Individual spiders that had mated prior to their capture could produce multiple egg cases over a period of months in the laboratory. Each individual egg case contained a clutch of multiple eggs. An egg represents a developing spider embryo "housed" within an egg shell. The average clutch size of the black widow, *Latrodectus hesperus*,

was significantly larger than that of the brown widow, *Latrodectus geometricus* (p=0.00001) [Table 1]. Moreover, the overall size of the eggs, and hence their volume, was greater for *L. hesperus* compared to *L. geometricus* [Table 1]. Despite the relatively smaller size of the eggs of L. geometricus, it was found that the overall lipid content of the eggs tended to be greater than that of L. hesperus [Table 1].

	Latrodectus hesperus	*Latrodectus geometricus*
Average number of eggs per clutch	150±50 (n=22)*	89±22 (n=12)*
Average egg volume	0.074 cm^3	0.038 cm^3
Time of Emergence (T_e)(days)	29 ± 7.6**	36 ± 4.8**
Average lipid content per egg	4.3 ± 2.1 µg (n=11)	11.2 ± 3.0 µg (n=6)
Average rate of weight loss (g per day)	$9.4x10^{-4} \pm 2.4x10^{-4}$§	$3.0x10^{-4} \pm 9x10^{-5}$§
*p=0.0001 **p=0.45 §p=0.0002		

Table 1

Time to Emergence

Spider development, including hatching from the egg and the first true molt, occurs within the egg case. The interval between egg case production and the exit of the first instar spiderlings from the egg case was defined as the time to emergence (T_E). It was found that the time between egg case production by the female spider and the emergence of the spiderlings from the egg case averaged 29 days for *L. hesperus* and 36 days for *L. geometricus* [Table 1]. This difference was not statistically significant (p=0.45)

Change in egg case weight

The weight of individual egg cases differed between individuals from within the same *Latrodectus* species and between the two species [Fig. 1]. It was found that the weight of both individual *L. hesperus* and *L. geometricus* egg cases decreased linearly over time. Both species demonstrated a consistent decrease in egg case mass with an R^2 correlation coefficient values ranging from 0.89 to 0.99. The average rate of change in egg case weight over time was greater for *L. geometricus* compared to *L. hesperus* [Table 1].

Lipid Content Per Egg in Successive Egg Cases

Widow spiders are capable of producing multiple egg cases while in the laboratory. Analysis of the lipid content of subsequent egg cases from both *L. geometricus* and *L. hesperus* showed no discernable pattern. The per egg lipid content varied widely both between spiders and even in the same female. There is no significant difference between the data of an individual spider's successive egg sacs or the spiders themselves. Lipid content per egg per egg sac for both species of spiders is shown in Figures 2A and B.

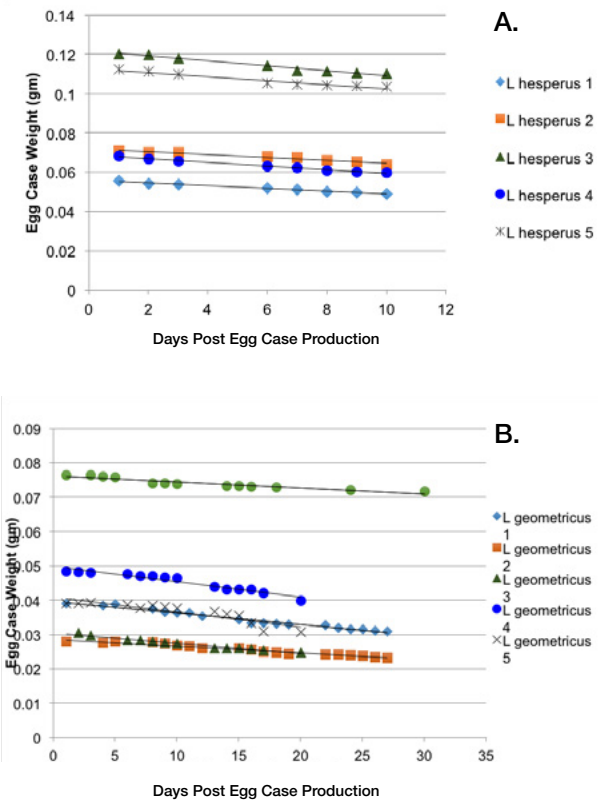

Figure 1. *Both L. Hesperus (A) and L. geometricus (B) egg cases were weighed on a day-to-day basis. Both species showed a consistent linear decrease in weight over time with L. geometricus displaying a smaller slope. Slope signifies the rate of metabolism.*

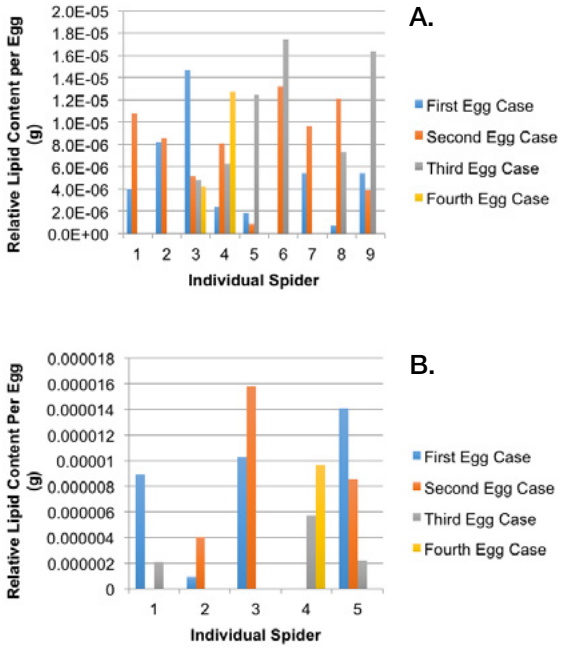

Figure 2. *Lipid content per egg for successive egg sacs for individual spiders. Some spiders produced more egg sacs than others hence the absence of bars. There is no apparent trend visible for L. hesperus (A) or L. geometricus (B).*

Discussion

Oocyte maturation occurs through the accumulation of yolk during the process of vitellogenesis [Trabalon, Pourie & Hartmann 1998; Pourie & Trabalon, 2003]. Vitellogenin proteins are produced by the spider's fat bodies and are taken up from the hemolymph into the oocytes through a process of receptor-mediated endocytosis [Foelix, 2011]. These proteins help bring lipids into the oocyte which accumulates into yolk granules in the mature egg. Each successive clutch of eggs requires a set amount of vitellogenin proteins and lipids per egg in order support the development of the spider embryos. While the spiders in this study were capable of producing multiple clutches of eggs, the amount of lipid per egg within a clutch was highly variable. All spiders were fed on a biweekly basis suggesting that the availability of nutrition was not responsible for this variation.

Despite the variation between clutches, the average lipid content per egg differed between *L. hesperus* and *L. geometricus*; with *L. geometricus* having a significantly greater lipid content. This result was unexpected since the size, and presumably the volume, of the *L. hesperus* egg is greater than that of the *L. geometricus* egg. Another result from this study was the observation that the number of eggs produced in the average *L. hesperus* clutch was significantly greater than the number of eggs in an average *L. geometricus* clutch. One possible explanation for these observations could be that the female spider has a finite nutritional supply that she can allocate to vitellogenesis and yolk production. Dividing a limited resource between a larger number of oocytes would result in a smaller "serving" per egg.

The lower lipid content in the eggs of *L. hesperus* implies that the increased quantities of eggs comes at a cost in quality in terms of transferring nutrients to the offspring. A higher quality egg is going to contain the necessary levels of lipid available to the developing spider. However, the timing of development of the two species, based on the emergence of the spiderlings from the egg case, was not significantly different. This observation may support the idea that the difference in the lipid content per egg is a consequence of unequal distribution of the lipid resources between eggs in a clutch. Only those eggs with sufficient nutritional resources will develop into a spiderling that is capable of leaving the egg case. It is possible that a population of inviable eggs contributed to over-estimating egg number. It has been observed that there is a size differential between the first instar spiderlings of *L. hesperus* compared to *L. geometricus* (personal communication) which may also support the idea of unequal distribution of nutrients.

Another interesting difference between the two *Latrodectus* species is the change in the weight of the egg cases over time during development. Since the silken egg case encloses the clutch of eggs, the loss in mass can only be accounted for by the potential loss of water and CO2 as a consequence of cellular metabolism within the eggs. The developing embryos are undergoing multiple mitotic cell divisions and cellular rearrangements. All of this cellular activity requires a constant supply of energy. Metabolic processes

necessary for the developing spider heavily rely on the lipids and proteins stored in the individual egg yolk. The loss of egg case weight, therefore, can be used as an indirect measure of the metabolic activity of the developing embryos. While both species took nearly the same amount of time to emerge from their egg cases, the rate at which the yolk material was metabolized differed. The metabolic rate for *L. geometricus* was significantly slower than that of *L. hesperus*. Again, this seems counter- intuitive given the differences in yolk content described above. It is important to remember that this study only examined the lipid content of the eggs, however, yolk also contains a protein component that contributes amino acids to the biochemical pathways of cellular respiration and ATP production. It is possible that *L. hesperus* relies on alternate metabolic pathways to generate energy.

Yolk stores must provide nutrition to the spiderling until it is able to feed independently [Foelix 2011]. Previous work from our lab has shown that first instar *L. hesperus* are more likely than equivalent *L. geometricus* to engage in sibling cannibalism. *L. hesperus* first instars have been observed feeding on viable unhatched embryos and other first instar siblings. Sibling cannibalism has been reported in other spiders [Ibarra, 1985; Wagner 1995]. It is possible that the tendency of *L. hesperus* and not *L. geometricus* to engage in sibling cannibalism is a consequence of the disparity in lipid content between the two species.

In conclusion, this study has shown that differences exist between the lipid content of the eggs from the two species of *Latrodectus* commonly found in southern California. The success of the non-native *L. geometricus* may be due, in part, to the high lipid content that the female spider provides to her oocytes. In future, it would be interesting to determine the survival rate of the *L. geometricus* spiderlings. Does the increased nutrition and smaller clutch size of the *L. geometricus* egg case result in more spiderlings reaching adulthood more quickly? Conversely, is the lower lipid content and larger clutch size of the *L. hesperus* egg case a competitive disadvantage? This dynamic might help accounting for the apparent reduction in the number of the native black widows in our local environment.

References

Foelix, R.F. *Biology of Spiders third edition*. New York: Oxford University Press, 2011.

Ibarra, N.G. 1985. Egg feeding by *Tegenaria* spiderlings (Araneae, Agelenidae). *Journal of Arachnology* 13:219-223.

Pourie, G. and Trabalon, M. 2003. The role of 20-hydroxyecdysone on the control of spider vitellogenesis. *General and Comparative Endocrinology* 131: 250-257.

Salomen, M., Mayntz, D., Lubin. 2008. Colony nutrition skews reproduction in a social spider. *Behavioral Ecology* 19:605-611.

Trabalon, M., Pourie, G., and Hartmann, N. 1998. Relationships among cannibalism, contact signals, ovarian development and ecdysteroid levels in *Tegenaria atrica* (Araneae, Agelenidae). *Insect Biochemistry and Molecular Biology* 28:751-758.

Wagner, J.D. 1995. Egg sac inhibits filial cannibalism in the wolf spider, *Schizocosa ocreata*. *Animal Behavior* 50:555-557.

Effects of Fire-related Changes in Coastal Sage Scrub and Grassland Vegetation on the Activity of Desert Cottontails

Kaitlyn Berry
Advisor: Dr. Paul Stapp

Department of Biological Science, California State University, Fullerton

Abstract

In the coastal sage scrub (CSS) ecosystem, wildfires destroy habitat for wildlife in the short-term, but can create new resources, such as shelter and food, as the plant community recovers. In turn, herbivorous mammals may influence post-fire vegetation recovery, especially along the fire's edge, because individuals that take refuge in unburned vegetation may forage in the open and take advantage of new plant growth. I used pellet counts to study the activity of desert cottontails (Sylvilagus audubonii) in CSS and non-native grassland habitats at the Robert J. Bernard Field Station in Claremont, California, one year after a fire at the field station. I hypothesized that cottontail activity would be greater in CSS than in grasslands, and greater at the edge between unburned and burned vegetation than in burned areas far from the edge. At approximately three-month intervals, I counted rabbit pellets in 0.78-m² plots placed every 20-m along three 160-m transects located perpendicular to the burn edge in both habitat types. Pellet densities varied greatly among plots and transects in any given sampling period, but mean pellet density was significantly higher along CSS transects than in grasslands. In CSS, pellet densities were consistently highest in the edge and burned plots, whereas, in the grasslands, there was no consistent spatial pattern in pellet densities. Overall rabbit activity, expressed as mean pellet accumulation rate (pellets/m²/week), increased from February to August 2015 and was consistently lowest in unburned CSS as compared to the edge and burned areas. In August and November 2015, rabbit activity declined in edge plots relative to burned plots, perhaps because intense foraging near the edge eliminated palatable plants, forcing rabbits to forage farther away from refuge. Information on small-scale habitat characteristics at individual sampling plots may be necessary to explain the high variability in rabbit activity among plots and transects.

Introduction

Wildfires are an important source of disturbance and mortality for both plants and animals. Although the most obvious and immediate effect of a fire is the destruction of aboveground vegetation, fires can also decrease local plant diversity, affect soil moisture and nutrients, and reset ecological succession (Otten and Holmstead 1996; Francl and Small 2013). In some ecosystems, such as coastal sage scrub (CSS), however, wildfires are a form of disturbance that is essential to remove dead material, restore soil nutrients, and maintain the native plant community (Francl and Small 2013). CSS plants such as sugar bush (*Rhus ovata*) leafy California buckwheat (*Eriogonum fasciculatum*), laurel sumac (*Malosma laurina*), and western poison oak (*Toxicodendron diversiobum*) require the heat of a fire to germinate their seeds (National Park Service 2016; Ainsworth and Doss 1995). Some grasses and perennial herbaceous plants produce more seeds after a wildfire than in previous years without fire (Bock and Bock 1996). However, even with increased seed production, CSS vegetation may not fully recover for two to four years (Valone et al. 2002).

A fire can kill individual animals directly or may indirectly alter habitat and food resources for wildlife through its effects on vegetation structure and plant communities. In turn, wildlife species can influence post-

fire vegetation recovery by consuming plants and seeds, or creating soil disturbances that affect seed germination (Otten and Holmstead 1996). The loss of shrubs, for example, may eliminate escape cover and habitat for small mammals (Kundaeli and Reynolds 1972). Small mammal diversity often declines immediately following a fire and can take three years to return to pre-fire diversity levels (Francl and Small 2013).

One CSS mammal that may be particularly affected by fires is the desert cottontail, *Sylvilagus audubonii* (Fig. 1). The desert cottontail is common throughout low-elevation, shrub-dominated areas of the western United States (James and Peeters 2004). These rabbits are crepuscular or nocturnal and live in burrows during the day (Orr 1940). Cottontails feed primarily on plants, including grasses, forbs, woody plants, and some fruits (Chapman and Willner 1978). Desert cottontails usually live close to their food sources, but can travel to find food. Male rabbits range over 6.1 ha in one day, whereas females tend to have much smaller daily ranges (0.41 ha; Ingles 1941).

Figure 1. *Desert cottontail (Sylvilagus audubonii). Photo credit: San Francisco Bay Wildlife 2009.*

Rabbits also use vegetative cover for protection from predators, which may include coyotes (*Canis latrans*), raccoons (*Procyon lotor*), striped skunks (*Mephitis mephitis*), red-tailed hawks (*Buteo jamaicensis*), great horned owls (*Bubo virginianus*), rattlesnakes (*Crotalus sp.*), and domestic cats and dogs (*Felis catus, Canis familiaris*; Chapman and Willner 1978). Upon encountering a predator, a rabbit may freeze, dodge, or run away (Ingles 1941). Shrubs provide the best protection and shelter for cottontails, although fallen trees and other woody debris can provide similar cover (Kundaeli and Reynolds 1972). Fires that destroy vegetation and food plants therefore affect cottontail behavior and populations. For example, Otten and Holmstead (1996) found higher levels of rabbit activity in unburned control plots than in seeded areas that had been burned.

Because cottontails live in dense vegetation, are most active at night, and are hard to capture, it is difficult to estimate population density directly (Chapman and Willner 1978; Southern 1940). Indirect measures of relative abundance can be obtained by spotlighting or flush counts. Counts of fecal pellets in fixed plots or transects are also used to estimate activity and population size indirectly (Kundaeli and Reynolds 1972). However, there are some disadvantages of this method. First, some pellets might be overlooked if the substrate or ground cover is dense. Second, the rate of deterioration of pellets is sensitive to weather; pellets deteriorate faster in humid environments than in dry ones (Julander et al. 1962). Pellet decomposition rate is also affected by the rabbit's diet, making it difficult to determine the exact age of the pellets. To use pellet counts to estimate population density, the number of pellets expelled by a rabbit per day must be known. For example, Ingles (1941) found in the laboratory that one desert cottontail left 488 pellets in a 15-hour period, whereas another rabbit deposited 540 pellets over the same time period. Rabbits dropped pellets while they moved and ate, but not in the areas near their burrows (Ingles 1941). Sampling plots therefore must be widely distributed around a study site to sample all possible areas used. Pellet counts may be best considered as a way to obtain some measure of the level of rabbit activity in an area (Julander et al. 1962).

I used pellet counts to investigate the effects of fire on desert cottontail activity in CSS and non-native, annual grassland habitats at one study site in southern California. I hypothesized that rabbit activity would be greater in CSS than in non-native grassland, and greater at the edge between unburned and burned vegetation than in burned areas far from the edge. I predicted that rabbit activity would be greater along the edge rather than the unburned or burned areas because the edge would provide both available cover and an abundance of

new plant growth in the adjacent burned area. Lastly, I predicted that cottontail activity would be greater in unburned than burned CSS because of the absence of vegetation cover in the burned area.

Study Area

My research project was conducted between November 2014 and November 2015 at the Robert J. Bernard Field Station (BFS) in Claremont, California. Vegetation at the 35-ha site is mostly coastal sage scrub and non-native grasslands, along with some coast live oaks (*Quercus agrifolia*) and western sycamores (*Plantaus racemosa*) near the paved roads and buildings (Hamlett 2015). In addition to desert cottontails, other small mammals at the BFS include the California ground squirrel (*Otospermophilus beecheyi*), Botta's pocket gopher (*Thomomys bottae*), Pacific kangaroo rat (*Dipodomys agilis*), deer mouse (*Peromyscus maniculatus*), and big-eared and San Diego desert wood rats (*Neotoma macrotis*; *Neotoma lepida intermedia*; Hamlett 2015). Although black-tailed jackrabbits (*Lepus californicus*) were historically present, the desert cottontail is the only rabbit species currently at the site. In September 2013, employees of the local water company accidentally started a brush fire in the southeastern portion of the BFS (Hamlett 2015). This 8-ha fire primarily burned CSS and grassland vegetation. Both areas had shown significant recovery by the start of my surveys, although the effects of the fire were still obvious some 26 months later.

Methods and Materials

Pellet sampling plots (0.78 m^2) were established at nine stations along three 160-m long transects placed perpendicular to the burn edge in both CSS and grassland vegetation types (Fig. 2). Transects were at least 40 m apart, with plots spaced at 20-m intervals. Plots were placed 1 m from the path used to walk between plots to minimize disturbance. Each plot was marked with a permanent stake-wire flag at its center. At the time of sampling, all pellets were counted within a 56.4-cm radius of the flag. Once counted, all pellets were discarded outside of the plot.

Figure 2. *Layout of the study area at the Bernard Field Station, Claremont, California, showing the locations of three transects in CSS (left) and three in the grasslands (right), each with nine sampling plots (yellow circles). The edge of the fire is visible in the middle of each transect, especially the in CSS. Source: Google Earth. Image accessed February 17, 2015.*

Initial pellet densities were recorded on November 11, 2014, and all pellets were removed. Plots were re-sampled approximately three months later on February 27, May 8, August 18, and November 13, 2015. I chose this frequency of sampling to allow multiple weeks for new rabbit pellets to accumulate in the plots.

Pellet densities were first estimated for each plot and transect to compare variation in pellet densities between plots and transects and across the unburned-burned gradient in a given habitat type. Prior to calculating densities, pellet counts were natural-log transformed to reduce the effects of high variability in counts among plots. Pellet densities were averaged at each distance category to estimate how mean pellet density varied relative to the burn edge in CSS and grassland habitats. Pellet densities were compared by examining the overlap in 90% confidence intervals (CI) for each distance category. A paired t-test was performed to compare the mean pellet densities at each distance. Mean pellet accumulation rates (pellets/m^2/week) were calculated for each sampling period for both habitat types. Plots were grouped into three distance zones (unburned, -80 to -40 m; edge, -20 to 20 m; and burned, 40 to 80 m), with a total of nine plots per zone. Note that it was not possible to calculate accumulation rates for the initial November 2014 survey because it was impossible to know how long the original pellets had been in the plots. For a given sampling period and habitat type, I used a Kruskal-Wallis test to determine if accumulation rates differed between zones.

Results

Pellet densities were significantly higher along CSS unburned and burned transects than along grassland transects during each sampling period (paired t-tests, $P<0.01$, d.f. = 8; Fig. 3). Densities were particularly high 20 m into the unburned CSS (-20 m) during November 2014, February 2015, and May 2015, but then decreased in the August and November 2015 plot checks. Densities were similarly high at 80 m into the burned CSS areas during each survey.

Pellet densities were consistently low far into the unburned CSS (-80 m; Fig. 3). Counts in grassland transects were highly variable among plots and transects during each sampling period. Pellet densities greatly increased across all grassland plots in August and November 2015. Pellet densities varied greatly between plots and transects in both CSS and grasslands across all sampling periods.

Figure 3. *Mean density of rabbit pellets at different distances from the edge of a fire in CSS and grassland areas of the Bernard Field Station, Claremont, California, surveyed on five occasions in 2014-2015. Densities during the November 2014 survey (top left) represent pellets that had accumulated over an unknown length of time, whereas other surveys were 10-15 weeks apart. Negative distances indicate unburned plots. Counts were ln(count+1)-transformed. Values are mean + 90% CI, with n = 3 plots per distance in each vegetation type. The dashed line indicates a mean value of 100 pellets in a plot and is shown for reference.*

Vegetation type	Sampling period	No. of weeks	Unburned	Edge	Burned	K-W statistic
CSS	Feb 2015	15	1.68 ± 1.36	5.76 ± 6.05	4.97 ± 4.99	2.92
	May 2015	10	6.60 ± 6.13	15.85 ± 7.39	12.45 ± 8.52	6.62*
	Aug 2015	15	4.58 ± 3.99	6.57 ± 3.32	14.05 ± 11.82	5.85*
	Nov 2015	12	1.59 ± 0.85	4.93 ± 3.12	14.11 ± 11.15	14.95*
Grasslands	Feb 2015	15	0.18 ± 0.39	0.36 ± 0.60	0.13 ± 0.25	0.08
	May 2015	10	1.32 ± 2.88	0.78 ± 1.02	0.19 ± 0.42	1.83
	Aug 2015	15	1.13 ± 1.18	1.75 ± 1.22	1.03 ± 1.00	2.70
	Nov 2015	12	1.00 ± 1.24	2.55 ± 3.21	2.29 ± 2.91	0.68

Table 1. *Mean accumulation rate (pellets/m^2 /week) of pellets of desert cottontails in CSS and grassland areas of the Bernard Field Station, Claremont, California. Pellet surveys were conducted on five occasions from November 2014 to November 2015, although accumulation rates could not be estimated for the 2014 survey because pellets were first removed from plots in November 2014. Plots were placed in zones based on their distance from the fires edge, as follows: unburned (-80, -60, -40 m), edge (-20, 0, 20 m), and burned (40, 60, 80 m). Values are means ± 90% CI, with n = 9 plots per zone. Kruskal-Wallis tests were used to compare accumulation rates among zones for each sampling period. Asterisks (*) denote surveys when accumulation rates differed significantly among zones ($\alpha = 0.10$; $X^2 = 4.61$, d.f. = 2).*

Rabbit activity, based on pellet accumulation rates, was consistently highest in CSS and within CSS, along the edge of the fire and in the burned area (Table 1). However, rabbit activity increased in the burned area and decreased in the edge in August and November 2015 (Table 1). Rabbit activity was very low in the grassland area and did not differ significantly between zones, although activity tended to increase in edge and burned grassland areas later in 2015 (Table 1).

Discussion

Patterns of pellet density, and especially, pellet accumulation rates, across my five surveys suggest that activity of desert cottontails is greater in CSS than grasslands. This was not surprising given the affinity of cottontail rabbits for habitats with significant shrub cover (Ingles 1941). Cottontail activity is often associated with higher shrub densities because shrubs provide the best cover from predators (Kundaeli and Reynolds 1972). One year after the fire, rabbit activity in CSS tended to be highest near the edge of the burn early in the year, but increased in the burned vegetation in late summer and autumn. At the edge of burned CSS, rabbits have the benefit of proximity to shrub refuges as well as access to nutritious new growth in the recently burned vegetation (Ingles 1941). Thus the edge may provide both protection and nutritious food. This might be particularly important in spring, when the first substantial new growth appeared after the fire. By late summer, it is possible that rabbits had consumed most of the new growth near the shrubby edge and were forced to forage farther away and deeper into the burned area (Chapman and Willner 1978). This might explain why rabbit activity increased during summer and autumn. By this time, however, other taller plants, especially yerba santa (*Eriodictyon californicum*) and royal penstemon (*Penstemon spectabilis*) had emerged in large numbers in the burned area, and therefore may have provided sufficient overhead cover for rabbits.

Pellet accumulation rates serve as a good measure of rabbit activity because they account for both plot area and the number of pellets deposited over time. Accumulation rates can be used to estimate population densities if the relationship between pellet density and population density can be independently established (Ingles 1941). This relationship also depends upon an understanding of the number of pellets deposited by an individual rabbit each day, which may vary with the quality of the rabbit's diet and by the rate of pellet decomposition in the environment, which is influenced by weather and the type of substrate (Sanchez et al. 2009). Unfortunately, such data do not exist for desert cottontails in CSS environments, which makes it difficult to determine rabbit population density from pellet counts alone.

Future Studies

Pellet densities varied considerably between plots and transects, and between sampling periods for the same plots. To more reliably track changes in rabbit activity as the vegetation recovers, it may be necessary to increase the number of transects and sampling periods, although this may not be practical for the 2013 fire at the BFS, given this fire's relatively small size (8 ha). The high variability among plots and transects might also reflect small-scale variation in the availability of cover or food plants at a given sampling plot. Detailed habitat measurements taken at each plot might help explain variation in pellet densities among plots within a habitat type. Spotlight or mark-recapture surveys could be conducted to provide an independent estimate of cottontail abundance at the BFS, which could then be used to determine the relationship between rabbit abundance and pellet accumulation rate.

Acknowledgements

I would like to thank the Bernard Field Station and its director, Dr. Wallace M. "Marty" Meyer III, for permission to work at the field station. I also thank Angela Castanon, Brian Rivas, Emily Estrada, Skip Berry, Peggie Berry, Michelle Berry, Kristal Healy, Riley Morse, and Alicia Berry for their invaluable assistance with data collection in the field, and Dr. Michael Horn for research advice.

References

Ainsworth, J., and T. A. Doss. 1995. Natural history of fires and flood cycles. http://www.coastal.ca.gov/fire/ucsbfire.html. Accessed on 1 February 2016.

Bock, C. E., and J. H. Bock. 1996. Factors controlling the structure and function of desert grasslands: a case study from southeastern Arizona. USDA Forest Service, Rocky Mountain Research Station pp. 9-13.

Chapman, J. A. and G. R. Willner. 1978. *Sylvilagus audubonii*. Mammalian Species 106:1-4.

Francl, K. E. and C. J. Small. 2013. Temporal changes and prescribed-fire effects on vegetation and small-mammal communities in central Appalachian forest, creek, and field habitats. Southeastern Naturalist 12:11-26.

Hamlett, N. 2015. The Robert J. Bernard Biological Field Station: An academic resource of the Claremont Colleges. http://www.bfs.claremont.edu/index.html. Accessed on 24 February 2015.

Ingles, L. G. 1941. Natural history observations on the Audubon cottontail. Journal of Mammalogy 22:227-250.

James, E. W. Jr., and H. J. Peeters. 2004. California natural history guide: Mammals of California. University of California Press. Los Angeles, California.

Julander, O., R. B. Ferguson, and J. E. Dealy. 1962. Range research methods: a symposium. U.S. Department of Agriculture Forest Service 940:102-108.

Kundaeli, J. N., and H. G. Reynolds. 1972. Desert cottontail use of natural and modified pinyon-juniper woodland. Journal of Range Management 25:116-118.

National Park Service: U.S. Department of the Interior. 2016. Coastal sage scrub and southern maritime chaparral communities. http://www.nps.gov/cabr/learn/nature/coastal-sage- 12 scrub-and-southern-maritime-chaparral-communities.htm. Accessed on 29 January 2016.

Orr, R. T. 1940. The rabbits of California. Bulletin of the California Academy of Sciences 19:1-227.

Otten, M. R. M., and G. L. Holmstead. 1996. Effects of seeding burned lands on the abundance of rodents and leporids on Naval Petroleum Reserve No. 1, Kern County, California. Southwestern Naturalist 41:129-135.

Sanchez, D. M., J. L. Rachlow, A. P. Robinson, and T. R. Johnson. 2009. Survey indicators for pygmy rabbits: temporal trends of burrow system and pellets. Western North American Naturalist 69:426-436.

San Francisco Bay Wildlife. 2009. Desert cottontail – *Sylvilagus audobonii*. www.flickr.com/photos/sfbaywildlife/6338665873/. Accessed on 24 February 2015.

Southern, H. N. 1940. The ecology and population dynamics of the wild rabbit (*Oryctolagus cuniculus*). Annals of Applied Biology 27:509-526.

Valone, T. J., S. E. Nordell, and S. K. M. Ernest. 2002. Effects of fire and grazing on arid grassland ecosystem. Southwestern Naturalist 47:557-565.

Companion Plant Density Effects Of Basil (*Ocimum Basilicum*) On Tomato Plant (*Solanum Lycopersicum*): Growth Rate, Herbivory, And Productivity

Brandon Betancourt
Advisor: Dr. Joel K. Abraham

Department of Biological Science, California State University, Fullerton

Abstract

Food insecurity, the lack of consistent access to nutritious and affordable food, is a global societal concern. Small-scale urban gardens are an increasingly popular approach to addressing local food insecurity, but pest management requires new approaches. Companion planting, co-planting of crops to reduce pests and improve productivity through ecological interactions, may be effective but little research has been done on this approach. In this study the impact of companion planting of tomato (Solanum lycopersicum), with different densities of basil (Ocimum basilicum), on tomato growth rate, productivity, and herbivory was explored. It was hypothesized that basil would negatively affects tomato growth and productivity at high densities, but reduce herbivory at any density. Individual tomato plants with zero (0 basil plants/replicate), low (3 basil plants/replicate), and high (6 basil plants/replicate) basil density treatments were planted at the Seeds of Hope Community Garden in Fullerton, CA, which serves people experiencing low to marginal food insecurity. Height, tomato production and quality, and herbivory was recorded from planting through harvest. No differences were found among treatments in growth, tomato productivity and quality, or herbivory rates. However, a significant difference was found in the average mass of tomatoes produced; low-density basil tomato plants produced the smallest average tomato size. No evidence was found of increased pest reduction, tomato growth, or productivity, through high density companion planting. Given the importance of productivity for gardens that serve the community, these results suggest that garden-level productivity can be increased through companion planting to help address local food insecurity.

Introduction

1. Food Security

Food security is defined as when people at all times have adequate access to sufficient, safe, nutritious food to maintain a healthy and active lifestyle (Food Security, n.d.). Global food insecurity is a significant societal issue that affects both western and third world countries, and this concern is only expected to increase as the population grows. Growing human populations and the need for food production exposes major societal concerns, with some consequences already being evident. A recent study conducted on dietary intake values among Minnesotan youth by Smith and Richards in 2008 exposes the societal concern and impact which food insecurity may have on people within the general populous. The study revealed that the majority of homeless Minnesotan youth possessed inadequate dietary intake levels for essential nutrients including vitamins A, C, D, E and calcium, potassium, phosphorous, foliate, and zinc (Smith and Richards, 2008). Proper essential nutrient composition is needed for healthy physiological functions and cellular health. These recent findings produced by Smith and Richards on the nutrient poor diets of the Minnesotan homeless youth not only exemplify the issues of food insecurity within society, but also the need for locally accessible nutrient dense foods within the community.

Although locally produced nutrient dense food is an apparent need for the health and well being of individuals within societies worldwide, this demand is often substituted for a mass produced form of agriculture known as monoculture agriculture. While the agricultural method of growing crops within a monoculture enables for the mass production of crops, the monoculture design is associated with

unsustainable practices that necessitates the need for additives. As a result, numerous ecological and human health threats stem from this form of food production.

II. Monocultures

Monocultures are the agricultural practice of growing one type of crop within a given area (Parloin, 2009). The homogeneity of monocultures allows for standardization of crop requirements, resulting in large agricultural yields. Growing one crop species minimizes harvesting labor, due to the use of developed harvesting machines. The use of monocultures as the primary means for agricultural food development possesses the potential for large agricultural yields. Although the very concept that defines monocultures and the practices needed to sustain consistent food production and harvests do come with the tradeoff of various ecological issues and potential public health concerns, critical analysis is needed in order to development alternative means to alleviate food security.

The defining characteristic of homogeneity within the monoculture design allows for mass production of crops, but the dense concentration of one type of plant over large areas is often not seen within nature, and thus human intervention is needed in order to sustain an adequate production from this system. Specific crop species possess specific nutrient requirements for proper developmental growth, and will often deplete the shallow topsoil of these specific nutrients. Topsoil depletion can lead to reduction in soil fertility and, in extreme cases where monocultures have been ill practiced, desertification of large areas of land. Certain practices target topsoil depletion through remediation of the soil by methods such as crop rotation. Although the practice of crop rotation has been accredited for some of the remediation of topsoil nutrients, this practice is often insufficient in restoring all of the nutrients lost by repeated monoculture practices, and thus is supplemented with additives such as fertilizers.

The uniform crop orientation that comprises a monoculture does not allow for the biodiversity of varying plant species. The limitation on the biodiversity of plants species is problematic for agriculture. Secondary plant species provide suitable habitats for and enable the development of natural predators of agricultural pests (Balmer et al., 2013). The limitation of plant diversity and suitable habitats for many natural pest predators do not allow for the establishment of viable predator populations and help contribute to the increase in pest populations (Balmer et al., 2013). Without the necessary predators needed to control pest populations, and the close proximity and abundant supply of primary crops serving as food, crop specific pest populations can increase to detrimental proportions and result in high agricultural losses.

Moreover, the homogeneity of the monoculture design not only increases susceptibility to pests, but also the increases susceptibility to disease. The genetic diversity of crops within a given monoculture is very uniform and similar to one another, due to the expression of desirable phenotypes. This intensive and close grouping of genetically similar plants, results in an inability for these crop plants to adapt and combat certain diseases that may decimate an entire crop harvest.

III. Pesticides

Monoculture agriculture is recognized for the standardization and mass production of crops, but the reduction in plant diversity in monocultures disrupts the natural ecological regulation between the predator and pest species (Parloin et al., 2012). With an abundant food source available in the monoculture design, and a reduction in plants that serve as suitable habitats for predatory insects pests populations are allowed to increase to proportions that can be detrimental to the agriculture industry. In response to the large growth rates of pest population within monocultures pesticide application is usually needed to compensate for the lack of natural pest predators and thus suppress the pest populations to manageable proportions. As defined by the USDA, pesticides are considered to be any chemical or substance, used to repel, mitigate, suppress, or destroy any pest (About Pesticides, n.d.). The use of pesticides may be contingent with the large agricultural yields associated with monocultures, but the practice of using pesticides with monocultures are responsible for multiple ecological and social issues.

Pesticides application can be administered through subterranean soil application or by foliar spray application. Larger crop areas associated with

monoculture design typically rely on foliar pesticide application (Jusake et al., 2009). Foliar application is regularly used as the application method of pesticides within monocultures due to the efficiency of aerial application that can target large crop areas in shorter periods of time. This pesticide application method may help farmers administer pesticides over large areas in relatively short periods of time, but there is a trade off for the convenience of aerial foliar pesticide application. With aerial application of pesticides environmental factors such as wind and rain displace the applied pesticides, and disperse the pesticides into the surrounding environment resulting in environmental contamination (Carvalho, 2006).

The negative attributes of pesticide application cannot only be associated with environmental contamination. Pesticides are nondiscriminatory, and when applied pesticides can negatively impact the ecology within the agriculture design through the extermination of both targeted pest species and beneficial non-targeted pest species (Carvalho, 2006). The extermination of beneficial non-targeted species through foliar pesticide application parallels a positive feedback loop that further enhances the need for pesticide application. With a decrease in suitable habitat and the regular application of pesticides, the role of beneficial insects within the agriculture are disrupted.

The consistent application of pesticides possesses larger ecological impacts, which are evident by the development of pesticide resistance in pest species. Similar resistance build up has been seen in the medical field and different strains of bacteria such as methicillin resistant *Staphylococcus aureas*. Consistent exposure to pesticides impacts the natural selection and evolution of that pest species to develop pesticide resistance. Thus, new agricultural pests are evolving pesticide resistance, further increasing the need for more potent and toxic chemical based pesticides.

The application and use of pesticides in monocultures additionally creates social issues, in addition to ecological issues. When agricultural pesticides are applied to crops and proper food prepping practices are not made aware to the consumer, pesticide consumption results as the greatest process for pesticide intake values (Jursake et al., 2009). With adverse health effects being well documented with pesticide exposure, the social and ethical issue regarding pesticide use is made apparent.

Recognizing the inherit need for additive supplementation for consistent agricultural yields within monocultures emphasizes this as an unsustainable agricultural practice. The application of pesticides as a compensation for the inherent flaws created by the deformation of the ecological environment within monocultures lends itself responsible for the negative impacts monoculture practices have on the ecology, health, and social aspects of society. Examination of current monoculture practices epitomizes the need for other sustainable and alternative agricultural practices to increase societal food security.

IV. Intercropping

Alternative methods for agricultural food production have been developed, but much discredit has been given regarding the potential importance to such alternative agricultural practices, such as the alternative agricultural practice of intercropping. Intercropping is the agricultural practice of growing one primary crop with one or more species of secondary plants, in order to receive a beneficial reaction or response on the primary crop plant (Parloin et al., 2012). Intercropping differs from monocultures in multiple ways. Instead of the reliance of additives for consistent agricultural yields and productivity that monocultures use, intercropping is dependent on the ecological interactions and niches of specific plant species to benefit crop development and yield. Due to the reliance on the ecological interactions between plant species for promotions in agricultural yields and plant development, intercropping is recognized as a sustainable agricultural practice. Surprisingly the alternative agricultural practice of intercropping is not a new practice to agriculture. The recognition of the importance of intercropping and the development of one of the most well known intercropping examples was identified by the Native Americans, with the planting of maize, bean, and squash together. The planting of these three crops together is known as the “three sisters” and is a valid example for demonstrating that ecological niches and interactions that complement one another increase agricultural yields.

Intercropping on large-scales for agricultural food production has not been well established for several reasons. When compared to monocultures, the manual labor involved in harvesting the crops in an intercropped environment is vastly greater due to the insufficient developments in harvesting machinery specific to intercropped environments. Intercropping has also not witnessed large-scale agricultural production because of the complexity associated with the ecological relationships. Intercropping recommendations are plentiful within the gardening community, but scientifically validated understandings of the various intercropping combinations and the ecological interactions remain to be defined.

V. Companion Planting

Large-scale agricultural food production by intercropping may not contribute significantly to societal food security, but smaller scale intercropping, known as companion planting, within urban gardens may have a promising future and importance in alleviating societal food insecurities. With the establishment of urban gardens becoming more common in communities, and relevant topics of discussion within members of the community, companion planting and advances in the understanding of companion plant interactions has the potential to alleviate societal food insecurities. Companion plants possess various interactions that coincide with the beneficial development of primary crops and include pest suppression, increased pollination, reduced weed prevalence, enhanced crop taste, and higher agricultural yields (Bomford *et al.*, 2004). A recent studied conducted in 2004 examined different pests and their coinciding herbivore preferences on crops that were either intercropped or monocropped (Bukovinszky *et al.*, 2004). The results from the study indicated that herbivore populations were greater on the monocropped plants than the intercropped plants, and that there were differences in crop preference depending on the developmental stage of the herbivore. This study demonstrates not only the tendency for monocropped plants to attract more pests, but also the complexity of the ecological interactions experienced in companion planting.

With companion planting possessing a significant potential to alleviate some societal dependence on monoculture agriculture and societal food insecurities it is a topic that needs more research and understanding in order to benefit the community and society. This study will investigate companion plant competition and how it affects tomato agricultural productivity, herbivory, and growth rates. Secondly, it will apply these findings into surrounding community gardens to increase tomato agricultural yield, and discourage the use of synthetic garden additives through sustainable companion plant practices.

Materials and Methods

On March 20, 2015 *Solanum lycopersicon* and *Ocimum basilicum* were planted grown in the Fullerton Arboretum greenhouse. *Solanum lycopersicon* and *Ocimum basilicum* seeds were grown in Pro-Mix Ulitimate Seeding Mix and watered every other day throughout the initial six week germination stage. Seedlings were transferred into 10 raised beds at the St. Andrew's Seeds of Hope Community garden on May 2. Soil pH was assessed and treated with peat moss prior to transplantation. Azomite supplementation was applied through subterranean application during transplantation of basil and tomato plants. Position of plant treatments within the raised beds was randomized. Stems within six inches of the soil were removed to discourage the onset of powdery mildew.

Planting Design

Three treatment groups were utilized to assess the effects of basil density on tomato growth rate, herbivory, and productivity. Recommended plant spacing with garden literature determined different treatment group planting designs. Recommended plant spacing between each tomato plant was 50cm. The recommended plant spacing between two basil plants was 25cm, and the recommended plant spacing between individual basil and tomato plants was also 25cm. Control treatment group planting design consisted of singular tomato plants with no plants planted within a 50 cm diameter. Low-density treatment group utilized an equilateral triangle planting design that incorporated three equally spaced basil

plants planted 25cm away from the central tomato plant. High-density treatment group consisted of six basil plants planted around one central tomato plant in a hexagonal planting design. Yielding to the recommended plant spacing, the hexagonal planting design utilized 25cm spacing between each basil plant, and 25cm spacing between the one central tomato plant and its surrounding basil plants. Spacing between each tomato plant of different treatment groups was 100cm in order to minimize the aromatic effects of basil on neighboring treatment groups.

Growth Rate Assessment

Growth rates of tomato took place over a ten week time period from May 18, 2015 to July 31, 2015. Tomato growth rates were determined by weekly height measurements. Height was measured from the soil to the topmost leaf.

Herbivory Assessment

Aromatic effects of basil on tomato herbivory was assessed through visual pest surveys of aphids, and by the assessment of ripe fruit damaged by tomato hornworm herbivory. Aphid abundance was estimated through counting surveys that took place from June 1 through July 31, 2015. Surveys consisted of randomly selecting one leaf from the low, middle, and high canopy regions of each tomato plant and counting the number of aphids on each leaf.

The effects of basil companion planting on tomato hornworm herbivory was assessed through a weekly harvest during an eight week harvest period from July 11, 2015 until August 29, 2015. Ripe fruit negatively affected by hornworm herbivory was counted and weighed.

Productivity Assessment

Companion plant density effects of basil on tomato plant productivity were assessed through weekly harvest counting and weighing of ripe fruit. Ripe fruit was harvested weekly until September 15, 2015. Weekly harvest consisted of counting and weighing of ripe fruit and was centered on human consumption criteria. Harvested fruit was discriminated based on whether it was fit for human consumption. Fruit severely damaged was considered not fit for human consumption.

Results

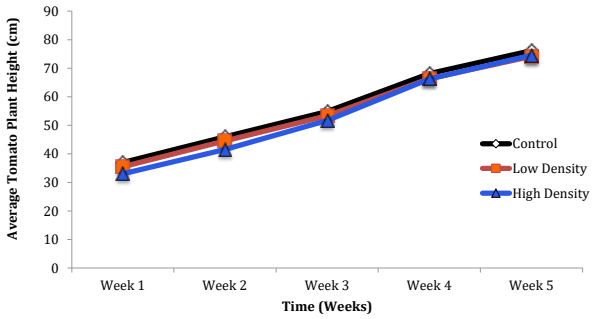

Figure 1. *Tomato plant growth rate as a function of varying basil densities. Each point represents an averaged tomato plant height across different basil density treatment groups. Tomato growth rate was not significantly affected by different basil companion plant densities. Error bars are that of standard error.*

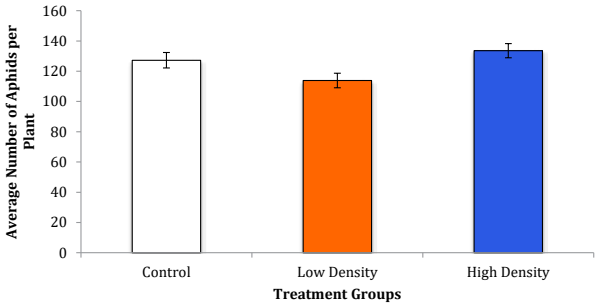

Figure 2. *Relationship between the average number of aphids per plant and different basil density treatment groups. Error bars are of standard error. Treatment groups with varying basil densities did not reveal significant differences in the average number of aphids per plant.*

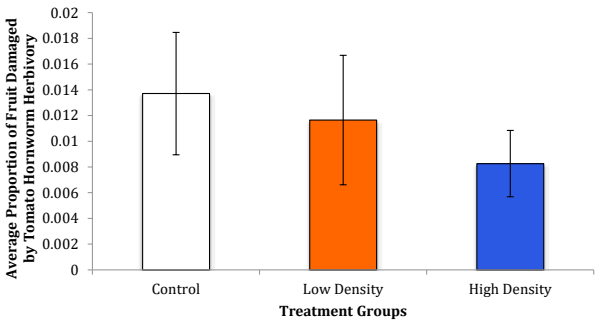

Figure 3. *Relationship between the average proportion of fruit damaged by hornworm herbivory and different basil density treatment groups. No significant difference in the proportion of fruit lost to hornworm herbivory between the different basil density treatment groups (Kruskal-Wallis chi-squared= 0.206, df = 2, $p > 0.05$). Error bars are of standard error.*

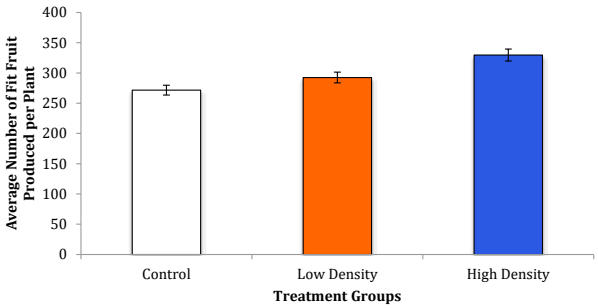

Figure 4. *Average number of fit fruit produced as a function of different basil treatment groups. There was no significant difference in the average number of fit fruit produced between treatment groups (Kruskal-Wallis chi-square = 3.9028, df = 2, p > 0.05). Error bars are of standard error.*

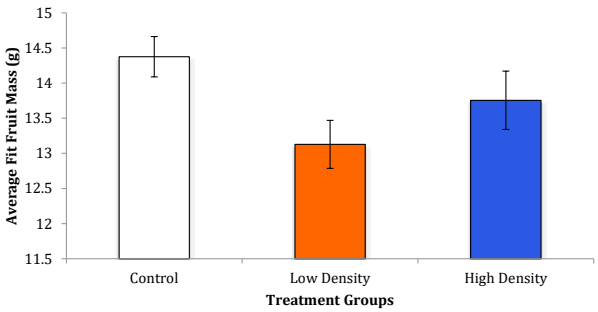

Figure 5. *Average fit fruit mass across different basil density treatment groups. There was a significant difference between the control and low density treatment groups (p < 0.05). Error bars are that of standard error.*

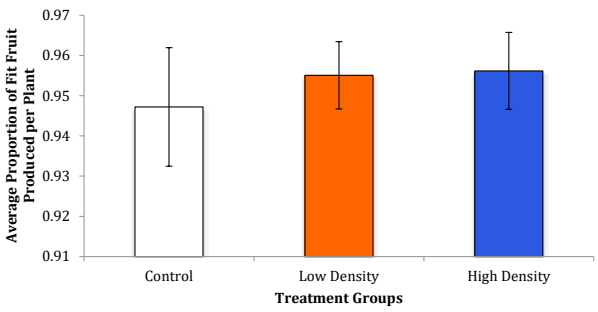

Figure 6. *Average proportion of fit fruit produced per plant between different basil treatment groups. There was no significant difference between the different treatment groups (Kruskal- Wallis chi-squared = 0.0499, df = 2, p > 0.05). Error bars are that of standard error.*

Discussion

Contrary to previous expectations concerning the effects of interspecific plant competition in intercropped systems (Bukovinszky et al., 2004), differences in basil companion planting densities did not significantly affect the growth rates, productivity, and herbivory of tomato plants with the exception of a significant difference in the average fit fruit mass between the control and treatment groups. The results suggest that basil companion planting did not significantly affect tomato growth rates. This finding may be due to the fact that tomato plant heights were measured one week after the initial transplantation. The basil and tomato plants during this measurement time frame were not mature plants, and as a result, the early developmental stages and lack of fully develop canopy levels within the basil plants may have allowed for sufficient light levels to reach the tomato plants. If tomato plant heights were assessed a couple of weeks after the initial transplantation, the more developed basil canopy foliage may have interfered with the photosynthetic abilities of tomato plants through interspecific plant competition, and possibly contribute to different tomato growth rate results.

When compared to the original hypothesis of high basil companion planting densities negatively affecting productivity, the results reveal that tomato plants within the high basil density planting design treatment group did not experience significant differences in productivity. This finding supports the null hypothesis in that there is no relationship between reduced tomato productivity and high basil companion planting densities. Companion planting competition between basil plants in high densities and individual tomato plants was not significant enough to affect tomato productivity when the average number of fit fruit produced per plant, average fit fruit mass, and average proportion of fit fruit produced were analyzed. High basil companion planting may have not resulted in significant negative impacts on tomato productivity due to the trellie support systems used in this study. The trellie support systems may have allowed tomato plants to attain proper height to escape the shade imposed by the lower basil canopy levels, diminishing the negative impacts of sunlight resource competition on the tomato plants.

Results revealed significant differences in average fit fruit mass between control and low- density treatment groups. Absence of basil companion plants may have allowed for greater soil and sunlight resource availability for tomato plants in the control treatment group, and thus enable these tomato plants more resources to be allocated in fruit development. While this explanation gives a plausible account for the control tomato plants producing the largest average fit fruit mass, the lowest average fit fruit mass results exhibited by the low density treatment group does not coincide with the same theory. If the previous resource availability theory were to be the prevailing theory, the high basil density treatment group would be expected to possess the lowest fit fruit mass. Thus, the current experimental findings warrant greater investigation.

Contrary to popular belief basil did not appear to demonstrate repellent aromatic properties towards aphids or tomato hornworms. Basil companion planting did not significantly affect aphid or tomato hornworm herbivory. Aphid surveys did not reveal significant differences in aphid populations between the planting designs. In addition, analysis of the proportion of fruit negatively affected by tomato hornworm herbirvory revealed that planting designs did not vary significantly in tomato hornworms herbivory levels.

Conclusion

The use of small-scale urban gardens for food production provides a promising alternative for alleviating societal food insecurity. Alternative companion planting practices within urban gardens allow for sustainable food production, but space is often a limiting factor in this type of setting. Therefore, knowledge on best companion planting practices are needed for the greatest produce yields in limited areas. As a result of ecological interactions between plant species, companion plant competition is a concern when different plant species are grown in close proximity to each other. While this study did not reveal many beneficial findings between basil companion planting and tomato growth rate, productivity, and herbivory, this study did reveal that high density basil companion planting did not negatively affect tomato growth rate, productivity, and herbivory. In the context of urban gardens, the findings from this study indicate that high basil companion planting does not result in negative competition interactions between the two different plant species. Thus, community garden can grow tomato plants with relatively high basil densities for maximum food production in small garden settings.

References

Adedipe, F., Park, Y.L. (2010). Visual and olfactory preference of *Harmonia axyridis* (Coleoptera: Coccinellidae) adults to various companion plants. *Journal of Asia-Pacific Entomology*. 13, 319-323. DOI 10.1016

An, L., Pan, Y., Wang, Z., Zhu, C. (2011). Heavy metal absorption status of five plant species in monoculture and intercropping. *Plant Soil*, 345, 237-245

Balmer, O., Pfiffner, L., Schied, J., Willareth, M., Leimgruber, A., Luka, H., Traugott, M. (2013). Noncrop flowering plants restore top-down herbivore control in agricultural fields. *Ecology and Evolution*, 3, 2634-2646. DOI 10.1002

Bukovinszky, T., Trefas, H., Lenteren, J.C., Vet, L.E.M., Fremont, J. (2004). Plant competition in pest-suppressive intercropping systems complicates evaluation of herbivore responses. *Agriculture, Ecosystems and Environment*, 102, 185-196

Jaworski, C.C., Bompard, A., Genies, L., Amiens-Desneux, E., Desneux, N. (2013). Preference and prey switching in a generalist predator attacking local and invasive alien pests. *PLOS One*, 8, 1-10. DOI 10.1371

Juraske, R., Anton, A., Castells, F., Huijbregts, M.A.J. (2007). Human intake fractions of pesticides via greenhouse tomato consumption: comparing model estimates with measurements of captan. *Chemosphere*, 67, 1102-1107

Jusake, R., Castells, F., Vijay, A., Munoz, P., Anton, A. (2009). Uptake of persistence of pesticides in plants: measurements and model estimates for imidacloprid after foliar and soil application. *Journal of Hazardous Materials*, 165, 683-689

Medeiros, M., Sujii, E.R., Morais, H.C. (2009). Effect of plant diversification on abundance of South American tomato pinworm and predators in two cropping systems. *Horticultura Brasileira*. 27, 300-306

Mutiga, S.K., Gohole, L.S., Auma, E.O. (2010). Effect of integrating companion cropping and nitrogen application on the performance and infestation of collards by *Brevicoryne brassicae*. *Entomologia Experimentalis Et Applicata*. 134, 234-244

Parloin, P., Bresch, C., Desneux, N., Brun, R., Bout, A., Boll, R., Poncet, C. (2012). Secondary plants used in biological control: A review. *International Journal of Pest Management*. 58, 91-100

Parloin, P., Bresch, C., Poncet, C., Desneux, N. (2012). Functional characteristics of secondary plants for increased pest management. *International Journal of Pest Management*. 58, 368-376

Roosta, H., Hamidpour, M. (2011). Effects of foliar application of some macro- and micro- nutrients on tomato plants in aquaponic and hydroponic systems. *Scienta Horniculturae*. 129, 396-402. DOI 10.1016

Song, Y.Y.,Ye, M., Li, Y.L., Wang, R.L., Wei, X.C., Luo, S.M., Zeng, R.S. (2013). Priming of anti-herbivore defense in tomato by arbuscular mycorrhizal fungus and involvement of jasmonate pathway. *Journal of Chemical Ecology*, 39, 1036-1044. DOI 10.1007

Tyson, R.V., Simonne, E.H., Davis, M., Lamb, E.M., White, J.M., Treadwell, D.D.(2007). Effect of nutrient solution, nitrate-nitrogen concentration, and pH on nitrification rate in perlite medium. *Journal of Plant Nutrition*. 30, 901-913. DOI 10.1080

Jones, B. (2012). "Growing Tomatoes". Retrieved August 10, 2014. (http://www.growingtomatoes.com)

EPA. "About Pesticides". Environmental Protection Agency, n.d. Web <http://www.epa.gov/pesticides/about/>

WHO. "Food Security". World Health Organization. Retrieved from <http://www.who.int/trade/glossary/story028/en/> <http://www.epa.gov/pesticides/about/>

The Effect of Learning Styles on Student Performance in an Undergraduate Biology Course

Precious Daileg
Advisor: Dr. Merri Lynn Casem

Department of Biological Science, California State University, Fullerton

Abstract

Not everyone learns in the same way. In a classroom, different students have different learning styles. The manner in which a course is taught may favor one learning style over another. Therefore, students with a learning style that aligns with a course's pedagogy should perform better in that course. Students in Biology 172 were asked to complete a Learning Styles Assessment (https://www.engr.ncsu.edu/learningstyles/ilsweb.html). The survey uses a 44 item questionnaire to place students along a scale of +11 to -11 for learning style categories: Visual-Verbal, Sequential-Global, Active- Reflective, and Sensing-Intuitive. A student's score along that scale indicates whether they are "well- balanced", or show a "moderate preference" or a "strong preference" within each of the learning style categories. Students in a first semester cellular and molecular biology course were divided into three populations based on their overall performance in the lecture portion of the course. High performing students were defined as having earned at least an 80% in lecture. Average performing students were characterized as having earned between 70-79% and under-performing students earned below 70%. The pattern of learning style preferences for each population overlapped, indicating that performance in the class was independent of a student's learning style preferences. Interestingly, as a group, students in the course showed a strong preference for "sensing" and "visual" learning; suggesting that these students will do best in a class that emphasizes real-world connections while using visual aides to illustrate course concepts.

Introduction

There is no single right way to learn and each student will acquire and integrate information in their own, unique way. The characterization of how an individual learns is their *learning style*. A learning style is the way that a person receives, processes, and recalls information most effectively (James and Gardner, 1995) It is also the way in which students are influenced by different factors around them such as their environment, their psychological and emotional makeup and their various needs (Ballone and Czerniak, 2001). In an academic setting, students primarily receive their information from their instructors. Felder (1993) mentions that if the teaching and learning styles are compatible between student and teacher, the students perform better. As an instructor, being able to adapt the curriculum to accommodate every learning style will ensure that each student can capture the information one way or the other (Edens, 2014).

CSU Fullerton offers a lower division cellular and molecular biology class (Biology 151) as part of the lower division biology core biology for the major. The course is a prerequisite for upper division biology classes.

The Felder-Silverman Learning/Teaching Style model focuses on the way that students receive their information (Felder and Silverman, 1988). The learning style categories are grouped into antagonistic pairs: Active-Reflective, Visual-Verbal, Sensing-Intuitive and Global-Sequencing. Science courses in general present a large amount of information that students often have a hard time learning. Biology courses contain a lot of processes, vocabulary terms and concepts. Being aware of what type of learning style is most effective in obtaining large amounts of information will benefit the students because they would know how they learn

best. Some students struggle through the course either because they have not found an effective study habit or they do not know how to utilize their prevalent learning style. They accept the way the information is presented to them and do not find other ways in which they could understand the material better. The way that a class is taught depends on how the instructor learned the subject themselves and how they found it most effective to teach (Hawk and Shah, 2007). Thus, this creates a difference in teaching styles between instructors teaching the same subject. Both factors greatly affect the way that a student effectively learns the material in a course.

The learning styles that are most effective when learning material in a science course are active, visual, sensing and sequencing (Tanner and Allen, 2004). Students' success has been shown to be higher when they are receiving the information in a their preferred learning style (Ballone and Czerniak, 2001). However, this is not saying that those whose learning styles differ from that of the instructor or do not align with the pedagogy of a course will never succeed. Students will always need to be able to adapt to various educational situations and turn the material into something they can easily internalize. In this study, the learning styles of students in an undergraduate biology was assessed to determine if there was a correlation between learning style preference and student success.

Methods

CSUF undergraduate students enrolled in a lower division biology course were given the opportunity to complete the North Carolina State University-hosted online Learning Styles Assessment (https://www.engr.ncsu.edu/learningstyles/ilsweb.html) as an extra credit assignment. A total of 233 students over two semesters (fall 2014 and fall 2015) participated in the assessment. The assessment is composed of 44 questions asking students to indicate their preferences or actions to a range of situations related to learning. The website analyzes the students' responses and generates individualized reports illustrating the student's preferences along a scale of -11 to +11 for each of the four learning style antagonistic pairs. A score of -3 to +3 indicates that the student is well-balanced between the pair of learning styles. A score of -7 to +7 indicates a moderate preference to one learning style over the other. Scores in the range of -11 to +11 indicate a strong preference for one of the paired learning styles.

Individual student reports were collected by the instructor. Numeric scores for each of the four learning style categories was coded into an Excel spreadsheet. At the end of the semester, students were assigned to one of the three populations (high performing, average performing or underperforming) based on their overall performance in the lecture portion of the course. The distribution of students along the -11 to+11 preference scale for each antagonistic learning pair was determined and graphed using Excel. All work was performed in accordance with an approved IRB protocol.

Results

The assessment used in this research project characterizes student learning styles for four antagonistic pairs; Active-Reflective, Visual-Verbal, Sensing-Intuitive, and Sequential-Global. The majority of students in this first semester biology majors' course demonstrated a balance between active and reflective learning styles (Fig. 1). A similar pattern was found for sequential and global learning styles, although there was a slight preference towards sequential learning (Fig. 4). This population of students showed a stronger preference for visual and sensing learning styles compared to verbal and intuitive learning styles, respectively (Fig. 2 and 3).

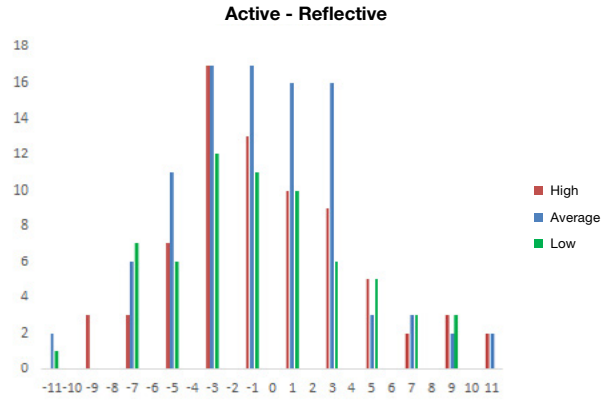

Figure 1. *Active learners are those who learn best when they are actively applying or using their knowledge (ie, explaining it to others). Reflective learners prefer to process the information quietly by themselves. Overall student population showed that they are well-balanced between the Active and Reflective Learning Style.*

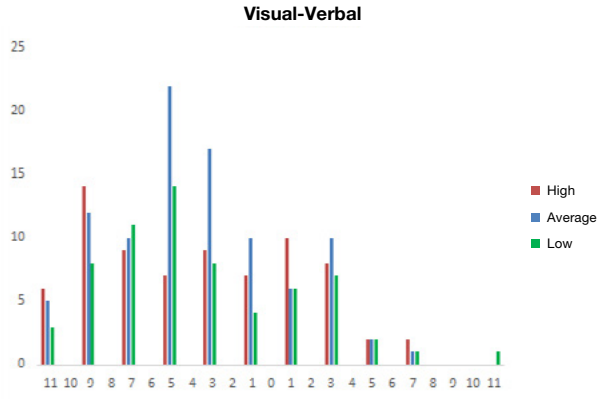

Figure 2. *Visual learners obtain information best with pictures, diagrams, timelines or anything they can see. Verbal learners prefer to acquire their information through written or spoken material such as lectures or discussions. Overall student population showed a preference in the Visual Learning Style. The High Population had an equal value between visual learning style preference and being well-balanced. The Average and Low populations showed a moderate preference to the visual learning style.*

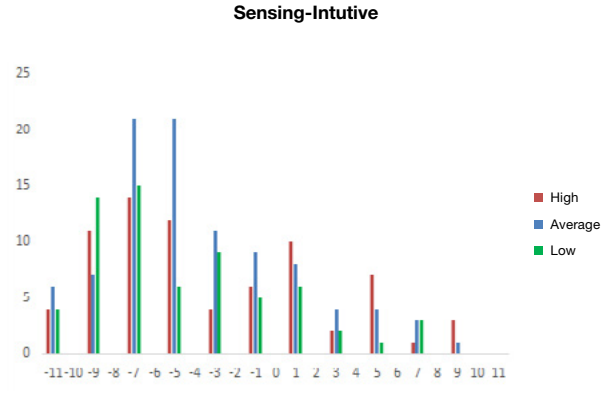

Figure 1. *Sensing learners retain information that are based on facts and have a low tendency for change or surprises. They are focused on learning the details and good with memorization. Intuitive learners are innovative and like to find new ways to look at things. They focus more on the larger concept rather than the details. Overall student population showed a preference toward the Sensing Learning Style.*

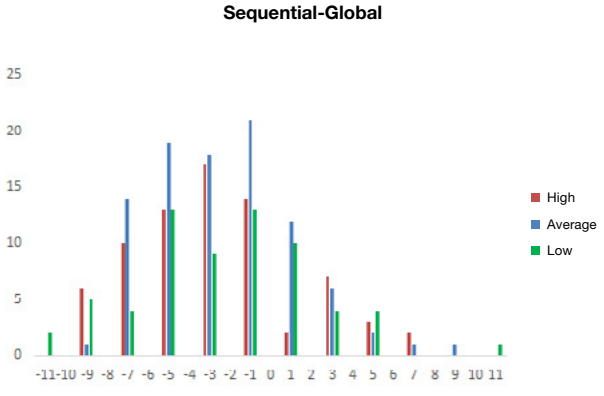

Figure 4. *Sequential learners understand material that is presented in logical steps. Global learners obtain various pieces and parts of the material, initially not aware of their connections. Eventually, all the information will just "click" in their head. The High and Average Populations had moderate preference to the sequential learning style.. The Low population was well-balanced.*

Analysis of the learning style data relative to overall performance in the course failed to show any difference in the preferences of any of the populations [Figs 1-4]. In general, students from each of the performance populations can be found across the preference scale. The few exceptions were a small number of underperforming students that manifested a strong preference for verbal (n=1), sequential (n=2) or global (n=1) learning styles.

Discussion

The distribution of students' scores for each of the populations across each of the learning style scales overlapped indicating that student success in the course was not correlated with a student's learning styles. Other factors that might impact student success include students' background and their early learning experiences (Tai, *et al*, 2005).

The majority of students in all three performance groups fell within the definition of "well- balanced" for the scale that describes Active versus Reflective learners. Active learners do best if they can discuss or apply information while reflective learners prefer to think about information. A slightly greater proportion of average performing students demonstrated a preference for active learning. In a biology course, most of the time students are bombarded with facts each time they go to class. The inclusion of in- class activities, "clicker" questions and small group work would support active learners. Students also have access to Supplemental Instruction in which their application of their knowledge can be further developed and used for their benefit through small discussion and activities with their peers. Furthermore, science classes primarily include various lab work that engages the mind as the students learn different skills and concepts.

As a group, students in this course showed a preference towards visual learning. Visual learners benefit from the use of pictures, diagrams, flow charts and demonstrations. A small number of low performing students demonstrated a preference of verbal learning. These individuals would benefit from written or spoken instruction. Lectures and assigned readings are a regular part of the learning environment for this class, so these students should have had their needs met. The course also included lots of visual information provided in PowerPoint slides and some demonstrations. There is also an increased amount of access to visual aids such as videos, animations and pictures to help portray concepts that are not well understood in class (Tanner and Allen, 2004).

A majority of students showed a preference toward the sensing learning. Sensing learners do very well with memorizing facts and details. These students benefit in this class because biology is full of facts and details. The majority of the exam includes recall questions which should be easy to answer for these types of learners. Though memorization is a proven strength, it is also crucial for them to understand the broader concepts of the topics. This can help improve their critical thinking skill and apply it through problem-solving.

Most students showed a preference for sequential learning. The low performing students were "well-balanced" between the two styles. Sequential learners understand the material when it is presented in logical steps. Since Biology contains various processes with steps, sequential learners could be able to grasp the topics faster than others. Global learners will require more guidance in terms of developing the connections to the pieces they have acquired.

Although students have different aspects that make up their learning styles, it is still the responsibility of their instructor to create a multifaceted curriculum that will accommodate every learning style (Edens, 2014). In this case, the instructor was able to administer the information in a way that every type of learner can benefit from. Extra resources were also made available online for the students to use. This could be a possible explanation as to why student success is not correlated to their learning style. The diversity of how the information was presented was able to create an "equal ground" where other factors, such as self-motivation and perseverance, could have contributed more to the students' success. In this case, it is up to the students to utilize their knowledge, the available resources and their learning styles to get their desired grade. Administering this survey early in the semester could be beneficial in that, they can be aware of which learning style they most likely have. The instructor can provide different study tips that each type of learner can utilize to optimize their study time and, hopefully, improve their grades (Leithner, 2011). For future studies, data will be collected from non-science majors to compare their learning styles.

References

Ballone, L.M., and Czerniak, C.M. (2001). Teacher's Beliefs About Accommodating Students' Learning Styles in Science Classes. Electronic Journal of Science Education. 6(2).

Edens, S. (2014). Who Will You Teach? Consideration of Learning Styles in Teaching a Core Course PL300: Military Leadership.

Felder, R.M., and Silverman, L.K. (1988). Learning and teaching styles in engineering education. Engr. Educ, 78(7), 674-681

Felder, R.M. (1996). Matters of Style. ASEE Prism, 6(4), 18-23.

Hawk, T.H., and Shah, A.J. (2007). Using Learning Style Instruments to Enhance Student Learning. Decision Sciences Journal of Innovative Education. 5, 1-19.

James, W.B. and Gardner, D.L. (1995). Learning styles: Implications for distance learning. New Dir. Adult Contin. Educ., 67, 19-32.

Leithner, A. (2011). Do Student Learning Styles Translate to Different "Testing Styles"? Journal of Political Science Education, 7(4), 416-433.

Tai, R. H., Sadler, P. M. and Loehr, J. F. (2005), Factors influencing success in introductory college chemistry. J. Res. Sci. Teach., 42: 987–1012. doi: 10.1002/tea.20082

Tanner, K. and Allen, K. (2004). Approaches to Biology Teaching and Learning: Learning Styles and the Problem of Instructional Selection – Engaging All Students in Science Courses. Cell Biology. 3, 197-201.

Freeman, S., O'Connor, E., Parks, J.W., Cunningham, M., Hurley, D., Haak, D., Dirks, C., and Wenderoth, M.P. (2006). Prescribed Active Learning Increases Performance in Introductory Biology. CBE – Life Sciences Education. 6, 132-139.

The Relationship between Food Safety and Handling Knowledge and Practice Among Elementary Aged Children

Desiree Jacoby
Advisor: Dr. Joel K. Abraham

Department of Biological Science, California State University, Fullerton

Abstract

Despite the programs and information provided to the public, there is still an increase in foodborne illness outbreaks every year. Knowledge of proper food safety and handling practices is the key to preventing these outbreaks. However, knowledge of food safety and handling may not translate into actual practice, which could contribute to foodborne illness outbreaks. The relationship between food safety and handling practice and knowledge has been examined in adults, college students, high school students, and even middle school students, but not in elementary aged students. An evidence-based intervention was designed to learn about their knowledge and practice habits as well as teach the students proper food safety and handling in hopes of improving their handling and food safety knowledge and skills. A questionnaire and card sorting activity were given out one week prior to the lesson and two weeks after the lesson. The lesson covered proper washing, separating, and chilling according to the CDC. Results from the questionnaire and card sorting activity showed no relationship between knowledge and practice however personal observations during the intervention showed otherwise.

I. Introduction

Foodborne illnesses are responsible for 48 million Americans falling ill, 128,000 hospitalizations, and 3,000 deaths every year (CDC, 2012). Despite efforts to prevent foodborne illnesses, there are still outbreaks occurring all over the United States (Merkle, 2014). Foodborne illnesses, caused by microorganisms such as *Salmonella*, can produce severe symptoms including diarrhea, abdominal cramps, and nausea (CDC, 2012). Most adults can fight off invading microbes and recover with ease; however children are more susceptible to foodborne illnesses than adults (CDC, 2012). Commonly consumed items by children can spread foodborne illnesses. Apple juice batches, for example, have led to E. coli poisoning (Cody, et al., 1999). In this case, seventy people were infected from the apple juice; 25 of whom were hospitalized, 14 hemolytic uremic syndromes, and one death. Traces of arsenic have also been found in apple juice in amounts higher than the Food and Drug Administrations recommended safe levels (Marshall, 2014). Children that are uneducated in proper food safety and handling are at high risk of acquiring dangerous foodborne illnesses.

There are steps that are being taken to prevent such outbreaks from recurring. Those who work with food are required to take a food safety and handling course and be certified their entire time of working with food (ServSafe, 2012). The course must be renewed every 2-4 years and workers can be asked questions by authoritative workers throughout their employment to make sure they remember the information from their training. For those who handle food professionally, there is shown to have been a decrease in microbiological counts after training was completed (Soares, et al., 2013). Even though providing training courses for those who work with food is important, it is also important to remember that everyone works with food at some point in their lives and without knowledge, people are at risk of acquiring a foodborne illness.

The training that is being provided as well as the knowledge gained, is not being put into practice (Rowell, et al., 2013). Rowell et al. performed pre and post training and observation for managers in three different grocery stores. The results showed that there was no significant change in store performance by the managers. There is also an economical benefit for putting the gained knowledge into practice (Ribera, et al., 2012). Ribera et al. found that it costs more for producers to deal with the outbreaks after they occur than to prevent them. This reveals a dissociation in knowledge and practice specifically in adults.

There is an insufficient amount of knowledge being provided to people on food safety and handling. People regularly underestimate the importance of food safety and handling (Machado, et al., 2014). For instance, people often underestimate the danger of foodborne illnesses from fruits and vegetables relative to meats (Berger, et al., 2010).

Machado et al. (2014) found that there is a weak perception on proper food safety and its importance by the food-handlers in schools, which can affect student's health. Children, who are already highly susceptible to foodborne illnesses, have an insufficient knowledge on proper food handling as well as a lack of seriousness towards the issue of food safety. Quick et al. (2013) found that middle school youth had insufficient food safety knowledge. Although students had been instructed to wash hands and food, information was not provided about when and how hand washing should occur. Students also showed a range of attitudes about the practice. These studies show that there might be a foundation to build on when teaching youth, but teaching is needed nonetheless.

When it comes to education, adults have learned so much and built routines and habits that are hard to break with age (Rothman et al., 2009). On the other hand, according to Eves, et al. (2010), behaviors that are taught a young age can be changed more easily and are resistant to then changing with age compared to being taught at a later age. With this in mind, reaching out and teaching children in elementary school when these skills are being taught and developed might be key to preventing foodborne illnesses later once they grow up. Teachers in schools are teaching little about food safety and handling and are generally basing it on personal knowledge and experience rather than on fact and research findings (Eves et al., 2010).

With an increase in interactive gardens at schools (Ozer, 2007), there are additional dangers and opportunities regarding food safety. Although more children are now participating in food handling and preparation, lessons on food safety may be better contextualized, which can improve learning outcomes (Ozer, 2007). These learned practices and knowledge can be brought home with them and their families can learn these proper skills as well.

In this study, the relationship between food safety and handling knowledge and practice in elementary aged children was explored. The goal was to determine student's current knowledge on proper washing and handling of fruits and vegetables and develop an evidence-based intervention to teach food safety and handling and improve food knowledge and practice in elementary-aged children. These children are at an ideal age to learn new ideas and concepts, and therefore by teaching them about food safety and handling, foodborne illness outbreaks can hopefully be prevented in the future.

II. Materials and Methods

I developed a short questionnaire to measure student knowledge of fruit and vegetable handling and safety, rates of fruit and vegetable handling, as well as awareness of food-borne illnesses. Through IRB (Institutional Review Board), I was given approval for this protocol in addition to working with the teachers to get parental consent and student assent. The study was performed at a local elementary school in southern California with students ranging in ages between six and nine years old. I observed the students food handling practices using a card sorting activity to understand if they take their knowledge and put it into practice. I used a hands-on tutorial designed around the Next Generation Science Standards within a one hour lesson plan upon which students will be introduced to proper food handling and safety, microorganisms, and how to separate foods appropriately.

Code	Performance Expectation	Disciplinary Core Idea
MS-LS1-1	Conduct an investigation to provide evidence that living things are made of cells; either one cell or many different numbers and types of cells.	
LS1.A		All living things are made up of cells, which is the smallest unit that can be said to be alive. An organism may consist of one single cell (unicellular) or many different numbers and types of cells (multicellular). (MS-LS1-1)
3-LS4-3	Construct an argument with evidence that in a particular habitat some organisms survive well, some survive less well, and some cannot survive at all.	
LS4.C		For any particular environment, some kinds of organisms survive well, some survive less well, and some cannot survive at all (3-LS4-3).
3-LS4-4	Make a claim about the merit of a solution to a problem caused when the environment changes and the types of plants and animals that live there may change.	When the environment changes in ways that affect a place's physical characteristics, temperature, or availability of resources, some organisms survive and reproduce, others move to new locations, yet others move into the transformed environment, and some die (LS2.C). Populations live in a variety of habits, and change in those habitats affects the organisms living there (LS4.D).
4-PS4-3	Generate and compare multiple solutions that use patterns to transfer information	Different solutions need to be tested in order to determine which of them best solves the problem, given the criteria and the constraints (ETS1.C)
4-ESS3-2	Generate and compare multiple solutions to reduce the impacts of natural Earth processes on humans.	A variety of hazards result from natural processes. Humans cannot eliminate the hazards but can take steps to reduce their impacts (ESS3.B).
3-5-ETS1-3	Plan and carry out fair tests in which variables are controlled and failure points are considered to identify aspects of a model or prototype that can be improved.	Different solutions need to be tested in order to determine which of them best solves the problem, given the criteria and the constraints (ETS1.C).

Table 1. *Next Generation Science Standards alignment with intervention.*

	Yes	**No**	**N/A**
Worked in the School Garden	100%	100%	0%
Help Adults Prepare Meals	86%	86%	0%
Vegetarian	7%	7%	0%
Vegan	7%	7%	57%
Had a Previous Food Safety/Handling Lesson	79%	79%	0%
Grade		**Gender**	
1st	36%	**Boy**	43%
2nd	36%	**Girl**	57%
3rd	29%		

Table 2. *Demographics of students regarding to food habits and previous endeavors.*

Tutorials

When seeking to change practices, lectures are rarely an effective form of teaching; hands-on tutorials tend to lead to greater changes in behavior (Rothman et al., 2009). Thus, I sought to develop a more interactive lesson that would allow students to engage with the material and bring their own perspectives into the lesson. The lesson plan was aligned with the Next Generation Science Standards (NGSS) and consisted of three main topics including washing, separating, and chilling. The washing portion of the lesson plan included washing their hands, surfaces, and utensils before and after handling food. The separating portion focused on separating work spaces and utensils when working with food as well as separating fruits and vegetables and meats. The chilling portion comprised of when food goes in the refrigerator and pantry, checking when food needs to be thrown away, and knowing when to put food away after being prepared. The three main topics were chosen based on student comprehension of the material and recommended topics by the CDC. The materials that were used for the lessons were pictures of microorganisms that are the common cause of foodborne illnesses, pictures of pantry and refrigerator items for the students to separate accordingly, and a matching game of food hazards.

Assessment

A pre and post questionnaire was given to students which consisted of questions asking students about if they think anything lives on their fruits and vegetables and if so what as well as questions pertaining to handling and washing practices of their fruits, vegetables, hands, and surfaces. The questionnaire was given one week prior to the lecture and two weeks after the lecture.

The students were observed before and after the lecture via a card sorting activity. The sorting of the cards according to the given scenario was documented as to prevent a possible bias in their questionnaire responses. I compared results from the pre and post-intervention questionnaires and my observations of how students order the cards before and after the intervention.

III. Results

Demographics

Of those who participated in the study, 72% were in 1st or 2nd grade, while 29% were in 3rd with 43% of those students being male and 57% being female (Table 2). All of the students who participated in the study and whose data was used had worked in the school garden before (Table 2). Only 14% of students claimed that they do not help out adults when it comes to preparing meals as well as 21% of students had not had a previous lesson in food handling and safety (Table 2). Interestingly, one student claimed to be a vegetarian and another student claimed to be vegan.

Knowledge

For the questionnaire, there was an increase in responses that were non applicable because they either did not answer the question or their answer could not be interpreted. There was an overall increase in the answer “Never” from pre to post questionnaire. On the contrary, there was a general decrease in the answer “Every Time” from pre to post questionnaire. There wasn’t much of a change in the response “Sometimes” from pre to post questionnaire. The in class worksheet provided more insight into students’ knowledge on microorganisms and food safety. Results showed 63% of the students drew bacteria and 75% said that infectious microorganisms make them sick (Table 3). Of all of the students who participated, 16% of the students said that they can give you cancer or that they fight blood cells (Table 3). Two students talked about how they can make you sick but that’s why we wash our hands so that doesn’t happen and that some microorganisms are good for us (Table 3). One student claimed that infectious microorganisms are good on food but it’s when we eat them that they become bad and make us sick (Table 3).

Practice

For the card sorting activity, there was an increase in the correct order of the cards for the first scenario but a decrease in the correct order for the second scenario.

IV. Discussion

In this study, there does not appear to be a direct relationship between food safety and handling knowledge and practice. Some problems with the data may come from the fact the students were organized into groups for the pre-questionnaire because of the available seating so it is possible that they worked together and didn't want to be embarrassed by answering "Never" or "Sometimes". However, the seating for the post-questionnaire was more spread out and individualized so that the students worked more on their own and more quietly. These may have obscured some of the students' answers from pre- to post-questionnaire. Another problem faced with the card sorting activity was that the students had difficulties understanding the activity despite the numerous examples provided to help them comprehend what was being asked of them. A limitation to the study in general was that there were more 1st and 2nd graders than there were 3rd (Table 2) so maybe they were not at a proper level to understand how the card sorting activity was done and how to answer the questions on the questionnaire.

For the questionnaire, the students' scored more poorly after the lesson (Figure 1). The questions were designed so that the ideal answer for all of the questions would be all the time but majority of the students answered never when they filled out the post-questionnaire after the lesson. The students also changed answers from pre to post questionnaire that were surprising. For example, for the pre questionnaire the students helped out and cooked more often than they did for the post questionnaire (Figure 2). This could be that after taking the questionnaire for a second time, students had a better understanding of what the question was asking and therefore answered differently. However, only some answers improved from pre to post questionnaire. The question about whether or not the students thought anything lived on their fruits and vegetables improved from more students saying yes after the intervention than before (Figure 3). From what was observed during the entire study, the students really did know how to properly wash their hands, when to do it, and did it quite often. However, their responses on the questionnaire did not reflect that same knowledge.

What do you think an infectious microorganism looks like?	
Bacteria	63%
Virus	4%
N/A	33%
What do infectious microorganisms do to you?	
Makes you sick	75%
Gives you cancer	8%
Kills you	8%
Germs fight red blood cells	8%

Table 3. *In Class worksheet student responses.*

The card sorting activity did not seem to accurately show their practice and behavior when it came to food safety and handling. There were only a few students who had consistent answers for the activity, but a majority of the students had the wrong order or did not participate in the activity (Figure 4). Regardless of this, it seemed that the students' correct order of the cards increased from pre to post activity for the first scenario, but there was a decrease in the amount of cards put in the correct order for the second scenario (Figure 5). One explanation for this is that the second scenario was made to be a little more complicated than the first scenario so their level of understanding may have not been fit for that scenario.

It is interesting to note the students responses on the in class worksheet because they displayed a lot of knowledge in their answers and drawings that does not seem to be reflected in their questionnaire and card sorting answers. The students knew how infectious microorganisms can make people sick, can cause cancer, and that they even fight our blood cells and can lead to death if not taken care of properly (Table 3). As for their drawings, although it is difficult to say exactly what they intended to draw, it seemed like most of the students drew bacteria with some worms and even a couple of viruses. What is notable here is that all of the students had an answer and drew something for the worksheet showing that they knew about infectious organisms and how they can make us sick, however only about half of them stated that they thought that something lives on their food. This response changed to all but a few students answering yes to something living on their food for the second questionnaire after the lesson plan. In future studies, the wording of the worksheet should match the wording on the questionnaire and refer to something living on their food as microorganisms instead or vice versa for the worksheet.

Overall, the data collected from the questionnaire and card sorting did not match my personal observations. The data shows that there is no relationship between food safety and handling knowledge and practice in elementary aged children. This is most likely due to the age group, the questions being asked, and the card sorting activity difficulty level that made the data the way that it is. For future studies, more care should be taken in the wording and structure of the intervention as to not confuse the students. Also, the setup of the students in the classroom proved to be an essential component in that separation of the students from each other would most likely have greatly benefited the honesty of the answers. Additional research is required to fully understand the extent to which elementary aged students put their knowledge into practice and the possible ways that curriculums can be altered to help students put their knowledge into practice.

Figure 1. *Student response to the question, "Do you wash your hands before touching food?" from questionnaire, pre-intervention and post-intervention.*

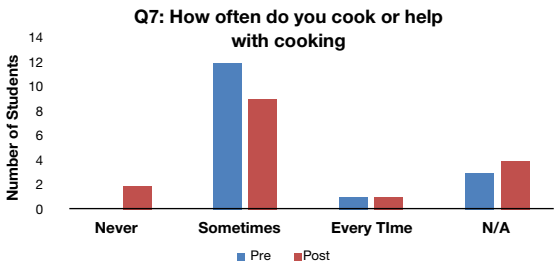

Figure 2. *Student response to the question, "How often do you cook or help with cooking?" from questionnaire, pre-intervention and post-intervention.*

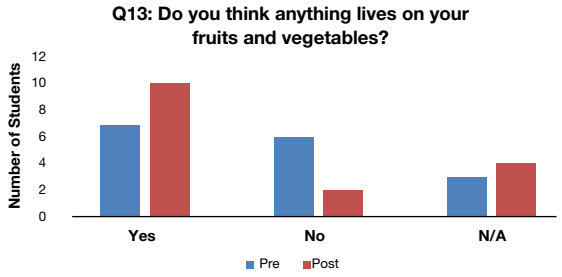

Figure 3. *Student response to the question, "Do you think anything lives on your fruits and vegetables?" from questionnaire, pre-intervention and post-intervention.*

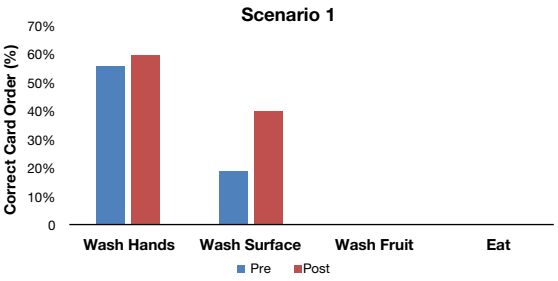

Figure 4. *Percentage of students who put the correct cards in the correct order from scenario 1, pre-intervention and post-intervention*

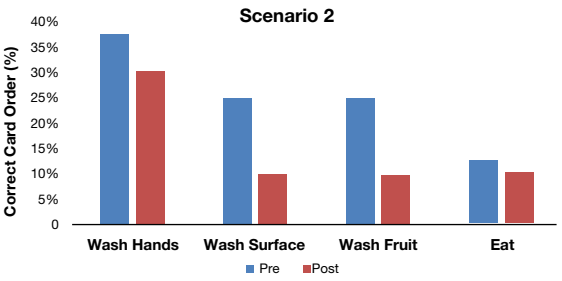

Figure 5. *Percentage of students who put the correct cards in the correct order for scenario 2, pre-intervention and post-intervention.*

References

Berger, C. N., Sodha, S. V., Shaw, R. K., Griffin, P. M., Pink, D., Hand, P., & Frankel, G. (2010). Fresh fruit and vegetables as vehicles for the transmission of human pathogens. *Environmental Microbiology*, 12(9), 2385-2397.

CDC (2012). Foodborne Illness, Foodborne Disease, (sometimes called "Food Poisoning"), Food Safety. Retrieved from http://www.cdc.gov

Cody, S. H., Glynn, K., Farrar, J. A., Cairns, K. L., Griffin, P. M., Kobayashi, J., . . . Vugia, D. J. (1999). An outbreak of Escherichia coli O157:H7 infection from unpasteurized commercial apple juice. *Annals of Internal Medicine*, 130(3), 202-209.

Eves, A. , Bielby, G. , Egan, B. , Lumbers, M. , Raats, M. , et al. (2010). Food safety knowledge and behaviours of children (5-7 years). *Health Education Journal*, 69(1), 21-30.

Machado[1], M. G., Monego, E. T., & Hidalgo Campos, M. R. (2014). Risk Perception of Food Safety by School Food-handlers. *Journal of Health, Population & Nutrition*, 32(1), 19-27.

Marshall, T. (2010, March 14). ARSENIC IN APPLE JUICE A CONCERN; Testing of the popular kids' drink reveals a level of the poison that may be a potential health hazard. *St. Petersburg Times* [St. Petersburg, FL], p. 1A. Retrieved from http://ic.galegroup.com/ic/ovic/NewsDetailsPage/NewsDetailsWindow?failOverType=&query=&prodId=OVIC&windowstate=normal&contentModules=&display-query=&mode=view&displayGroupName=News&limiter=&currPage=&disableHighlighting=false&displayGroups=&sortBy=&search_within_results=&p=OVIC&action=e&catId=&activityType=&scanId=&documentId=GALE%7CA221265606&source=Bookmark&u=csuf_main&jsid=fe3d5ebe5429c4088d337080a1524224

Merkle, S. (2014). Food Safety Tools and Products for Environmental Health Practitioners. *Journal of Environmental Health*, 76(7), 44-46.

Ozer, E. J. (2007). The effects of school gardens on students and schools: Conceptualization and considerations for maximizing healthy development. *Health Education & Behavior*, 34(6), 846-863.

Quick, V., Byrd-Bredbenner, C., & Corda, K. W. (2013). Determinants of safe food handling behaviors among middle school youth. *Nutrition & Food Science*, 43(6), 543-553. doi: 10.1108/NFS-08-2012-0086

Ribera, L. A., Palma, M. A., Paggi, M., Knutson, R., Masabni, J. G., & Anciso, J. (2012). Economic Analysis of Food Safety Compliance Costs and Foodborne Illness Outbreaks in the United States. *HortTechnology*, 22(2), 150-156.

Rothman, A. J., Sheeran, P., & Wood, W. (2009). Reflective and automatic processes in the initiation and maintenance of dietary change. *Annals of Behavioral Medicine*, 38, S4-S17.

Rowell, A. E., Binkley, M., Alvarado, C., Thompson, L., & Burris, S. (2013). Influence of Food Safety Training on Grocery Store Employees' Performance of Food Handling Practices. *Food Policy*, 41, 177-183. doi: http://www.sciencedirect.com.lib-proxy.fullerton.edu/science/journal/03069192

ServSafe (2012), ServSafe Food Handler Program, ServSafe California Food Handler. Retrieved from www.servsafe.com

Soares, K., García-Díez, J., Esteves, A., Oliveira, I., & Saraiva, C. (2013). Evaluation of food safety training on hygienic conditions in food establishments. *Food Control*, 34(2), 613-618. doi: 10.1016/j.foodcont.2013.06.006

Biochar Feedstock Effects on Crop Yield: A Comparison Between Palm Frond and Commercial Biochar

Jarret Jones
Advisor: Dr. Joel K. Abraham

Department of Biological Science, California State University, Fullerton

Abstract

Palm trees, found in all counties in Southern California, regularly shed their fronds. These fronds are difficult to dispose through municipal waste streams, and methods such as shredding and composting are ineffective. The use of palm fronds as feedstock for biochar, which is charcoal used as a soil amendment to improve plant growth, may be a possible solution. The aim of this research was to compare palm frond biochar to that of a commercially available biochar with respect to crop yield in three common garden plants: radish (*Raphanas sativus*), Genovese basil (*Albahaca genovesa*), and spinach (*Spinacia oleracea*). Palm fronds were collected and converted into biochar with a custom made kiln. Three treatments were established: Palm biochar, commercial biochar, and a non-biochar control (n =10). Soil in the biochar treatments was amended with 70 grams of ground biochar. Plants were harvested at the appropriate time for each crop, and dry biomass was measured. Control radishes were significantly larger than radishes from either biochar treatment, while commercial biochar radishes were significantly smaller than the two other treatments ($p < 0.001$). Overall poor plant growth made inferences about the impact of biochar difficult. However, the reduction of plant size in both biochar-amended treatments may have been due in part to insufficient nutrients in the soil and specific application methods used. However, the higher growth of radishes in palm frond versus commercial biochar suggests that further research on palms as a biochar feedstock is warranted.

Assessing CSUF Student Knowledge and Practices of Safe Produce Handling

Phyllis Liang
Advisor: Dr. Joel K. Abraham

Department of Biological Science, California State University, Fullerton

Abstract

Fruit and vegetable consumption has numerous health benefits and United States health policy recommends that most Americans increase consumption. However, fruits and vegetables can be contaminated with heavy metals, pesticides, and microbes, which can lead to food-borne illnesses. Although proper food handling practices can mitigate these concerns, many consumers do not know about or regularly practice safe produce handling. Unsafe produce handling practices appear to be particularly common in some sub-populations, including college graduates. It is also important to note that many students begin to cook for the first time in college, and thus, it is important to understand, and ultimately improve, their produce handling practices and knowledge. In this study, produce handling knowledge and practices in undergraduate students at California State University, Fullerton (CSUF) was documented. A web-based survey was administered to student volunteers on their produce handling knowledge and practices. Although CSUF students report that they regularly wash produce in general, most neglect to wash fruits that are peeled before consumption, such as cantaloupes and bananas, which still pose health threats. Students were most aware of chemical-based and microorganismal contaminants, but rarely acknowledged the possibility of heavy metal contamination. Reported produce handling practices did not differ between organic and conventional produce. Students appear to lack basic knowledge of proper produce washing methods. This knowledge can help develop future food handling tutorials and intervention to improve the knowledge and practice of produce handling procedures.

I. Introduction

Fruit and vegetable consumption has numerous benefits for consumer health, such as supplying important nutrients to the body and lowering the risks to many diseases (CDC, 2013). However, fruits and vegetables are susceptible to contamination as they are grown, harvested, packaged, and shipped before entering the consumer's home; throughout this process, there are a myriad of opportunities for contamination by microbes, heavy metals, and pesticides (Core, 2002). These contaminants can lead to serious health repercussions when ingested. For instance, microorganisms, such as *Escherichia coli O157:H7*, *Salmonella enteritis*, and *Listeria monocytogenes*, can cause illness or even death when ingested by contaminated foods (Kilonzo- Nthenge, Chen, and Godwin, 2006). For foodborne illnesses, the Center for Disease Control (CDC) (2012) estimates about 63,000 cases of *E. coli*, 42,000 cases of *Salmonella*, and 1,600 cases of *Listeria* are reported per year in the United States. Heavy metal contaminants such as lead, iron, zinc, and cadmium are quite common in produce grown in soil and can cause numerous neurological problems when ingested (Ismail, 2005). Pesticide contamination on produce can negatively affect the nervous (Weiss, 2004) and reproductive systems in humans as some pesticides are persistent and accumulate in the body causing long-term exposure (Keikotlhaile, Spanoghe, and Steurbaut, 2010).

Although consumers may be aware of some potential contamination sources, there are many non-intuitive sources of contaminants that are overlooked (Losasso et al, 2012). For example, plant uptake of heavy metals from the soil is a common concern in urban environments (Sterrett et al, 1996). However,

Sterrett et al (1996) found that consuming urban garden lead contaminated soil far outweighs the danger of consuming produce that has taken up lead. To reduce heavy metal ingestion, washing the produce before consumption is recommended. To address consumer pesticide concerns, the USDA Pesticide Data Program (PDP) tests for the overall pesticide residue on produce to ensure that pesticide levels are below the tolerance levels established by the U.S. Environmental Protection Agency (USDA, 2013). The PDP emulate consumer practices and wash the produce samples before testing the pesticide residue (USDA, 2013). The PDP found that over a nine-year period, over 90 percent of the sampled peaches, apples, and strawberries had average detectable pesticide residue (Punzi et al, 2005).This means that consumers regularly consume small amounts of pesticide residue after washing their produce, likely contrary to their belief. In situations where produce are not tested, they likely have higher levels of pesticide residue when sold to consumers. These examples demonstrate the importance of safe produce handling; proper practices can reduce both intuitive and non-intuitive sources of contamination.

Another non-intuitive source of contamination is from organic produce. Since organic farms are subject to strict regulations (Winter and Davis, 2006), many consumers buy organic produce under the assumption that they are safer and healthier (Hughner et al, 2007). However the PDP found pesticide residue in 23% of 127 organically labeled produce samples (Winter and Davis, 2006). Organic farms are not allowed to use synthetic pesticides; however, there are exceptions where synthetic substances such as soap-based herbicides, water disinfectants such as calcium hypochlorite, and insecticides such as boric acid, elemental sulfur, and oils can be used (Winter and Davis, 2006). Like conventionally grown produce, organic produce is still susceptible to heavy metal and microorganismal contamination. Pesticide, heavy metal, and microorganismal contamination could be introduced through animal manure, which is permitted in organic agriculture (Coleman, 2012). This practice could lead to variation in contamination levels in organic produce, again highlighting the need for safe food handling practices.

Although safe food handling practices, such as proper food storage and washing can reduce these potential health risks, many consumers do not know about them or do not regularly practice them (Scott, Pope, and Thompson, 2009). Phang and Bruhn (2011) found that consumers typically do not wash their produce enough before consumption and commonly violate safe food handling during routine food preparation. This appears to be especially true for particular sub-populations. Li-Cohen and Bruhn (2002) found that subpopulations such as college or post-college graduates, men, higher-income households, and people under the age of 65 are more likely to practice unsafe food handling methods than non-college graduates, women, lower-income households, and people 65 years or older.

Given the higher education, it seems counterintuitive that college students practice unsafe food handling than non-college graduates; one might think that people who have a higher education would be more knowledgeable and practice safer food handling methods than those who do not. One study suggests this pattern: college students were confident in their food handling methods, but their knowledge and behaviors indicated that they were not practicing safe food handling methods (Stein, Dirks, and Quinlan, 2010).

There are a number of possible reasons why students would not practice safe food handling. One reason could be that students are not in the kitchen helping while food is being prepared at home. Another reason could be that students are not formally taught how to properly handle food because home economics classes have been reduced or eliminated from secondary schools (Beard, 1991). Health and nutrition classes in college focus more on sexual behavior, alcohol and substance abuse, and nutrition rather than on food safety practices (Morrone and Rathbun, 2003).

College students are the ideal subjects to assess their produce knowledge and practices as they are usually cooking for themselves for the first time and are also more likely to start working in the food industry serving food to the public (Stein et al, 2010). Jevšnik, Hlebec, and Raspor (2008) stated that educational programs should focus on the younger members of the population to spread food safety methods. As students are the next generation to have families, take care

of the elderly, and become mentors to the following generation, it is important for students to know and practice safe food handling skills. Given these reasons, college students and post-college graduate food handling practices are of particular interest.

Safe produce handling is an important national health issue, and is less often practiced by college students. To help address this problem, California State University, Fullerton students' knowledge and behaviors of safe food handling were assessed. The data collected was used to answer the following questions:

1. How are CSUF students handling their produce?

2. What is their knowledge of produce contaminants based conventionally, organically, or urban garden grown produce?

This knowledge can help develop future food handling tutorials and intervention to improve produce handling behaviors.

II. Methods

Different target produce and the correct practices associated with each type were identified. Once the target produce was determined, a survey that addressed how CSUF students handle their produce and what their knowledge of produce contaminants based on where the produce was grown was designed. The survey was administered online campus-wide to college students at CSUF in Spring 2014.

Determining Correct Practices for Target Produce
Produce that would span the range of approaches to safe produce handling with regards to microorganisms, heavy metal, and pesticide contaminants were identified. The seven types of produce focused on in this study were apples, bananas, blueberries, broccoli head, whole cantaloupe, lettuce head, and potatoes as these produce characterize much of the range of fruit and vegetable types consumed regularly in the US. Apples are a typical fruit with a waxy coating and smooth surface that can harbor contaminants (Kilonzo-Nthenge et al, 2006). Bananas and whole cantaloupe are fruits that most consumers do not consider washing or rinsing before consumption because the peel is not consumed (Li-Cohen and Bruhn, 2002). However, these fruits can be cross-contaminated from cutting or peeling the fruit, then making contact with the inside flesh (Verrill, 2012). Blueberries are an example of fragile or soft fruits that consumers might not consider washing or rinsing because they are too delicate or too time consuming to wash (Li-Cohen and Bruhn, 2002). Broccoli is a vegetable type that has numerous nooks and crannies in which contaminants can linger (Kilonzo-Nthenge et al, 2006). Lettuce, like many leafy greens and vegetables, is commonly consumed raw (Doménech et al, 2013). Potatoes are a rough-skinned vegetable type, with crevices that can harbor contaminants (Rowe, 2007).

The correct washing methods for the range of produce that were focused on in this study were then identified. Apples should be washed by running it under running water while rubbing it with ones hands (Zander and Bunning, 2010). Under the broad category of "Peaches, plums, and other soft fruits", bananas should be washed under running water (Zander and Bunning, 2010). Rowe (2007) stated that bananas should be rinsed off. Since "washing" and "rinsing" are commonly used synonymously, it is difficult to decipher what the authors actually mean. For this study, the correct washing method for bananas was determined to be holding it under running water. Blueberries should be gently washed collectively under cool running water in a colander (Bolton et al, 2013; Driessen, 2013; Rowe, 2007; Zander and Bunning, 2010). There are conflicting methods in the literature regarding the proper technique for washing heads of broccoli. Bolton et al (2013) stated that a broccoli head should be soaked in cold clean water, while Zander and Bunning (2010) said to soak it and then hold it under running water. However, Bruhn and Li-Cohen (2004) says that soaking is not recommended as cross-contamination could occur. Based on the literature review and recommended methods from similar vegetable crops, the correct method for washing broccoli head was decided to be holding it under running water. This method increases the likelihood of dislodging soil particles, while reducing the risk of cross-contamination by inserting hands

into standing water. Whole cantaloupe and potatoes should be washed by running the fruit or vegetable under running water and scrubbing it with a vegetable brush (Bolton et al, 2013; Bruhn and Li-Cohen, 2004; Driessen, 2013; Rowe, 2007; Zander and Bunning, 2010). For lettuce heads, Zander and Bunning (2010) and Bolton et al (2013) recommend soaking in cool water and then rinsing, while Rowe (2007) recommends rinsing lettuce under running water. Because Bruhn and Cohen (2004) state that soaking is not recommended in general due to possible cross-contamination, the correct method was determined to be to rinse under running water.

Survey Development and Administration

The majority of the survey questions were modeled after the Center for Food Safety and Applied Nutrition 2006 and 2010 Food Safety Surveys, which gathered information on consumer knowledge, behaviors, perceptions, and attitudes on various food topics (Lando and Carlton, 2010). Additional questions were added to measure student knowledge about possible contaminants on conventionally, organically, and urban grown produce, and their behaviors regarding pre-washed produce. A pilot test was administered to six CSUF undergraduate students for readability prior to distribution.

The online program Qualtrics was used to create the survey. The survey was IRB approval (application # HSR-14-0068; Assurance # FWA00015384) and distributed through a link on the California State University, Fullerton student portal messaging system and through flyers placed around the campus. Two Kindle e-readers were raffled as an incentive for participation. Over a four-week period, 177 responses were collected.

Data Analysis

Chi-square analyses were used to compare students' washing behavior between organic and conventionally grown produce (R Development Core Team 2013). For the produce contaminants, the COUNTIF function was used to determine the types of contaminants that the students listed and then put into broader categories (Microsoft Excel 2007). General produce washing methods were calculated by percentages.

III. Results

	Respondents	CSUF Population
Gender	n=142	
Female	73%	55%
Male	23%	45%
Prefer not to answer	5%	-
Ethnicity	n=156	
Caucasian	24%	25%
Asian	23%	22%
African American	3%	2%
Hispanic or Latino	37%	37%
Native American or Alaska Native	1%	0%
Native Hawaiian / Pacific Islander	3%	0%
Prefer not to answer	6%	4%
Other	3%	9%
Academic Level	n=142	
Freshamn (0-30 units)	13%	13%
Sophmore (31-60 units)	14%	12%
Junior (61-90 units)	22%	25%
Senior (91>units)	35%	37%
Post-baccalaureate / Graduate	16%	14%
College	n=131	
College of the Arts	3%	6%
Mihaylo College of Business and Economics	16%	22%
College of Communications	9%	10%
College of Engineering and Computer Sciences	9%	9%
College of Health and Human Development	31%	18%
College of Humanities and Social Sciences	14%	20%
College of Natural Sciences and Mathematics	18%	8%

Table 1. *Demographic data of survey respondents and CSUF population. The CSUF population is based on Fall 2013 data.*

There was an overrepresentation of females (73%) and an underrepresentation of males (23%) in the survey compared to the CSUF population (Table 1). However; there was no difference between survey respondents and CSUF population regarding ethnicity, academic level, and college of the students (Table 1).

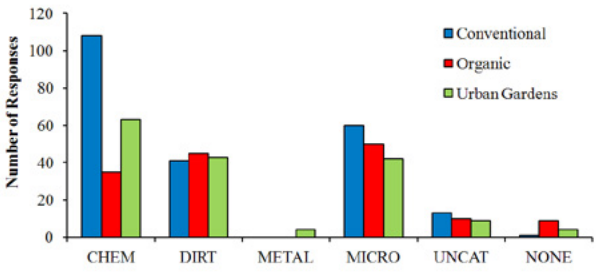

Figure 1. *Student assessment of produce contaminants for conventional (n=114), organic (n=106), and urban garden grown (n=107) produce. Sample sizes denote the number of student responses for each free-response question. One response could have stated multiple contaminants for one or more categories. CHEM = pesticides, herbicides, fertilizers, pollutants. DIRT = dirt, bugs, insects. METAL = Heavy metals. MICRO = bacteria, parasites, E. coli, germs, mold, viruses, fungi. UNCAT = fecal matter, GMOs, toxins.*

Students were asked to list the types of contaminants that they thought were associated with produce grown conventionally, organically, or in urban gardens. For conventionally grown and urban garden grown produce, the main sources of contamination that students reported were chemical and microorganismal contaminants (Figure 1). For organically grown produce, students reported microorganismal and dirt contaminants as the main sources of contamination (Figure 1). In all cases, students reported chemical and microorganismal contaminants, but rarely reported heavy metals as a source of contamination (Figure 1).

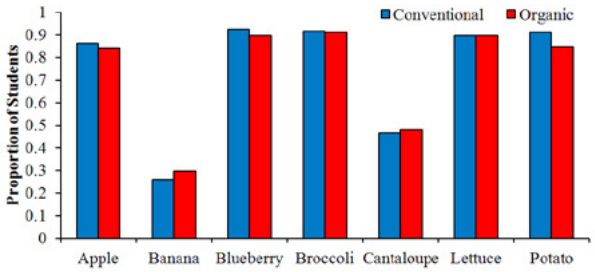

Figure 2. *Proportion of students who reported washing fruits and vegetables MOST or ALL of the time prior to consumption. A high proportion of students reported washing apples (conv: n=146; org: n=145), blueberries (conv: n=145; org: n=145), broccoli (conv: n=146; org: n=145), lettuce (conv: n=145; org: n=145), and potatoes (conv: n=144; org: n=144) MOST or ALL of the time. A low proportion of students reported washing bananas (conv: n=146; org: n=145) and cantaloupe (conv: n=146; org: n=144) MOST or ALL of the time. Washing behavior does not differ between conventional and organic produce ($p > 0.05$ for all chi-square tests).*

For the rest of the survey, conventionally and organically grown produce were focused on as they are commonly found in grocery stores and, which was assumed, would be the most accessible to students. In the survey, students reported that they purchase the majority (86%) of their produce from a grocery store (data not shown). To assess if there was a difference in washing behaviors, students were asked how frequently they washed different types of produce that were conventionally or organically grown. The "Most or All of the time" responses were focused on as it would give insight to differences among produce types and the gaps that students might have. There was no significant difference in student washing behaviors between conventional and organic produce for any of the produce types for most or all of the time responses ($p > 0.05$ for all tests) (Figure 2). For the majority of the different produce types, many students reported washing their produce most, or all of the time, prior to consumption; however, less than 50% of students reported washing bananas or cantaloupe (Figure 2).

When students did wash their produce, they varied in their practice of washing different produce types, and often used incorrect practices to wash their produce (Table 2). The majority of students (62%) wash their apples correctly by rubbing them with their hands under running water (Table 2). However, 58% of students do not wash their bananas at all, while only 13% hold them under running water (Table 2). For blueberries, only a third of students correctly wash them by either holding them under running water (Table 2). For broccoli head, 48% of students incorrectly wash them by rubbing them with their hands under running water, while only 32% hold them under running water (Table 2).

Fruit or Vegetable	Do not wash	Use cleaner	Soak in container	Hold under running water	Scrub with brush*	Rub with hands**
Apples (n=178)	3%	4%	3%	22%	5%	62%
Bananas (n=11)	58%	1%	1%	13%	3%	25%
Blueberries (n=188)	1%	3%	16%	35%	2%	44%
Broccoli Head (n=183)	2%	3%	15%	32%	2%	48%
Cataloupe (n=166)	34%	2%	3%	22%	4%	35%
Lettuce Head (n=183)	1%	3%	13%	31%	2%	51%
Potatoes (n=188)	3%	3%	10%	18%	18%	48%

*Modified. Survey stated: "Rub them under running water with a brush"
**Modified. Survey stated: "Rub them under running water with your hands"

Table 2. *General produce washing methods used by student respondents. Percentages can be greater than 100% because more than one method could have been selected. Shaded areas denote correct washing methods*

For whole cantaloupe, one third of students reported not washing them at all while another third of students incorrectly wash by rubbing them with their hands under running water; only 4% of students correctly wash cantaloupe by scrubbing. For lettuce head, 51% of students incorrectly wash by rubbing them with their hands under running water, while only 31% correctly wash by hold them under running water. For potatoes, 48% of students incorrectly wash them by rubbing them with their hands under running water, while only 18% of students correctly wash them by scrubbing them with a vegetable brush under running water.

IV. Discussion

Proper food handling can drastically decrease foodborne illnesses; poor food handling causes more cases of illness than do foods that are high risk for contamination (Hillers et al, 2003). However, safe produce handling practices are surprisingly rare, particularly in some subpopulations (Scott, Pope, and Thompson, 2009). In this study, California State University, Fullerton (CSUF) student self-reported knowledge and practice of food handling was documented. Since college students are one of the sub-populations that regularly practice unsafe food handling (Li-Cohen and Bruhn, 2002), this information may help guide future interventions to improve food safety.

Students mostly reported chemical and microorganismal types of contaminants, while heavy metals were rarely mentioned as a possible produce contaminant (Figure 1). This could be due to common knowledge of pesticides and produce recalls from the media, while heavy metals are more associated with non-consumable products such as paint and toys. However, it is important to think about heavy metals as possible produce contaminants as urban gardens are becoming more popular and are susceptible to heavy metal contamination due to surrounding buildings, construction, and car pollutants (Alloway, 2004). For example, zucchini and tomatoes that were grown in urban gardens nearby roads had higher heavy metal deposition and accumulation compared to those grown 60 m away and suggested that these produce should be carefully washed before consumption (Antisari, 2015).

Students reported washing the majority of their produce items most or all of the time; however, the proportion of students was nearly halved with regard to produce with peels (bananas and whole cantaloupe). In anticipation of low frequencies of washing, a follow-up question was asked when students did not answer "most of the time" or "all or nearly all of the time" to any of the produce types. For bananas and whole cantaloupe, students commonly reported (71%) that they did not wash these fruits because they do not eat or serve them with the peel on. However, both produce types can cause serious illness through cross-contamination between the peel and the inside flesh when handling and thus need to be washed (Verrill, 2012). One specific example of the importance of produce washing was the *Salmonella* outbreak due to imported cantaloupe from Agropecuaria Montelibano in which 51 illnesses in 16 states and 9 illnesses in Canada in 2008 (Food and Drug Administration, 2008). Because consumers do not consume the rind of the cantaloupe, most do not think to wash them; however if consumers knew proper produce handling, then the number of cases and illnesses could have been reduced and possibly avoided.

Common organic buyer belief is that organic produce is healthier and cleaner than conventional produce (Winter and Davis, 2006), which could alter handling behavior to infrequently wash organic produce. According to Cicia et al (2002), regular organic food buyers are usually associated with alternative lifestyles such as vegetarianism, active environmentalism, and alternative medicine. As the majority of students (92%) were neither vegetarian nor vegan in this study, it makes sense that student behavior on washing conventional or organic produce did not differ in this study (Figure 2).

Although the majority of students frequently wash their produce, their approaches to washing different produce type are generally insufficient for reducing contamination risks, based on published guidelines. Students frequently use incorrect methods to wash produce; for instance, washing potatoes by running under water while rubbing them with their hands is a common, but incorrect, approach (Table 2). One possible factor contributing to poor practice is the confusing or conflicting information about best practices in the literature. For example, several produce items in this study had multiple correct conflicting washing methods due to conflicting literature. However, the most likely explanation for poor practice is the lack of food safety training in schools as health and nutrition classes primarily focus on nutrition, sexual behavior, alcohol and substance abuse (Morrone and Rathbun, 2003).

Although students reported high rates of produce washing, because this study is based on self-report data, it could be an overestimate of what students actually practice. Although the study population captured much of the range of ethnicities and majors at CSUF, women were overly represented in the data (Table 1). This may also tie in with another confounding factor that is that students who were more inclined to practice produce washing may have been more likely to take this survey which may not represent

the CSUF student population's actual produce handling.

There is a clear need for more research and consensus on how to properly handle different types of produce and a standardized way for consumers to gain the knowledge to reduce the risk of foodborne illnesses. Given the importance of improving college student food handling practices, it is crucial to inform college students and consumers about safe food handling practices and improve instructional interventions to prevent Foodborne illnesses.

Acknowledgments

This research was funded in part by USDA NIFA HSI Grant 2011-38422-30838 and the Department of Biological Science at CSU Fullerton. I thank my advisor Dr. Joel K. Abraham, Dr. Sara Johnson, and the fellows of the Urban Agriculture Community-based Research Experience (U-ACRE), as well as Abraham Lab members, for providing support and guidance throughout this process.

References

Alloway, B. J. (2004). Contamination of soils in domestic gardens and allotments: a brief overview. *Land Contamination & Reclamation*, *12*(3), 179-187.

Antisari, L., Orsini, F., Marchetti, L., Vianello, G., & Gianquinto, G. (2015). Heavy metal accumulation in vegetables grown in urban gardens. *Agronomy for Sustainable Development*, *35*(3). doi:10.1007/s13593-015-0308-z

Beard, T. (1991). Haccp and the home: The need for consumer education. *Food Technology*, 45, 123-124.

Bolton, J., Bushway, A., Crowe, K., & El-Begearmi, M. (2013). Best Ways to Wash Fruits and Vegetables. Retrieved November 2015 from University of Maine Department of Food Science and Human Nutrition, and Cooperative Extension. Retrieved from: http://umaine.edu/publications/4336e/

Bruhn, C., Li-Cohen, A., Harris, L. J., & Spitler-kashuba, A. (2004) Safe Handling of Fruits and Vegetables. Retrieved November 2015 from University of California Division of Agriculture and Natural Resources. Retrieved from: http://anrcatalog.ucanr.edu/pdf/8121.pdf

CDC. (2013). *State Indicator Report Fruits and Vegetables Median Daily Vegetable Intake* (pp. 1–14).

Centers for Disease Control and Prevention (2012). What is Salmonellosis? http://www.cdc.gov/salmonella/general/index.html

Centers for Disease Control and Prevention (2013). Listeria (Listeriosis) statistics. http://www.cdc.gov/listeria/statistics.html

Cicia, G., Giudice, T., & Scarpa, R. (2002). Consumers' perception of quality in organic food: a random utility model under preference heterogeneity and choice correlation from rank- orderings. *British Food Journal*, *104*(3/4/5), 200–213. doi:10.1108/00070700210425660

Coleman, P. (2012). Guide For Organic Crop Producers. https://attra.ncat.org/attra-pub/summaries/summary.php?pub=67

Core, J. (2002). Scientists seek to sanitize fruits and vegetables. *Agricultural Research*, *50*(3), 12. Article database.

Doménech, E., Botella, S., Ferrús, M., & Escriche, I. (2013). The role of the consumer in the reduction of Listeria monocytogenes in lettuces by washing at home. *Food Control*, *29*(1), 98–102.

Driessen, S. (2013). Handling Fresh Fruits and Vegetables Safely. Retrieved November 2015 from University of Minnesota Extension. Retrieved from: http://www.extension.umn.edu/food/food-safety/preserving/fruits/handling-fresh-fruits-and-vegetables-safely/

Food and Drug Administration. (2008). Limited Recall of Cantaloupe (Due to Salmonella). Retrieved December 2015. Retrieved from: http://www.fda.gov/NewsEvents/PublicHealthFocus/ucm179164.htm

Hillers, V. N., Medeiros, L., Kendall, P., Chen, G., & DiMascola, S. (2003). Consumer food handling behaviors associated with prevention of 13 foodborne illnesses. *Journal of food protection*, *66*(10), 1893–9.

Hughner, R., McDonagh, P., Prothero, A., Shultz, C., & Stanton, J. (2007). Who are organic food consumers? A compilation and review of why people purchase organic food. *Journal of Consumer Behaviour*, *6*(2-3), 94–110. doi:10.1002/cb.210

Ismail, B. S., Farihah, K., & Khairiah, J. (2005). Bioaccumulation of Heavy Metals in Vegetables from Selected Agricultural Areas. *Bulletin of Environmental Contamination and Toxicology*, *74*(2), 320–327. doi:10.1007/s00128-004-0587-6

Jevšnik, M., Hlebec, V., & Raspor, P. (2008). Consumers' awareness of food safety from shopping to eating. *Food Control*, *19*(8), 737-745.

Keikotlhaile, B. M., Spanoghe, P., & Steurbaut, W. (2010). Effects of food processing on pesticide residues in fruits and vegetables. *Food Engineering & Ingredients*, *35*(2), 34– 36.

Kilonzo-Nthenge, A., Chen, F. C., & Godwin, S. L. (2006). Efficacy of home washing methods in controlling surface microbial contamination on fresh produce. *Journal of Food Protection*, *69*(2), 330-334.

Lando, A., & Carlton, E. (2010). 2010 Food Safety Survey. Retrieved February 7, 2015, from http://www.fda.gov/downloads/Food/FoodScienceResearch/ConsumerBehaviorResearch/ UCM407008.pdf

Li-Cohen, A. E., & Bruhn, C. M. (2002). Safety of consumer handling of fresh produce from the time of purchase to the plate: A comprehensive consumer survey. *Journal of Food Protection*, *65*(8), 1287-1296.

Losasso, C., Cibin, V., Cappa, V., Roccato, A., Vanzo, A., Andrighetto, I., & Ricci, A. (2012). Food safety and nutrition: Improving consumer behaviour. *Food Control*, *26*(2), 252-258.

McIntosh, W. A., Christensen, L. B., & Acuff, G. R. (1994). Perceptions of risks of eating undercooked meat and willingness to change cooking practices. *Appetite*, 22, 83e96.

Morrone, M., & Rathbun, A. (2003). Health education and food safety behavior in the university setting. *Journal of Environmental Health*, 65(7), 9-15.

Phang, H. S., & Bruhn, C. M. (2011). Observations of consumer salad preparation. *Food Protection Trends*, *31*(5), 274.

Punzi, J. S., Lamont, M., Haynes, D., & Epstein, R. L. (2005). USDA PESTICIDE DATA PROGRAM : Pesticide residues on fresh and processesd fruit and vegetables, grains, meat, milk, and drinking water. *Outlooks on Pest Management*, 131–137. doi:10.1564/16jun12

Rothman, A. J., Sheeran, P., & Wood, W. (2009). Reflective and automatic processes in the initiation and maintenance of dietary change. *Annals of Behavioral Medicine*, 38, S4-S17.

Rowe, B.R. (2007). Washing Fruits and Vegetables. Retrieved November 2015 from Utah State University Cooperative Extension. Retrieved from: https://extension.usu.edu/files/publications/publication/FN_FC_2007-01.pdf

Scott, A. R., Pope, P. E., & Thompson, B. M. (2009). Consumer's Fresh Produce Food Safety Practices: Outcomes of a Fresh Produce Safety Education Program. J*ournal of Food Science Education*, *8*(1), 8–12. doi:10.1111/j.1541-4329.2008.00062.x

Stein, S. E., Dirks, B. P., & Quinlan, J. J. (2010). Assessing and addressing safe food handling knowledge, attitudes, and behaviors of college undergraduates. *Journal of Food Science Education*, *9*(2), 47-52.

Sterrett, S., Chaney, R., Gifford, C., & Mielke, H. (1996). Influence of fertilizer and sewage sludge compost on yield and heavy metal accumulation by lettuce grown in urban soils. Environmental Geochemistry and Health, 18(4), 135-142.

U.S. Department of Agriculture. (2013). Quick facts about the Pesticide Data Program (PDP). Available at: http://www.ams.usda.gov/AMSv1.0/getfile?dDocName=STELDEV3003252

U.S. Department of Agriculture. (2013). Quick facts about the Pesticide Data Program (PDP). Available at: http://www.ams.usda.gov/AMSv1.0/getfile?dDocName=STELDEV3003252

U.S. Food and Drug Administration. (2008). FDA warns of *Salmonella* risk with cantaloupes from Aropecuaria Montelibano. Available at: http://www.fda.gov/NewsEvents/Newsroom/PressAnnouncements/2008/ucm116869.htm. Accessed 27 September 2015.

Verrill, L., Lando, A. M. & O'Connell K. (2012). Consumer vegetable and fruit washing practices in the United States, 2006 and 2010. *Food Protection Trends*, 32(4), 164-172.

Weiss, B., Amler, S., & Amler, R. W. (2004). Pesticides. *Pediatrics*, 113(4), 1030–1036.

Winter, C. K., & Davis, S. F. (2006). Organic Foods. *Journal of Food Science*, *71*(9), R117–R124. doi:10.1111/j.1750-3841.2006.00196.x

Yarrow, L., Remig, V. M., & Higgins, M. M. (2009). Food Safety Educational Intervention Positively Influences College Students' Food Safety Attitudes, Beliefs, Knowledge, and Self-reported Practices. Vol. 71, pp. 30-35. DENVER:(National Environmental Health Association).

Zander, A., & Bunning, M. (2010). Guide to Washing Fresh Produce. Fact Sheet No. 9.380. Retrieved November http://extension.colostate.edu/docs/pubs/foodnut/09380.pdf

Reproductive Physiology of Pacific Sanddab (*Citharichthys sordidus*) Collected Near a Wastewater Outfall Site in Southern California

Velvet L. Park
Advisor: Dr. Kristy L. Forsgren

Department of Biological Science, California State University, Fullerton

Abstract

Over a billion gallons of treated wastewater, also known as wastewater effluent, is discharged off the coast of southern California daily. Wastewater effluent may contain endocrine disrupting compounds (EDCs), chemicals that mimic naturally synthesized hormones in animals, which can affect the physiological processes in marine organisms. We hypothesized that the reproductive physiology of Pacific sanddab (*Citharichthys sordidus*) collected at an outfall site would be different compared to fish collected at a reference site not directly receiving wastewater effluent. Female Pacific sanddab were collected from a wastewater outfall site (n=97) and a reference site (n=110) in southern California (Orange County) during July and October 2014 and January and July 2015. Fish weight (g), standard length (cm), and ovarian weight (g) were recorded. Gonadosomatic index (GSI), that is gonad weight as a proportion of total body weight, was calculated (gonad weight/body weight x 100). Ovarian tissue was dissected, fixed, and embedded in paraffin wax for histological analysis. Using a light microscope, ovarian follicle stage (primary, secondary, or vitellogenic stages) was determined and ovarian follicle diameter measured (to the nearest μm). Ovarian follicle volume was calculated using diameter measurements ($4/3\pi\ r^3$). Female sanddab standard length and weight were significantly greater ($p<0.001$ length; $p<0.005$ weight) at the outfall site during all months with the exception of January 2015. Pacific sanddab GSI was only significantly greater ($p<0.001$) in July 2014. The composition of ovarian follicles (i.e., developmental stages) in fish collected from the outfall or reference sites in July 2014, was not significantly different ($p=0.356$ primary; $p=0.155$ secondary; $p=0.432$ vitellogenic). However, in October 2014, more primary ovarian follicles advanced to the secondary stage ($p=0.050$) and vitellogenic stage ($p=0.020$) compared to ovaries from fish collected at the reference site. In January 2015, more primary ovarian follicles advanced to the secondary ($p=0.013$) stage compared to the reference site (Figure 1). Vitellogenic follicles were not present in the ovarian tissue from fish at either site in January 2015. In July 2014, primary ovarian follicle volume did not differ significantly ($p=0.468$) between the outfall and reference sites. The volume of secondary and vitellogenic ovarian follicle stages were significantly greater (secondary $p<0.001$; vitellogenic $p<0.001$) at the outfall site than at the reference site. During October 2014, the ovarian follicle volume of all stages of ovarian follicles was significantly greater ($p<0.001$) at the outfall site compared to the reference site. In January 2015, the volume of primary and secondary ovarian follicles were significantly greater (primary $p=0.020$; secondary $p<0.001$) at the outfall site (Figure 2). Our data indicate the reproductive physiology of female Pacific sanddab displays considerable temporal and spatial variability. Currently, histological analyses for fish collected during July 2015 is being conducted. Since sex steroid hormones are important during ovarian follicle growth, especially estrogens during secondary and vitellogenic ovarian follicle development, the presence of estrogen-mimicking EDCs in wastewater effluent are likely to have promoted the ovarian follicle development at the outfall site. Continued investigation of wastewater outfall sites will be important in order to conclusively establish a pattern of reproductive advancement in demersal organisms and/or determine the long-term effects of exposure to EDCs on reproductive physiology.

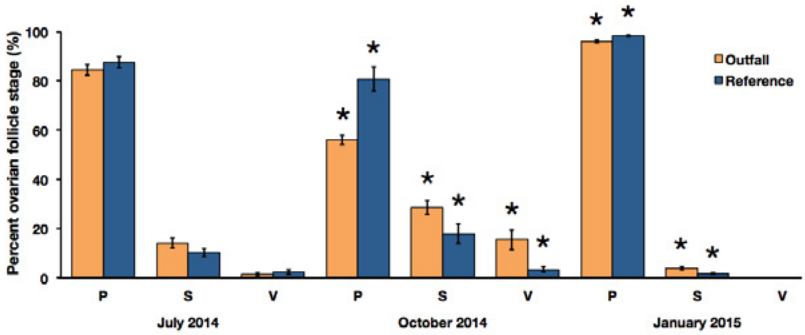

Figure 1. *Percentage of ovarian follicles at primary (P), secondary (S), and vitellogenic (V) stages of development (mean ± SE; n=5 sections per individual) of Pacific sanddab ovaries collected at an outfall site and a reference site in July of 2014, October 2014, and January 2015. Asterisks denote significant differences (p<0.001).*

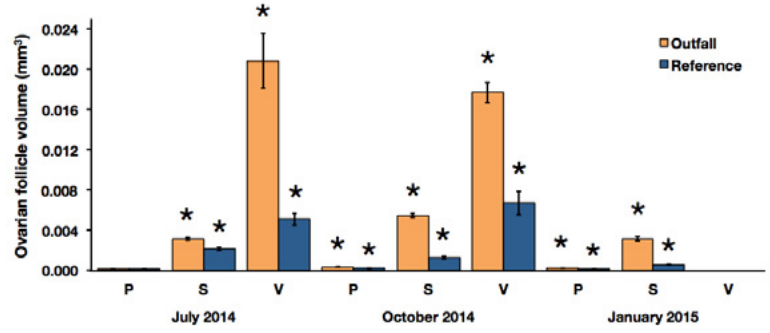

Figure 2. *Ovarian follicle (volume mean ± SE) of Pacific sanddab ovaries collected at an outfall and reference site (n=5 fish per stage; n=15 oocytes per fish). Asterisks denote significant differences (p<0.02). Note: no vitellogenic follicles were observed in fish at either site in January 2015*

Description of the Reproductive Morphology of a Viviparous Fish, the Black Perch (*Embiotoca jacksoni*) using Histological Methods

Evelyn Ruelas
Advisor: Dr. Kristy L. Forsgren

Department of Biological Science, California State University, Fullerton

Abstract

Black perch are a common southern California reef fish. During mating, male black perch transfer a spermatophore (capsule containing mature sperm) to the female via an intromittent organ. Females store the mature sperm within the ovarian cavity until the ova become fertilized. Embryonic and larval development takes place within the ovarian cavity until the female gives live birth five months later. The objective of our study was to describe ovarian and testicular development of black perch in addition to describing the pathway of spermatophore transfer. Black perch were collected along the southern California coast throughout the year. Gonadal tissues were dissected, embedded in paraffin wax, and examined under a light microscope. The percent composition of ovarian follicles and spermatophore development were determined. Female black perch only had one fully developed ovary. All stages of ovarian follicles (primary 78.7%, secondary 7.1%, tertiary 12.4% and fertilized ova 1.8%) were observed in ovarian tissues from females 50 - 100mm SL (n=5). In females 100 -150 mm SL (n = 4), in addition to all ovarian follicle stages being present (primary 69.2%, secondary 18.9%, tertiary 11.1%, fertilized ova 0.8%), one female had two developing young within the ovary. All stages of ovarian follicles (primary 4.0%, secondary 7.0%, tertiary 89%) were present in the ovarian tissue of females >150mm SL (n = 2); one female had eight developing young within the ovary. The intromittent organs of male fish 100 -150 mm SL (n =4) consisted of a white patch with no external protrusion. Spermatogonia (12.1%), spermatocytes (37.0%), spermatids (30.5%), and spermatozoa (20.3%) were present within the testicular tissue of fish 100 - 150 mm SL (n = 4). The intromittent organs were enlarged and protruded from the anal fin in males >150 mm SL (n = 2) and testicular tissue contained spermatocytes (31.3%), spermatids (28.3%), spermatozoa (34.3%) as well as spermatophore development (6.1%). By histologically describing the gonadal development of black perch and examining the pathway of spermatophore transfer, we will significantly contribute to our understanding of reproductive biology of the perch family (Embiotocidae) and viviparous fishes.

Introduction

The black perch (*Embiotoca jacksoni*) are a common southern California reef fish (Isaacson and Isaacson 1966, Behrens 1977, Baltz 1984). Black perch can be found in various habitats including: eelgrass, kelp beds, rocky and sandy bottoms, and bays and estuaries (Baltz 1984, Allen and Pondella 2006, and Froeschke et al. 2007). Black perch are distributed among varying depths, but are more commonly observed in deeper habitats where kelp beds are dense (˜10m; Hixon, 1980, Ebeling and Laur 1985). Despite a ubiquitous population of black perch off the coast of southern California, the reproductive biology and gonadal development of black perch have not been thoroughly described including reproductive maturation (Isaacson and Isaacson 1966, Baltz 1984,). Additionally, conflicting literature on black perch make understanding this viviparous fish difficult.

Viviparity is a unique form of reproduction, most commonly associated with mammals, in which the fertilized egg is retained within the female body cavity during embryonic development (Dunbrack and Ramsay

1989). The number of developing young a female fish can gestate at one time is directly correlated to the size of the female; the larger the female, the more young she can energetically support (Isaacson and Isaacson 1966, Turner 1938, Froescke et al. 2007). The smallest female black perch found to have developing young was 121 mm standard length (SL; Isaacson and Isaacson 1966, Froeschke et al 2007,). In some perch fishes (Family: Embiotocidae; e.g., shiner perch, dwarf perch), fish are sexually mature at birth (20-30 mm SL; Wiebe 1968, Liu and Avise, 2011). Black perch have been reported as being sexually mature between one and two years of age (40-50 mm SL; Isaacson and Isaacson 1966, Behrens 1977, Baltz 1984).

During the mating season, black perch mate by internal fertilization in which the male transfers sperm contained within a spermatophore via paired intromittent organs located on the anal fins (Blake 1868, Tarp 1952, Bernardi 1999, LaBrecque, 2014,). While spermatophore transfer in black perch has not been documented, in shiner perch (*Cymatogaster aggregata*), the spermatophore remains intact in the efferent sperm ducts of the male until transferred into the female reproductive tract (Gardiner 1978). The spermatophore rapidly dissolves and mature sperm are no longer encapsulated (Gardiner 1978). The sperm head embeds into the ovarian wall in a viable state, until ovarian follicles are fertilized (Gardiner 1978).

Froeschke (et al. 2007) suggested that black perch mate between July and November. However, gravid females have not been reported until December, which has led researchers to believe that females retain sperm within the ovary for 5 - 6 months until ovarian follicles are mature and able to be fertilized (Turner 1938, Wiebe 1968, Shaw 1971, Gardiner 1978, Froeshcke et al. 2007). Although much is known about the reproduction of shiner perch, little is known about the reproductive biology of black perch. The development of ovarian and testicular tissues has not been documented, and would provide insight into reproductive maturity, presence of spermatophores, and developing young. The objectives of our study were to document seasonal reproductive development of black perch gonadal tissues, and describe the male intromittent organ and its association with the testis to better understand transfer of the spermatophore to the female.

Materials and Methods

Specimen Collection

Black perch were collected in eel grass beds in Orange, Los Angeles, and San Diego Counties with at least two sites per location using a beach seine and hook and line methods. Fish were euthanized using an overdose of tricane methanesulfonate (MS-222) of purity at least 98% (1 g: 5,000 ml seawater). Standard length (SL) to the nearest mm and weight (g) were recorded. Gonadal tissue was dissected from body cavity, weighed (g), then cut into cross or longitudinal sections. Ovarian sacs with developing young were dissected from the body cavity. Developing young were dissected out of the ovarian sac, weight and standard length were recorded. Developing young were cut into whole body cross sections. Additionally, all male reproductive structures were dissected including the intromittent organs on both sides of the anal fin. All tissues were fixed and prepared for histological processing (see below).

Histological Procedures

Dissected tissues were placed in Bouin's fixative for 48 hours then transferred to 70% ethanol until histological processing. Fixed gonadal tissue fragments were processed by dehydration in a series of graded ethanols, cleared with xylene, infiltrated and embedded in paraffin wax. Tissues were sectioned using a rotary microtome to a thickness of 5μm and stained with hematoxylin and eosin. Tissues were examined using a light microscope with a digital camera mounted to take photos. Micrographs were captured at several magnifications.

Gonadal tissue was staged based on morphological characteristics previously established for teleost fishes. Ovarian follicles were staged as: 1) primary ovarian follicles, 2) secondary ovarian follicles, 3) tertiary ovarian follicles, and 4) fertilized ova, (Turner 1938). Sperm development was staged as: 1) spermatogonia, 2) spermatocytes, 3) spermatids, 4) spermatozoa, and 5) spermatophores (Gardiner 1978).

Gonadal Tissue Analysis

Ovarian follicle diameter (mm) was measured using Image J software (NIH, version 1.48). Five tissue sections separated by at least 5μm were analyzed, measuring 10 follicles per stage (e.g., primary, secondary, and tertiary ovarian follicle stages, and fertilized ova). In an effort to avoid psuedoreplication

of ovarian follicles measured, only those ovarian follicles in which the nucleus was at the center of the ovarian follicle were diameters measured. Fertilized ova were ellipsoid in shape, thus three measurements were taken: horizontally, vertically and diagonally. The diameter was calculated based on an average of these three measurements. The percent of each ovarian follicle stage was determined by dividing the number of each ovarian follicle stage by the total number of ovarian follicles and fertilized ova within the ovary and multiplied by 100. The percent of each sperm stage was determined by dividing the number of each sperm stage by the total number of sperm stages and spermatophore formations in the testes and multiplied by 100.

Results

Female black perch were divided into three size classes: 50 - 100 mm SL (n = 5), 101 - 150 mm SL (n = 4), and >151 mm SL (n = 2). The ovarian tissue dissected from females indicated that only one fully functional ovary was present (Fig. 1). A second structure, which did not contain ovarian follicles was always associated with the ovary (Fig. 1, 2).

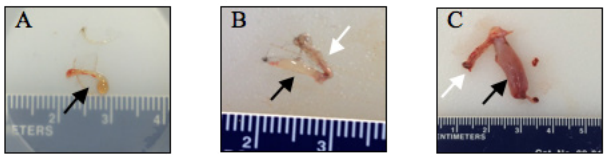

Figure 1. *Female black perch ovarian tissue from females (A) 50–100 mm SL (B) 101–150 mm SL, and (C) >151 mm SL. Black arrow is pointing to ovary, and white arrow is pointing to secondary structure.*

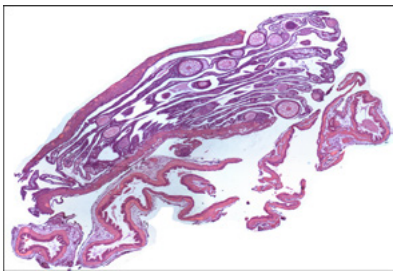

Figure 2. *Micrograph of ovary containing ovarian follicles (solid arrow pointing to ovary), and its association with the secondary structure (broken up arrow pointing to secondary structure) with no follicular development.*

Ovarian follicle development differed between females in the three different size classes (Figure. 3). Primary 78.7%, secondary 7.1%, tertiary 12.4% and fertilized ova 1.8%, were present in females 50-100 mm SL (n=5; Fig. 4). All ovarian follicle stages (n=4; primary 69.2%, secondary 18.9%, tertiary 11.1% and fertilized ova 0.8%) were also present in females 101-150 mm SL (Fig. 4). Additionally, one female (110 mm SL) was observed to have two developing young within the ovarian sac, each with a standard length of 30 mm SL, weighing 0.5g. Ovarian follicle stages (n=2; secondary 4%, tertiary 7%, and fertilized ova 89%) were present in females >151 mm SL (Fig. 4) primary ovarian follicles were not observed.

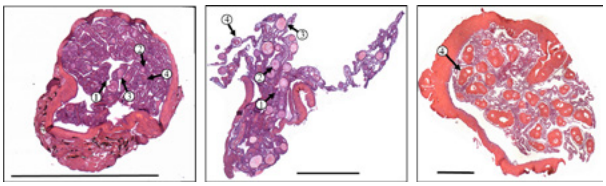

Figure 3. *Black perch ovarian histology of females (A) 50-100 mm SL, (B) 101-150 mm SL, and (C) >151 mm SL. Numbers represent: 1. Primary follicles, 2. Secondary follicles, 3. Tertiary follicles, and 4. Fertilized ova. (Scale bars equal 1 mm).*

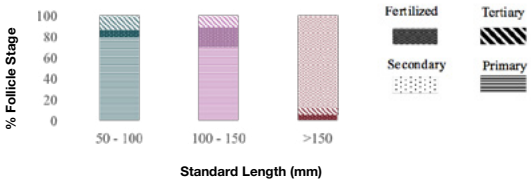

Figure 4. *Percent composition of ovarian follicle stages in female black perch (A) 50-100 mm SL; n=5, (B) 100-150 mm SL; n=4, and (C) >151 mm SL; n=2.*

One female (165 mm SL) was observed to have eight developing young within the ovarian sac (39.8 ± 0.46 mm SL and 1.3 ± 0.02 g; Fig. 5). Developing young were dissected from ovarian sac. The young appeared to be developing in multiple sacs found within the single ovary (Fig. 5). Additionally, follicle diameter (mm) increased as the follicle matured from primary follicle stage to tertiary follicle stage in females from all size classes (Fig. 6).

Fertilized ova from females 50-100 mm SL and 101-150 mm SL appeared to be smaller than all other follicles found in the ovary. Fertilized ova in females >151 mm SL had the largest diameter.

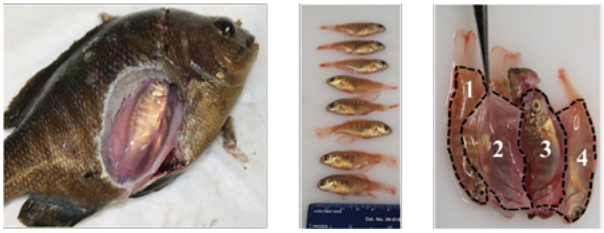

Figure 5. *(A) Dissection of a gravid female black perch displaying ovary containing developing young, (B) Developing young dissected from ovarian sac, and (C) Dorsal view of the ovarian sac with visible pockets containing young.*

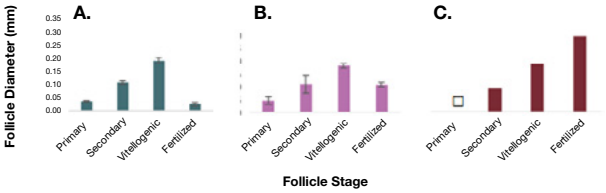

Figure 6. *Average follicle diameter of female black perch (A) >50-100 mm SL; n=5, (B) 100 -150 mm SL; n=5 and (C) >150 mm SL; n=2. Error bars represent standard error of mean.*

Sperm stages (Spermatogonia 12.1%, spermatocytes 37%, spermatids 30.5% and spermatozoa 20.3%, were present within the testicular tissue of fish 100-150 mm SL (Fig. 9). Spermatophore formations were not present, and the intromittent organs on the anal fin consisted of a white patch with no external protrusion (Fig. 7).

Figure 7. *Left side of male black perch <100 mm SL. Paired intromittent organs not fully developed on anal fin, but visible by a white patch (black box represents magnified image).*

Testicular tissue from males > 151 mm SL contained spermatocytes 31.3%, spermatids 28.3%, spermatozoa 34.3%, and the development of spermatophores 6.1% (Fig. 9). Spermatogonia were not observed, and the intromittent organs were enlarged and protruded from the anal fin (Fig. 8).

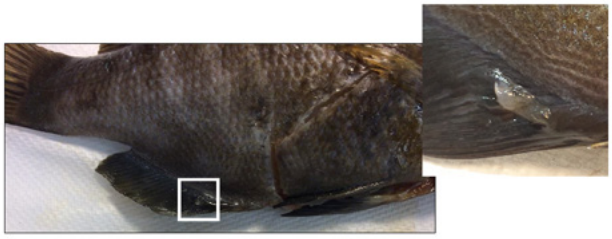

Figure 8. *Right side of a male black perch >151 mm SL. Paired intromittent organ visible on anal fin (white box represents magnified image).*

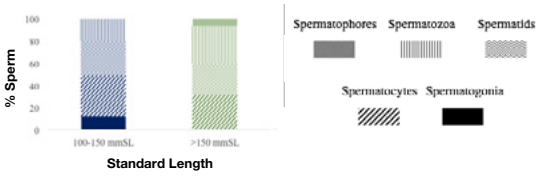

Figure 9. *Percent composition of sperm stages in male black perch (A) 100-150 mm SL; n=4, (B) >150 mm SL; n=2.*

Further observations on the testicular tissues of males 50-100 mm SL are currently being analyzed. Histological analyses on the relationship between the testis and intromittent organ confirm the presence of efferent ducts, which lead to a main sperm duct, possibly leading to the intromittent organs (Fig. 10).

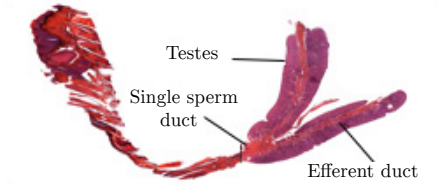

Figure 10. *Reproductive structure of male black perch (A) Efferent ducts of testes appear to fuse to a single sperm duct that leads directly to paired intromittent organs, and (B) Histological micrograph of anal fin, arrow pointing to intromittent organ.*

Discussion

The ovaries of all black perch had only one fully developed and functional ovary associated with a secondary structure. Our findings of a single ovary conflicts with previous published literature. It was believed that female black perch ovaries were fused (Behrens 1977). The secondary structure did not have developing ovarian follicles as evidenced by histological examination, thus ruling out the presence of a second ovary. The secondary structure may be associated with the process of internal fertilization, possibly receiving the spermatophore capsule from the male during copulation. The differences in the composition of ovarian follicles within the ovary, indicated that ovarian follicles are maturing during the year, which can aid in elucidating the timing of mature ovarian follicles and reproductive maturity of female black perch.

The percent of ovarian follicle stages aided in determining the reproductive status of females in different size classes. Females had the highest percentage of primary ovarian follicles 78.7%, followed by tertiary follicles 12.4%, secondary follicles 7.1%, and fertilized ova 0.8%, in females 50-100 mm SL (Fig. 3). Females 101-150 mm SL also contained a high percentage of primary ovarian follicles 69.2%, followed by secondary follicles 18.9%, tertiary follicles 11.1%, and <1% of fertilized ova. Ovarian tissues from females >151 mm SL had the highest percentage 89%, of fertilized ova. Our results indicate that larger females have a higher reproductive success than do the smaller females. Larger females may have accessibility to more nutrient resources, thus being able to expend more energy in follicle development leading to a higher a percentage of fertilized ova. It was interesting, however, that fertilized ova were observed in females <100 mm SL, which are considered to be a young-of-the-year. Previous literature has stated that females do not become sexually mature until one to two years of age.

Ovarian follicle diameter increased as the ovarian follicle progressed through subsequent developmental stages, as is expected. As the ovarian follicle develops it accumulates yolk within the cell's cytoplasm, and the upregulation of proteins cause the cell to increase in diameter (Forsgren and Young 2012, Bobe and Labbé 2010). The largest diameters were found in fertilized ova in females >151 mm SL. Fertilized ova in females 50-100 and 101-150 mm SL had smaller fertilized ova diameters compared to most other ovarian follicles present. The results may have been due to a histological artifact. Due to previous literature we were not expecting to find fertilized ova in young-of-the-year females, thus we only sectioned far enough into the ovarian tissues to calculate diameters of all other ovarian follicle stages present.

Gravid females were observed in females 100-150 and >151 mm SL. Interestingly, previous literature indicated that the smallest female to have developing young was 121 mm SL (Isaacson and Isaacson 1966, Froeschke et al 2007). Our study found that a female of 110 mm SL had two developing young within the ovarian sac. Gravid females had developing young within the ovary, thus not only is the black perch ovary the site of ovarian follicle development, but also the location of the five-month gestational period. The black perch ovary in the female 110 mm SL consisted of two longitudinal pockets where single young developed within each pocket. The ovary in the female >151 mm SL consisted of 4 longitudinal pockets where multiple young developed within each pocket. Dissected young from ovarian sac were all at the same stage of larval development.

Spermatogonia 12.1%, spermatocytes 37%, spermatids 30.5% and spermatozoa 20.3% were present in males <100 mm SL (Fig. 9). Spermatophores were not present in any males <100 mm SL. Males >151 mm had spermatocytes 31.3%, spermatids 28.3%, spermatozoa 34.3%, including the formation of spermatophores 6.1%. Spermatogonia were not present in the testes of males >150 mm SL. The sperm aggregations, otherwise known as spermatophores seemed to accumulate at the center of the cross section where the efferent duct was located. Spermatophores may be aggregating near the center to get into position to be released through the efferent ducts, to the single sperm duct and to the paired intromittent organs on the anal fin. Further investigation on the male reproductive structures will be conducted to locate spermatohpores and elucidate the pathway of the spermatophore from the male to the female during copulation.

Overall, spermatophore formations were not present in small males and the intromittent organs

were not fully developed on the anal fin. These data may indicate that young-of-the-year male black perch are not physically capable of copulating with a female. Interestingly, young- of-the-year females (<100 mm SL) were found to have fertilized ova within the ovary. Previous literature on black perch behavior have observed that males and females only mate with partners of equal size (Froeschke et al. 2007). Our results suggest that larger, mature, males >100 mm SL are mating with mature young-of the-year females <100 mm SL.

Future work will consist of analyzing the reproductive maturity of the developing young in the ovarian sac and juvenile black perch <50 mm SL. Observations of the intromittent organ are currently being conducted to determine the tissues that make up the organ and how the spermatophore is transferred to the female. We also aim to determine the fate of the transferred spermatophore once within the female reproductive tract. The development of ovarian and testicular tissues has not been documented, and would provide insight into reproductive maturity of the black perch and how they "fit" in with other perch species. It is important to understand that perch species in the same family (Embiotocidae) may differ in reproductive maturity, thus it cannot be assumed that all perch exhibit the same reproductive mechanisms. Histologically describing the gonadal development of black perch will significantly contribute to our understanding of reproductive biology of the perch family (Embiotocidae) and viviparous fishes.

Acknowledgements

Thank you to the Southern California Ecosystem Research Program (SCERP) for funding our research under the National Science Foundation (URM-DBI 1041203) and the CSUF Biology Department. I would also like to thank Prarthana Shankar, Cristy Rice, Matt Scanlon, Stacy Schkoda, Velvet Park, Austin Xu, Jordan Abney, Joseph Gamez, Sean Zulueta, Javier Jacob and Harrison Huang.

References

Allen, L. G., and D.J. Pondella II. 2006. Surfzone, coastal pelagic zone, and harbors. Pages 149- 166 in L.G. Allen, D.J. Pondella II, and M.H. Horn eds. The Ecology of marine fishes; Calfiornia Press, Berkeley.

Baltz, D. (1984). Life history variation among female surfperches (Perciformes: Embiotocidae). Environmental Biology of Fishes, 10(3), 159-171.

Behrens, D.W. (1970). Fecundity and Reproduction of the Viviparous Perches Hypsurus caryi (Agassiz) and Embiotoca jacksoni Agassiz. California Department of Fish and Game 63: 234-252.

Bernardi, G. (1999). Barriers to Gene Flow in Embiotoca Jacksoni, a Marine Fish Lacking a Pelagic Larval Stage. Evolution, 226-226.

Blake, J. (1868). On The Anal Fin Appendages of Embiotocoid Fishes. Journal of Anatomy and Physiology, 491-494.

Bobe, J. and Labbé, C. (2010). Egg and Sperm Quality in Fish. General Comparative Endocrinology, 535-548.

Dunbrack, R.L. and Ramsay, M.A. (1989). The Evolution of Viviparity in Amniote Vertebrates: Egg Retention versus Egg Size Reduction. The American Naturalist, 133(1), 138-148

Froeschke, B., Allen, L., and Pondella, D. (2007). Life History and Courtship Behavior of Black Perch, Embiotoca jacksoni (Teleostomi: Embiotocidae), from Southern California. Pacific Science, 61(4), 521-531.

Forsgren, K.L., and Young G. (2012). Stage-Specific Effects of Androgens and Estradiol-17beta on the Development of Late Primary and Early Secondary Ovarian Follicles of Coho Salmon (Oncorhynchus kisutch) In Vitro. Biology of Reproduction, 87(3),1-14

Gardiner, D. (1978). Cyclic changes in fine structure of the epithelium lining the ovary of the viviparous teleost, Cymatogaster aggregata (Perciformes: Embiotocidae). Journal of Morphology, 367-379.

Isaacson, P., and Isaacson, D. (1966). Notes on the Life History of the Black Perch, Embiotoca jacksoni, Agassiz. Transactions of the American Fisheries Society, 107-109.

LaBrecque, J., Alva-Campbell, Y., Archambeault, S., and Crow, K. (2014). Multiple paternity is a shared reproductive strategy in the live-bearing surfperches (Embiotocidae) that may be associated with female fitness. Ecology and Evolution, 4(12), 2316-2329.

Liu, J., and Avise, J. (2010). High degree of multiple paternity in the viviparous Shiner Perch, Cymatogaster aggregata, a fish with long-term female sperm storage. Marine Biology, 893-901.

Shaw, E., J. Allen and R. Stone. (1974). Notes on Collection of Shiner Perch, Cymatogaster aggregata, in Bodega Harbor, California. Calif. Fish and Game 60: 15-22.

Tarp, F.H. (1952). A Revision of the Family Embiotocidae (The Surfperches). Calif. Fish and Game 88:99-101

Turner, C. (1938). Histological and cytological changes in the ovary of Cymatogaster aggregatus during gestation. Journal of Morphology, 351-373.

Wiebe, J.P. (1968). The Reproductive Cycle of the Viviparous Surfperch, Cymatogaster aggregata Gibbons. Canadian Journal of Zoology, 46:1221-1234

Assessment of the Reproductive Physiology of the California Mussel (*Mytilus californianus*) in Southern California

Prarthana Shankar
Advisors: Dr. Jennifer L. Burnaford and Dr. Kristy L. Forsgren

Department of Biological Science, California State University, Fullerton

Abstract

The California mussel (*Mytilus californianus*) is a common suspension feeding bivalve in the intertidal zone. California mussels have the potential to spawn continually throughout the year, and in California, recruitment is thought to peak in the summer. Our objective was to assess the degree of variability of certain reproductive traits in sites that are located close together in southern California. We hypothesized that because of the close proximity of three southern California sites, mussels will not show differences in reproduction across the sites. California mussels were haphazardly collected in April and July 2015 from three sites: San Pedro, Corona Jetty, and Dana Point Jetty. Soft body tissue was removed from the mussel shell and weighed (g). Gonad tissue (i.e., ovaries, testes) was dissected from the soft body tissue and weighed (g). The gonadosomatic index (GSI) was calculated to determine the gonad mass as a proportion of total soft body mass [(gonad mass/soft body tissue mass)*100]. Gonad tissues were fixed and embedded in paraffin wax for histological analysis. Using a light microscope, the sex of individuals was determined, and ovarian follicles and spermatocytes were developmentally staged. Ovarian follicle diameter was measured (μm) and used to calculate ovarian follicle volume (μm^3). Female GSI at San Pedro was significantly lower in July than in April, while at Corona Jetty, GSI was significantly greater in July than in April (ANOVA on raw data: Site – $F = 1.684$, $DF = 2$, $p = 0.2032$; Season – $F = 3.970$, $DF = 1$, $p = 0.0558$; Site*Season – $F = 10.28$, $DF = 2$, $p = 0.0004$). Most females during the two sampling seasons had ovarian tissue with only previtellogenic ovarian follicles. However, at Dana Point Jetty in July, 60% of females had evidence of a recent spawning event with the presence of ruptured follicular walls. Ovarian follicle volume at San Pedro was significantly smaller in April than in July (ANOVA on raw data: Site – $F = 8.489$, $DF = 2$, $p = 0.0002$; Season – $F = 8.015$, $DF = 1$, $p = 0.0047$; Site*Season – $F = 4.269$, $DF = 2$, $p = 0.0141$). Male GSI at Corona Jetty was significantly greater in July than in April (ANOVA on raw data: Site – $F = 2.329$, $DF = 2$, $p = 0.1160$; Season – $F = 1.670$, $DF = 1$, $p = 0.2068$; Site*Season – $F = 8.072$, $DF = 2$, $p = 0.0017$). In July, at all three sites, the majority of males were in the developing stage, indicating they were not sexually mature. Thus, California mussel reproduction in southern California appears to vary across the three sites and also between seasons. There may be many potential explanations for our results, including biotic factors and local environmental conditions like salinity, temperature and food abundance, all of which are thought to be exogenous cues for reproduction in the California mussel. Future work includes processing reproductive tissue of California mussels collected in November 2015 and February 2016, in order to gain a comprehensive understanding of the reproductive physiology of the California mussel along the coast of southern California.

Comparing Seed Viability and Harvest Consistency Across Sites and Years for the Federally Endangered Plant *Eriastrum densifolium* ssp. *sanctorum*

Ignacio Vera
Advisor: Dr. Darren Sandquist

Department of Biological Science, California State University, Fullerton

Abstract

The Santa Ana River woolly star, Eriastrum densifolium spp. sanctorum, is a federally- listed, endangered plant species native to the Santa Ana River floodplain in Redlands, CA. Woolly star has a specific habitat preference for young sand deposits that develop after periodic flooding. A major reason for its protection is the lack of such flooding from the Santa Ana River due to regional flood control measures. Suitable woolly star habitat is now significantly reduced and only supports small populations. A seed reserve of approximately 77,000 viable woolly star seeds was created as part of a larger restoration project. Seed collections involved formalizing a simplified method for harvesting, sorting, counting, testing viability, and storing the seeds. The methods were tested at three sites and across two years with slightly lower-than-normal precipitation (2012 and 2013). The objective was to achieve consistent and reproducible seed recovery across years and sites. Variation across sites was larger than expected, but recovery between years was consistent. These results indicate that the harvest method appears to be reliable for consistent seed recovery, but that seed production can differ significantly between sites.

Introduction

Endangered organisms are an important part of the world's biodiversity and any and all action to protect endangered organisms should be taken. This includes organisms that are not in the general public's eye and may be of little economic interest. Conservation of endangered organisms also does not have to be a financial burden and can serve as cultural value to a locality. Eriastrum densifolium ssp. sanctorum (family

Polemoniaceae), the Santa Ana River Wooly Star, or more commonly woolly star is a federally endangered plant located along the Santa Ana River floodplains of Redlands, CA. Like many endangered taxa, the woolly star is restricted to a small and unique habitat that is the Santa Ana River floodplain (Harper, K.T., 1979). Natural flooding of this floodplain would normally occur every few years and would eliminate competition, bring in new soil and nutrients, and replenish ground water. Unfortunately, due to flood control measures, these natural floods are less frequent and at a much smaller scale.

The woolly star is a perennial sub-shrub that grows to a maximum height of 1 m with blue-purplish flowers. Its common name, Santa Ana River Woolly Star, derives from its characteristics: being located near the Santa Ana River, having white woolly colored pubescent hairs on its stem, and flower having five petals in the shape of a star. It is fairly similar looking to other subspecies such as ssp. elongatum, but two characteristics identify the ssp. sanctorum from ssp. elongatum: geographic location and an elongated corolla tube or "flower depth" (Patterson, R. and Tanowitz, B.D., 1989). In a previous study, hybridization among various E. densifolium subspecies was successful, thereby challenging the need for more than simply two subspecies (Brunell, M.S. and Whitkus, R., 1998).

The primary pollinators of E. densifolium spp. sanctorum are hummingbirds, bumble bees, hallictid bees, and digger bees (Dorsett et. al, 2001). In the fall, the flowers fall off of the flower heads and seedpods develop. Individuals can have 2-100 flower heads, with

each flower head containing 2-20 seedpods, and each seedpod containing about 5 seeds. Thus an individual plant can contain 10 to10,000 seeds.

This study is a part of a broader program to maintain a viable E. densifolium spp. sanctorum population for perpetuity. As part of this program, a seed reserve is required for restoring populations or establishing plants in a new location. Collecting this seed reserve is one of the main objectives of the study.

The goal was to collect 30,000 viable seeds in 2012 and 2013. Viable seeds,which tend to be larger (1.5 to 3.0 mm in length) and generally grow into healthier individuals, were specifically needed (Skogen et. Al, 2010 and Seiwa, K. and Kikuzawa, K., 1996); seedlings that come from larger seeds are able to grow faster and produce more flowers than seedlings that come from smaller seeds (Stanton, 1984). In addition, I examined variation in seed yield and viability among different E. densifolium spp. sanctorum sub-populations to determine whether or not some sub-populations were producing healthier seeds than others. A final goal was to see if seed collections could be done in a cost effective manner.

Materials and Methods

Figure 1: *Field site locations: A-D in Redlands, CA. Boxes do not represent the entire range of the woolly star population of each site, only the area of the site that was used for seed collection. The Santa Ana River is dried up in this figure and the arrow depicts the natural flow when the river is present. The freeway in the middle of the figure is the Foothill Freeway (CA State Highway 210).*

Collection of woolly star seeds was done across field sites: A-D (Figure 1) in 2012 and A-C in 2013 in the Santa Ana River floodplain in Redlands, CA. Site D was not collected from in 2013 because the majority of the plants were dormant during the collecting period. These sites offer a good representation of woolly star populations as they offer various population sizes. Sites A and B are the larger sites, with several hundreds of individuals, Site D is a medium size population of a few hundred individuals, and site C is a smaller size population with less than a hundred individuals.

Because no previous methodology for collecting woolly star seeds had been published, one objective was to develop a standardized protocol for collecting, counting, and testing woolly star viability. The number of plants sampled was not recorded because the goal was to collect as much as possible.

Sampling occurred between late August and early November. During this period plants have open seedpods with seeds ready to be dispersed; only plants with at least half of their flower heads open were sampled. Plants were shaken firmly and falling seeds and debris were collected in large mixing bowls. The resulting mixture of seed and debris was designated as a “field sample”. “Field samples” were returned to the lab for sorting. Sorting was done with a two-sieve system: one size 14 soil sieve followed by a size 10 soil sieve. The size 14 sieve prevented debris larger than 3 mm from passing through, but allowed woolly star seeds to pass. The size 10 sieve trapped large woolly star seeds, but allowed small non-viable ones, and other minute debris smaller than 1 mm to pass through. The isolated seeds and any debris retained in the size 10 sieve were designated a “sieved sample”.

Physically counting 30,000 1.5 – 3-mm long seeds would take a large amount of time, so seed-to-mass regressions were used to give accurate estimates of how many seeds were actually collected. The regressions were based on small subsamples of “sieved samples” ranging in mass from 0.1 to 0.8 g. Actual counts of “potentially viable” seeds (i.e. seeds that were between 1.5 – 3 mm in length and not visibly shriveled) were made for each subsample so that seed-to-mass regressions could be generated. Subsample masses and corresponding seed counts were plotted in Excel and a linear regression line, $y = mx + b$, fitted for each site in each year, where y is the potentially viable seeds of a sample, x is the sample mass, and m and b are the empirically determined slope and y- intercept.

Viability tests of potentially viable seeds from each site in each year were conducted through germination experiments. Using small flowering pots filled with natural Santa Ana River floodplain gravel, 100 “potentially viable” seeds from each site each year were germinated to give each site a “viability percentage”. Over a 36-hour period seeds were misted over in a misting chamber collecting 33 cm of water. The flowering pots were then placed inside a germination chamber where they were exposed to a night-day cycle of light (12h light: 12h dark) for 14 days. This “viability percentage” was then used to adjust seed counts for each site and thereby estimate the total number of “viable seeds” collected from a site for a given year.

Results

Site A consistently produced more “potentially viable” seeds each year than the other sites, followed by site B, and then site C (Figure 2). Site D had similar yield as site A, but was not collected from in 2013. The “percent viabilities” were very different across sites in 2012 (Table 1), but did not vary much in 2013 (Table 2). In 2013, “percent viabilities” were also drastically lower than those of 2012. This drop in “percent viability” severely decreased the number of “viable seeds” despite collecting more “sieved sample” mass in 2013. In 2012, a total of 34,972 “viable seeds” were collected and, in 2013, the total was 15,194 “viable seeds.”

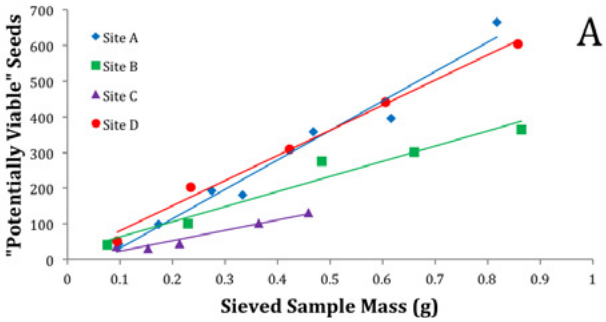

Figure 2: *Seed-to-mass regressions of the “potentially viable” seeds to “sieved sample” mass collected from the four sites in 2012 (A). Seed-to-mass regressions of the “potentially viable” seeds to “sieved sample” mass collected from the three sites in 2013 (B).*

	"Sieved Sample" Mass(g)	"Potentially Viable"Seeds	"Viability Percentage"	"Viable Seeds"
Site A	27.293	22,421	78	17.617
Site B	21.068	8,939	78	5,006
Site C	2.752	785	67	523
Site D	35.804	25,161	47	11,826
Total	**86.917**	**57,306**		**34,972**

Table 1: *2012 “Sieved Sample” mass, “Potentially Viable” seeds based on regressions estimate, “Viability Percentage” from germination trials, and the resulting estimated number of “Viable Seeds” collected for each site.*

	"Sieved Sample" Mass(g)	"Potentially Viable"Seeds	"Viability Percentage"	"Viable Seeds"
Site A	7.002	5,442	32	1,741
Site B	31.370	16,240	38	6,171
Site C	78.600	40,352	39	7,281
Total	**116.972**	**69.440**		**15,194**

Table 2: *2013 “Sieved Sample” mass, “Potentially Viable” seeds based on regressions estimate, “Viability Percentage” from germination trials, and the resulting estimated number of “Viable Seeds” collected for each site*

Discussion

Site A produced more “potentially viable” seeds than the other sites, but the reason why is not clear. It could be due to river proximity, as site A is the closest to the main drainage of the Santa Ana River, or it could be a result of greater soil nutrients. Site B is two kilometers East of Site A and still on the Santa Ana River drainage. Sites C and D are furthest from the drainage about a kilometer North of Site B. All of these sites may not be getting access to as much water as Site A. Sites C and D are also located next to an operational sand mine, but it is not clear if the mine is negatively impacting the woolly star environment.

Site C produced the least amount of “sieved sample” due to fewer plants in this population. It is also a fragmented population, with plants growing in small groups of 3- 8 plants and often several meters apart. There are also other plants and weeds in this site that likely compete with the woolly star for space and resources. This could be the reason for

fragmentation of this sub-population, however further testing would be required to determine how well woolly star competes with invasive species in the area.

Rain also plays a role in the woolly star life-cycle. The timing of rainfall is especially important for the emergence of seedlings, as seedlings have specific time frames in which they need rainwater to emerge. Woolly star specifically needs rain in late winter to early spring between January and March. If it rains outside the critical window, the rains are relatively useless for germination. Any global climate change that alters timing of rain events could negatively impact the woolly star natural emergence and hinder plant growth (Seiwa, K., 1999). If required temperatures, sunlight, and rainfall events do not occur simultaneously, seeds may remain dormant or worse, lose germination ability.

Restoration managers can use this methodology to recreate this project for various other plants of different seed sizes. It is low cost and would only need to adjust the type of sieves used to accommodate the plant of interest's seed size. The whole process needs to be followed as one can not assume on an average year of rain fall to get "Viability Percentage" in the 60-70% range and in years with below average rainfall "Viability Percentage" in the low 30%. If one was to use this methodology to go and collect 10,000 viable seeds of another plant; I would recommend doing a test run first going out in the field with collecting bowls or other apparatus to capture falling seeds. Then to take this "Field Sample" and sieve it through a two sieve system and measure the mass of the "Sieved Sample". Next to count the number of "Potentially Viable Seeds" in the "Sieved Sample" and follow up with a germination test to measure the "Viability Percentage" using a portion of those "Potentially Viable Seeds". Applying the "Viability Percentage" to the number of "Potentially Viable Seeds" gives us a more accurate "Viable Seeds" count and an idea of how much sampling of the desired plant needs to be done relative to the test run's size. However if one is collecting from several sites that are a kilometer or more apart site, variation may occur as some sites may be producing healthier seeds than other sites. This is something to keep in mind when conducting a project such as this.

The overall cost and manpower needed for this type of conservation project was relatively minor. At a total of 70 man-hours plus $1,160 resulted in the collection of 50,000+ viable seeds. This is a small expense for the assurance of protecting populations of a federally endangered plant that faces extinction.

References

Allen, L. G., and D.J. Pondella II. 2006. Surfzone, coastal pelagic zone, and harbors. Pages 149- 166 in L.G. Allen, D.J. Pondella II, and M.H. Horn eds. The Ecology of marine fishes; Calfiornia Press, Berkeley.

Baltz, D. (1984). Life history variation among female surfperches (Perciformes: Embiotocidae). Environmental Biology of Fishes, 10(3), 159-171.

Dorsett, D.K., Jones, C.E., and Burk J.H., The Pollination biology of Eriastrum densifolium ssp. sanctorum (Polemoniaceae), an endangered plant. Madroño, 2001. Vol. 48, No. 4, pp. 265-271

Harper, K.T., Some reproductive and life history characteristics of rare plants and implications of management, Great Basin Naturalist Memoirs, 1979. No. 3: pp. 129-137

Patterson, R. and Tanowitz, B.D. Evolutionary and Geographic Trends in Adaptive Wood Anatomy in Eriastrum densifolium (Polemoniaceae). American Journal of Botany, 1989. Vol. 76, No. 5, pp. 706-713

Primack, R.B., Regulation of seed yield in Plantago, Journal of Ecology, 1978. Vol. 66, No. 3, pp. 835-847

Seiwa, K., Effects of seed size and emergence time on tree seedling establishment: importance of developmental constraints. 1999. Oecologia. 123:208-215

Skogan, K.A., Senack, L., and Holsinger, K.E., Dormancy, small seed size and low germination rates contribute to low recruitment in Desmodium cuspidatum (Fabaceae), The Journal of the Torrey Botanical Society, 2010. Vol. 137, No. 4, pp. 355-365

Stanton, M. L., Seed variation in wildlife radish: effect of seed size on components of seedling and adult fitness, Ecology, 1984. Vol. 65, No. 4, pp. 1105-1112

Stone, D.R., Pollinator effectiveness and assemblages in three populations of Eriastrum densifolium (Benth.) mason (Polemoniaceae). 1995. Master's Degree Thesis, California State University, Fullerton

The Effects of Elevated Soil Nitrogen Levels and Drought on Radish (*Raphanus sativus*) Leaf Characteristics and Palatability for Brown Garden Snails (*Cornu aspersum*)

Daniel Weiherer and Britney Brown
Advisor: Dr. Joel K. Abraham

Department of Biological Science, California State University, Fullerton

Abstract

Recent environmental changes in California, including elevated levels of nitrogen in soils and a higher frequency of drought, can increase the concentration of nitrogen in plant leaves. This can make plants more appealing as food sources to herbivores as well as weaken their herbivory defense mechanisms. In this experiment, radishes were grown under various conditions of nitrogen and water levels and their leaves were analyzed. Herbivory trials were conducted using brown garden snails. Elevated nitrogen levels decreased leaf trichome density and increased leaf mass, and area. Food-appeal also increased, leading to higher rates of herbivory in nitrogen- rich leaves. Drought was found to have no effect on leaf characteristics, but drought-stressed leaves were found to experience more herbivory. These findings indicate that anthropogenic nitrogen increases could have meaningful impacts on plant herbivory rates.

Introduction

Climate change and land use change have altered environmental conditions worldwide. For instance, the distribution of nitrogen across landscapes can become concentrated by leaching into soils where humans fertilize crops, raise livestock, dump waste, and process food (Follett, 1995). The over-nitrification of habitats can create problems such as eutrophication in aquatic habitats, water toxicity, alteration of plant assemblages, interferences in nutrient cycling, and raised levels of greenhouse gas emissions from soils (Fenn et al., 2003).

As global mean temperatures increase, drought will occur more frequently and in larger areas. Scientists expect to see lower than normal levels of water in rivers, lakes, and soils as well as insufficient water availability for farming (Union of Concerned Scientists, 2011). Environmental changes such as these can have direct and indirect effects on plant assemblages. Directly, they can affect plants by altering resource availability. If levels of water drop, plants may suffer from desiccation and nutrient deficiency since wet soils are required to allow for the movement nutrients into roots. If levels of nitrogen increase, plants will absorb more nitrates into their tissues. Indirectly environmental changes can affect plants by influencing insect herbivore populations, which in turn influences plants.

In most cases, herbivory has negative impacts on a plant's health and fitness. When a plant's total leaf area is reduced, its photosynthetic capacity drops. Thus plants will produce lower amounts of energy after a period of herbivory, which can limit primary production. If the amount of energy is insufficient, plants may experience stress and an increased risk of death. For example, it has been found that increased insect abundance on a plot of land decreased coarse root production and subdominant plant species' biomass (Blue et al., 2011). This demonstrates that the reduction in a plant's mass is not only due to the loss of leaf mass consumed by herbivores, but that physiological effects in the plant that result from herbivory hinder plant growth.

Plants are sessile and cannot evade herbivores; thus in numerous cases, evolution has produced many types of defense mechanisms to guard against herbivory. Plants may defend themselves chemically with a wide range of carbon and nitrogen based

compounds, such as alkaloids, cyanogenic glycosides, terpenoids, or tannins (Freeman and Beattie, 2008). Plants may also defend themselves mechanically using trichomes or thorns to prevent access to tissues or sting attackers; they may have thick leaves that are tough to chew, slippery leaves that are difficult to grasp, or they may produce sticky liquids which trap insects. These defense mechanisms are not mutually exclusive. For instance, radishes (*Raphanus sativus*) make use of cyanogenic glycosides and trichomes to defend against herbivores (Agrawal, 1998). Trichomes, a constitutive defense, are always present on radish leaves. However, cyanogenic glycosides are induced in radishes only during herbivory. When herbivory disrupts leaf tissue, the enzyme β- glucosidase comes into contact with and activates cyanogenic glycosides, which are toxic to most animals (Møller, 2010). These variables are not only contingent to plants; they also depend on environmental conditions.

Changes in environmental conditions may influence herbivory rates through changes in the quality or quantity of plant defenses. Nitrogen levels in leaves can both increase and decrease rates of herbivory. For example, plants with higher tissue nitrogen content become more favorable food sources to insects because they are more nutritious (Lemoine et al., 2014). When a population of insects feeds on leaves high in nitrogen, more insects are likely to survive and their abundance will increase, elevating rates of herbivory (White, 1984). Additionally, nitrogen can make leaves more appetizing to insects. Lemoine et al. (2013; 2014) found that when temperatures increased, some insect species preferred to eat leaves that were higher in nitrogen.
However, nitrogen is a key component in cyanogenic glycosides; in some instance, plants that grow in nitrogen-rich soil have greater amounts of cyanogenic glycosides in their tissue (Gleadow and Møller, 2014). This provides plants with a more potent defense against herbivory, making them less palatable for many organisms, including snails (Griffiths, 2013). Thus, in the case of elevated soil nitrogen levels, it is hard to predict whether leaf palatability would increase or decrease.

Drought may also increase or decrease leaf palatability. Insufficient water availability stresses plants, which can cause more nitrogen to become available in their tissues (White, 1984). When a section of a plant is stressed, nitrogen is dissolved in that section to be transported away. With higher levels of accessible nitrogen, leaves may experience higher levels of herbivory due to the same reasons explained in the previous paragraph (White, 1984; Lemoine et al., 2013; Lemoine et al., 2014). As drought limits plant growth, the concentration of cyanogenic glycosides can increase (Gleadow and Møller, 2014). This on the other hand would provide plants with a stronger chemical herbivory defense. Much like nitrogen, drought impacts on herbivory appear to be idiosyncratic.

Given the rate of change of environmental conditions due to human activities, the rate of herbivory may be altered in many plant communities. Consequently, it is important to know if plants will be able to adequately defend themselves against herbivory in the future. This study was designed to learn how elevated soil nitrogen levels and drought affect radish leaves and their palatability. It was hypothesized that nitrogen-rich plants have greater palatability because while even though increasing the concentration of nitrogen in their leaves should increase the concentration of cyanogenic glycosides, it also increases their food-appeal to some herbivores and this could outweigh the elevated level of cyanogenic glycosides. It was hypothesized that drought-stressed plants have greater palatability because drought can hinder plants' health which in turn may hinder plants' ability to defend itself. It was hypothesized that the combination of nitrogen-rich and drought-stressed plants also has greater palatability since it was postulated that each treatment independently makes leaves more palatable. To test these hypotheses, radishes were grown under varying levels of nitrogen and water in a greenhouse. Leaf characteristics were measured to confirm that the nitrogen and water were transferred into the leaves at concentrations proportional to their treatments, to see how leaf characteristics correlated with growing conditions, and to compare the strength of herbivory defense mechanisms across treatments. Herbivory trials were conducted using brown garden snails (*Cornu aspersum*) to see how the growing conditions, strength of defense mechanisms, and nutrient content affected leaf palatability. Greater rates of herbivory were predicted in the experimental plants compared to the control plants since they were hypothesized to be more palatable.

Methods

Radishes are part of the Brassicaceae family. Domestic radish, *Raphanus sativus*, may have originated in Asia or the Eastern Mediterranean and has since been distributed worldwide (Henslow, 1898). This annual plant grows rapidly and may be harvested in less than one month. *R. sativus* is commonly farmed for its swollen taproot; the roots are usually eaten raw in salads for their crisp, spicy flavor which is in part due to the plant's cyanogenic glycoside content (IARC, 2004). The Radishes' herbivory defenses are so potent that it can be grown alongside other crops to help deter pests such as ants, aphids, and hornworms from the area (Ready, 1982). Despite this and its fast growth, it can still suffer from pests such as *Delia radicum*, *Phyllotreta striolata*, and *Contarinia nasturii* (Seamen, 2013). The brown garden snail is part of the class Gastropoda and has been introduced into many parts of the world. These snails are originally from Europe but were introduced into California to be used for escargot in the 1850s. They prefer non-stressed habitats with sufficient moisture, and yet they have managed to become thriving herbivores in California (Dekle and Fasulo, 2001).

In February 2015, 120 radish seeds were sown in forty pots inside a greenhouse, with three individuals per pot. Each pot was 6 cm in diameter and 20 cm deep with a well-draining bottom. The plants were watered with 300 mL of water on Mondays, Wednesdays, and Fridays. Each treatment had ten pots per group. Twelve days after sowing, the following adjustments were made to the pots: 1) seedlings were randomly thinned to a single individual per pot, 2) nitrogen-rich plants and the combined-conditions plants were given 0.616 mL of blood meal (a nitrogen fertilizer), and 3) the drought-stressed plants and the combined-conditions plants were only watered once a week (300 mL) on Wednesdays. The pots were arranged evenly so that each row (of four pots) contained one plant from each group of conditions, but the arrangement of plants within the rows was random. The plants were rotated once per week. These procedures were taken to reduce the likelihood of spatial confounding factors.

Over forty snails were collected and housed in containers in the greenhouse during this time period. The containers had openings for ventilation and a layer of soil and peat moss was placed on the bottom. This layer of bedding was moistened and the snails were fed one entire head of Romaine lettuce on Mondays, Wednesdays, and Fridays. However, seven days prior to the start of the herbivory trials, the snails were starved to encourage herbivory. No additional water was ever supplied to the snails for drinking.

In April, once the plants had matured, one high quality leaf from each plant was removed in order to measure leaf characteristics. Leaf quality was determined as a compromise between size and greenness. The mass of each leaf was recorded. The greenness of each leaf was assigned a number by matching the color of the leaf to a color from a series of green paint swatches. The swatches had been given numbers ranking 1 to 5 from least to most green. Trichome density was measured under a microscope by counting the number of trichomes in the area of the field of view. Samples were taken at two locations on the upper surface of each leaf and the densities were averaged. The area of each leaf was measured using a computer program, ImageJ. The leaves were placed in a drying oven for three days, and then their dry mass was recorded.

It was necessary to confirm whether the various growing conditions had any impacts on the nitrogen and water concentrations in the leaves. Leaf greenness was used to compare the amount of nitrogen in the plant. Greener plants have more nitrogen in them because nitrogen is a component of chlorophyll (Hunt, 2012). Therefore leaves with a higher greenness number were said to have greater concentrations of nitrogen. To calculate the concentration of water, the difference between wet mass and dry mass was divided by the area of the leaf.

Leaf palatability was said to be influenced by both the strength of herbivory defense mechanisms and the food-appeal due to the concentration of nitrogen. First, to compare the strength of defense mechanisms, trichome density and leaf toughness were ananlyzed. Leaf toughness was defined as leaf mass per area (LMA) which was calculated by dividing dry leaf mass by leaf area. To compare the food-appeal, leaf greenness was analyzed. Since the greenness of leaves is due to the concentration of nitrogen, the

food-appeal of a leaf was defined as being directly related to its greenness. Finally, to compare leaf palatability in its entirety, herbivory trials were conducted. Leaves that experienced higher rates of herbivory were said to be more palatable to snails.

Herbivory trials were conducted at night because snails are nocturnal (Dekle and Fasulo, 2001). One high quality leaf was removed from each radish and its mass was recorded. A snail was also weighed and then stimulated by submerging in water for one second. The leaf and the snail were placed in a sealed plastic container. The snails were allowed ten minutes to find the leaf and begin eating. Once herbivory was initiated, it was allowed to continue for ten minutes, then the snail was removed and the leaf was weighed again. This was repeated for each radish plant and a new snail was used each time. The mass of leaf that each snail consumed was calculated and subtracted the average amount of mucus added to each leaf. To account for the possible bias of larger food consumption by larger snails, this measurement was standardized by dividing it by the mass of the snail. Then the value was multiplied by 6 to calculate the standardized rate of herbivory per gram of snail per hour.

The data from leaf characteristics and herbivory rates were analyzed by making comparisons between the four groups using average values and standard errors. When correlations were made between leaf characteristics and herbivory rates, linear trend lines were generated in Microsoft Excel to obtain R^2 values. Statistical significance was tested using ANOVA.

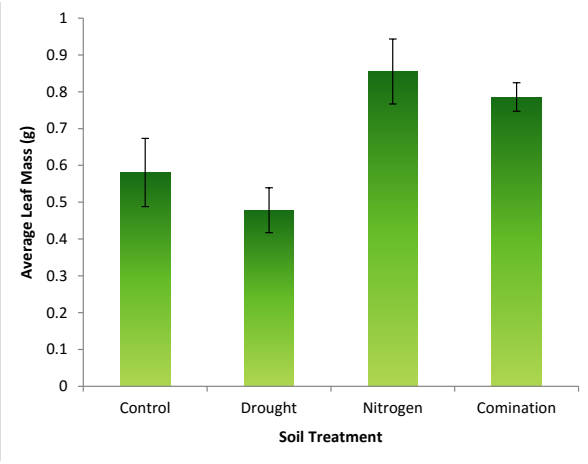

Figure 1. *Average leaf mass produced across various growing conditions. Error bars are standard error.*

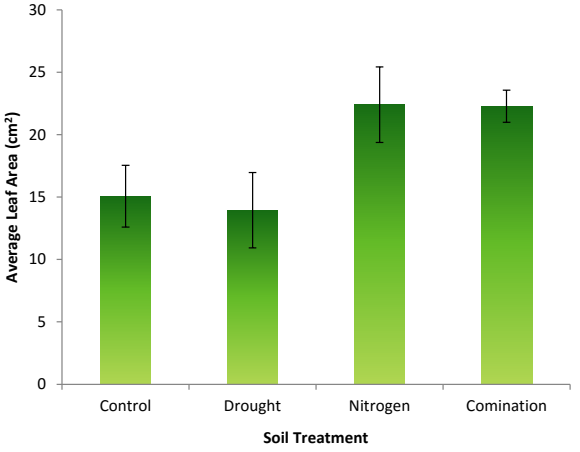

Figure 2. *Average leaf area produced across various growing conditions. Error bars are standard error.*

Results

Leaf mass and leaf area had the same responses to the soil treatments (Figures 1 and 2). Elevated nitrogen levels significantly increased leaf mass ($p = 0.045$) and area ($p < 0.001$). Although drought conditions lowered leaf mass and area, the differences were not significant.

To confirm if there was less water in the leaves of plants grown in drought-simulated growing conditions, the concentration of water in leaves throughout the four treatments were compared (Figure 3). Pots that had the lower water levels had lower average water concentrations in their leaves. The plants from the drought soil treatment had significantly lower concentrations of water than the control and the nitrogen-rich plants ($p = 0.028$), but the combination plants only had significantly lower water concentrations compared to the control plants.

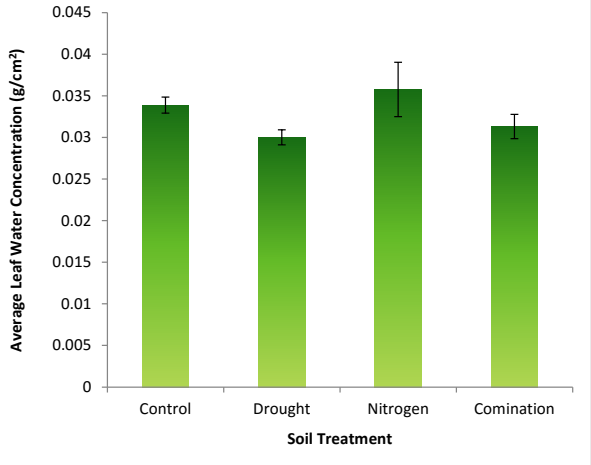

Figure 3. *Average water concentration in leaves from the four growing conditions. Error bars are standard error.*

To confirm if there were higher concentrations of nitrogen in leaves from plants grown in soils with elevated nitrogen levels, the greenness of leaves throughout the four treatments were compared (Figure 4). Greener leaves were said to have higher concentrations of nitrogen. Greenness was also used to determine food appeal. The plants that were grown in the combination of soil treatments had leaves that were significantly greener than the control and drought leaves.

The strength of herbivory defense mechanisms was compared by analyzing trichome density and leaf toughness (Figure 5 and 6). Leaves from plants grown in nitrogen-rich soils had a significantly lower trichome density than leaves from plants that were not ($p = 0.045$). Leaves from plants grown in the combination of conditions only had a significantly lower trichome density than leaves from the control plants. No significant differences were found in leaf toughness.

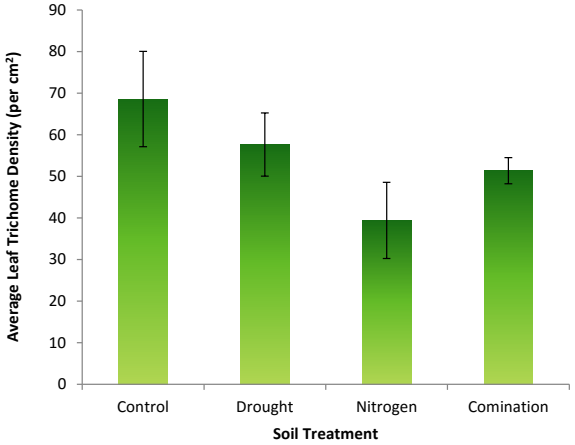

Figure 5. *Average trichome density of leaves across soil treatments. Error bars are standard error.*

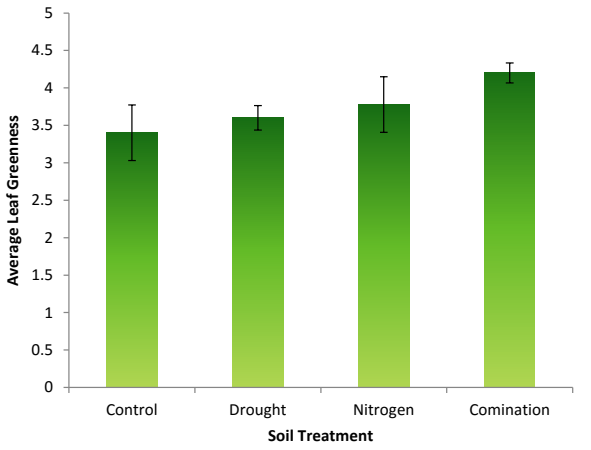

Figure 4. *Average leaf greenness determined by soil treatments. Error bars are standard error.*

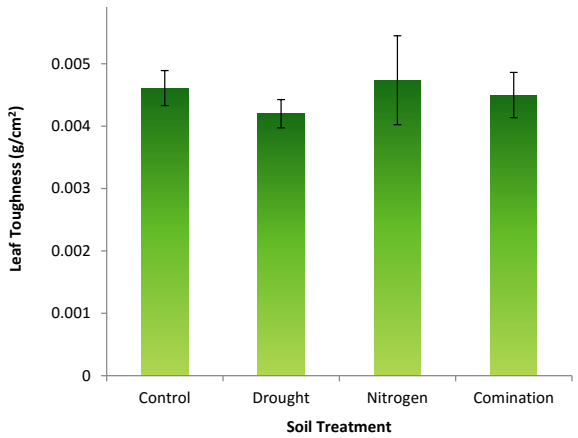

Figure 6. *Average toughness of leaves across soil treatments. Error bars are standard error.*

Leaf palatability was compared by conducting herbivory trials (Figure 7). All plants from experimental groups had a greater number of leaves that experienced herbivory than the control treatment. The control experienced zero instances of herbivory, the drought plants experienced three, the nitrogen plants experienced four, and the combination plants experienced five. The rate of herbivory was significantly higher in leaves that grew in the nitrogen-rich and combined- conditions soils.

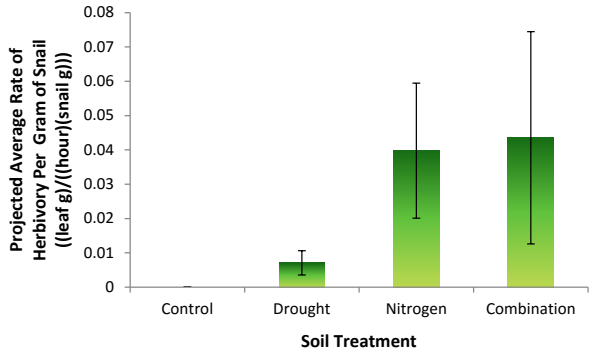

Figure 7. *Average rate of herbivory per gram of snail per hour due to different growing conditions. The masses consumed were standardized for snail mass and the rate of herbivory was projected into units of hours instead of ten minutes. Error bars are standard error.*

Greener leaves were found to experience higher rates of herbivory (Figure 8). A negative correlation ($R^2 = 0.7246$) was found between trichome density and the rate of herbivory (Figure 9). No correlation was found between leaf toughness and the rate of herbivory because there were no significant differences in leaf toughness. Lastly, a summary statistics are given for all of our data in table 1.

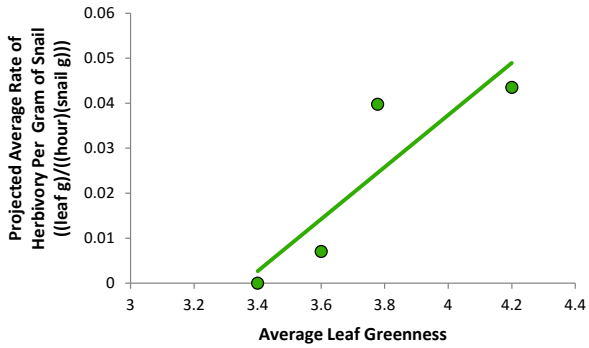

Figure 8. *Average standardized rate of herbivory per gram of snail per hour at various leaf greennesses. R2 = 0.7841.*

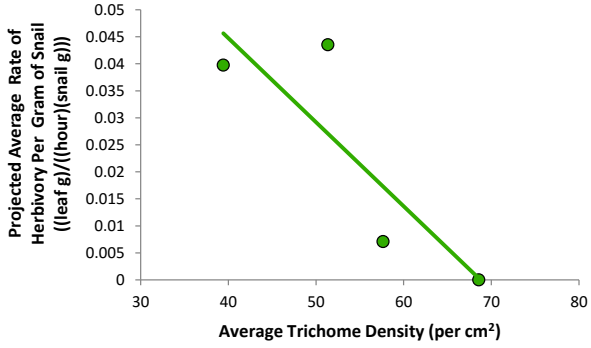

Figure 9. *Average standardized rate of herbivory per gram of snail per hour at various trichome densities. R2 = 0.7246*

		Control Leaves	Drought-stressed Leaves	Nitrogen-rich Leaves	Combined-conditions Leaves
Initial Leaf Mass (g)	Avg.	0.581	0.478	0.855	0.786
	S.D.	0.293	0.193	0.264	0.123
	S.E.	0.093	0.061	0.088	0.039
Greenness Index Measure	Avg.	3.4	3.6	3.8	4.2
	S.D.	1.2	0.5	0.8	0.4
	S.E.	0.4	0.2	0.3	0.1
Trichome Density (per cm^2)	Avg.	68.56	57.64	39.42	51.34
	S.D.	36.22	23.97	27.47	9.92
	S.E.	11.45	7.58	9.16	3.13
Leaf Area (cm^2)	Avg.	15.07	13.95	22.40	22.28
	S.D.	7.82	5.32	9.07	4.05
	S.E.	2.47	1.68	3.02	1.28
Dry Leaf Mass (g)	Avg.	0.064	0.057	0.092	0.097
	S.D.	0.025	0.021	0.023	0.016
	S.E.	0.008	0.007	0.008	0.005
Specific Leaf Area (cm^2/g)	Avg.	226	246	258	237
	S.D.	50.4	49.9	125	65.8
	S.E.	15.9	15.8	41.7	20.8
Water Mass (g)	Avg.	0.517	0.421	0.763	0.689
	S.D.	0.271	0.173	0.255	0.117
	S.E.	0.086	0.055	0.085	0.037
Water Concentration (g/cm^2)	Avg.	0.0339	0.0300	0.0358	0.0313
	S.D.	0.0031	0.0029	0.0098	0.0046
	S.E.	0.0010	0.0009	0.0033	0.0015
Toughness (g/cm^2)	Avg.	0.0046	0.0042	0.0047	0.0045
	S.D.	0.0009	0.0007	0.0021	0.0012
	S.E.	0.0003	0.0002	0.0007	0.0004
Herbivory Rate [(leaf g)/ ((snail g)(hour))]	Avg.	0	0.0071	0.040	0.044
	S.D.	-	0.0061	0.039	0.069
	S.E.	-	0.0035	0.20	0.031

Table 1. *Summary statistics of all data. Averages (avg.), standard deviation (s.d), and standard error (s.e.) are stated for all measurements.*

Discussion

It was hypothesized that the drought, nitrogen, and combination groups would all be more palatable than the control group. The hypothesis was demonstrated to be correct as seen by higher rates of herbivory in all experimental groups. The plants that received less water had significantly lower concentrations of water in their leaves than control plants. This means that the treatments were effective and valid conclusions concerning drought could be drawn from the differences in leaf characteristics and rates of herbivory.

Plants that grew in higher levels of nitrogen had greener leaves than the control leaves, but the difference was only significant in the combined-conditions plants. This means that the treatments may have been only partially successful; it is only know for certain that valid conclusions concerning increased nitrogen levels amidst drought, not nitrogen levels alone, can be drawn from our results. Chlorophyll is made from nitrogen (Hunt, 2012). Therefore since the combined-conditions plants' leaves were greener, it can be inferred that they contained greater concentrations of nitrogen. Thus, these leaves should be more appealing food sources, which should increase rates of herbivory (Lemoine, 2013; Lemoine, 2014). However, since they contained more nitrogen, they could have also contained more cyanogenic glycosides, which should decrease the rate of herbivory. Yet a correlation in our herbivory results indicated that the more appetizing effect of added nitrogen outweighed the repelling effect of greater cyanogenic glycosides; it was

found that greener leaves experienced higher rates of herbivory ($R^2 = 0.7841$). One possible explanation for this is that our radishes may not have had the correct alleles to code for cyanogenic glycosides. According to Griffiths (2013), natural selection selects for cyanogenic glycosides in radishes when populations experience more herbivory. The seeds used could have come from populations that did not experience frequent herbivory, so they may not have had a strong cyanogenic glycoside herbivory defense mechanism. This would explain why adding nitrogen did not seem to have an effect on the strength of this particular defense mechanism.

Increasing the level of nitrogen in the soils increased leaf mass and area. This result can be expected because nitrogen is usually a limiting nutrient. It is in agreement with the work of Blue (2011) who showed that increasing nitrogen levels can increase primary production. In this study, leaves from plants that grew in conditions with elevated nitrogen levels also had a significantly lower trichome density than did plants in the control treatment. This is probably because leaves in nitrogen-rich plants had greater leaf areas. Based on this finding, it can be hypothesize that the number of trichomes does not scale with the area, but is fixed; so as leaf area increases, trichome density decreases. Having a lower trichome density should decrease the ability of a plant to defend against herbivores. This was evidenced by a correlation in the results from the herbivory trials: plants with lower trichome densities experienced higher rates of herbivory ($R^2 = 0.7246$). One possible explanation for this is that when trichomes are less dense, snails get pricked less often and are not as discouraged to continue eating. However, it is also possible that if the leaves were also more appetizing due to increased nitrogen, the rates of herbivory could have been faster regardless of trichome density. For a definitive correlation, a test could be conducted in which trichomes were removed from leaves in one group of plants while the concentration of nitrogen was held constant between this group and a control group. In conclusion, it is evidenced that nitrogen-rich plants have weaker herbivory defense mechanisms and greater food appeal, thus their palatability should be greater.

Nitrogen-rich and drought-stressed leaves were expected to be more palatable and to have higher rates of herbivory. Our prediction was correct; both nitrogen-rich leaves and drought- stressed leaves had significantly higher rates of herbivory than the control which had a rate of herbivory of zero. This suggests that in the future, when drought and nitrogen is more prevalent, plants will face greater levels of herbivory. Furthermore, nitrogen-rich leaves had significantly higher rates of herbivory than the drought-stressed leaves. Therefore the most effective way to prevent herbivory levels from increasing may be to prevent natural plant assemblages from receiving too much nitrogen. The upper limit of nitrogen levels which is considered damaging for a plant may be considerably lower than the level where effects of over-nitrification are directly damaging. At high levels where plants still appear healthy they can be indirectly more prone to damage due to higher rates of herbivory.

The major difficulty in this experiment was compelling the snails to eat. Even though they were starved and experiments were performed at night, just over 30% of the snails ate leaves. This introduced greater possibility of error and produced a lower significance in the data. It is recommend that future experiments eliminate the possibility of no herbivory occurring by extending the time in which herbivory has the opportunity to occur. Instead of ten minutes with a leaf, a snail could be contained with an entire living plant for a whole night. Moreover, to address the issue of alleles not coding for cyanogenic glycosides, the experiment could be extended over generations of radishes. The plants could be grown on plots of land, each with a contained population of snails that was allowed to freely feed. Over time, the consistent pressure of herbivory should select for radishes with strong cyanogenic glycoside defenses and different results may be observed.

Another issue that arose was that all of our plants appeared to have been watered on one day when they weren't supposed to be. This occurred between gathering the leaf data and the herbivory trials. Therefore, if this event was significant, there may have been a difference in the rate of herbivory of the drought-stressed and combined-conditions leaves.

It would be interesting to change the direction of this research. It is possible that plants may be able to handle the tradeoff of higher rates of herbivory for

more nitrogen; they may even grow better in higher nitrogen conditions, despite the herbivory. This is important to find out. However, there must be some level where the tradeoff is no longer beneficial. The level of nitrogen that acts as the threshold between benign and damaging rates of herbivory could be experimentally determined. Those results could be applied by environmental agencies to regulate the amount of nitrogen input into the environment by farmers and nitrogen oxide polluters. This could prevent herbivory not only in wild plant assemblages, but crops as well, perhaps reducing the need for pesticides.

Unfortunately, there seems to be potential for a severe snowball effect due to the warming of Earth's climate and increased levels of nitrogen in its soils. These changes can affect herbivory in many ways other than leaf palatability. As the temperature increases, insects may expand their ranges, affecting more plant species in greater numbers (Backhaus, 2014). Higher temperatures can increase the metabolic rate of insects, also resulting in higher rates of herbivory (Lemoine, 2014). In addition, some insects that use plants as a water source will be required to consume more plant biomass only to obtain the same amount of water since the concentration of water was found to be lower in drought-stressed leaves. It was already mentioned that drought can stress plants and free up the available nitrogen in tissues, but high temperatures and herbivory, itself can stress plants as well. Once the nitrogen is readily available, it not only makes leaves more appetizing, but their increased nutritional content also increases the fitness of insect populations that feed on them. This increases the number of insects, increasing the rate of herbivory (White, 1984). Furthermore, herbivory adds nitrogen to the soil. As insect populations feed, they increase the rate of leaf deposition into the leaf litter, they add their excrement and carcasses into the leaf litter, and they speed up the decomposition rate of the leaf litter (Belovsky, 2000). As a result, the plant populations may absorb higher concentrations of nitrogen. If environmental conditions continue to change as they have been, all of these results will be multiplied, and any single effect can act as a feedback loop for any of the other effects. Humans are constructing this dangerous system that may threaten countless plant species. Therefore it is important to prevent these changes before they cannot be undone.

Acknowledgements

I thank Britney Brown, my partner, for helping conduct this research. I thank Edward Read, the CSUF greenhouse manager, for letting us use his facilities and supplying equipment. I thank Dr. Abraham, my professor, and Jarret Jones, my classmate, for reviewing this paper. Lastly, I thank the CSUF Department of Biological Science for providing funding for this work.

References

Agrawal, A. (1998). Induced Responses to Herbivory and Increased Plant Performance. *Science*, 279, 1201-1202.

Backhaus, S., Wiehl, D., Beierkuhnlein, C., Jentsch, A., & Wellstein, C. (2014). Warming and drought do not influence the palatability of *Quercus pubescens* Willd. leaves of four European provenances. *Arthropod-Plant Interactions*, 8, 329-337.

Belovsky, G., & Slade, J. (2000). Insect herbivory accelerates nutrient cycling and increases plant production. *Proceedings of the National Academy of Sciences*, 97(26), 14412-14417.

Blue, J., Souza, L., Classen, A., Schweitzer, J., & Sanders, N. (2011). The variable effects of soil nitrogen availability and insect herbivory on aboveground and belowground plant biomass in an old-field ecosystem. *Oecologia*, 167, 771-780.

Dekle, G., & Fasulo, T. (2001). Brown Garden Snail, Cornu aspersum (Müller, 1774) (Gastropoda: Helicidae). *UF IFAS Extension*, 1-4.

Fenn, M., Baron, J., Allen, E., Rueth, H., Nydick, K., Geiser, L., ... Neitlich, P. (2003). Ecological Effects of Nitrogen Deposition in the Western United States. *Bioscience*, 53(4), 404-420.

Follett, R. (1995, September). Fate and Transport of Nutrients: Nitrogen. Working Paper No. 7, USDA, Agricultural Research Service, Soil-Plant Nutrient Research Unit.

Freeman, B.C. and G.A. Beattie. (2008). An Overview of Plant Defenses against Pathogens and Herbivores. *The Plant Health Instructor*.

Gleadow, R., & Møller, B. (2014). Cyanogenic Glycosides: Synthesis, Physiology, and Phenotypic Plasticity. *Annual Review of Plant Biology*, 65, 155-185.

Griffiths, J., & Bonser, S. (2013). Is Sex Advantageous in Adverse Environments? A Test of the Abandon-Ship Hypothesis. *The American Naturalist*, 182(6), 718-725.

Henslow, G. (1898). The History of the Radish. *Gardeners Chronicle*. 23, 389.

Hunt, E., Doraiswamy, P., Mcmurtrey, J., Daughtry, C., Perry, E., & Akhmedov, B. (2012). A visible band index for remote sensing leaf chlorophyll content at the canopy scale. *International Journal of Applied Earth Observation and Geoinformation*, 21, 103- 112.

IARC. (2004). Cruciferous Vegetables, Isothiocyanates and Indoles. IARC Handbook of Cancer Prevention, 9.

Lemoine NP, DrewsWA, Burkepile DE, Parker JD. (2013). Increased temperature alters feeding behavior of a generalist herbivore. *Oikos* 122:1669–1678

Lemoine, N., Burkepile, D., & Parker, J. (2014). Variable effects of temperature on insect herbivory. *PeerJ*, 1-18.

Møller, B. (2010). Functional diversifications of cyanogenic glucosides. *Current Opinion in Plant Biology*, 338-347.

Ready, B. (1982). Garden Companions and Enemies. *Earthwood*.

Seaman, A. (2013). "Turnips and Radishes". *Integrated crop and pest management guidelines for commercial vegetable production*. Cornell Cooperative Extension. Retrieved Feb. 16, 2016.

Union of Concerned Scientists. (2011). Extreme Dry. Retrieved May 14, 2015.

White, T. (1984). The Abundance Of Invertebrate Herbivores In Relation To The Availability Of Nitrogen In Stressed Food Plants. *Oecologia*, 63, 90-105.

Structure-Function Studies of *Deinococcus radiodurans* ADP Glucose Pyrophosphorylase: Role of Ser48 in Allosteric Regulation*

Ashley Le-Pham, Jeries Qoborsi, Leo Ong, Dr. Andrew Orry and Dr. Christopher R. Meyer

Department of Chemistry and Biochemistry, California State University, Fullerton

Abstract

Adenosine Diphosphate Glucose Pyrophosphorylase (ADPG PPase) is an allosterically regulated enzyme that functions as the rate-limiting step of starch synthesis in plants and glycogen synthesis in bacteria. Because starch is a source of renewable and biodegradable carbon, ADPG PPase is an attractive target for protein engineering to increase biomass yield in crops. The microbial versions of this enzyme are quite diverse in their regulatory and physical properties; some of these properties would be useful to incorporate into transgenic crops to enhance starch production. While a number of ADPG PPases have been kinetically characterized, there is only one published x-ray structure (PDB 3BRK) of an inhibited form. Very little is known about the enzyme from *Deinococcus radiodurans* (*D. rad*), an extremophile that is resistant to ionizing radiation and harsh growth conditions. When comparing the amino acid sequence of this enzyme to other characterized ADPG PPases, it was noted that position 48 differed with a serine substituted for alanine in a region known to be important for allostery. To probe the role of Ser-48, the S48A enzyme was generated by site-directed mutagenesis and the recombinant altered *D. rad* ADPG PPases were successfully expressed in *E. coli* and purified via a scheme that includes anion exchange chromatography, size exclusion chromatography, and affinity chromatography. Initial studies on the S48A enzyme in the absence of activators have shown a dramatic 20-fold increase in the apparent affinity for the substrate ATP, a 3-fold increase in apparent affinity for the cofactor magnesium, and a 4-fold increase in V_{max} compared to wild-type. Interestingly, in the presence of the activator fructose 1,6- bisphosphate (FBP) there was little change in the apparent binding affinity for substrates or V_{max} compared to WT which displays a 14-fold increase in V_{max} and 12-fold and 3-fold increase in apparent affinity for ATP and magnesium, respectively. Similarly, in the presence of fructose-6-phosphate (F6P), there were not a very large increase in V_{max} or higher apparent affinity for ATP for the S48A enzyme, but there was a 9-fold difference in V_{max} and a 12-fold and 2-fold increase in apparent binding affinity for ATP and magnesium for WT, respectively. The WT enzyme also displayed higher apparent affinity for FBP and F6P compared to the S48A enzyme. The alanine substitution appears to result in an enzyme form that is partially activated but relatively insensitive to activators. Further kinetic characterization of S48A in the presence of sulfate and the inhibitor phosphate is in progress. With respect to physical characterization, two crystallization conditions for S48A, one including imidazole and the other with lithium sulfate and PEG, were found to yield preliminary results. Further crystallization trials are in progress as a first step in elucidating the three-dimensional structure.

**Supported in part by NSF and NSF BIO MCB grant #0448676*

Analysis Of The Predicted Strong Isomer Dependence Of Phenols When Reacted With Nitrogen Dioxide To Produce Nitrous Acid

Salim Soubra
Advisor: Dr. Scott Arthur Hewitt

Department of Chemistry and Biochemistry, California State University, Fullerton

Abstract

Humic acid is a complex mixture in soil, composed of long-chain hydrocarbons with carboxyl and phenolic groups. Simple phenolic compounds can be used as model compounds to study the reaction of nitrogen dioxide with humic acid. Computational work from Dr. Tao's research group predicts that these reactions lead to the formation of HONO, a precursor of the very important atmospheric oxidizer, the OH radical. Nitrogen dioxide was reacted with phenol and isomers of methoxyphenol. Under consistent parameters and in a glass reaction cell, the following was performed in order to compare rate constants between the varying isomers. Samples from the reaction cell were removed using solid-phase micro extraction. The phenolic reactants and products were monitored by GC/MS analysis. The experimental results indicated that the rate of reaction with NO2 increased from phenol, to 2-methoxyphenol (ortho), to 3-methoxyphenol (meta), and then to 4-methoxyphenol (para). This contradicts Dr. Tao's research group's prediction, that the activation energies of the NO2 reactions with 2-methoxyphenol and 4-methoxyphenol are much lower than those with phenol and 3-methoxyphenol. Their calculations assumed that it is a gas-phase reaction. Reasons for the discrepancies are discussed.

Introduction

The Earth's ground is known to contain humic matter as the most abundant organic species.[1] This matter is created from the biodegradation of organic compounds by microorganisms within the soil to produce macromolecules, providing nutrients to plants. Humic acid consists of interconnected aromatic rings containing phenolic and carboxylic substituents, among other side chains that include carbon, hydrogen, nitrogen, and oxygen atoms. Humic matter is composed of highly complex macromolecules in soil, containing multiple fragments with various rings of different degree of substitution, resulting in its chemistry not being fully characterized.[2] Overall, the different types of individual humic substances found in nature contain a great amount of similarity with each other. They are derived from plant-based lignin and generally composed of phenolic moieties with hydrocarbon, hydroxyl, carboxyl, and amino side chains, as shown in Figure 1 below.[2]

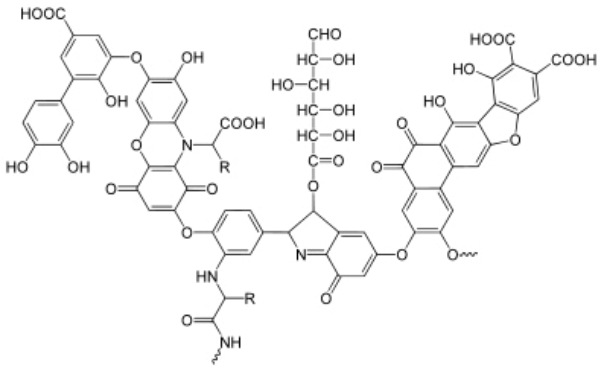

Figure 1: *Generic humic acid structure including the major substituents.*

In this research, our main focus is to study the production of the air pollutants in the troposphere, the lower atmosphere region. Many of the pollutants emitted from the atmosphere become reactive in the presence of the light, which then reacts with other gases in the air

and produces harmful chemicals to the environment. For example, nitrogen dioxide undergoes photodissociation in the presence of light, producing NO and an oxygen atom,[3] which then reacts with the molecular oxygen in the air to produce tropospheric ozone. However, ozone can react with the NO to produce NO_2 and O_2, and this regeneration cycle continues to produce nitrogen dioxide and ozone in the atmosphere.[4]

$$NO_2 + h\nu \rightarrow NO + O \quad (1)$$
$$O + O_2 \rightarrow O_3 \text{ (ozone)} \quad (2)$$
$$NO + O_3 \rightarrow NO_2 + O_2 \quad (3)$$

Typically, the NO_2 is not the only molecule that plays a big role in the creation of the air pollution, the volatile organic compounds (VOCs) released in the atmosphere are also a big source of the air pollution. NO_2, VOCs, and sunlight all interact to form tropospheric ozone and other toxic species that not only affects human health, but damages crop productions.[5] NO is formed through emissions of internal combustion engines. Stemmler et al. (2006) reported that "soil and other surfaces containing humic acid exhibit an organic surface photochemistry, producing reductive surface species, which then reacts with nitrogen dioxide to produce nitrous acid (HONO)".[3]

During the daytime, the sunlight photolysis of HONO produces hydroxyl (OH) radicals. These OH radicals play a big part in the daytime chemistry of both polluted and clean atmospheres. The HONO photolysis reaction is shown as follows:[14]

$$HONO + h\nu \rightarrow OH + NO \quad (4)$$

The removal processes of many species in the atmosphere are initiated by reactions with the hydroxyl radical, followed by the succeeding oxidation reactions. These oxidation processes are important for many atmospheric phenomena such as photochemical smog and particle formation. It all begins with the OH radical, which is the most important oxidizing species in the daytime atmosphere. The OH radical is considered to be the 'detergent' of the atmosphere, because it primarily participates in the removal of natural and manmade sources of pollutant compounds.[7]

Humic acid-like surfaces have been reacted with NO_2.[8] Giving the assumption that the surface irradiates with substituted aromatic compounds, producing HONO. Possibly explaining the daytime source of HONO. Su et al. stated that in the soil nitrite can be formed by microorganisms and that it can then react with water to produce HONO, while not necessarily needing organic species.[9]

HONO is considered to be a key player for OH. Its photolysis is fastest in the early daylight hours.[10] During the daytime, HONO concentrations are lower since it is in the stationary state, meaning there is no net production as it is rapidly photolyzed right after it is formed. It is estimated that 20% of the integrated OH concentration is formed from photolysis of HONO immediately after sunrise when compared to other sources such as formaldehyde and VOCs.[11] However, it can also react to produce more ozone or other secondary pollutants, such as nitric acid and peroxyacyl nitrate. Since the discovery of HONO more than three decades ago, its sources have yet to be determined.[12]

The importance of understanding where HONO comes from is beneficial in terms of reducing air pollution, because the production of hydroxyl radical can lead to more nitrogen dioxide production and increase the ozone concentration in the troposphere. If the reactions of HONO are fully understood and all the major pathways that contribute to its nighttime and daytime concentrations are known, then it may be possible to diminish OH production in the early morning by at least 20%.

Dr. Tao's research group assumed that HONO might be formed from the gas- phase reaction of NO_2 with phenols, acting as the humic substance. The theoretical results of Dr. Tao's group take into assumption that phenol reacts with nitrogen dioxide to form nitrous acid (HONO), shown in the equation below:[14]

$$C_6H_5OH + .NO_2 \rightarrow C_6H_5O. + HONO \quad (5)$$

Then, through the HONO photolysis reaction (Equation 4), nitrous acid (HONO) could form OH radicals. Dr. Tao's research group performed computational analyses on the reaction of nitrogen dioxide with varying substituted phenols to produce HONO. Dr. Tao's group's computational results are displayed in figure 2 (below).

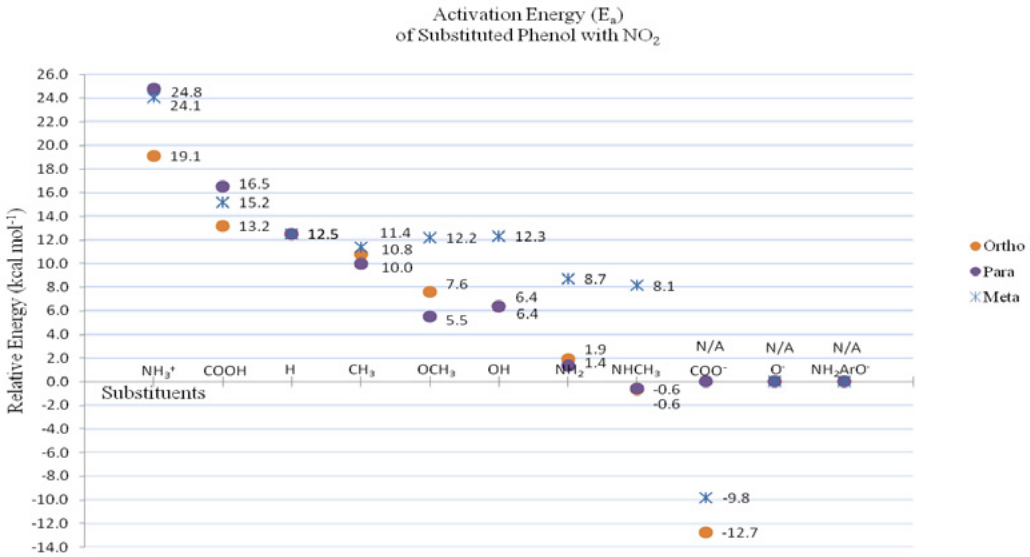

Figure 2: *Dr. Tao's predicted activation energies for various substituted phenols.*

The attention should be focused on the activation energies of phenol and the three methoxyphenol isomers (Figure 2) for the particular study. Phenol and *meta*- methoxyphenol have the highest activation energies, followed by *ortho*-methoxyphenol, then by *para*-methoxyphenol. Higher activation energies indicate that it takes more energy to pass over the threshold for the reaction to occur. Therefore, the larger the activation energy, the more time it will take to pass that threshold, resulting in a slower rate of reaction.

Dr. Hewitt's previous lab group studied if NO_2 reacts with phenols or mesitylene. The results indicated that a reaction was observed for both compounds, separately reacting with NO_2. In addition, the lab group attempted to research if HONO was produced from the reaction of NO_2 with phenol. After Fourier Transform Infrared Spectrometer (FTIR) and Ultraviolet Visible Spectrometer (UV-VIS) analysis, no HONO peaks were observed in the assumed wavelength range. However, Dr. Hewitt's previous lab group concluded that a reaction involving NO_2 and phenol does occur.

For the following research, phenols with varying locations of methoxy groups were used as model soil compounds (humic substance) to see how readily they react with nitrogen dioxide in a controlled atmosphere. The phenolic compounds used were: phenol, *meta*-methoxyphenol, *ortho*-methoxyphenol, and *para*-methoxyphenol. The structure of these compounds are displayed in figures 3a-3d. The research goal is to study the reaction of nitrogen dioxide with varying isomers of methoxyphenol to better understand the rates of reaction with humic acid. The rate of reaction is the rate at which the reactants are transformed into the products of the reaction. Since nitrogen dioxide and phenols react as soon as they are mixed together, the phenol reactant and products are analyzed after a 5-minute reaction time. The percent reaction obtained was then compared to the computational activation energy results from Dr. Tao's research group.

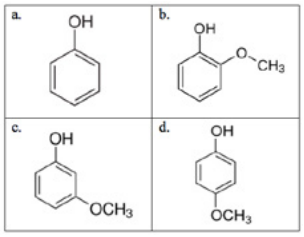

Figures 3a-3d:
The molecular structures of the phenolic compounds that will be reacted with NO_2 in the study.
a) phenol.
b) 2-methoxyphenol (ortho),
c) 3-methoxyphenol (meta),
d) 4-methoxyphenol (para)

Analysis will be performed using Gas Chromatography/Mass Spectrometry (GC/MS) techniques. Gas chromatography is one of the most popular techniques in industry. GC/MS analysis requires small samples with minimal preparation and is efficient at separating complex mixtures into individual components. It has low detection limits (minimum detection concentration), fast rate, high resolution, accuracy and reproducibility.[13] This technique is usually used for analyzing samples that have high volatility and a low molecular weight, such as phenolic groups, making GC/MS the preferred technique for the following research. The sample is inserted in the inlet where it is immediately vaporized, then pressurized by an inert carrier gas. The carrier gas – Helium – is continually flowing from a gas regulator through the injector and into the GC column. The flowing gas "carries" the vaporized sample in the column. The gaseous or liquid analyte is eluted through a column by a mobile phase over a stationary phase on the inside of the column. The mobile phase is the solvent passing through the column that is either a gas or liquid. The stationary phase is dependent on polarity in which it remains in place inside the column.

Different compounds elute at different retention times due to the varying interactions each compound undergoes with the stationary phase. The stronger the interaction between the sample and stationary phase, the longer it will take for the sample to flow through the column. The same is true for the reverse situation. Therefore, a non-polar column will take longer to elute a non-polar sample, due to the strong interactions with substances with same polarities. On the other hand, a polar sample will elute much faster out of the non-polar column, due to weaker or no interactions between polar and non- polar substances.

It is important that the column is heated enough to provide enough vapor pressure for analytes to be eluted. The process launches at a low temperature to determine the low boiling point mixtures and then increases to resolve the less volatile, high boiling point elements throughout the separation in a method known as temperature programming. The separated analytes move through a detector that is sustained at a higher temperature than the column to ensure that all analytes are gaseous.

Experimental

Nitrogen dioxide was reacted with varying phenolic compounds in a 2.0 L reaction cell. With the final pressure in the reaction cell being a consistent 14 Torr throughout the study. Samples were removed using a solid phase micro extraction (SPME) fiber, and then injected into the GC/MS for further analysis. The resulting chromatograms were reviewed to determine the percent products formed compared to the remaining percent of reactants. By knowing the percent of products formed for each isomer, one can determine the relative rates of reaction.

Conditions

Experiments were conducted in a 2.0 L reaction cell at 25°C and 15 Torr. In a previous study, it was difficult to approximate how much phenol actually went into the reaction cell, since it was being pushed into the cell by Ultra-pure N_2. Due to the fact that a couple of the methoxyphenols were light sensitive, the reaction cell was completely wrapped in black electrical tape and reactions were run in a dimly lit room. A consistent amount of 10 mTorr for each isomer was put in the reaction cell during each separate experiment. All individual vapor pressures of phenol, *ortho-*, *meta-*, and *para-* methoxyphenol were measured. 10 mTorr was suggested as a reasonable pressure to use, since the phenolic compound with the lowest vapor pressure was 4-methoxyphenol at ~12 mTorr. While the vapor pressure for phenol was ~400 mTorr, 2-methoxyphenol had a vapor pressure of ~500 mTorr, and 3-methoxyphenol had a vapor pressure of ~30 mTorr.

Also, each experiment involved putting 28.5 Torr of the NO_2/O_2 gas mixture, from the attached bulb, into the reaction cell. The final pressure in the reaction cell was 14.8 Torr of the NO2/O2 gas mixture. The gas mixture in the bulb is Nitrogen Dioxide and Oxygen at a ratio of [1:79], respectively. Therefore, 14.8 Torr of the NO_2/O_2 gas mixture is equivalent to having 185 mTorr of NO_2. All conditions and parameters were consistent and equal throughout the study. The final pressure of the NO_2/O_2 mixture in the reaction cell was 14.8 Torr, it was previously determined to be enough for the reaction to occur. However, if the pressure were to be brought up to sea level (760 Torr), it would take a good amount of time to reach that point. By that time the reaction between NO_2 and the phenolic compound may have already begun, which may cause inaccurate results.

Sampling

Samples were removed from the reaction cell using a solid phase micro extraction (SPME) fiber (SUPELCO 100 μm PDMS). A delay time of 5.0 minutes was given to each experiment, allowing the same amount of time for reaction to occur in the reaction cell for each individual experiment. The SPME fiber was inserted into the reaction cell through a septum, and allowed to adsorb the gases for 2.0 minutes. Then, the SPME fiber with the absorbed sample was injected into the gas chromatograph (Agilent Technologies 6890N Network GC System) that was running the PRODUCT STUDIES (SOIL-2) method. The fiber was left in the GC inlet for 30 seconds, each time, to allow all adsorbed gases to be heated and released through the GC column. All samples were analyzed by the mass spectrometer (Agilent 5973 inert Mass Selective Detector) attached to the GC.

Product Studies Method: (Soil-2)

Product studies (soil-2) GC/MS parameters include an overall time of 18.02 minutes, an inlet temperature of 260°C and detector temperature of 280°C. An Agilent DB-5 GC Column was used. With a length of 60 meters and an inner diameter of 0.250 mm lined with a film 0.10 μm thick. Thin film columns are used to minimize the retention of high boiling and high molecular weight solutes. Also, thin film columns are less inert and have lower capacities. The film inside the column is known as the stationary phase. The DB-5 column is non-polar consisting of a film made of (5%-Phenyl)-methylpolysiloxane. Different compounds interact differently with the stationary phase. The stronger the interaction between the sample and stationary phase, the longer it will take for the sample to flow through the column. The same is true for the opposite. Therefore, a non-polar column will take longer to elute a non-polar sample, due to the strong interactions with substances with same polarities. On the other hand, a polar sample will elute much faster out of the non-polar column, due to weaker interactions between polar and non-polar substances.

The oven temperature is divided into three ramps: 1, 2, and 3. The oven temperature initially reaches 100°C and has a hold time and run time of 2 minutes each. Ramp 1 increases the oven temperature at a rate of 40 °C/min until it reaches 111 °C, remaining at this temperature for an additional 0.50 s. Overall, level one lasts about 2.78 minutes. The Ramp 2 increases the oven temperature at 2 °C/min until it reaches 130 °C, immediately followed by Ramp 3. Overall, Ramp 2 lasts for approximately 12.28 minutes. The Ramp 3 increases the oven temperature at 40 °C/min until it reaches 200 °C, remaining at that temperature for an additional 4 minutes.

Chemicals and Glass Line

The reactants used in the air-soil experiments were: phenol (Sigma-Aldrich, 99%), 2-methoxyphenol (Sigma-Aldrich, 99%), 3-methoxyphenol (Sigma-Aldrich, 99%), and 4-methoxyphenol (Sigma-Aldrich, 99%). The gas in the bulb was made by mixing 9 Torr of compressed Nitrogen Oxide (PRAXAIR, CAS: 10102-43-9) and 715 Torr of excess compressed Oxygen (Oxygen Service Co., CAS: 7782-44-7). The resulting gas mixture in the bulb was Nitrogen Dioxide and Oxygen at a ratio of [1:79], respectively.

A glass vacuum line is used to prepare the nitrogen dioxide bulb and the reactions in the reaction cell. The phenolic compounds are kept in a U-tube completely wrapped in black electrical tape. The tape keeps light from getting to the phenolic compounds, since two of the methoxyphenols are known to be light sensitive. The placement of the U-tube is directly next to the reaction cell, giving the phenolic compounds a much shorter distance to travel until reaching the reaction cell. This is important since phenol and the methoxyphenols are fairly adhesive substances. Pressure is measured using a capacitance manometer (MKS Instruments Inc., Model 122BA), for pressures above 300 mTorr, and a thermocouple gauge (Duniway stockroom corp., DST-531), for making sure the vacuum pumps were working and that there were no leaks. The glass line was evacuated using a diffusion pump, and a duo-seal rough pump (Welch, model 1400).

Procedure

A glass vacuum line was set up with a reaction cell and U-tube line consisting of the varying phenolic compound that will be analyzed (phenol, 2-, 3-, or 4- methoxyphenol). Both knobs at the ends of the U-line were closed off. The entire vacuum line was

pumped down. The glass line to vacuum was then closed off. The U-line was opened, bringing 10 mTorr of phenolic vapor from the U-tube to the reaction cell. The reaction cell containing ~10 mTorr of phenol vapor was closed. Again, the glass line was pumped down by vacuum. The glass line to vacuum was closed off. The NO_2/O_2 bulb was opened to the glass line, and then closed off when the pressure inside of the glass line reached 28 Torr. The total amount of NO2 can be calculated according to the ratio of the gas mixture, $1(NO_2) : 79(O_2)$. The gas mixture at a pressure reading of 28 Torr is calculated to contain 350 mTorr of nitrogen dioxide. The glass line to vacuum was closed. Reaction cell to the glass line was opened to mix phenolic vapor and NO_2, total pressure was 14 Torr. The reaction cell (~14 Torr) was closed off. Allowing a 5-minute delay time for the reaction to proceed. Then a SPME fiber was injected into the reaction cell for 2 minutes to absorb molecules. Finally, the SPME fiber was transferred from the reaction cell to be injected in the GC/MS for analysis.

Results

In this research, the relative rates of reaction of nitrogen dioxide with varying phenolic compounds were studied using gas chromatography mass spectrometry (GC/MS) method. The result section shows the gas chromatograms for each different experiment/isomer collected during the research. The first section discusses the obtained results of phenol, *ortho-*, *meta-*, and *para-* methoxyphenol when reacted with nitrogen dioxide. The second section tabulates the results of the percent reactants and products that were present when each experiment was performed. The concluding results were then compared with the theory predicted by Dr. Tao's research group. Experimental chromatograms are on the next page.

Gas Chromatograms

Figure 4 (below) show an example of a gas chromatogram of ion abundance vs. retention time for the nitrogen dioxide reaction with phenol. The peak of reactant, phenol, can be seen at 5.165 min. and the peaks of the products, 2-nitrophenol and 4-nitrophenol, can be seen around 7.213 min and 15.799 min.

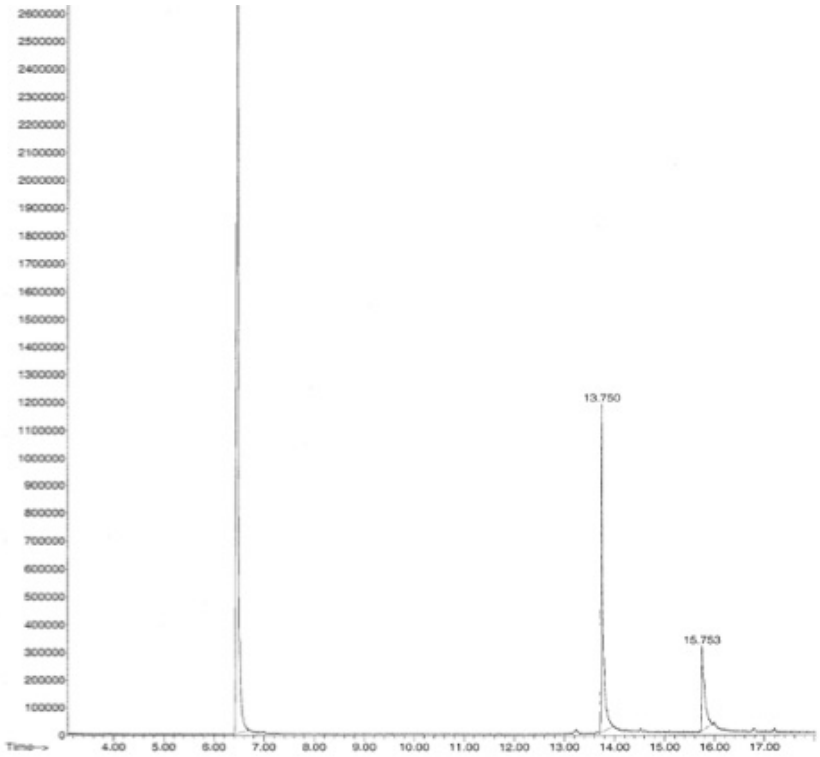

Figure 4. *GC/MS chromatogram of ion abundance vs. retention time for nitrogen dioxide when reacted with phenol.*

Figure 5 (below) shows an example gas chromatogram of ion abundance vs. retention time for the nitrogen dioxide reaction with 2-methoxyphenol. The peak of reactant, 2-methoxyphenol, can be seen around 6.470 min. and the peaks of the products, 3-hydroxy-4-methoxynitrobenzene and 4-nitroquaiacol, can be seen around 13.747 min and 15.732 min.

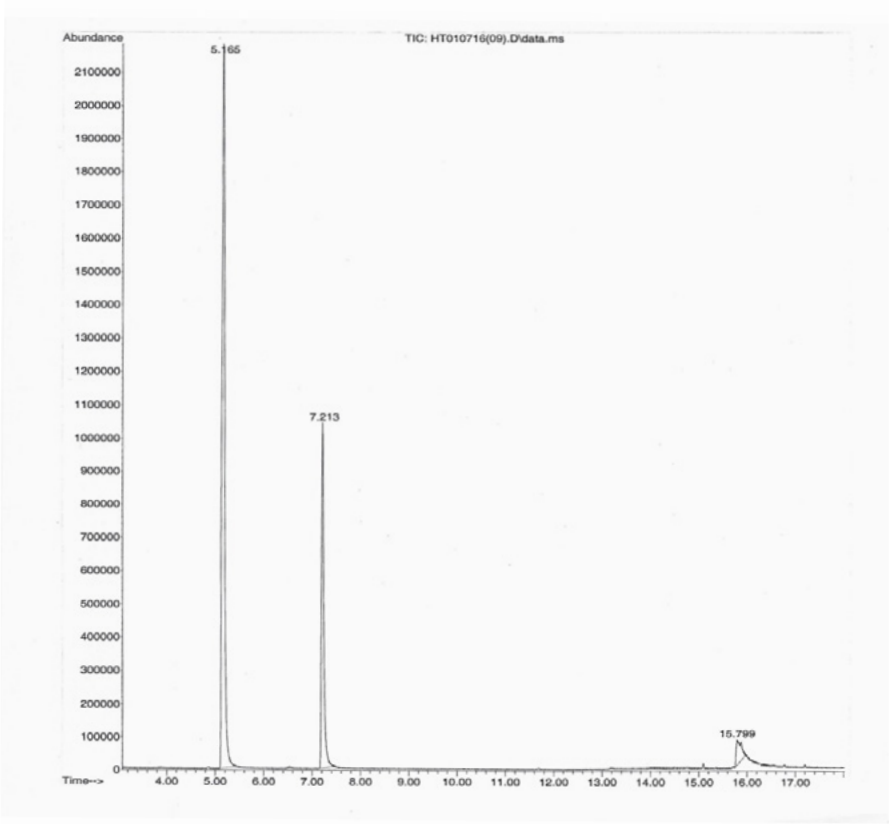

Figure 5. *GC/MS chromatogram of ion abundance vs. retention time for nitrogen dioxide when reacted with 2-methoxyphenol.*

Figure 6 (below) shows an e xample gas chromatogram of ion abundance vs. retention time for the nitrogen dioxide reaction with 3-methoxyphenol. The peak of reactant, 3-methoxyphenol, can be seen around 8.919 min. and the peaks of the combined products, 4-Nitroguaiacol, Hexamethyl benzene, and 4-methoxy-2-nitrophenol, can be seen around 13.975 min., 14.222 min., and 14.439 min.

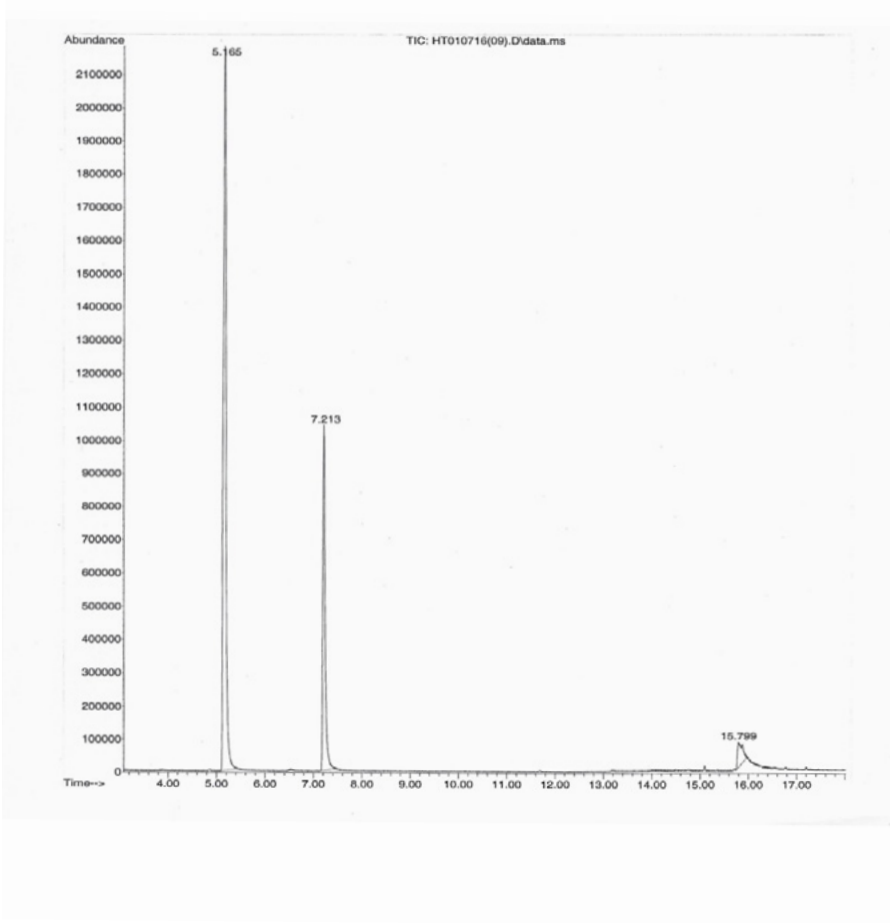

Figure 6. *GC/MS chromatogram of ion abundance vs. retention time for nitrogen dioxide when reacted with 3-methoxyphenol.*

Figure 7 (below) shows an example gas chromatogram of ion abundance vs. retention time for the nitrogen dioxide reaction with 4-methoxyphenol. The peak of reactant, 4-methoxyphenol, can be seen around 7.694 min. and the peaks of the products, 4-Nitroguaiacol and 4-methoxy-2-nitrophenol, can be seen around 13.027 min and 14.715 min.

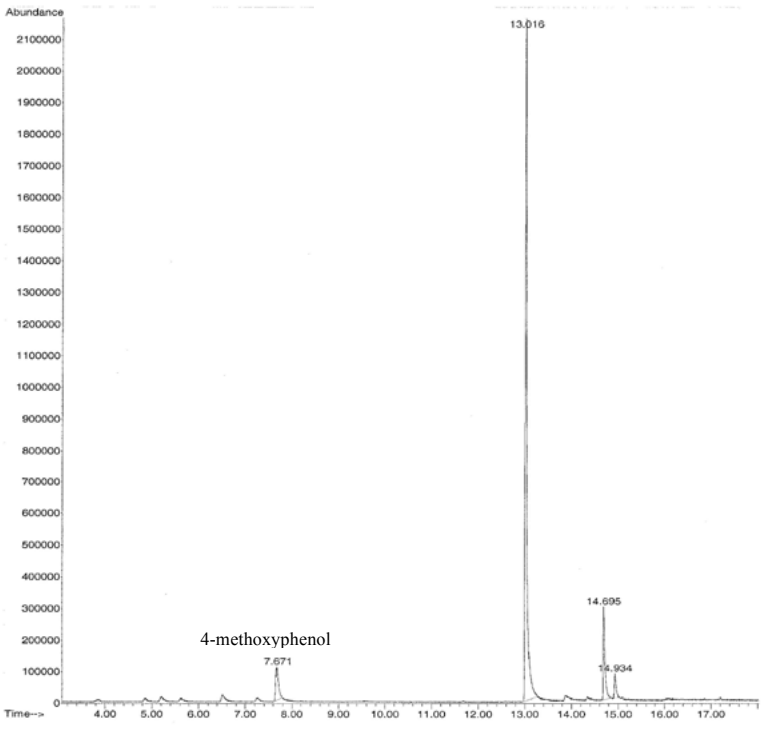

Figure 7. *GC/MS chromatogram of ion abundance vs. retention time for nitrogen dioxide when reacted with 4-methoxyphenol.*

Data Tables

In this research, the relative rates of reaction of nitrogen dioxide with varying phenolic compounds were studied using gas chromatography mass spectrometry (GC/MS) method. The result section shows the gas chromatograms for each different experiment/isomer collected during the research. The first section discusses the obtained results of phenol, *ortho*-, *meta*-, and *para*-methoxyphenol when reacted with nitrogen dioxide. The second section tabulates the results of the percent reactants and products that were present when each experiment was performed. The concluding results were then compared with the theory predicted by Dr. Tao's research group. Experimental chromatograms are on the next page.

Compound reacting with Nitrogen Dioxide	Reactant (%)	Product (%)
Phenol	69.1 ± 2.6	30.9 ± 2.6
2-methoxyphenol (*ortho*-)	65.7 ± 1.9	34.3 ± 1.9
3-methoxyphenol (*meta*-)	32.8 ± 4.3	67.2 ± 4.3
4-methoxyphenol (*para*-)	7.8 ± 2.2	92.2 ± 2.2

Table 1: *Shows the average percent of reactant and products present after the 5 minute reaction involving NO_2 and the varying phenolic compounds.*

Isomers	Reactant Lost (molecule/cm^3)	Rate Constant, k (cm^3/molecule•s)
Phenol	1.00 x 10^{14}	7.59 x 10^{-20}
2-methoxyphenol (*ortho*-)	1.10 x 10^{14}	8.34 x 10^{-20}
3-methoxyphenol (*meta*-)	2.17 x 10^{14}	16.42 x 10^{-20}
4-methoxyphenol (*para*-)	2.98 x 10^{14}	22.54 x 10^{-20}

Table 2: *Lists the calculated amount of reactant lost and the rate constant for the reactions of the varying phenolic compounds with NO_2.*

Calculations for Table 2 (above):

$$\frac{[\textit{Phenolic Isomer lost}]}{360 \text{ seconds}} = \textit{Rate} = k \cdot [\textit{Phenolic Reactant}] \cdot [\textit{Nitrogen Dioxide}]$$

Isomers:	Phenol ≤ 3-methoxyphenol << 2-methoxyphenol << 4-methoxyphenol
Experimental:	Phenol ≤ 2-methoxyphenol << 3-methoxyphenol << 4-methoxyphenol

Table 3: *Dr. Tao's predicted computational results vs. the experimental results obtained in this study.*

Discussion

The chromatograms obtained were of samples taken under the same parameters and same reaction time interval. The reaction involving phenol and NO_2 produced 2-nitrophenol and 4-nitrophenol as products. The second reaction involving 2-methoxyphenol reacting with NO_2 produced 3-hydroxy-4-methoxynitrobenzene and 4-nitroquaiacol as products. The third reaction involving 3-methoxyphenol reacting with NO_2 produced 4-nitroguaiacol, Hexamethyl benzene (may not be in the headspace for methoxyphenol), and 4-methoxy-2-nitrophenol as products. The fourth reaction involving 4-methoxyphenol reacting with NO_2 produced 4-nitroguaiacol and 4-methoxy-2-nitrophenol as products.

In the chromatogram, a large relative peak of products is directly related to a larger percentage of products present at the end of reaction Therefore, a larger relative peak area of products, means the larger percentage of products present after reaction, formulating the determination of a faster reaction. The amount of products present at the end of the first reaction with phenol was 30.9% (± 2.6). The amount of products present at the end of the second reaction with 2-methoxyphenol was 34.3% (± 1.9). The amount of products present at the end of the third reaction with 3-methoxyphenol was 67.2% (± 4.3). The amount of products present at the end of the fourth reaction with 4-methoxyphenol was 92.2% (± 2.2).

The rate constant for each reaction was calculated, assuming that an elementary bimolecular reaction occurred, the rate constants were reported in (cm^3/molecules). The larger the rate constant, the faster a reaction will occur. Finally, after analysis of the following data, it was determined that the reaction of NO_2 with 4-methoxyphenol is about three times faster than that with phenol. The NO_2 reaction with 3-methoxyphenol is about twice as fast as that with phenol. The NO_2 reaction with 2-methoxyphenol is only about 10% faster than that with phenol.

However, Dr. Tao's research group provided results suggesting otherwise. Dr. Tao's research group computationally determined the activation energies when NO_2 reacts with the previously stated phenolic compounds. Their computational results agreed with the experimental results, such that, the fastest rate of reaction was that involving 4-methoxyphenol and NO_2, and the slowest rate of reaction was that involving

phenol and NO_2. However, their proposed predictions regarding 2-methoxyphenol and 3-methoxyphenol were not consistent with the experimental results. They predicted that the rate of reaction for 3-methoxyphenol is slower than that of 2-methoxyphenol, when reacted with NO_2. While the experimental results indicate that 2-methoxyphenol is slower than that of 3-methoxyphenol. Therefore, the only dissimilarity between the two groups' results is between the 2-methoxyphenol and 3-methoxyphenol.

As for the *para-* isomer (4-methoxyphenol), it has the fastest rate of reaction; this is similar to what Dr. Hewitt's previous lab research has observed for the reactions of chlorine atoms with Halotoluenes. It could be that we cannot detect all product peaks, which might throw off our calculated percent products. Also, it could be that the adsorption/desorption efficiencies, with the SPME fiber, for the different reactants and products are not the same. This would throw off the calculated percent products. Since the computational calculations for Dr. Tao's research group were performed under gas- phase reaction conditions. It may be assumed that instead of a gas-phase reaction occurring, it can be a heterogeneous reaction of water molecules occurring on the surface.

It is assumed that the reaction of phenolic compounds with nitrogen dioxide will form HONO. Then during the daytime, the sunlight photolysis of HONO produces hydroxyl (OH) radicals. These OH radicals play a big part in the daytime chemistry of both polluted and clean atmospheres. However, the lifetime of these phenolic compounds is fairly important. The lifetime is the time it takes a compound to drop to 1/e of its original concentration. This is important since the phenolic compound has to be present throughout the night reacting with NO_2, forming HONO, which later photolysis during the daytime from the sunlight. The lifetimes of phenol and 2-methoxyphenol were calculated to be around 992 hours and 903 hours, respectively, using the rate constants from the experimental results. The lifetimes of 3-methoxyphenol and 4-methoxyphenol were around 458 hours and 334 hours, respectively. Hence, there shouldn't be an issue with the phenolic compounds not being present during the nighttime, which is about 12 hours of no sunlight. Until the produced HONO undergoes photolysis early in the daytime, producing the OH radicals.

Conclusion

Humic acid is a complex mixture in soil, composed of long chain hydrocarbons with carboxyl and phenolic groups, was used as model compounds to study the reaction of nitrogen dioxide with humic acid. Computational work from Dr. Tao's research group predicted that these reactions lead to the formation of HONO, a precursor of the very important atmospheric oxidizer, the OH radical. Nitrogen dioxide was reacted with methoxyphenol isomers and phenol, under consistent parameters, in a glass reaction cell, followed by GC/MS analysis. The study established which reaction with nitrogen dioxide occurred the fastest for varying phenolic compounds, under consistent parameters.

The experimental results indicated that the reaction with NO_2 and 4-methoxyphenol is about three times faster than that with phenol. The NO_2 reaction with 3-methoxyphenol is about twice as fast as that with phenol. The NO_2 reaction with 2-methoxyphenol is only about 10% faster than that with phenol. This contradicts Dr. Tao's research groups' prediction, suggesting that the rate of the reaction with 3-methoxyphenol proceeds slower than 2-methoxyphenol.

Lastly, comparing our results to Dr. Tao's results assume that the pre-exponential factors are the same, however, this may not be the case. Their calculations were performed assuming that it was a gas-phase reaction. Nonetheless, it has been hypothesized that there may also be heterogeneous reactions of water molecules occurring on the surface. Future studies reacting NO_2 with isotopically substituted phenols and analyzing with FTIR; will provide the necessary information to test the hypothesis.

Future Studies

The following research should also be performed using Fourier Transform Infrared Spectroscopy (FTIR). Since the use of FTIR would allow the direct detection of the production of HONO in the reaction with NO_2. In addition, to ensure that the H in HONO comes from the hydrogen of the reactive specie, phenol. Rather than coming from the H_2O molecules on the surface. The future experiment would determine if a

heterogenous reaction occurs, rather than the assumed gas phase reaction. be involved in analyzing isotopically substituted C_6H_5O-D, instead of the phenolic compounds. Since it can be used to distinguish between the gas-phase NO_2 and C_6H_5O-D reaction (DONO product) and the heterogeneous NO_2 and H_2O reaction (HONO product) using FTIR.

I would like to thank Dr. Scott Hewitt for providing us the opportunity and his guidance for this research project. I would also like to acknowledge and thank Dr. Fu-Ming Tao for providing us with his theory behind this research project. I also want to thank California State University, Fullerton for the funding and the use of their facilities. Last but not least, I would like to greatly appreciate the members of Dr. Hewitt's laboratory; Billal Zayat and Abbas Sizar, for their countless assistance in the completion of this research project.

References

[1] Batjes, N. H. Total carbon and nitrogen in the soils of the world. *European Journal of Soil Science* 1996, *47*, 151-163.

[2] Wilson, E. Nitrous Acid From Sun And Soil. *Chem. Eng. News* 2006, *84*, 11.

[3] Stemmler, K. , Ammann, M. , Donders, C. , Kleffmann, J. , & George, C. (2006). Photosensitized reduction of nitrogen dioxide on humic acid as a source of nitrous acid. Nature, 440(7081), 195-198.

[4] Finlayson-Pitts, B., Pitts, J. (2000). Chemistry of the Upper and Lower Atmosphere: Theory, Experiments and Applications. San Diego, Calif.: Academic Press

[5] Logan, J. A. Tropospheric ozone: Seasonal behavior, trends, and anthropogenic influence. *Journal of Geophysical Research* 1985, *90*, 10463-10482.

[6] http://en.wikipedia.org/wiki/Humic_acid

[7] Crutzen, P. J. ; Zimmermann, P. H. The changing photochemistry of the troposphere. *Tellus B* 1991, *43*, 136-151.

[8] George, C. ; Strekowski, R. ; Kleffmann, J. ; Stemmler, K. ; Ammann, M. Photoenhanced uptake of gaseous NO2 on solid organic compounds: a photochemical source of HONO. *Faraday Discuss.* 2005, *130*, 195-210.

[9] Su, H. ; Cheng, Y. ; Oswald, R. ; Behrendt, T. ; Trebs, I. ; Meixner, F. X. ; Andreae, M. O. ; Cheng, P. ; Zhang, Y. ; Pöschl, U. Soil nitrite as a source of atmospheric HONO and OH radicals. *Science* 2011, *333*, 1616-1618.

[10] Winer, A. M. Air Pollution Chemistry," *in Handbook of Air Pollution Analysis (R. M. Harrison and R. Perry, Eds.), 2nd ed. Chap. 3*; Chapman and Hall, London, 1985.

[11] Alicke, B.; Geyer, A.; Hofzumahaus, A.; Holland, F.; Konrad, S.; Pätz, H.; Schäfer, J. ; Stutz, J. ; Volz-Thomas, A. ; Platt, U. OH formation by HONO photolysis during the BERLIOZ experiment. *J. Geophys. Res* 2003, *108*, 8247.

[12] Perner, D. ; Platt, U. Detection of nitrous acid in the atmosphere by differential optical absorption. *Geophysical Research Letters* 1979, *6*, 917-920.

[13] Berger, T. A. Chromatographia 1996, 42, 63-71.

[14] Tao, F. Shenghur, A.: Nitrous Acid formation by the reaction of Nitrogen Dioxide with organic molecules in the atmosphere: *A Quantum mechanical study*. A thesis presented to the faculty of California State University, Fullerton.

Examining the Geochemical Relationships Between the Twentynine Palms and Queen Mountain Plutons in Joshua Tree National Park

Alexander Arita and Lizzeth Flores
Advisor: Dr. Valbone Memeti

Department of Geological Sciences, California State University, Fullerton

Abstract

Plutonic studies increasingly show that plutons spend a lot of their hypersolidus time as magma mush. Over time, they may build vertical magma mush pathways in arcs and interact at various degrees with other magmas. How extensive these magma mushes are, which magma processes dominate and if and how much interplutonic interaction between different plutons takes place at the emplacement level is not well understood.

A place where these questions can be investigated is in the northern part of Joshua Tree National Park, California, which contains outcrops of a Triassic arc magma plumbing system consistent of two contemporaneous plutons: the ca. 235 Ma Twentynine Palms pluton (TPP) and the Queen Mountain pluton (QMP). The TPP is a megacrystic quartz monzonite composed of 1-20 cm blocky K-feldspar phenocrysts in a medium grained, equigranular matrix of largely plagioclase, hornblende, and minor quartz, biotite and accessories. The size of the K-feldspar varies substantially between different pluton domains. The QMP is a medium grained granodiorite with plagioclase, K-feldspar, quartz, biotite, hornblende and accessories. In addition, both plutons contain small pendants and blocks (TPP) and smaller, cm-dm pieces and biotite clots (QMP) of Pinto gneiss, the host rock into which the magmas intruded. Together, the plutons form a roughly bull's-eye shape map pattern with the megacrystic TPP forming the outer rim and the QMP, the interior of the complex. The contact between the two plutons is steep and sharp to gradational where exposed and dikes of the QMP intruded the TPP. The QMP contains sparse Alkali-feldspar phenocrysts up to 4 cm large, which resemble smaller phenocrysts in the TPP. Both plutons exhibit local solid-state deformation with the strongest fabric along the TPP margin.

Given these field relationships and concurrent crystallization of both plutons, we are investigating through petrography and element and isotope geochemistry the hypothesis that the two units may be related to one parent magma and are potentially representing a fractionate (QMP) and cumulate (TPP) pair. If our hypothesis is confirmed, this would suggest that we may be looking at a cross section of a horizontally and vertically extensive magma mush zone that underwent extensive open system differentiation and efficient crystal-melt separation.

Geochemical Analysis of Basalts from White Mountains and Horse Thief Hills, California by X-ray Fluorescence Spectroscopy (XRF)

Jacob Kato
Advisor: Dr. Jeffrey R. Knott

Department of Geological Sciences, California State University, Fullerton

Abstract

White Mountains and Horse Thief Hills are located to the in between Death Valley and Bishop, Ca. Horse Thief Hills is located to the south-east of Deep Springs Valley and to the north-west of the Last Chance Range. Miocene-Pliocene age (10.8 Ma) olivine basalts lie on the valley floor and atop the White/ Inyo Mountains to the west and the Deep Springs Range to the east. Previous geologic mapping shows the basalts in the White Mountains, Deep Springs Valley (DSV) and Horse Thief Hills (HTH) of the Last Chance Range (LCR) as the same geologic unit.

To determine if olivine basalts found in the White Mountains and HTH have the same source as the DSV basalts, samples were collected in the White Mountains and HTH. Samples were powdered and analyzed for major and minor trace element composition by X-Ray Fluorescence Spectrometer (XRF).

Trace element plots (e.g., Ba, Nb, Zr, Y, Ce, etc.) show that White Mountain and HTH basalts are similar to the DSV basalts and are likely from the same source. The White Mountain/DSV/HTH basalts are distinct and differ from LCR basalt. This geochemical correlation shows that basalt flowed from NW to SE in a paleochannel 10.8 M.a from the White Mountains to the HTH prior to formation of DSV.

Introduction

Questions exist about the different possible dispersal pathways of various ancient species such as the pupfish. Early hypotheses suggested pupfish in the southwestern U.S. dispersed along the ancient rivers and lakes that existed during the Last Glacial Maximum (15-20 ka; Blackwelder, 1933). However, biological studies show that this is an insufficiently short time period and a possible Colorado River connection in the last 3 My is also infeasible (Smith et al., 2002; Brown and Rosen, 1995). A 4 Ma time frame defined by the molecular clock (Smith et al., 2002) is more realistic geologically because tectonic activity would have had a larger impact on migratory pathways.

Based on unpublished major oxide data, Reheis and Sawyer (1997) hypothesized that basalt flows of the White Mountains flowed southeast across Deep Springs Valley (DSV) and onto the Horse Thief hills (HTH), possibly as far as Fish Lake Valley Death Valley. Case (2014) found that isolated outcrops of basalt across DSV are geochemically similar and from the same flow.

To further test the hypothesis of Reheis and Sawyer (1997), in this study, I collected samples of basalts found in the White Mountains west of DSV and in the HTH east of DSV to compare the geochemical composition of these baslts with the DSV basalts and determine if these flows have the same source.

Location

The White Mountains are located 20 km (12 miles) east of Bishop, California in the rain shadow of the Sierra Nevada Mountains (Figure 1). The highest elevation is White Mountain at 4342m (14,246 feet) above sea level (asl). Deep Springs Valley is east of the White Mountains and 35 km (22 miles) east of Bishop. The HTH are an informally named northwest-southeast trending upland 48 km (30 miles) east of Bishop. The HTH reach an elevation of 1783 m asl (5853 ft asl). East of the HTH is Fish Lake Valley

with an elevation of 1588 m asl (~5200 ft asl). Pliocene basalt flows are located at the top of the ridge and trend towards the southeast (McKee and Nelson, 1967). Pliocene basalt flows stop at the low lying basin of Fish Lake Valley. Flows are located on both the east and west sides of Fish Lake Valley separated by alluvial fan deposits.

Background

Using potassium-argon dating, Dalrymple (1963) determined a whole-rock age of 10.8±1.0 Ma (Miocene) on an olivine basalt in the White Mountains. A rhyolite tuff underlying the basalt was dated at 10.9±0.2 Ma. He postulated that the basalt rested on an extensive erosion surface that predated formation of DSV.

Nelson (1966) mapped these same olivine basalts (Tb) in the northeast part of the Blanco Mountain Quadrangle of the White Mountain/Inyo Range (Figure 2). He speculated that the age was Pliocene. One prominent basalt outcrop is on Bucks Peak (3235 m asl; 10,600 ft asl) 3.81 km (2.37 miles) southeast of the White Mountain Research Station Crooked Creek Laboratory. At Bucks Peak, Nelson (1966) mapped the basalt as non-conformably overlying the Precambrian Wyman Formation and Jurassic quartz monzonite of Beer Creek. Nelson (1966) also mapped olivine basalt on a saddle north of the North Fork of Crooked Creek 3.5 km (2.17 miles) due east of the White Mountain Research Station.

McKee and Nelson (1967) mapped locally scoriaceous olivine basalt flows (Tb) spanning northern DSV to Piper Mountain and across to the HTH. Across DSV the basalt flows are offset by a series of normal faults as they cross (McKee and Nelson, 1967). Basalt in the HTH are underlain by a medium to coarse-grained porphyritic quartz monzonite (Jm) and Tertiary tuff (Tt). Basalts in Fish Lake Valley to the east have similar stratigraphic relations (McKee and Nelson, 1967).

Krauskopf (1971) also mapped olivine basalts in several locations of the Mt. Barcroft Quadrangle, north and northwest of the Blanco Mountain and Soldier Pass Quadrangles, respectively. Krauskopf listed a 4.8 Ma K/Ar age for scoriaceous olivine basalts in Fish Lake Valley, northeast of the White Mountains. Krauskopf mapped rhyolite tuff underlying basalt north of Cottonwood creek. This is most likely the location of Dalrymple's (1963) 10.8 Ma basalt and 10.9 Ma rhyolite tuff (Case, 2014).

Ormerod et al (1988) proposed that the trace element composition of basalts in the western Basin and Range may identify two distinct mantle sources and the stage of eruption. The element Niobium (Nb) indicates ocean island basalts (OIB) whereas low Nb signifies continental flood basalts (Ormerod et al., 1988). The low Nb concentration of western Basin and Range basalts requires substitution of Zr. Ormerod et al. (1988) found that Ba/Zr ratio separates different magmas. Lavas with $Zr/Ba<0.20$ reflect contributions from subducted oceanic material or lithospheric mantle, whereas lavas with $Zr/Ba>0.20$ resemble ocean island basalts (Ormerod et al, 1988).

Ba/Zr ratios also indicate the stage of eruption. Older, lithosphere-dominated magmatism resulted in $Ba/Zr<0.20$, compared with $Ba/Zr>0.20$ for younger, asthenosphere-dominated magmatism (Ormerod et al, 1988). In other words, major elemental basaltic components can represent locations of large-scale melting events.

Based on unpublished major oxide composition, Reheis and Sawyer (1997) proposed that basalts located in Deep Springs/Eureka Valley and White/Inyo Mountains had the same source. Pluhar et al. (2005) used X-ray Fluorescence spectroscopy (XRF) to distinguish basalts from the Coso volcanic field 166 km south of Bishop. Pluhar et al. (2005) used Harker diagrams and Sr/Zr and Rb/Nb plots to show distinctive compositional fields.

Manoukian (2012) analyzed basalts by XRF from the Last Chance Range southeast of the HTH. Case (2014) analyzed samples from the basalt outcrops across DSV using XRF as well. Case (2014) found that the basalts across DSV are the same flow and that these basalts have a different source from the Last Chance Range basalts of Manoukian (2012). There are currently no published geochemical analyses of the basalt in the White Mountains.

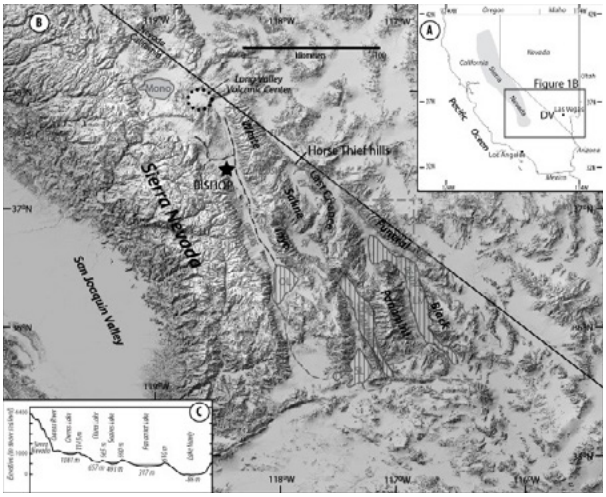

Figure 1: *A location map of southwest U.S. B: Shaded relief of eastern California-western Nevada showing the paleo-Ownes River drainage system, prominent mountain ranges (after Blackwelder, 1933), including the Horse Thief hills, and Death Valley National Park boundaries (dashed line). Mono Lake (shaded) is the only remaining lake in the Owens Lake system with extent (vertical lines) of pluvial Owens Lake (OL), China/Searles Lake (SL), Lake Gale (LG or Panamint Lake) and Lake Manly (LM) also shown. Key valleys are Death Valley, Deep Springs Valley (DSV), Eureka Valley (EV), Fish Lake Valley (FLV), Owens Valley, Panamint Valley and Saline Valley (SV). C: Paleo-Owens River system in cross section showing basin and still elevations.*

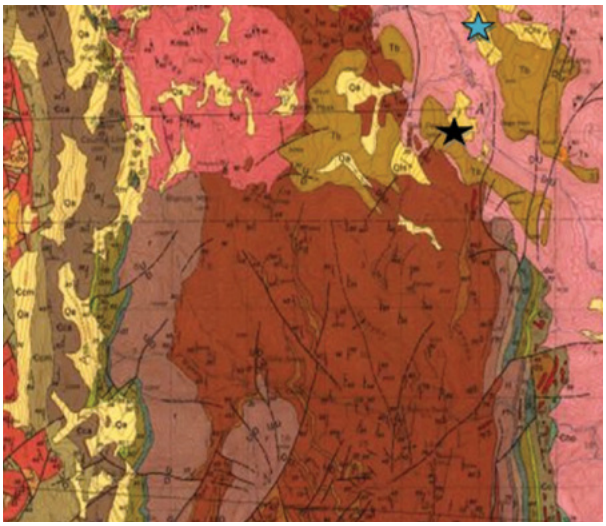

Figure 2: *Portion of the geologic map of the Blanco Mountain Quadrangle (Nelson, 1966). Brown units are olivine basalts (Tb). Black star indicates sample location of JKK-082314-1. Blue star indicates sample location of JKK-082314-2.*

Objectives

In this study, I will test the following hypotheses by completing XRF analysis on basalt samples in the White Mountain/Inyo Range and the HTH:

1. If basalt samples found in the White Mountains and HTH are the same basalt found in DSV, then the basalts should have the same geochemical composition.

2. If White Mountains and HTH basalts are from a different magmatic source, then the basalt should have different geochemical composition.

3. If the White Mountains, DSV, Last Chance Range, and HTH basalt compositions indicate the same source, then the basalt flowed from the White Mountains to the HTH and Last Chance Range as hypothesized by Reheis and Sawyer, (1997).

4. If the White Mountains, DSV and HTH basalt compositions differ, then the basalt flows had one or more sources.

Methods

Two basalt samples were collected from Bucks Peak and north of the North Fork of Crooked Creek in the White Mountains. A third basalt sample was collected from the HTH.

Basalt samples were crushed and powdered at CSU Fullerton. Samples were taken to the Department of Geology at Pomona College, weighed into graphite crucibles along with a flux to promote melting. The graphite crucibles were melted in a furnace at 1000°C, powdered and melted again to form glass beads. The glass beads were polished and then analyzed using an X-ray Fluorescence spectrometer (XRF) to determine geochemical composition of major and minor trace elements.

The major oxides were plotted on a TAS diagram. Plots of trace elements included a chondrite-normalized spider diagram and a trace element ratio. These geochemical data was compared previous basalt data from the region.

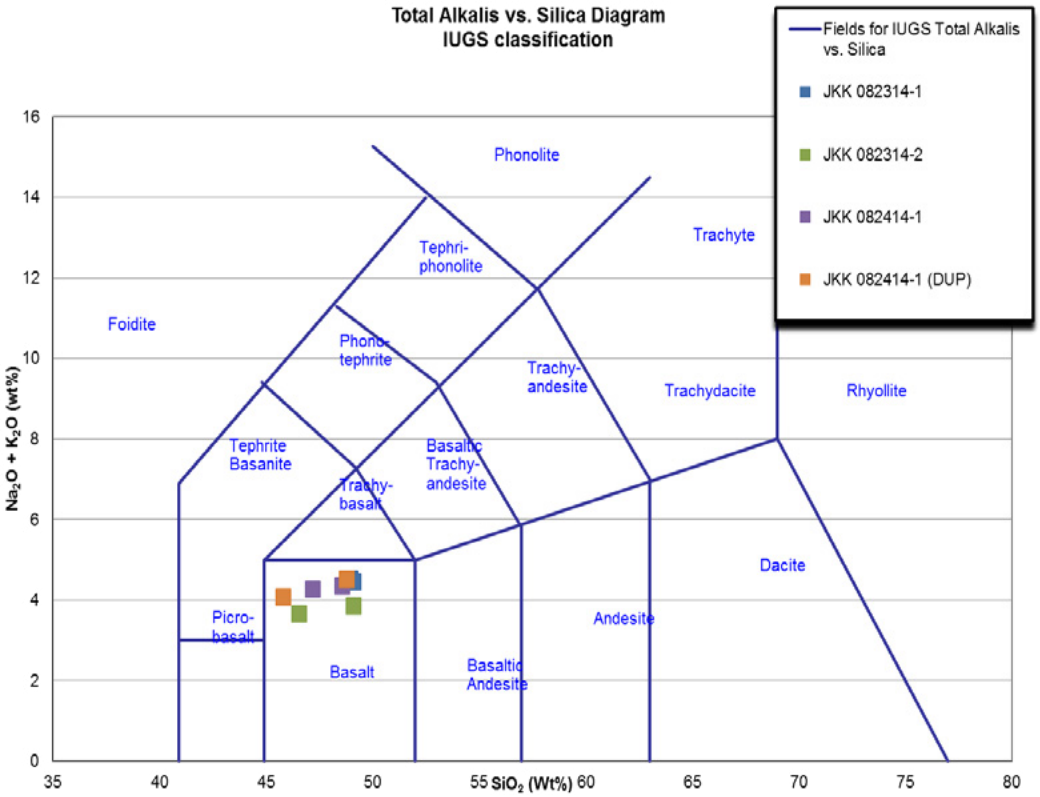

Figure 3: *TAS Diagram (ww.neiu.edu/~kbartels/DrBartelsExcelSpreadsheetModel.xls)*

Results

The Total Alkali Silica diagram (Figure 3) distinguishes volcanic rocks geochemically using silica and total alkali content. The JKK samples plot in the basalt field. A spider diagram plot shows that the JKK samples are nearly identical at a trace element level. On a Ce/Y vs Zr/Ba plot (after Ormerod et al., 1988), the JKK samples have a Zr/Ba ratio less than 0.2 (Figure 4).

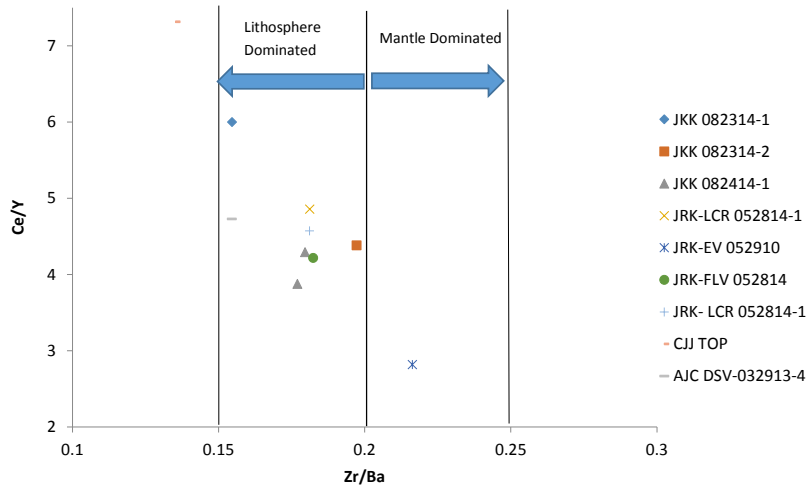

Figure 4: *Ce/Y vs Zr/Ba. Ormerod et al. (1988)*

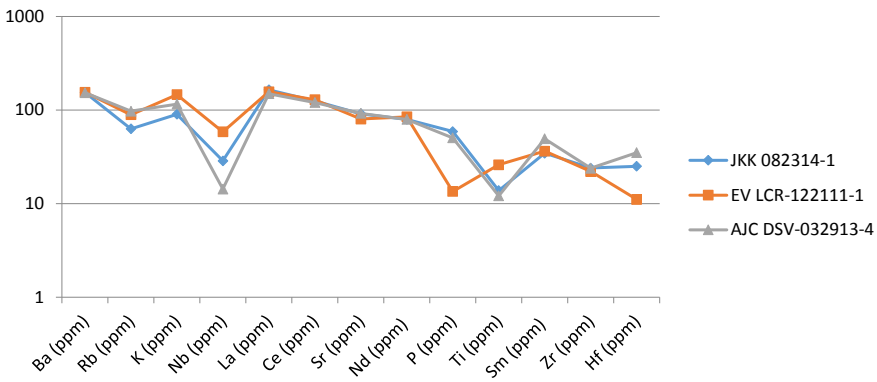

Figure 6: *XRF analysis of samples JKK 082314-1, EV LCR-122111-1, and AJC DSV-032913-4 normalized with chondrite data.*

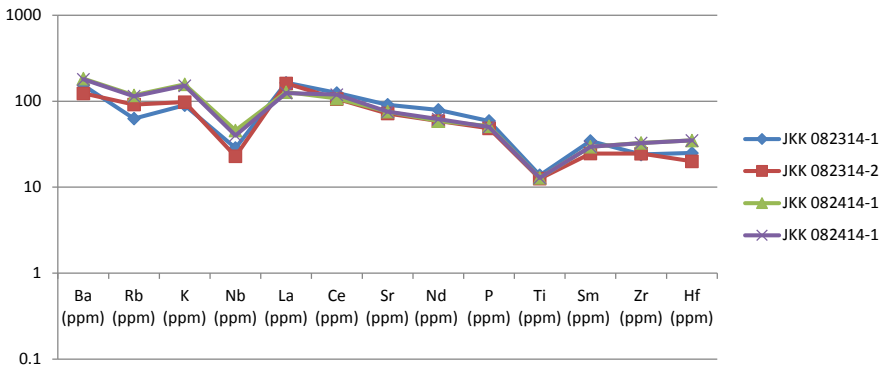

Figure 5: *XRF analysis of sample numbers JKK-082314-1, JKK-082314-2, JKK-082414-1, and JKK-082414-1 (DUP) normalized to chondrite.*

Discussion

In this study, I wanted to explore the following hypotheses:

1. If basalt samples found in the White Mountains and HTH are the same basalt found in DSV, then the basalts should have the same geochemical composition. The trace element composition of a DSV basalt (AJC-DSV-052913-4) with a sample from the White Mountains (JKK-082314-1) are indistinguishable. The greatest differences are Nb and Hf. Ormerod et al. (1988) previously noted that Nb concentrations in western Basin and Range basalts are too low for quantitative comparison.

2. If White Mountains and HTH basalts are from a different magmatic source, then the basalt should have different geochemical composition. The Ce/Y and Zr/Ba ratios of the White Mountain (JKK 082314-1) basalt and the HTH basalt (JKK 082414-1) are similar and are probably from the same flow. The Ce/Y ratio (Figure 4) for JKK 082314-1 is higher than the other samples. This is possibly due to the lack of weathering of this sample. The olivine at Bucks Peak was not oxidized whereas the olivine elsewhere was altered. Ratios $Zr/Ba<0.2$ are also consistent with Ormerod et al.'s hypothesis that these basalts have lithospheric contamination produced by the subducted Farallon plate.

3. If the White Mountains, DSV, Last Chance Range, and HTH basalt compositions indicate the same source, then the basalt flowed from the White Mountains to the HTH and Last Chance Range as hypothesized by Reheis and Sawyer, (1997).The basalts from the White Mountains (JKK 082315-2), Last Chance Range (EV LCR-122111-1) and DSV (AJC-DSV-052913-4) are different (Figure 5). The Last Chance Range basalt is clearly different from the other two and must have a different source.

4. If the White Mountains, DSV and HTH basalt compositions differ, then the basalt flows had one or more sources. The White Mountain (JKK 082314-2), DSV (AJC samples) and HTH basalts (JKK 082414-1) are similar and, therefore, have the same source (Figure 6). HTH sample (JKK 082414-1) lies at the same geomorphic position as AJC DSV 032913-4 atop the HTH. HTH basalt units labeled, "QTb", are southwest of DSV. HTH sample Zr/Ba ratio $x<0.2$ indicates that it originated from a lithospherically dominated magma (Ormerod et. al, 1988). When compared between HTH and DSV, ratios of Zr/Ba and Ce/Y data are similar. This indicates they could have been the same flow. The CJJ Top (Figure 4) sample is also atop a range, in this case the Last Chance Range; however, CJJ Top is not consistent with the HTH samples indicating that these basalts have different sources.

Conclusions and Future Work

Geochemical data suggests that DSV basalts are different from LCR basalts. Geochemical markers indicate that White Mountains, Deep Springs Valley and Horse Thief Hills are all from the same source and may be the same flow. A topographic low (e.g. ancient river channels) would have allowed basalts to flow from White/Inyo Mountains to Horse Thief Hills. However, data shows that basalts differ in composition and age in Deep Springs, Eureka Valley, and Last Chance Region. As to whether the channel extended further to the east towards Death Valley or to the south remains unknown.

For future work, samples of additional basalts should be taken farther east. Along with additional sampling, Ar/Ar chronology should be done to see if samples are similar in age.

References

Case, A. J., 2014, Geochemical Correlation of Basalts in Northern Deep Springs Valley, California. B.S. Thesis California State University, Fullerton. p. 1-16. Department of Geological Sciences. Faculty Advisor Jeffrey R. Knott, Ph.D.

Dalrymple, G. B., 1963, Potassium-argon dates of some Cenozoic volcanic rocks of the Sierra Nevada, California: Geological Society of America Bulletin, v. 74, p. 379–390.

Knott, J. R., Machette, M. N., Klinger, R. E., Sarna-Wojcicki, A. M., Liddicoat, J. C., Tinsley, J. C., David, B. T., and Ebbs, V. M., 2008, Reconstructing late Pliocene - middle Pleistocene Death Valley lakes and river systems as a test of pupfish (Cyprinodontidae) dispersal hypotheses, in Reheis, M. C., Hershler, R., and Miller, D. M., eds., Late Cenozoic drainage history of the southwestern Great Basin and lower Colorado river region: Geologic and biotic perspectives: Boulder, Colorado, Geological Society of America Special Paper 439, p. 1-26.

Krauskopf, K.B., 1971, Geologic Map of the Mt. Barcroft Quadrangle, California-Nevada: U.S. geologic Survey Geologic Quadrangle Map GQ-960, scale 1:62500

McKee, E.H. and Nelson, C.A., 1967, Geologic map of the Soldier Pass quadrangle, California and Nevada: U.S. Geological Survey, Geologic Quadrangle Map GQ-654, scale 1:62,500

Nelson, C.A., 1966, Geologic map of the Blanco Mountain quadrangle, Inyo and Mono Counties, California: U.S. Geological Survey, Geologic Quadrangle Map GQ-529 scale 1; 62,500.

Ormerod, D.S., Hawkesworth, C.J., Rogers, N.W., Leeman, W.P., Menzies, M.A., May, 1988, Tectonic and magmatic transitions in the Western Great Basin, USA. Nature: v.333, p 349-353.

Pluhar, C.., Coe, R.S., Sampson, D.E., 2005, Lava fingerprinting using paleomagnetism and innovative X- ray fluorescence spectroscopy: A case study from the Coso volcanic field, California. Geochemistry, Geophysics and Geosystems. Vol. 6, Issue 4.

Reheis, M.C., Sawyer, T.L., March, 1997, Late Cenozoic history and slip rates of the Fish Lake Valley, Emigrant Peak, and Deep Springs fault zones, Nevada and California. Geological Society of America Bulletin Vol. 109, Issue 3, pp 280-299.

Ross, D.C., 1967, Generalized Geologic Map of the Inyo Mountains Region, California: U.S. Geological Survey, scale 1:125000

Trace Elemental Analysis of Productivity and Oxygenation Conditions within the Western Canada Sedimentary Basin following the Permian-Triassic Extinction

Anthony A. Macias
Advisor: Dr. Adam Woods

Department of Geological Sciences, California State University, Fullerton

Abstract

Approximately 251 million years ago, towards the end of the Permian, Earth experienced a mass extinction event that resulted in the extinction of almost 90% of species on the planet. Recovery from the extinction event did not happen at the same time everywhere; instead, recovery from the extinction was strongly related to environmental conditions. To understand how organisms rebounded following such a devastating crisis, it is necessary to examine the reestablishment of primary productivity and its relationship to environmental conditions, specifically oxygenation levels, during this period as a whole. Samples previously collected and powdered from the Montney Formation from 2 drill cores from the Pedigree-Ring/ Border-Kahntah River area of northeastern British Columbia and northwestern Alberta (16-33-84/18W6M and B-24-H/94-H-16) underwent trace elemental analysis to determine oxygenation and productivity recovery rates within the region. Trace elemental analysis of core B-24-H/94-H-16 reveals low productivity levels and anoxic conditions that shift up section to euxinic conditions. Analysis of core 16-33-84/18W6M reveals anoxia and possible euxinic conditions that correlate with enhanced productivity, which likely drove the anoxic conditions found in the core. Anoxic to euxinic conditions found within the Pedigree-Ring/ Border-Kahntah River area therefore are driven by a combination of upwelling of nutrient -rich deep waters (16-33-84/18W6M) and the impingement of deep, anoxic water masses along the western margin of Pangea (B-24-H/94-H-16). Results derived from this study suggest that post-extinction recovery rates are strongly influenced by environmental conditions that are driven by processes acting at both the regional and global scale, and careful, multiproxy analysis is necessary to determine which processes are active in any given area.

Search for the Source of Cogstones in Southern California

Ryan McKay, Sierra Patterson and Crystal Cortez
Advisor: Dr. Valbone Memeti

Department of Geological Sciences, California State University, Fullerton

Abstract

Cogged stones are 6000-3500 BC old Native American artifacts carved in a way that look like a cog gear. They have been only found in southern California and are dominantly made out of a variety of scoria basalt. The use and significance of these stones is unknown and no flawless theory has yet been agreed upon. The location of the basaltic source rock for the stones is also not known, however, multiple basalt locations crop out in southern California and it is possible the source rocks were derived from nearby. Thus finding the location of the source rocks may help narrow down the possibilities of what the stones were used for and reveal more about the lifestyle of Native Americans in Southern California.

We use petrography and geochemical analysis on four cogged stone fragments (CS1-CS4) collected at different sites in Orange County. We are comparing these to scoria basalt collected on the SE side of Catalina Island near Two Harbors (CL1B), a site known to have been inhabited by Native Americans, the Santa Monica Mountains near La Vina Gomez de Malibu along Mulholland Highway (SAM), at Van Winkle Mountains (SW Mojave National Preserve; VW1) and at Fossil Falls along Hwy 395 (FF1). Three of the four cogged stones are vesicular basaltic scoria and one is volcaniclastic tuff. Petrographic analysis revealed the cogged stones are plagioclase rich with various amounts of olivine, pyroxene, oxides and iddingsite and varying grain size. Samples SAM and VW1 were eliminated as source rocks for these particular stones based on differences in petrography. The texture, grain size and mineralogy of samples CL1B and FF1, however, could be both possible matches for cogged stone CS3. XRF major oxide and trace element analysis shows similarities in chemistry between FF1 and CS3 with only minor differences in SiO2, CaO, Ba, Ni, Cu and Nb content. Samples CL1B and CS3 yield some overlap in major oxide and trace element concentrations, but enough variance to indicate a match is probably less likely. However, more geochemical analyses are underway to further test our working hypotheses. If the analyses yield positive match results with Fossil Falls (FF1) and Catalina Island (CL1B), then there is a possibility that Native Americans had a reason to travel far to collect cogged stone source rocks, however, other potential source rock comparisons have indicated possible nearby locations as well.

Locating The Volcanic Source Rock Of Prehistoric Cogged Stones From Southern California: Were They Carved From El Modena And Santa Rosa Basalts?

Sierra Patterson, Ryan McKay and Steven R. James
Advisor: Dr. Valbone Memeti

Department of Geological Sciences, California State University, Fullerton

Abstract

Cog stones, hand-size Native American artifacts carved in the shape of cogs, have only been found in Orange County, CA and are dominantly made of basaltic scoria. The use of cog stones is unknown with ca. 40 different potential uses proposed to date. The purpose of this study is to identify the volcanic source location from which the cog stones were carved. This may help reveal the significance of the cog stones to 6000-3500 BC Native Americans.

To identify the source location of basaltic cog stones four cog stones fragments unearthed in Orange County were used for analysis. We focused on two potential source locations: the El Modena volcanics, which have been previously suggested as a likely source for the cog stones, and the nearby Santa Rosa volcanics in Riverside County. Petrographic observations and whole rock XRF geochemistry are used to compare the cog stones with the potential source samples. Given the variability in the composition of basaltic cog stones, it is unlikely that all cog stones are from the same volcanic source.

Preliminary results from petrographic analysis of thin sections of the cog stones show that they have porphyritic texture and are composed of mainly plagioclase laths with varying amounts of ortho- and clinopyroxene, olivine, opaque minerals, and iddingsite. Petrographic analysis of Santa Rosa basalt has the same mineralogical composition and texture as cog stone CS3. We are further testing this potential match through XRF analysis. Mineralogy and texture of the El Modena basalts do not resemble that of any of the cog stones analyzed, however XRF analyses of two El Modena samples suggest similar geochemical compositions to CS2. They contain ca. 55 wt.% SiO_2, 20-21 wt.% of Al_2O_3, 5-6.5 wt.% Fe_2O_3, 8-9 wt.% of CaO, and similar trace element concentrations, e.g. 200-230 ppm Zr, 320-400 ppm Ba, 16-20 ppm Nb, and 600- 700 ppm Sr. El Modena basalt has smaller plagioclase exhibiting a sieve structure, lower vesicle and matrix abundance, and does not contain clinopyroxene and olivine. More analyses are underway to further examine these relationships. If we can confirm that both El Modena and Santa Rosa volcanics were sourced to carve cogged stones, it would suggest that Native Americans collected these rocks perhaps because they were soft to carve and found nearby; the collection site may have not been important.

Evaluation of the Big Pine Volcanic Field Contact Relationships along the Sierra Nevada Frontal Fault Zone north of Goodale Creek in Owens Valley, California

Amanda Shellhorn
Advisor: Dr. Phillip A. Armstrong

Department of Geological Sciences, California State University, Fullerton

Abstract

This study investigates the contact relationships between basalt flows and cones of the Quaternary Big Pine Volcanic field (BPV) and the predominantly granitic rocks of the eastern Sierra Nevada Mountains between Goodale and Taboose Creeks along the Sierra Nevada Frontal Fault Zone (SNFFZ). The SNFFZ marks the western boundary of the Basin and Range Province and separates the Sierra Nevada Mountains from Owens Valley. This zone is composed mostly of NNW-striking, east-dipping normal faults, which generally are assumed to dip 60°. However, previous work north of Bishop and farther south near Lone Pine and Independence has shown that the SNFFZ faults dip much shallower (26 to 52°). The BPV contact with the Sierra Nevada Mountains generally trends NNW and is parallel to the mountain front. The contact locally V's up and over ridges at the range front and along the SNFFZ and is consistent with an overall east dip. Our working hypotheses are that the contact formed by (1) basaltic flow deposition buttressed against the mountain front; (2) localized basalt emplacement and extrusion along the SNFFZ; and (3) faulting after emplacement of the basaltic rocks. Field and GPS mapping along the contact combined with Google Earth map analysis are being used to test the hypotheses. Field mapping and preliminary 3-point analysis along the contact yields an average dip of 24° E. This dip is similar to the dip of SNFFZ faults farther north and south suggesting that the contact may locally be a fault. Plane-fitting analysis of GPS- and Google Earth-derived x,y,z positions will be utilized for a more precise orientation of the contact and to assess its potential as a fault. A shallow SNFFZ dip affects long-term extension rate calculations and the kinematic history of this part of the western Basin and Range and Eastern California Shear Zone.

Reconstructing Hydrologic Change Over the past 96,000 Years Using Sediments from Baldwin Lake, San Bernardino County, California

Emily Silveira
Advisor: Dr. Matthew Kirby

Department of Geological Sciences, California State University, Fullerton

1. Introduction

Records of the last glacial in coastal Southern California (CSC) are incredibly sparse (Blazevic et al., 2009; Kirby et al., 2010). In fact, terrestrial climate records spanning the entirety of the last 96,000 years in southern California are presently non-existent. In this study, we present a new paleohydrologic record derived from a sediment core obtained from Baldwin Lake in summer 2012, which extends our knowledge of water variability in CSC back into the last Interglacial (MIS 5c; Table 1). Blazevic et al. (2009) have shown that Baldwin Lake does provide a reliable record of past environmental change for the region back to 65,000 years. Also, it has been shown that data from Baldwin Lake can be extended to the entire coastal southwestern region of North America and correlated to hemispheric paleoclimatic records such as those from ice cores in Greenland (Kirby et al., 2006). This thesis uses a variety of sedimentological measurements to reconstruct the hydrologic history of Baldwin Lake at Milankovitch timescales over the past 96,000 years. The initial isolation, and thus formation, of Baldwin Lake is also hypothesized.

Today, CSC faces a perennial fresh water shortage, which brings increased importance to studying the past climate of the region. Climate variability has a direct impact on the availability of freshwater in CSC (Kirby et al., 2010). Cities in the southern California area use twice as much water as is naturally available (Hanak, 2011). Also, population trends in 2001 were projected to increase by 30% by 2020. This population growth will increase demand on the already limited water resources (Apple, 2001). Regional drought coupled with this population growth ensures that CSC will remain freshwater-poor. Perennial water shortages cause the region to be especially susceptible to hydrologic variability such as drought (MacDonald et al., 2008); thus, it necessary to have an understanding of natural hydrologic variations in the past.

Significantly, the results of this study extend knowledge of past hydrologic change in CSC back to the end of the last Interglacial (96,000 years before present, MIS 5c). The study of past water availability, particularly during the last Interglacial, is increasingly significant as the last Interglacial may provide a potential analog for future global warming (Muhs et al., 2006). Importantly, global temperatures during the past Interglacial were slightly higher than today (North Greenland Ice Core Project members, 2004; Muhs et al., 2006). Therefore, understanding past climatic change during the last Interglacial will provide potential insight into how southern California will change in the future as global warming continues.

An in-depth study of the glacial climate in CSC also has implications for understanding future climate change. When making predictions for future change, it is essential to be aware of the natural range of hydrologic variability, as well as the amplitude of changes. The glacial period provides a good basis for studying these two aspects, as it was a time that was characterized by high amplitude and high frequency changes in climate (Kirby et al., 2006). Examining the end of the last glacial also allows an exploration of hydrologic responses to potential abrupt climatic "surprises" such as that akin to the Younger Dryas (Overpeck, 1996).

2. Objectives And Hypotheses

The objectives of this study are: (1) to explore the ontogeny of Baldwin Lake; and, (2) to reconstruct the lake's Milankovitch scale hydrologic variability over the past 96,000 years. The hypotheses of this study are: (1) The origin of Baldwin Lake is related to valley isolation as linked to extension of the Sugarloaf Fan; and, (2) In general, deep lake conditions existed during full glacial conditions and shallow or dry lake conditions existed during interglacials.

3. Background

3.1 Geologic Setting

The San Bernardino Mountains are a relatively young range, located in the eastern extension of the Transverse Ranges Geomorphic Province of California (Leidy 2003). The Baldwin Valley watershed is located in the north block of the mountain system. During the Tertiary and early Quaternary periods, the north block was part of the Mojave Desert and eroded to a low relief and dissected by streams (Leidy, 2003; Stout, 1976). The region which now contains Bear Valley and Baldwin Valley was traversed by a small valley prior to uplift (Stout, 1976). The block was subsequently elevated 1520 -2130 m and tilted northward toward the Mojave Desert by late Quaternary time (Leidy, 2003). Due to lateral movements of the San Andreas Fault system and the Pinto Mountain Fault, the mountain blocks were rapidly uplifted during the Pasadenan Orogeny, approximately 300,000-500,000 years BP (Stout, 1976).

The basin containing Bear Valley and Baldwin Valley formed by tilting and thrusting along the northern and eastern sides of the valley (Stout, 1976). It is believed that early sediment deposition in the valley is closely related to the age of this original thrusting, which began in the mid-Pleistocene, prior to the Pasadena Orogeny, and continued through the late Pleistocene (Leidy, 2003). According to geologic cross-sections of the region, approximately 30 m of lacustrine sediment were deposited on top of about 60 m of older alluvium (Leidy, 2003). Though the region is still tectonically active, only minor uplift has occurred during the last 10,000 years.

3.2 Baldwin Lake

Baldwin Lake is an alpine-playa lake located at 2,040 m above sea level; it is located 3 km east of Big Bear Lake in San Bernardino County, CA. The lake lies within the east-west trending Big Bear Valley which likely originated from geologically recent thrust faulting (Blazevic et al., 2009). Quaternary age unconsolidated alluvium, as well as metasedimentary Precambrian(?) and Paleozoic basement rocks, surround Baldwin Lake, while the valley is enclosed by Precambrian(?) and Paleozoic-aged metamorphic rocks (Blazevic et al., 2009).

Baldwin Lake has a small (78 km^2) drainage basin, which is surrounded by mountain crests and separated from Big Bear Lake by the Sugarloaf Fan (Blazevic et al., 2009). Under modern conditions, it remains dry for an average of 3 to 4 years every 10 years (Blazevic et al., 2009). The lake is a closed basin, allowing it to serve as a precipitation gauge or "evaporation pan". Due to the closed nature of the basin, Baldwin Lake is a sensitive recorder of hydrologic changes (Blazevic et al., 2009; Kirby et al., 2006). Today, there is a positive correlation between total regional winter precipitation and lake level at Baldwin Lake (Kirby et al., 2006). This relationship is expected to continue into the past for as long as Baldwin Lake was characterized by a closed basin geometry.

3.3 Modern Regional Climate

Southern California has a Mediterranean climate, characterized by dry, hot summers and cool, wet winters (Bailey, 1966). Average daily summer temperatures in Big Bear Valley range from 15.5°C to 21.1°C, while average daily winter temperatures are between 1.6°C and 4.4°C (Flint et al., 2012). Annual precipitation in the valley varies; however, the region in which Baldwin Lake is situated receives an average of 45 to 55 cm. Precipitation in southern California is dictated by the average position of the winter season polar front in relation to changes in the position of the eastern Pacific subtropical high pressure zone (Kirby et al., 2006). A weakened subtropical high allows storm tracks to shift southward, thus increasing the frequency of winter storms across CSC. The frequency of winter storms and their associated moisture determine whether or not CSC experiences a wet or dry winter. Dryer winters, on the other hand, are caused by a stronger high pressure zone, as storms are diverted to

the Pacific Northwest. In addition to the interaction between atmospheric circulation and Pacific Ocean sea-surface conditions, interannual precipitation variability in southern California is influenced by El Niño-Southern Oscillation (ENSO) and Pacific-Decadal Oscillation (PDO) (Kirby et al., 2009).

ENSO is arguably the most prominent factor in CSC's interannual climate variability (Tudhope et al., 2001; Mantua and Hare, 2002; Ryu et al., 2008; Zhang et al., 2010). The driving mechanism of ENSO is debatable; however, there is a clear connection between sea surface temperature (SST) and atmospheric circulation, which has a direct impact on hydrologic variability in CSC (Zhang et al., 2010). During an El-Niño event, SSTs along the western coast of North America increase as well as CSC winter precipitation; meanwhile, a La Niña event is characterized by cooler SSTs and less winter precipitation (Tudhope et al., 2001; Kirby et al., 2005). The period of ENSO is variable ranging from 2.5 to 7 years; however, it is usually focused within a 3 to 5 year band (Tudhope et al., 2001).

While ENSO is a primary driver of interannual climate variability, the PDO is equally important to interdecadal climate variability (Mantua and Hare, 2001; Kirby et al., 2010). A positive PDO is linked to similar effects as an El-Niño event, including increased precipitation in CSC (Kirby et al., 2010). A notable difference between ENSO and the PDO is the length of events. According to Mantua and Hare (2001), typical modern ENSO events persist for 6 to 18 months, while a typical PDO "event" persists for 20 to 30 years.

3.4 Interglacial and Glacial Climate

This study covers the past 96,000 years including MIS 5a-c (74 – 96 ka), MIS 4 (57 – 74 ka), MIS 3 (29 – 57 ka), MIS 2 (12.9 – 29 ka), and the present Interglacial (Table 1).

The Last Interglacial (LIG) correlates to Marine Isotope Stage 5 (MIS 5a-e: 130,000 to 74,000 years before present), and is thought to have peaked between 125 and 130 thousand years before present (ka) (Oppo et al., 2006; Sime, 2013). Temperatures during the LIG, based on the maximum isotopic value in a Greenland ice core, were approximately 5°K warmer than the present (North Greenland Ice Core Project members, 2004). This is supported by an examination of fauna in the eastern Pacific Ocean, as the ~120 ka fossils represent warmer- than-modern marine waters (Muhs et al., 2006). Grain size analysis of a core from the Gulf of Mexico implies that absolute precipitation was not more intense during the LIG in comparison to the present (Montero-Serrano, 2011). The end of the LIG occurred in a gradual cooling, rather than an abrupt climate change (North Greenland Ice Core Project members, 2004). By 80 ka, Pacific Ocean fauna began to reflect cooler-than-modern marine temperatures (Muhs et al., 2006).

Beginning around 75 to 70 ka, corresponding with the onset of MIS 4, North America experienced the onset of the glacial period as the Laurentide Ice Sheet (LIS) and Cordilleran Ice Sheet (CIS) both grew rapidly over the continent (Barry, 1983). Coastal southwestern North America experienced an increased frequency of winter storms during glacial growth, from about 65 ka to 50 ka (Kirby et al., 2006). Deep sea sediment records suggest that equatorial Pacific SSTs were 2°C to 3°C cooler as the ice sheets progressed to their maximum, from 70 ka to 30 ka (MIS 3-4; Tudhope et al., 2001). Advances of mountain glaciers in the San Bernardino Mountains of CSC also occurred during MIS 2 (Owen et al., 2003).

The Last Glacial Maximum (LGM), when global ice sheets reached their maximum integrated volume, occurred from 26.5 to 19.0 ka during the start of MIS 2 (Clark et al., 2009). Heusser and Sirocko's (1997) analysis of polliniferous sediments deposited in the Santa Barbara basin suggests that southern California experienced an increase of up to 700 mm of precipitation and a decrease of 9°C in average temperature during full glacial conditions. Increased precipitation in the region can be attributed to a shift in the position of the jet stream due to the extent of the North American ice sheets. As the jet stream shifted southward, the coastal southwestern United States experienced an increased frequency of winter storms (Kirby et al., 2006). For example, the LGM is characterized by substantial glacial advances in the San Bernardino Mountains of CSC (Owen et al., 2003); however, lake status during the LGM is yet unknown for CSC (Kirby et al., 2013). Clark et al. (2009) propose the retreat of the CIS and LIS began between 19 and 20 ka.

A general drying trend ensued after the end of the last glacial, corresponding to the end of MIS 2, which can be divided into three phases: (1) the Oldest Dryas (19-14.7 ka BP; OD), (2) the Bølling-Allderød (14.7-12.9 ka BP; BA), and (3) the Younger Dryas (12.9-11.7 ka BP; YD). The OD was characterized by a wetter-than-modern climate in CSC (Kirby et al., 2013). The southward displacement of the polar front jet stream at this time caused more winter precipitation, causing at least one significant advance of glaciers in the San Bernardino Mountains (Owen et al., 2003). The abrupt transition in the BA marked a shift to a less wet climate in CSC. Decreased winter precipitation, coupled with higher summer temperatures, likely led to a retreat of glaciers in the San Bernardino Mountains (Owen et al., 2003). A recent Lake Elsinore sediment record is used to infer smaller magnitude or less frequent winter storms during the BA (Kirby et al., 2013). The transition from the BA to the YD was abrupt; however, regional responses were varied. While eastern and inland sites experienced conditions wetter than the BA, more coastal sites, such as Lake Elsinore, experience conditions drier than the BA (Kirby et al., 2013). As a whole, these three stages marked the transition from a cold, wet glacial environment to a warm, drier Holocene environment.

4. Methods

4.1 Core Collection

Core BDL12 was extracted from Baldwin Lake in August 2012 using a truck-mounted hollow stem auger drill over a course of two days. The core is comprised of 41 sections which total 26.5 m of near-continuous material with 81.3% recovery. Following extraction, the core was split, photographed, described, and sampled by Ph.D. candidate Katie Glover at University of California, Los Angeles (UCLA).

4.2 Age Control

Age control for BDL12 was determined from seven accelerator mass spectrometry (AMS) ^{14}C dates and three infra-red stimulated luminescence (IRSL) dates. Bulk charcoal and macro-organics from the upper 8 m of the core were analyzed for AMS radiocarbon dates at the Keck Carbon Cycle AMS Lab at University of California, Irvine in early 2013. Sand grains from the lower sections of the core were analyzed for IRSL dates at UCLA's Earth and Planetary Science Optically Stimulated Luminescence Lab. IRSL was utilized rather than optically stimulated luminescence (OSL) due to possible feldspar and zircon inclusions in the quartz grains of sediments from the San Bernardino Mountains, which can skew OSL dates (Garcia et al., 2013).

4.3 Magnetic Susceptibility

Magnetic susceptibility was measured by Katie Glover (UCLA) using a Bartington MS3e magnetic susceptibility meter. Samples were extracted from the core for measurement at 1 cm contiguous intervals.

4.4. Total Organic Matter and Total Carbonate

Total organic matter and total carbonate were measured by Katie Glover (UCLA) using the loss-on-ignition (LOI) method (Dean, 1974). All samples were extracted from the core for measurement at 1 cm contiguous intervals.

4.4 Grain Size

Grain size analysis was performed every fifty centimeters using a Malvern Mastersizer 2000 laser diffraction grain size analyzer coupled to a Hydro 2000G. The sample interval was chosen to create a general core characterization. A higher resolution study may be performed in the future. The samples were pretreated by removing organic matter, carbonate, and biogenic silica. The organic matter was removed by treating the samples with ≥30 mL of 30% hydrogen peroxide on a 200oC hot plate. The samples were then treated to remove carbonates with 10 mL of 1 M HCl and allowed to sit overnight. Before the removal of biogenic silica, the samples were centrifuged twice and DI water was used to ensure the samples were clean. The supernatant was removed through decantation. The samples were treated to remove biogenic silica with 10 mL of 1 M NaOH for four hours on a 50oC hot plate. Following the removal of biogenic silica, the samples were again centrifuged twice with DI water and the supernatant was decanted.

When running the samples through the grain size analysis machine, a tuff standard with a known distribution was run to evaluate the reliability of the results (n = 9524, avg = 4.61, stndev = 0.22). The standard was run twice at the beginning of each day, once every ten samples, and once at the end of every day. For each sample, the analyzer measured it three times and calculated an average. Ten size classes are reported including mode, d(0.1), d(0.5), and d(0.9).

5. Results

5.1 Core Stratigraphy

Core stratigraphy and age control, radiocarbon dates and optically stimulated luminescence dates, are shown on Figure 1. Core BDL12 is characterized by several sedimentologically distinct sections. The top of the core, from 5 cm to 150 cm, the sediment is light brown massive clay. From 150 cm to 250 cm, the sediment transitions to a dark gray massive clay. From 250 cm to 1500 cm, the sediment is dominated by massive silt with variable banding. During this interval, the sediment varies from dark gray to a lighter gray. At a depth of 1500 cm to 1550 cm, the sediment transitions to light gray massive clay with variable banding still present. From 1550 cm to 1950 cm, the sediment is brown and shell-rich. At a depth of 1950 cm to 2150 cm, the sediment transitions to light gray massive clay with variable banding. From 2150 cm to 2300 cm, brown, shell-rich sediment is present. From 2300 cm to 2425 cm, the sediment is light gray massive clay. At a depth of 2425 cm to 2475 cm, the sediment is characterized by light gray inorganic poorly-sorted sand. From 2475 cm to 2600 cm, the sediment transitions to light gray massive clay. The bottom of the core, from 2600 cm to 2675 cm, the sediment is inorganic poorly-sorted sand.

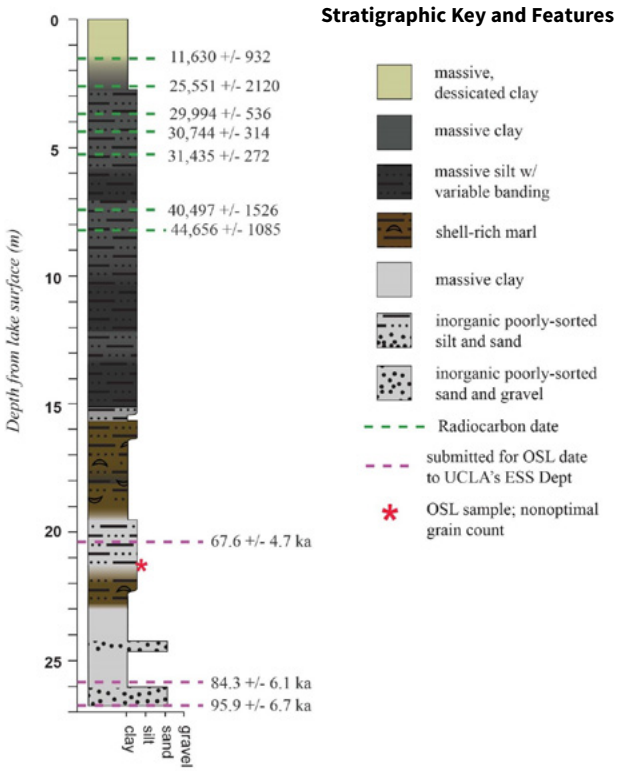

Figure 1: *Core stratigraphy, provided by Katie Glover (UCLA).*

Blazevic et al. (2009) presented a sediment core from Baldwin Lake, which extended to a depth of 1455 cm. Core BDL12 reveals similar trends in magnetic susceptibility, grain size, total organic matter, and total carbonate.

5.2 Age Model

The age model on the stratigraphic column represents a straight-line interpolation between dates. The age model of the site includes: basin inception at 95.9 +/- 6.7 ka BP during MIS 5c, determined by an IRSL date, up to late-Pleistocene/early-Holocene lake conditions at 11.6 +/- 932 ka BP determined by a ^{14}C date. This establishes that the sequence includes the entirety of MIS 2 (29 – 14 ka BP). The differences in errors between the radiocarbon dates and the IRSL dates are due to fundamental differences in the nature of the methods. Radiocarbon dating utilizes the AMS method, which is very precise back to ~40,000 years. IRSL, on the other hand, involves more unknowns and assumptions, which produces larger errors.

5.3 Magnetic Susceptibility

The magnetic susceptibility values of core BDL12 range from 5.55 x 10^{-6} m^3/kg to 9.94 x 10^{-4} m^3/kg. The average value is 7.06 x 10^{-5} m^3/kg. From the top of the core to 600 cm, values are generally high and stable; however, a prominent decrease is noted at 150 cm, while a sharp increase to 9.94 x 10^{-4} m^3/kg occurs at 300 cm. A general increasing trend is present from 350 cm to 1200 cm. Between 1200 cm and 1550 cm, values become uniformly high and stable. From 1600 cm to the bottom of the core, the values are characterized by high amplitude variation. Two distinct peaks exist at 2050 cm and 2450 cm.

5.4. Total Organic Matter and Total Carbonate

The total organic matter of core BDL12 ranges from 0.7% to 32.2%, with an average of 13.3%. From the top of the core to 250 cm, values are generally low and stable. At a depth of 250 cm to 1550 cm, the values have low amplitude, high frequency variability. Between 1550 cm and 2400 cm, the values have high amplitude variability with two distinct peaks at 1750 cm and 2200 cm. From 2450 cm to 2550 cm, the values transition to uniformly low and stable. The basal sediments contained a negligible amount of organic matter.

For core BDL12, the total carbonate values range from 0.7% to 20.9%, with an average of 7.07%. From the top of the core to 150 cm, values are generally high with a decreasing trend. Between 200 cm and 1750 cm, the values transition to low and generally stable, with two slight peaks at 700 cm and 1000 cm. At a depth of 1750 cm to 2250 cm, the values are characterized by sharp increase at 1750 cm followed by a general decreasing trend with low amplitude variability. Between 2250 cm and 2550 cm, the values transition back to general higher levels with a peak at 2400 cm. The basal sediments contained a negligible amount of carbonate.

Grain Size

The grain size distribution of core BDL12 is dominated by silt, with generally low levels of clay and sand content (Figure 2). From the top of the core to 150 cm, silt and clay content decreases, while sand content increases. Between 200 cm and 450 cm, grain size distribution is generally constant, with a slight increase in clay content. At 350 cm, however, there is a sharp increase of sand content and corresponding decrease in silt content, before a return to the general previous levels. From 500 cm to 650, grain size distribution is highly variable and alternates between high and low silt content with corresponding low and high sand content. There is a slight increase in clay content at 700 cm. Between 700 cm and 1000 cm, there is a decreasing trend in sand content and a corresponding increasing trend in silt content. At 1070 cm, there is an increase in grain size of the sediment. From 1100 cm to 1250 cm, there is a generally lower grain size with increased clay and silt content and decreased sand content. Grain size is highly variable between 1300 cm and 1500 cm, though there is a general increasing trend in overall grain size. Contrastingly, from 1500 cm to 1850 cm, there is an overall decreasing trend, as sand content steadily decreased and silt content steadily increased. At 1900 cm, there was a marked increase of grain size. Between 1950 cm to 2350 cm, the grain size distribution demonstrated high amplitude variability. While clay content decreased and remained generally low, sand content alternated between about 20% and 40% and silt content alternated between 50% and 70%. From 2400 cm to 2500 cm, there was a markedly lower overall grain size. Sand content was extremely low, while silt content and clay content increased. From 2550 cm to the bottom of core, there is a dramatic increase in grain size, as sand content increased to 89%, while silt content decreased to 9%.

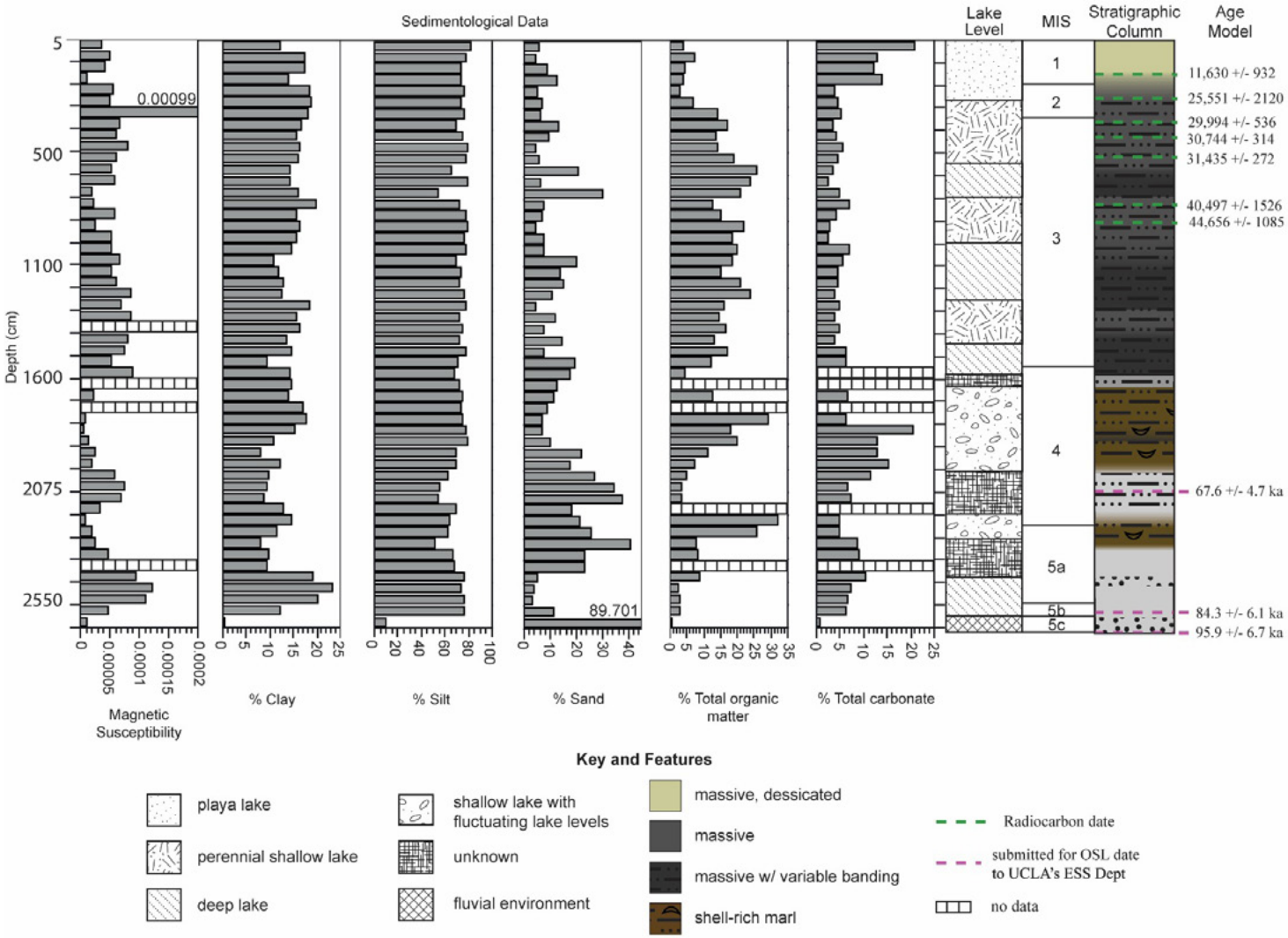
Sedimentological Data
Lake Level
MIS
Stratigraphic Column
Age Model
Depth (cm)
5
500
1100
1600
2075
2550
0.00099
89.701
1
2
3
4
5a
5b
5c
11,630 +/- 932
25,551 +/- 2120
29,994 +/- 536
30,744 +/- 314
31,435 +/- 272
40,497 +/- 1526
44,656 +/- 1085
67.6 +/- 4.7 ka
84.3 +/- 6.1 ka
95.9 +/- 6.7 ka
Magnetic Susceptibility
% Clay
% Silt
% Sand
% Total organic matter
% Total carbonate
Key and Features
playa lake
perennial shallow lake
deep lake
shallow lake with fluctuating lake levels
unknown
fluvial environment
massive, dessicated
massive
massive w/ variable banding
shell-rich marl
Radiocarbon date
submitted for OSL date to UCLA's ESS Dept
no data

6. Discussion

6.1 Lake Ontogeny

The basal sediments of core BDL12 are more than 85% sand, which is indicative of a high energy environment (Figure 2). The sand is relatively clean with low to negligible organic matter and carbonate (Figure 2). To determine the origin of this clean sand, we must first assume that Baldwin Lake did not exist before the valley became isolated via extension of the Sugarloaf Fan. Second, we must assume that a fluvial environment occupied the valley's pre- lake location with water flowing from Baldwin Valley into Bear Valley (Lower Bear Lake). Using these assumptions, the basal sand is inferred to represent a possible fluvial environment (channel bars? braided system?) in Baldwin Valley pre-95.9 ka. It is proposed that these sands predate the closure of Baldwin Valley by the Sugarloaf Fan, a large fanglomerate on the northerly side of Sugarloaf Mountain (Leidy, 2003). Sugarloaf Fan, itself, is postulated to have formed as a result of a large-scale landsliding event in Green Canyon. This debris subsequently separated Big Bear Valley and Baldwin Valley into two separate topographic depressions, the latter of which became host to Baldwin Lake ca. 95.5 ka (Leidy, 2003). Immediately following the damming of the valley, lacustrine sedimentation ensued covering the basal sands with organic poor, low carbonate clayey silts (Figure 2). The presence of this massive clayey silt possibly represents the initial flooding of the now isolated Baldwin Lake basin. The abruptness of this transition may also indicate that closure of the valley by the Sugarloaf Fan was single rapid event rather than a slow progression of the fan across the valley; however, our data cannot definitively prove the "rapid" closure hypothesis.

6.2 Milankovitch Timescale Hydrologic Variability

Reconstructing paleohydologic variability using sedimentological analyses such as magnetic susceptibility, total organic matter, total carbonate, and grain-size has been established as reliable in CSC, as well as in Baldwin Lake in particular (Blazevic et al., 2009; Kirby et al., 2006). A positive relationship has been noted between high lake levels and high magnetic susceptibility (Kirby et al., 2006); however, the relationship between low magnetic susceptibility values and lake level is less clear. Low values may be due to a reduction in the inflow of sediment to the basin, or the dissolution of magnetic materials under reducing conditions in a deep lake environment (Blazevic et al., 2009). Increasing total organic matter in a lake is considered a function of increasing water depth (Blazevic et al., 2009; Kirby et al., 2006). Total carbonate content is closely related to the precipitation and evaporation dynamics of the lake (Blazevic et al., 2009); that is, higher total carbonate values are generally indicative of an environment in which evaporation has occurred. Grain-size can be used to infer changes in the relative energy of the lake environment, as well as lake level (Blazevic et al., 2009). Within Baldwin Lake, deep lake conditions are inferred from fine-grained sediment, while coarser-grained sediment is indicative of a shallow to dry lake environment. With these relationships in mind, it is possible to differentiate between wetter and drier conditions at Baldwin Lake.

Since the lake's origin ca. 96,000 years ago, Baldwin Lake has been characterized by high amplitude, Milankovitch timescale hydrologic variability (Kirby et al., 2006; Blazevic et al., 2009). For example, during the last glacial (MIS 3), Baldwin Lake fluctuated between shallow and deep conditions, perhaps coeval to interstadial – stadial conditions as recorded in the Greenland ice core records. This is inferred from the presence of fine-grained sediment with high percentages of total organic matter and low percentages of total carbonate content. Wet conditions were made possible due to the interactions of the North American ice sheets and the polar front jet stream. As both the Cordilleran and Laurentide ice sheets grew over the continent, the polar front jet stream shifted southward with the glacial boundary causing increased winter precipitation in the CSC region (Kirby et al., 2013). In contrast, during both the last interglacial and the modern interglacial, the polar front jet stream returned to a more northern position, leading to decreased winter precipitation. Dryer conditions at Baldwin Lake during these intervals are inferred from the presence of coarse-grained, organic poor sediment with higher values of total carbonate content.

7. Conclusion

Core BDL12 provides the first terrestrial paleohydrologic record extending the past 96,000 years from CSC. The conclusions of this study in relation to the project's hypotheses and objectives are summarized below:

1. *The origin of Baldwin Lake is related to valley isolation as linked to extension of the Sugarloaf Fan.* The basal sediments of core BDL12, which consists of relatively clean sand, are interpreted to represent a fluvial environment, which existed ca. 96,000 years. The extension of the Sugarloaf Fan approximately 95.5 ka subsequently dammed the valley creating two distinct topographic depressions: Big Bear Valley and Baldwin Valley. Immediately following damming, the initial flooding of Baldwin Valley is inferred from the presence of organic poor, low carbonate clayey-silts.
2. *In general, deep lake conditions existed during full glacial conditions and shallow or dry lake conditions existed during interglacials.* The sedimentological analyses of core BDL12 reveal Milankovitch timescale changes in hydrologic conditions. Deep lake conditions in Baldwin Valley are inferred from the presence of fine-grained, organic rich, and carbonate poor sediment, while shallow to dry lake conditions are inferred from the presence of coarser-grained, organic poor, carbonate rich sediment. From the sediment record, it has been determined that wet, deep lake conditions existed during MIS 3, while shallow to dry lake conditions existed during MIS 1 and MIS 5.

References

Allen, B.D., Anderson, R.Y. (1993). Evidence from Western North America for Rapid Shifts in Climate During the Last Glacial Maximum. *Science*, 260(5116): 1920-1923.

Apple, Diana D. (2001). *Evolution of U.S. Water Policy: Emphasis on the West*. Publication. United States Forest Service. Web. 22 July 2013.

Bailey, H. P. (1966). *The Climate of Southern California*. Berkeley and Los Angeles: University of California Press.

Barry, R. G. (1983). Late-Pleistocene Climatology. *Late-Quaternary Environments of the United States*. Ed. H. E. Wright and S. C. Porter. Vol. 1: The Late Pleistocene. Minneapolis: University of Minnesota, pp. 390-407. Print.

Blazevic, M.A., Kirby M.E., Woods, A.D., Browne, B.L., Bowman, D.D. (2009). A sedimentary facies model for glacial-age sediments in Baldwin Lake, Southern California. *Sedimentary Geology*, 219: 151-168.

California Department of Water Resources (2003). California's groundwater: Bulletin 118, update 2003: Sacramento, Calif., State of California, The Resources Agency, Department of Water Resources, accessed on July 13, 2013, at URL: http://www.dpla2.water.ca.gov/publications/groundwater/bulletin118/basins/pdfs_desc/8- 9.pdf

Camarero, J.J., Gutiérrez, E. (2004). Pace and Pattern of recent treeline dynamics: response of ecotones to climatic variability in the Spanish Pyrenees. *Climatic Change*, 63(1-2): 181- 200.

Clark, P.U., Dyke, A.S., Shakun, J.D., Carlson, A.E., Clark, J., Wohlfarth, B., Mitrovica, J.X., Hostetler, S.W., McCabe, A.M. (2009). The Last Glacial Maximum. *Science* 325(710): 710-714.

Dean, W.E. (1974). Determination of Carbonate and Organic Matter in Calcareous Sediments and Sedimentary Rocks by loss on ignition: Comparison with other methods. *Journal of Sedimentary Petrology*, 44(1): 242-248

Flint, L.E., and Martin, P., eds., with contributions by Brandt, J., Christensen, A.H., Flint, A.L., Flint, L.E., Hevesi, J.A., Jachens, R., Kulongoski, J.T., Martin, P., and Sneed, M. (2012). Geohydrology of Big Bear Valley, California: Phase 1—Geologic Framework, Recharge, and Preliminary Assessment of the Source and Age of Groundwater: U.S. Geological Survey Scientific Investigations Report 2012–5100, 112 p.

Garcia, A.L., Knott, J.R., Mahan, S.A., Bright, J. (2013) Geochronology and paleoenvironment of pluvial Harper Lake, Mojave Desert, California, USA. *Quaternary Research*.

Hanak, E., Lund, J., Dinar, A., Gray, B., Howitt, R., Mount, J., Moyle, P., Thompson, B. (2011). *Managing California's Water: From Conflict to Reconciliation*. Publication. Public Policy Institute of California.

Heusser, L., Sirocko, F. (1997). Millennial pulsing of environmental change in southern California from the past 24 k.y: a record of Indo-Pacific ENSO events?. *Geology*, 25(3): 243-246.

Kirby, M.E., Lund, S.P., Poulsen, C.J. (2005). Hydrologic variability and the onset of modern El- Niño-Southern Oscillation: a 19,250-year record from Lake Elsinore, southern California. *Journal of Quaternary Science*, 20(3): 239-254.

Kirby, M.E., Lund, S.P., Bird, B.W. (2006). Mid-Wisconsin sediment record from Baldwin Lake reveals hemispheric climate dynamics (Southern CA, USA). *Palaeogeography, Palaeoclimatology, Palaeoecology*, 241: 267-283.

Kirby, M.E., Lund, S.P., Patterson, W.P., Anderson, M.A., Bird, B.W., Ivanovici, L., Monarrez, P., Nielsen, S. (2010). A Holocene record of Pacific Decadal Oscillation (PDO)-related hydrologic variability in Southern California (Lake Elsinore, CA). *Journal of Paleolimnology*, 44: 819-839.

Kirby, M.E., Feakins, S.J., Bonuso, N., Fantozzi, J.M., Hiner, C.A. (2013). Latest Pleistocene to Holocene hydroclimates from Lake Elsinore, California. *Quaternary Science Reviews*, 76: 267-283.

Leidy, R. (2003). Prehistoric and Historic Environmental Conditions in Bear Valley, San Bernardino County, California. EIP Associates, Sacramento, CA.

MacDonald, G. M., Stahle, D.W., Diaz, J.V., Beer, N., Busby, S.J., Cerano-Paredes, J., Cole, J.E., Cook, E.R., Endfield, G., Gutierrez-Garcia, G., Hall, B., Magan, V., Meko, D.M., Mendez-Perez, M., Sauchyn, D.J., Watson, E., Woodhouse, C.A. (2008). Climate Warming and 21st-Century Drought in Southwestern North America, Eos Trans. AGU, 89(9), 82–82.

Mantua, N.J., Hare, S.R. (2002). The Pacific Decadal Oscillation. *Journal of Oceanography*, 58: 35-44.

North Greenland Ice Core Project members (2004). High-Resolution Record Of Northern Hemisphere Climate Extending Into The Last Interglacial Period. *Nature*, 431: 147-151.

Owen, L.A., Finkel, R.C., Minnich, R.A., Perez, A.E. (2003). Extreme southwestern margin of late Quaternary glaciation in North America: Timing and controls. *Geology*, 31(8): 729-732.

Overpeck, J.T. (1996). Warm Climate Surprises. *Science*, 271(5257): 1820-1821.

Ryu, J.H., Svoboda, M.D., Lenters, J.D., Tadesse, T., Knutson, C.L. (2010). Potential extents for ENSO-driven hydrologic drought forecasts in the United States. *Climatic Change*, 101: 575-597.

Stout, M.L. (1976). Pleistocene and Holocene geology of Big Bear Valley San Bernardino Mountains, Calif. In: Stout, M.L. (Ed.), Association of Engineering Geologists. Association of Engineering Geologists, Los Angeles, CA, pp. 70-112.

Tudhope, A.W., Chilcott, C.P., McCulloch, M.T., Cook, E.R., Chappell, J., Ellam, R.M., Lea, D.W., Lough, J.M., Shimmield, G.B. (2001). Variability in the El Nino-Southern Oscillation Through a Glacial-Interglacial Cycle. *Science*, 291: 1511-1517.

Zhang, X., Wang, J., Zweiers, F.W., Groisman, P.Y. (2010). The Influence of Large-Scale Climate Variability on Winter Maximum Daily Precipitation of North America. *Journal of Climate*, 23: 2902-2915.

Evaluating a potential connection between the Late Jurassic-Early Cretaceous Osa Creek ring complex and the Blackrock andesite, southern Sierra Nevada, CA

Rebecca Steever, Katie Pickett and Nancy Chen
Advisor: Dr. Diane Clemens-Knott

Department of Geological Sciences, California State University, Fullerton

Abstract

Recent exploration of the western edge of the Kern Plateau (Tulare Co.; 36.17 degrees N lat.) reveals a hornblende andesite that is buttressed against plutonic rocks south of Blackrock Mountain. Neogene lavas and cones decorate this part of the Kern Plateau, but the presence of biotite granite dikes crosscutting the Blackrock andesite supports the intriguing possibility that this non-metamorphosed volcanic rock is instead Mesozoic in age. We first hypothesize that the Osa Creek ring complex (OCRC), located 2.5 km to the west, reveals the shallow footprint of a stratovolcano and evaluate this magmatic center as a possible source for the Blackrock volcanic deposit. Interfingering arcuate dikes of biotite leucogranite and biotite-hornblende diorite, with rare pyroxene- hornblende gabbro, comprise the ring complex. Mineralogy and whole-rock geochemistry is broadly consistent with a comagmatic origin for the ring complex and the andesite, which contains comingled basalt pods. U-Pb LA-ICPMS dating of zircon separated from a biotite granite dike cross-cutting the andesite yields a latest Jurassic to earliest Cretaceous minimum age for the hornblende andesite (mean U-Pb date = 161.1 + 3.4 Ma; youngest population = 146.1 + 2.3 Ma). In places, cuspate contacts separate the granite dikes from the andesite, suggesting the granite dikes are coeval with the surrounding andesite. Zircon crystals separated from a hypabyssal-textured OCRC granite yield Early Cretaceous dates (mean U-Pb date = 147.6 + 0.7 Ma; youngest population = 137.7 + 2.0 Ma). Core-rim zircon dates document growth of individual, zoned zircon crystals over c.a. 4 m.y. and support our preferred interpretation that the youngest U-Pb zircon age population provides the best constraint of emplacement age. If correct, the Osa Creek ring complex is a rare exposed example of Early Cretaceous magmatism, and is c.a. 10 m.y. younger than the Blackrock andesite. Similar reasoning would indicate that the Blackrock andesite is coeval with the hornblende-rich Summit Gabbro, which crops out across the Kern Plateau, and with the regionally extensive Independence dike swarm. Future geochemical and geochronologic studies of the Kern Plateau are aimed at revealing details of Sierra Nevada arc evolution across the Jurassic- Cretaceous boundary.

Determining the Nature of the Contact Between the Eastern Sierra Nevada Mountain Front and the Big Pine Volcanic Field South of Goodale Creek in Owens Valley, California

Jazmine N. Titular
Advisor: Dr. Phil Armstrong

Department of Geological Sciences, California State University, Fullerton

Abstract

The Sierra Nevada Frontal Fault Zone (SNFFZ) located along the western boundary of Owens Valley is comprised of numerous Quaternary normal faults. These faults generally are assumed to dip 60° and long-term extension rates for Owens Valley are calculated assuming these steep dips. Recent studies conducted in the Independence and Lone Pine areas of Owens Valley and farther north in the Bishop area show shallow dips of 26-52°. These shallow dips affect long-term extension rate calculations and the kinematic history of Owens Valley. Quaternary Big Pine Volcanic field (BPV) basalt deposits that crop out along the mountain front offer an opportunity to evaluate potential SNFFZ fault orientations in this area. This study analyzes the contact between the mostly granitic rocks of the Sierra Nevada Mountains and the BPV in the vicinity of Aberdeen from just south of Sawmill Creek and north to Goodale Creek. Working hypotheses for this contact include: (1) it is a depositional contact along the mountain front and (2) it is a fault contact. These hypotheses are tested by mapping the contact and surrounding rocks in detail. GPS locations of the contact were taken where the contact is clear. In general, the basalt-granite contact trends NNW, however north of Sawmill Creek the contact steps west consistent with the mountain front and the faults of the SNFFZ. Locally, especially south of Sawmill Creek, the basalt deposits are present on ridges with granitic basement in the intervening valleys so that the contact V's to show an eastward dip, consistent with east-dipping fault contact. Preliminary 3-point calculations along the contact suggest the contact dips about 25° E. In other areas the contact is diffuse with thin scoria deposits located uphill from the presumed location of the frontal fault. The mapping is being correlated to detailed Google Earth images to better define the relationships between basalt exposure and fault locations. Where the contact can be clearly defined, plane-fitting analysis using GPS- and Google Earth-derived x,y,z locations may refine potential fault orientations. This work will lead to a better understanding of the relationships between the BPV distribution and SNFFZ faults and may help constrain the SNFFZ orientation for kinematic analysis.

Documenting Recovery From A Deep Water, Middle Triassic Section From Fossil Hills Member, Humboldt Range Locality, Southern Canyon, NV

Christine Tong
Advisor: Dr. Nicole Bonuso

Department of Geological Sciences, California State University, Fullerton

Abstract

Physical and chemical processes constantly alters Earth's delicate systems since the beginning of this planet, which gives scientists a more difficult job to determine how life was Earth millions of years ago. Among the processes, climate change contributes a huge factor towards living organisms' existence. During the End-Permian mass extinctions, volcanic eruptions spewed basaltic lava widespread. This deformed continental structures, increased oceanic temperatures, caused anoxic conditions in the sea and eliminated nearly all-living species. This extinction marks a significant time in our geological time scale because it affected almost all species in various locations as well as change the climate. Research indicates that some taxa survived during the early Triassic but most died out before the Middle Triassic. This study aims to document the deep-water fossils at Fossil Hill from American Canyon, NV during the Middle Triassic. Documenting at local paleocommunity structure of the Middle Triassic is needed to fully understand long lasting re-diversification. The hand samples Dr. Bonuso's lab collected from Fossil Hill, Humbolt Range locality, South American Canyon, Nevada were made into petrographic thin sections. The relative abundance of fossils and sedimentary grain within the rock was analyzed via thin section point counting of grids 75mm (21x 12). From the thin sections, majority of the samples are wackestone containing mainly thin bivalves, cephalopods, foraminifera, ostracods, and radiolarians. Samples were also all cemented by calcite grain. These indices support a high diversity of organisms located in an upper ocean basin.

Introduction

A mass extinction occurred between the Permian-Triassic boundary (252 million years ago). Multiple leading hypotheses describe how this extinction occurred, but most scientists agree that the Siberian traps released volatiles into the area (Payne and Clapham, 2015). As a result, an abundance of CO_2 released into the atmosphere causing marine hypoxia and anoxia most likely caused the extinction. Long-term recovery after this mass extinction is largely understudied and thus studying the Middle-Triassic American Canyon Fossil will provide new within a deep marine environment. Foraminifera comprise most of the fossils. This study aims to identify and track foraminifera abundance through time. Observation of community reconstruction through recovery phase of the end Permian Mass Extinction in the deep ocean will be done. Here we record a more complete initial recovery stage after the End-Permian mass extinction by documenting the fossil that persist beyond the early Triassic. While other students complete paleoecological studies in Middle Triassic shallow water sections, this study focuses on completing a paleoecological study of a Middle Triassic deep-water section. Thus, this study will provide a key component in document the overall marine community. We expect to find a diverse and abundant foraminifera community preserved in grain-supported thin sections.

Background

Study Site and Study Importance

The study conducted in American Canyon, NV near Lovelock, NV ~70 miles northeast of Reno, once flourished as an ocean, but now resides as an arid environment.

This specific study area focuses on Fossil Hill member of the Middle Triassic Favret Formation because this will reveal how life recovered after the end-Permian Mass Extinction. Post-Permian mass extinction has shown to be the longest rate of recovery within the Phanerozoic. Some research suggest that "survival in interval" took place after the early Triassic so most taxas that survived the mass extinction eventually died off before they made it to the Middle Triassic (Twitchett, 2004). The importance of the location is that these foraminifera are from the Middle Triassic, which continues to live on to become the Modern fauna. This is a marker for a forever changed marine community. This deep-water section is only one piece of the puzzle adding to a complete documentation of paleoecological study from shallow to deep-water environment. The samples collected within the deep ocean area of the shelf, which contained foraminifera is important because foraminifera are relatively abundant and usually the only fossils found in deep waters.

Foraminifera

Foraminifera are shelled, heterotrophic protozoa and are also valuable to biostratigraphy (Benton, 2009). They live by floating and drifting within the water column. The calcareous test makes it well preserved in oceanic sediments. They are usually preserved in the benthic areas. Foraminifera are great still for biostratigraphic studies because they have short lifespan and they live all over the world. They have a well-defined biostratigraphy range which is important to dating the stratigraphic record (Fadel 2012).

Methods

Upon this study, literary research was done to have a more in-depth idea of the geological concepts such as mass extinction and foraminifera. From there I have a two-part analysis on a macro and micro level.

Hand Sample Macro-Analysis

Hand samples were collected in 2007 from Fossil Hill, NV by Dr. Nicole Bonuso and later made into thin sections. The rock samples were cut and polished using a vibrating LAP machine: making fossil identification suitable for hand sample observation.

Thin Section Micro-Analysis

A thin-section is a laboratory rock preparation necessary for petrographic microscope analysis (Figure 2). Bulk samples were cut into 45 x 70 mm billets and sent to Burnham Petrographic (a service company that prepares rock thin-sections). From the thin sections, ten were selected and digitally imaged at Dr. Coretti's lab at USC, using a Zeiss automated microscope. Images were scanned and stitched together on AxioVision SE64 program under 2,5x objective. After thin-sections were prepared, I classified the carbonate material using the Dunham classification scheme (Dunham, 1962), along with modifications (Ashton F. Embry III and Klovan, 1971), to determine overall carbonate environment. This method classifies carbonate rocks according to depositional texture: for example, grain-supported carbonate rocks that contain small amounts of mud are classified as packstone (Dunham, 1962). To document the skeletal and mineral grain components of the thin-sections, I used a grid system 75mm (21x12) known as the point count method, and record where the grids intersect skeletal material and mineral grains. For this study, the focus are on skeletal material, and major voids are omitted (Jaanusson, 1972).

These methods enhance visibility, provide randomization, and properly document thin sections. The goals of these methods are to provide data for determining the abundance of skeletal material within carbonate facies, which helps determine whether the rocks are fossil or grain supported and provide evidence that support or refute my hypothesis.

Results

Lithological Evidence

The samples collected were all either mudstone or wackestone; mud matrixes of all the samples were all at least 49% or greater. FHAM8 has the lowest micrite abundance with 49.33%. FHAM6 has a fossil concentration of 30.13% and FHAM8 has a fossil concentration of 47.12%. The average fossil abundance from the twelve samples is 18.86%. Five of the twelve samples contained a type of foraminifera (A or B; Table 2). Most samples contain poor lamination with an exception of FHAM4, FHAM5, FHAM7, and FHAM9. All samples have a granular calcite cement/crust.

Lithological Evidence

The samples collected were all either mudstone or wackestone; mud matrixes of all the samples were all at least 49% or greater. FHAM8 has the lowest micrite abundance with 49.33%. FHAM6 has a fossil concentration of 30.13% and FHAM8 has a fossil concentration of 47.12%. The average fossil abundance from the twelve samples is18.86%. Five of the twelve samples contained a type of foraminifera (A or B; Table 2). Most samples contain poor lamination with an exception of FHAM4, FHAM5, FHAM7, and FHAM9. All samples have a granular calcite cement/crust.

Abundance and Diversity

During the recovery of the Permian-Middle-Triassic extinction, many organisms started flourishing. These modern faunas in ocean basins consisted mainly of thin-shelled bivalves and radiolarians (Flugel, 2004). The results may not have the best representation of the variety of fossils in the area because the counted points did not represent the entire range of fossils in the samples. The counted points were to show the ratio of biomass to matrix in the sample (Table 1). Most samples are micrite-rich with smaller proportion of allochem (sparite and fossils). The samples all have 3 or more different types of fossils excluding FHAM4 (1 type) and FHAM7 (2 types) showing a general diversity of skeletal grains. Exclusion of FHAM4, thin shelled bivalves were the most abundant fossil in all the samples.

Discussion

Depositional Environment

During the Middle-Triassic, polar caps were warmer resulting in high sea levels. The study area was also submerged under the Panthalassic Ocean allowing fine-grain mud to settle and accumulate. Most of the samples contained a large percentage of micrite to skeletal grains, although most of the samples are wackestone instead of mudstone suggesting an environment with a high level of mud. The fossils identified are bivalves, cephalopods, foraminifera, ostracods and radiolarians. These mollusks microfossils have a biostratigraphy in the upper middle ocean floor. Samples also exhibited poor lamination with a few slides that had bioturbation. It can be inferred that the samples collected are from the toe of the slope (SMF3) due to the diversity of fossils but contained mostly wackestone.

Conclusion

Based on the abundance count, during the Middle-Triassic there was a diverse stratum of mollusks up to six types in a sample. This may have occurred during the long period of recovery, where the study area remained undersea due to melting polar caps and rifting of Pangaea. This created a stable ocean above the study area for these benthic organisms to prosper.

There is also a strong indication that the study area may have been located on the upper ocean basin due to the amount of micrite in all the samples with the amount of lamination (Flugel, 2004). The presence of foraminifera is also a good indicator of depth due to its ability to biostratigraphic range. Conclusions can be made that the Fossil Hill member located in the Humboldt Range locality was once undersea in the upper basin ocean compared to its current arid environment. Sea levels have lowered allowing us to observe the types of organisms which once prospered.

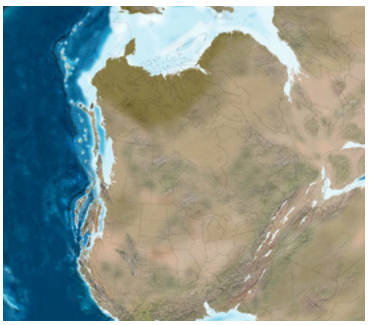

***Figure 1**. Paleogeographic map during the Middle-Triassic focusing on North America.*

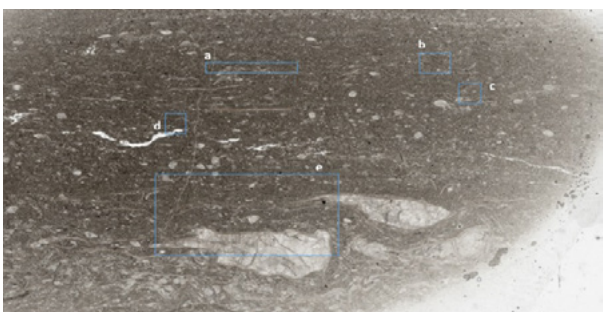

***Figure 2:** A thin section of foraminifera FHAM1. [a] Thin bivalve, [b] ostracod, [c] burrow of radiolarians, [d] foarmA, [e] cephalopod.*

Samples Name (Points counted)	Rock Classification (Dunham)	Fossils (Type and Abundance)	Concentration %	Full Description (color, texture % allochems, types of fossils)
FHAMI (208)	wackestone	• 8.65% bivalves • 6.73% cephalopods • 6.73% cephalopods (internal) • 1.44% ostracods • 0.48% foram A	**69.71% matrix 24.04% fossil**	• Light grey brown, poorly laminated, the fossils line up but they aren't in a good formation • Cephalopods, bivalves, foram A, foram B, radiolarians, ostracods
FHAM2B (207)	**wackestone**	• 9.18% bivalves • 2.89% radiolarians • 1.93% cephalopod • 1.45% foram A • 0.48% cephalopod (internal) • 0.48% ostracod	**75.85% matrix 16.42% fossil**	• Poorly laminated but still laminated in a linear fashion • Cephalopods, bivalves, ostracods, foram A, radiolarians
FHAM3 (203)*	**wackestone**	• 6.83% bivalves • 2.95% cephalopods • 1.47% foram A	**62.07% matrix 11.33% fossil**	• Poorly laminated • Cephalopods, bivalves, foarm A, radiolarians, ostracods
FHAM4 (187)	**mudstone**	• 2.14% cephalopod • 1.07% bivalves	**93.58% matrix 3.21% fossil**	• Bioturbated; the top left corner has another matrix going on • Bivalves, radiolarians
FHAM5 (140)	**mudstone**	• 3.78% bivalves • 3.57% radiolarians • 2.14% cephalopod	**94.29% matrix 2.14% fossil**	• Bioturbated/homogeneous matrix • Cephalopods, bivalves
FHAM6 (156)	**wackestone**	• 23.72% bivalves • 5.13% cephalopod • 0.64% radiolarians • 0.64% ostracods	**62.18% matrix 30.13% fossil**	• Laminated • Cephalopods, bivalves, radiolarians, ostracods
FHAM7 (249)	**wackestone**	• 12.46% bivalves	**61.85% matrix 16.46% fossil**	• Bioturbated • Bivalves, radiolarians, foarm A
FHAM8 (225)*	**wackestone**	• 45.77% bivalves • 0.44% foram A • 0.44% radiolarians • 0.44% ostracods	**49.33% matrix 47.12% fossil**	• Wavy lamination • Cephalopods, bivalves, radiolarians, foram A, foarm B
FHAM10 (203)*	**wackestone**	• 21.18% bivalves • 0.49% cephalopod • 0.49% cephalopod (internal) • 0.49% radiolarians	**64.53% matrix 23.15% fossil**	• Poorly laminated • Bivalves, foarm A, ostracods
FHAM11 (142)	**wackestone**	• 8.45% bivalves	**66.90% matrix 8.45% fossil**	• Poorly laminated • Cephalopods, bivalves
FHAM12* (225)	**wackestone**	• 10.22% bivalve • 2.67% cephalopod (internal) • 2.22% cephalopod • 1.78% ostracods	**73.78% matrix 16.89 fossil**	• Poorly laminated • Bivalves, ostracods, foram A, radiolarians
FHAM13 (229)	**wackestone**	• 21.40% bivalves • 2.62% cephalopod • 1.75% cephalopod (internal) • 0.44% foram A • 0.44% foram B • 0.44% ostracods	**60.70% matrix 27.07% fossil**	• Poorly laminated some bioturbation • Cephalopods, bivalves, foarm A, ostracods

Table 1: *Summary table of fossil abundance.*

References

Ashton F. Embry III, and Klovan, J. E., 1971, A Late Devonian Reef Tract on Northeastern Banks Island, N.W.T.: Bulletin of Canadian Petroleum Geology, v. 19, no. 4, p. 730-781.

Benton, M., & Harper, D. (2009). *Introduction to paleobiology and the fossil record* (1st ed.). Chichester, West Sussex, UK: Wiley-Blackwell.

Dunham, R. J., 1962, Classification of Carbonate Rocks According to Depositional Texture., in Hamm, W. E., ed., Classification of Carbonate Rocks, A Symposium. , American Association of Petroleum Geologists, p. 108-121.

Embry, A. F., and Klovan, J. E., 1971, A Late Devonian reef tract on Northeastern Banks Island, NWT: Canadian Petroleum Geology Bulletin, v. 19, p. 1-38.

Fadel, M. (2012). Biostratigraphic and geological significance of planktonic foraminifera. Amsterdam: Elsevier.

Jaanusson, V., 1972, Constituent analysis of an Ordovician limestone: Palaios, v. 5, p. 217-237. Knoll, Andrew H., Richard K. Bambach, Jonathan L. Payne, Sara Pruss, and Woodward W. Fischer. "Paleophysiology and end-Permian mass extinction." Science Direct 256: 295-313. Web. 11 Feb. 2007.

Payne, Jonathan L., and Matthew E. Clapham. "End-Permian Mass Extinction in the Oceans: An Ancient Analog for the Twenty-First Century?" Annual Review of Earth and Planetary Sciences 40.2012 (2012): 89-111. Web. 14 Jan. 2015.

Silberling, N.J. and Irwin, W. P., 1962. Stratigraphic distribution of Middle Triassic ammonites at Fossil Hill, Humboldt Range, Nevada: Jour. Paleontology, v 36. P. 153-160

Twitchett, R., Krystyn, L., Baud, A., Wheeley, J., & Richoz, S. (2004). Rapid marine recovery after the end-Permian mass-extinction event in the absence of marine anoxia. Geology,32(9), 805-808. doi:10.1130/G20585.1

A Cluster Theorem for Generalized Toeplitz Matrices

Allen Alvarez
Advisor: Dr. Tyler McMillen

Department of Mathematics, California State University, Fullerton

Abstract

We generalize a well known result about the clustering properties of the eigenvalues of Toeplitz matrices to generalized Toeplitz matrices. The class of matrices we are considering are generated by a symbol of two variables $a(s,t)$. We show that the extended range of $a(s,t)$ contains all of the eigenvalues except at most $o(n)$ of them.

I. Introduction

Toeplitz matrices have been studied extensively since the early 1900s and are arguably the most important matrices in applications. Consequently, there have been several results about Toeplitz matrices, many of which aid in understanding the asymptotic distribution of the eigenvalues. We intend to understand the asymptotic behavior of eigenvalues of a larger class of matrices introduced by Kac, Murdock, and Szegő [4, 2] called *generalized Toeplitz matrices*, defined as follows. Let $a(s,t)$ (the symbol of the matrix) be a complex valued function such that the Fourier series

$$a(s,t) = \sum_{k=-\infty}^{\infty} \hat{a}_k(s) e^{ikt} \tag{1}$$

is defined on $[0,\ 1] \times [-\pi,\ \pi]$. For each integer n, define the $n \times n$ matrix

$$T_n(a) = \left[\hat{a}_{j-i} \left(\frac{i+j}{2n+2} \right) \right]_{i,j=0}^{n-1} \tag{2}$$

(We will also use T_n for $T_n(a)$ throughout the paper.)

We impose the following condition throughout this paper

$$\sum_{k=-\infty}^{\infty} ||a_k|| < M < \infty \tag{3}$$

where $\|a_k\| = \sup_{s\in[0,1]} |a_k(s)|$. We denote the eigenvalues of T_n by

$$\lambda_1(T_n), \lambda_2(T_n), \lambda_3(T_n), \ldots, \lambda_n(T_n).$$

The goal of this paper is to find a cluster for the eigenvalues of T_n. That is, we want to find a set in the complex plane such that any of its neighborhoods contains all of the eigenvalues of T_n, except at most $o(n)$ of them. We begin by defining the essential range $\mathcal{R}(a)$, by:

$$\mathcal{R}(a) := \left\{ z \in \mathbb{C} : m\left\{ a^{-1}(D(z,r)) \right\} > 0, \forall r > 0 \right\}, \tag{4}$$

where $m(E)$ is the Lebesgue measure of E, and $D(z, r)$ denotes an open disk in the complex plane with radius r centered at z. In other words, the essential range is the range minus isolated points.

We will focus our attention on symbols $a(s,t)$ where $a \in L^\infty$, the spaces of all essentially bounded complex valued functions on $(-\pi, \pi)$. Consequently, $\mathcal{R}(a)$ is a compact set; hence its complement has just one unbounded connected component. Thus,

$$\mathbb{C} \backslash \mathcal{R}(a) =: U_0 \cup \bigcup_{j=1}^{\infty} U_j, \qquad U_i \cap U_j = \emptyset \text{ if } i \neq j, \tag{5}$$

where each U_j, $j \geq 1$, is a connected bounded open set, and U_0 is an unbounded connected open set. Using (5) we can define the *extended range* of the symbol a as

$$\mathcal{ER}(a) := \mathbb{C} \backslash U_0$$

Hence, the *extended range* $\mathcal{ER}(a)$ is the union of the range of a and all the bounded components of its complement. It is the range and everything inside the range.

We can now state the main result of this paper. The following is a generalization of a result of Paolo Tilli [6].

Theorem 1. *If $a(s,t)$ satisfies (3), then the extended range $\mathcal{ER}(a)$ is a cluster of the eigenvalues of $T_n(a)$. Then for any open set A containing $\mathcal{ER}(a)$ there holds*

$$\lim_{n \to \infty} \frac{\gamma(A, n)}{n} = 1, \tag{6}$$

where $\gamma(A,n)$ "counts" how many eigenvalues of T_n lie inside A.

This theorem states that any ε-neighborhood of $\mathcal{ER}(a)$ contains all of the eigenvalues of T_n except at most $o(n)$ of them.

2. Prerequisite Statements

We assume $a : [0,1] \times (-\pi, \pi) \to \mathbb{C}$ is essentially bounded and we denote T_n the $n \times n$ generalized Toeplitz matrix associated to a.

The following definition is used heavily throughout the paper.

Definition 1. *Given a matrix A, A^* denotes the Hermitian conjugate, and $||A||_F$ denotes the Frobenius norm given by $||A||_F^2 := trA^*A$.*

The following definition is used in Gershgoran's disc theorem. For a proof, see [3], p. 344.

Definition 2. *For an $n \times n$ matrix A, we define the ith Gerschgorin disk C_i to be the disk in the complex plane with center a_{ii} and radius*

$$r_i = \sum_{j \neq i} |a_{ij}|$$

that is,

$$C_i = \{z \in \mathbb{C} : |z - a_{ii}| \leq r_i\}$$

Theorem 2 (Gershgorin's disc theorem). *Let $A \in M_{n \times n}(\mathbb{C})$. Then every eigenvalue of A is contained in a Gerschgorin disk.*

The importance of this theorem is that it enables us to show that all of the eigenvalues of T_n lie in a compact set. The existence of this set is vital to proving the main results.

Lemma 1. *There exists a compact set G such that all eigenvalues of T_n are in G for all n = 1,2,3,....*

Proof. Since we are considering generalized Toeplitz matrices subject to the condition (3), Gershgorin's Theorem implies all the eigenvalues of T_n lie in the disk of radius $2M$ centered at the origin. □

For the proof of the main result we need to estimate the eigenvalues of polynomials of $P(T_n)$. For this we will use the following result which is proven in [1].

Theorem 3. *Let $\{T_n(a)\}$ be a sequence of generalized Toeplitz matrix. Then for any $r, k \in \mathbb{N}$, we have*

$$\lim_{n \to \infty} \frac{1}{n} Tr \left[T_n^r \left(T_n^*\right)^k \right] = \frac{1}{2\pi} \int_{-\pi}^{\pi} \int_0^1 a^r(s,t) \overline{a^k(s,t)} \, ds \, dt \tag{7}$$

From this theorem, we deduce the following lemma.

Lemma 2. *Let $P(z)$ be a polynomial in the complex variable z. If $\{T_n\}$ is a generalized Toeplitz matrix, then there holds*

$$\lim_{n \to \infty} \frac{1}{n} ||P(T_n)||_F^2 = \frac{1}{2\pi} \int_{-\pi}^{\pi} \int_0^1 |P(a(s,t))|^2 \, ds \, dt \tag{8}$$

Proof. Letting $P(z) = \sum_{i=0}^{d} c_i z^i$, we obtain

$$\frac{1}{n}||P(T_n)||_F^2 = \frac{1}{n}Tr\left[P(T_n)P(T_n)^*\right] = \frac{1}{n}\sum_{r,s=0}^{d} c_r\overline{c_s}Tr\left[(T_n^r T_n^{*k})\right]$$

Taking the limit, we have from (7)

$$\begin{aligned}\lim_{n\to\infty}\frac{1}{n}||P(T_n)||_F^2 &= \sum_{r,s=0}^{d} c_r\overline{c_s}\frac{1}{2\pi}\int_{-\pi}^{\pi}\int_0^1 a^r(s,t)\overline{a^k(s,t)}\,ds\,dt \\ &= \frac{1}{2\pi}\int_{-\pi}^{\pi}\int_0^1 |P(a(s,t))|^2\,ds\,dt.\end{aligned}$$

□

Next we have the key lemma used in the proof of the main result.

Lemma 3. *Let P be a complex polynomial in $\mathbb{C}$ and T_n be a generalized Toeplitz matrix, we have*

$$\sum_{j=1}^{n}|P(\lambda_j(T_n))|^2 \le ||P(T_n)||_F^2$$

Proof. We use the Schur's decomposition on $P(T_n)$. We have $P(T_n) = UTU^*$, where U is a unitary matrix and T is in upper triangular matrix. We have

$$\begin{aligned}P(T_n)P(T_n)^* &= UTU^*UT^*U^* \\ &= UTT^*U^*\end{aligned}$$

Which implies

$$tr(P(T_n)P(T_n)^*) = tr(TT^*)$$

Thus,

$$\begin{aligned}||P(T_n)||_F^2 &= ||T||_F^2 \\ &= \sum_{i,j}|t_{ij}|^2 \\ &= \sum_i |t_{ii}|^2 + \text{nonnegative terms} \\ &= \sum |\lambda|^2 + \text{nonnegative terms}\end{aligned}$$

Where the last sum is the sum of all the squares of the eigenvalues of $P(T_n)$. This implies, $\sum|\lambda|^2 \le ||P(T_n)||_F^2$. Therefore, $\sum_{j=1}^{n}|P(\lambda_j(T_n))|^2 \le ||P(T_n)||_F^2$.

□

The proof of the cluster theorem makes use of Mergelyan's Theorem, a proof of which can be found in [5], p. 390.

Theorem 4 (Mergelyan's Theorem). *A function F, continuous on a compact set K and holomorphic in its interior, can be uniformly approximated on K by polynomials, provided $\mathbb{C}\backslash K$ is connected.*

3. Proof of Cluster Theorem

Proof of Theorem 1. Choose some $z \notin \mathcal{ER}(a)$. Since $\mathcal{ER}(a)$ is closed, there exists some small open disk D centered at z such that $\overline{D} \cap \mathcal{ER}(a) = \emptyset$. Let $K = \mathcal{ER}(a) \cup \overline{D}$ and define F on K as

$$f(\xi) = \begin{cases} 1 & \text{if } \xi \in \overline{D} \\ 0 & \text{if } \xi \in \mathcal{ER}(a). \end{cases}$$

Since $\mathbb{C}\backslash K$ is connected, by the Mergelyan theorem we can find for every $\epsilon \in (0, 1)$ we can uniformly approximate F with a polynomial P so that $|P(\xi) - F(\xi)| \leq \epsilon$, for all $\xi \in K$. Let $\gamma(n)$ count how many eigenvalues of T_n lie inside D and let χ_D be the characteristic function of D. Since $1 - \epsilon \leq |C(\lambda)|$ whenever $\lambda \in D$, we have

$$\begin{aligned}(1-\epsilon)\gamma(n) &\leq \sum_{j=1}^{n} \chi_D(\lambda_j(T_n)|P(\lambda_j(T_n))| \\ &\leq \left(\sum_{j=1}^{n} \chi_D(\lambda_j(T_n)\right)^{1/2} \left(\sum_{j=1}^{n} |P(\lambda_j(T_n))|^2\right)^{1/2} \\ &= \lambda(n)^{1/2} \left(\sum_{j=1}^{n} |P(\lambda_j(T_n))|^2\right)^{1/2}\end{aligned}$$

Since $P(\lambda_j(T_n)) = \lambda_j(P(T_n))$, squaring we obtain

$$(1-\epsilon)^2\gamma(n) \leq \sum_{j=1}^{n} |P(\lambda_j(T_n))|^2 \leq ||P(T_n)||_F^2$$

The inequality above follows from lemma 3. Dividing by n and taking limits, we have, from Lemma 2,

$$\limsup_{n\to\infty}(1-\epsilon)^2\frac{\gamma(n)}{n} \leq \frac{1}{2\pi}\int_{-\pi}^{\pi}\int_{0}^{1} |P(a(s,t))|^2 ds dt \leq \epsilon^2$$

The last inequality holds since $|P(z)| \leq \epsilon$ whenever $z \in \mathcal{ER}(a)$. From the arbitrariness of ϵ, the last inequality implies $\gamma(n) = o(n)$.

Consider an arbitrary open set $A \supset \mathcal{ER}(a)$. We will show that at most $o(n)$ eigenvalues of T_n lie outside of A.

By lemma 1 there exists a compact set G such that all the eigenvalues of T_n lie inside G. Let $C := G \cap (\mathbb{C}\backslash A)$. If C is empty, then all of the eigenvalues of T_n lie inside A and we are done. If C is nonempty, for every $z \in C$ lies within some open disk D_z centered at z which contains only $o(n)$ eigenvalues of T_n. Thus, C can be covered by a family of open disks $\{D_z\}_{z\in c}$, each of which contains at most $o(n)$ eigenvalues. C being a compact set, a finite sub-covering exists; hence C itself contains only $o(n)$ eigenvalues of T_n. Since $C \cup A$ contains all the eigenvalues of T_n, equation (6) follows and the proof is complete since A was an arbitrary open set containing $\mathcal{ER}(a)$. □

4. Future Work

We have established that the extended range of a is a cluster for the eigenvalues of T_n; the question now becomes, What are the properties of this cluster? In the Toeplitz case the entries are taken from a symbol of one variable and the essential range is known to be a curve. For generalized Toeplitz matrices we have entries being taken from a symbol of two variables, so the essential range is more difficult to visualize. We will explore this numerically using MATLAB.

References

[1] Alain Bourget and Tyler McMillen. A first Szegő's limit theorem for a class of non- toeplitz matrices. Preprint.

[2] Ulf Grenander and G´abor Szegő's. T*oeplitz forms and their applications*. Chelsea Pub- lishing Co., New York, second edition, 1984.

[3] Roger A. Horn and Charles R. Johnson. *Matrix analysis*. Cambridge University Press, Cambridge, 1990. Corrected reprint of the 1985 original.

[4] M. Kac, W. L. Murdock, and G. Szegő. On the eigenvalues of certain Hermitian forms. *J. Rational Mech. Anal.*, 2:767–800, 1953.

[5] Walter Rudin. *Real and Complex Analysis*. McGraw-Hill Book Co., New York, third edition, 1987.

[6] Paolo Tilli. Some results on complex Toeplitz eigenvalues. *Journal of Mathematical Analysis and Applications*, 239(2):390–401, 1999.

On *k*th Roots in Semigroups of Order-preserving Partial Permutations

Ulysses Alvarez
Advisor: Dr. Scott Annin

Department of Mathematics, California State University, Fullerton

Abstract

This paper investigates the semigroup of partially ordered injections of an n-element set, $\mathrm{POI}(n)$, which is a submonoid of the symmetric inverse monoid. We present results aimed at characterizing the elements of $\mathrm{POI}(n)$ which possess k^{th} roots for fixed integers n and k. Using the software package Groups, Algorithms, and Programming (GAP), we collected data that led to several results in this paper involving the relationships between the domain and range patterns of the elements in $\mathrm{POI}(n)$. Through these results, among other things, we are able to completely characterize the elements of $\mathrm{POI}(n)$ for $n < 8$ that have square roots in $\mathrm{POI}(n)$.

I. Introduction

Classification of roots of elements in a variety of mathematical structures has been of growing interest in recent years. Useful applications in fields such as matrix theory and cryptography are well-known. This paper is an extension of recent work which characterized the elements in specific groups and semigroups that possess k^{th} roots (see [2] and [3]). In particular, this problem has been studied in the symmetric group, the alternating group, the symmetric inverse monoid, among others. In this paper, we shall discuss the same problem for the semigroup of order-preserving partial permutations. From now on, we denote this as $\mathrm{POI}(n)$.

$\mathrm{POI}(n)$ is an algebraic structure known as a semigroup. Before introducing related properties and examples of semigroups, we recall the definition of a more familiar algebraic structure closely related to semigroups, groups.

A **group** is a nonempty set G equipped with a binary operation * that satisfies the following axioms:

1. **Closure**: If $a \in G$ and $b \in G$, then $a * b \in G$.

2. **Associativity**: $a * (b * c) = (a * b) * c$ for all $a, b, c \in G$.

3. **Existence of an Identity**: An element $e \in G$ is called the identity element if $a * e = a = e * a$ for every $a \in G$.

4. **Existence of Inverses**: For each $a \in G$, there is an inverse element $d \in G$ such that $a * d = e$ and $d * a = e$.

The most important example of a group for our purposes in this paper is the symmetric group. It consists of the permutations of the set $\{1, 2, \ldots, n\}$. Its elements are expressible in a traditional two-line notation which we will later adapt for use in the semigroup POI(n). If the reader wishes to learn more about the symmetric group, please refer to [7]. A **semigroup** is a nonempty set S equipped with binary operation * that satisfies the first two axioms of a group, closure and associativity. Thus, every group is also a semigroup. However, there are many other semigroups, such as bands and the symmetric inverse monoid, that are not groups. By excluding the group properties of the existence of an identity element and the inverse elements, semigroups are a much more broad class of abstract algebraic structures than groups. For instance, while there are only two non-isomorphic groups with six elements, there are 15,793 non-isomorphic semigroups with six elements [6]! The semigroup of interest in this paper, POI(n), is a subsemigroup of the symmetric inverse monoid. The **symmetric inverse monoid**, denoted SIM(n), is an algebraic structure consisting of all partial permutations of the set $\{1, 2, \ldots, n\}$.

The collection POI(n) of **order-preserving partial permutations** inherits associativity from SIM(n) and is readily seen to be closed, hence forms a submonoid. The traditional two-line notation, often used to express elements of the symmetric group, is convenient for expressing the elements of POI(n) as well. This is simply because in order to determine whether an element of SIM(n) is also in POI(n), the integers listed on the bottom row have to be in increasing order. Let us understand this notation with an example.

Example 1.1. Consider $\alpha_1 = \begin{pmatrix} 1 & 2 & 3 & 4 & 5 & 6 & 7 \\ 4 & 5 & 6 & - & - & - & - \end{pmatrix}$,where 1 maps to 4, 2 maps to 5, 3 maps to 6, and 4, 5, 6, 7 map to nothing. Since the bottom row also has the integers increasing from left to right, we know that not only is α_1 in SIM(7), but it is also in POI(7).

Now, let $\alpha_2 = \begin{pmatrix} 1 & 2 & 3 & 4 & 5 & 6 & 7 \\ 2 & 4 & 7 & 5 & - & - & 6 \end{pmatrix}$,where 1 maps to 2, 2 maps to 4, 3 maps to 7, 4 maps to 5, 7 maps to 6, and 5, 6 map to nothing. Note that on the bottom row, if we read the numbers from left to right, 7 decreases to 5. This implies that while α_2 is in SIM(7), it is not in POI(7). Note here that α_2 is a square root of α_1, since

$$\begin{aligned} \alpha_2^2 &= \begin{pmatrix} 1 & 2 & 3 & 4 & 5 & 6 & 7 \\ 2 & 4 & 7 & 5 & - & - & 6 \end{pmatrix}^2 \\ &= \begin{pmatrix} 1 & 2 & 3 & 4 & 5 & 6 & 7 \\ 4 & 5 & 6 & - & - & - & - \end{pmatrix} \\ &= \alpha_1. \end{aligned}$$

However, α_2 does not belong to POI(7). Thus, α_1 has a square root in SIM(7), but, as the results later in this paper show, no square root in POI(7).

In terms of this notation, the definition of SIM(n) becomes more apparent. For example, *partial* is reflected by possible dashes in the second row, which means that the integer above it maps to nothing, and *permutation* means we cannot have any repeating numbers in the second row. For POI(n), the additional requirement is that the distinct elements appearing on the bottom row appear in strictly increasing order.

Definition 1.2. Let $\sigma \in \text{SIM}(n)$. The **rank** of σ is defined by the size of its domain or, equivalently, the size of its range.

Note that in Example 1.1, the rank of α_2 is 3 and the rank of α_1 is 5.

In order to better understand the structure of POI(n) and investigate our problem about the k^{th} roots described at the outset, we can gather data by using the GAP (Groups, Algorithms, Programming) program [5], which is a free software for computational discrete algebra. GAP generates the elements of POI(n) for small $n \in \mathbb{N}$. We can then raise each of these elements to the k^{th} power. The resulting list of kth powers constitutes precisely the set of elements that have kth roots. The size of POI(n), given by $\sum_{j=0}^{n} \binom{n}{j}^2$, grows rather quickly as the value of n is increased. Therefore, it is too time-consuming to collect the necessary data by hand. Here is GAP code that creates the list of k^{th} powers in POI(n) (Note that POI(n) is already a built-in semigroup in GAP):

$$
\begin{aligned}
gap > \; & squareElements := function(n, k) \\
& > local\ m, i, y; \\
& > m := Size(POI(n)); \\
& > y := []; \\
& > for\ i\ in\ [1..m]\ do \\
& > y[i] := Elements(POI(n))[i] \wedge k; \\
& > Print(y[i]); \\
& > od; \\
& > end;
\end{aligned}
$$

Note that *Size*(POI(n)) gives the number of elements in POI(n), and y[i] := *Elements*(POI(n))[i]^2 squares all of the individual elements and places the results in a list for the chosen value of n. GAP uses a different notation than the two-line notation we showed in Example 1.1 to present the elements of POI(n):

Notation. If $\sigma \in \text{POI}(n)$ and if $\text{rank}(\sigma) = m$, then GAP denotes σ as follows:

$$\sigma = [a_1, a_2, \ldots, a_m] \to [b_1, b_2, \ldots, b_m], \tag{1.1}$$

where $a_1, a_2, \ldots, a_m, b_1, b_2 \ldots, b_m \in \{1, 2, \ldots, n\}$, $a_i < a_{i+1}$, and $b_i < b_{i+1}$, for each $i \in \{1, 2, \ldots, m-1\}$.

Definition 1.3. Let $\sigma \in \text{SIM}(n)$ such that $\text{rank}(\sigma) = 0$. Then σ is the **null element** of SIM(n), which GAP denotes as $\langle$null of SIM(n)$\rangle$.

Definition 1.4. If $\sigma \in \text{POI}(n)$ with $\text{rank}(\sigma) = m$ and if $a_i = b_i$ for each $i \in \{1, 2, \ldots, m\}$, then σ is a **partial identity**. GAP denotes such elements as $\langle$ identity on $[a_1, a_2, \ldots, a_m]$ $\rangle$.

Remark. For every $\sigma \in \mathrm{POI}(n)$, there exists a positive integer k such that σk is a partial identity element or the null element.

Example 1.5. As an illustration of the Remark above, note that

$$([1,2,3,4,5] \to [1,2,3,5,6])^3 = \langle \text{identity on } [1,2,3] \rangle$$
$$\text{and}$$
$$([1,2,3,4] \to [2,3,4,5])^5 = \langle \text{null of SIM}(7) \rangle.$$

In [3], a theorem was proven that classifies the elements of SIM(n) that have k^{th} roots. We want to develop results that allow us to classify elements of POI(n) which have k^{th} roots in POI(n). Of course, for all elements of POI(n), [3] addresses whether or not a k^{th} root in SIM(n) exists. But our concern in this paper is whether or not such a k^{th} root exists in the subsemigroup POI(n).

Now that we have established the necessary definitions and notation, we are ready to introduce some tools that will help us approach our problem.

2. Preliminary Results

We begin this section with a useful remark that is self-evident, but which is worth recording since it will be used repeatedly in the results that follow.

Remark. Let $\tau \in \mathrm{POI}(n)$ and c be in the domain of τ. Then, since τ is order-preserving, observe that the sequence

$$\{c, \tau(c), \tau^2(c), \ldots, \tau^k(c), \ldots\} \tag{2.1}$$

is either constant, strictly increasing, or strictly decreasing. In the first case, the constant sequence carries on in an infinite sequence, whereas in the latter two situations, the number of defined terms of the sequence is necessarily finite.

Example 2.1. Let $\tau = \begin{pmatrix} 1 & 2 & 3 & 4 & 5 & 6 \\ - & 1 & 2 & 4 & 6 & - \end{pmatrix} \in \mathrm{POI}(6)$. Then for $c = 3$, the sequence (2.1) is strictly decreasing, for $c = 4$ it is constant, and for $c = 5$ it is strictly increasing.

Definition 2.2. Let $\sigma = [a_1, a_2, \ldots, a_m] \to [b_1, b_2, \ldots, b_m] \in \mathrm{POI}(n)$. Then, $\sigma^{-1} = [b_1, b_2, \ldots, b_m] \to [a_1, a_2, \ldots, a_m]$ is an **inverse** of σ. Note that $(\sigma^{-1})^{-1} = \sigma$, and that

$$\sigma \circ \sigma^{-1} = \langle \text{identity on } [b_1, b_2, \ldots, b_m] \rangle$$
$$\text{and}$$
$$\sigma^{-1} \circ \sigma = \langle \text{identity on } [a_1, a_2, \ldots, a_m] \rangle.$$

The next lemma is a direct consequence of Definition 2.2.

Lemma 2.3. *Let $k \geq 2$ and $\sigma \in \mathrm{POI}(n)$. Then, σ has a k^{th} root in $\mathrm{POI}(n)$ if and only if σ^{-1} has a k^{th} root $\mathrm{POI}(n)$.*

Proof By symmetry it suffices to prove the forward direction. Suppose that σ has a k^{th} root in $\mathrm{POI}(n)$, say τ. That is, $\tau^k = \sigma$. Now it is easy to see that $(\tau^{-1})^k = (\tau^k)^{-1} = \sigma^{-1}$, which proves that σ^{-1} has a k^{th} root in $\mathrm{POI}(n)$. □

Lemma 2.4. *Let $k \geq 2$ and $\sigma = [a_1, a_2, \ldots, a_m] \to [b_1, b_2, \ldots, b_m] \in \mathrm{POI}(n)$. If there exists an i such that $1 \leq i \leq m$ and $0 < |a_i - b_i| < k$, then σ does not have a k^{th} root in $\mathrm{POI}(n)$.*

Proof By way of contradiction, suppose that σ has a k^{th} root in $\mathrm{POI}(n)$, say τ, and that there exists an i with $1 \leq i \leq m$ such that $0 < |a_i - b_i| < k$. If $a_i < b_i$, then the sequence (2.1) for $c = a_i$ is strictly increasing. This implies that $b_i - a_i \geq k$ since for each $j \geq 0, \tau^{j+1}(a_i)$. Thus, we have a contradiction. If $a_i > b_i$, we obtain a similar contradiction. □

Example 2.5. The element $[1, 4, 6, 7] \to [3, 5, 9, 10]$ does not have a square root in POI(10), and $[3, 5, 6, 7, 8, 9, 10] \to [103, 104, 106, 107, 108, 109, 110]$ does not have a 100^{th} root in POI(110) by Lemma 2.4.

Lemma 2.6. *Let $k \geq 2$ and $\sigma = [a_1, a_2, \ldots, a_m] \to [b_1, b_2, \ldots, b_m] \in \mathrm{POI}(n)$. If $a_i = b_i$ or $a_{i+1} = b_i$ for some $1 \leq i \leq m-1$, then σ does not have a k^{th} root in $\mathrm{POI}(n)$.*

Proof By way of contradiction, suppose $\sigma = \tau^k$ for some $\tau \in \mathrm{POI}(n)$. This implies that for each $j \in \{1, \ldots, m\}$ we have $\tau^k(a_j) = b_j$. Fix $i \in \{1, \ldots, m-1\}$. If $a_i = b_{i+1}$, then the sequences

$$\{a_i, \tau(a_i), \tau^2(a_i), \ldots, \tau^{k-1}(a_i), b_i\} \tag{2.2}$$

and

$$\{a_{i+1}, \tau(a_{i+1}), \tau^2(a_{i+1}), \ldots, \tau^{k-1}(a_{i+1}), b_{i+1}\} \tag{2.3}$$

are strictly decreasing, since the notation in (1.1) requires that $b_{i+1} > b_i$ and $a_{i+1} > a_i$. It follows from (2.3) that $\tau(a_{i+1}), \tau^2(a_{i+1}), \ldots, \tau^{k-1}(a_{i+1})$ are strictly between a_i and a_{i+1} since $a_i = b_{i+1}$, hence not in the domain of σ. Furthermore, $\tau(a_i) = \tau(b_{i+1}) = \tau(\tau^k(a_{i+1})) = \tau^k(\tau(a_{i+1})) = \sigma(\tau(a_{i+1}))$, which implies that $\tau(a_{i+1})$ is in the domain of σ, a contradiction. If $a_{i+1} = b_i$, then we reach a similar contradiction by using (2.2). □

Example 2.7. Using Lemma 2.6, we can see immediately that none of the following elements have k^{th} roots for any $k \geq 2$:

$$[2, 10] \to [10, 16],$$

$$[1, 2, 10, 26] \to [1, 10, 16, 26],$$

$$1, 52, 53, 56, 58, 59, 60] \to [51, 52, 53, 54, 56, 59, 6$$

and

$$[56, 58] \to [54, 56].$$

Definition 2.8. For elements of POI(n) of rank m, say $\sigma = [a_1, a_2, \ldots, a_m] \to [b_1, b_2, \ldots, b_m]$, we will define the **spacing** of σ to be $d_1, d_2, \ldots, d_{m-1}/r_1, r_2, \ldots, r_{m-1}; c_1, c_2, \ldots, c_m$ where $d_i = a_{i+1} - a_i$, $r_j = b_{j+1} - b_j$, and $c_\ell = b_\ell - a_\ell$ with $i, j \in \{1, \ldots, m-1\}$ and $\ell \in \{1, \ldots, m\}$.

Remark. The reader has likely noticed that relationships exist among the parameters a_i, b_i, c_i, d_i, and r_i. With Definition 2.8, we have following equations, the first of which results by repeated application of the formula $a_{i+1} = a_i + d_i$:

$$a_{i+k} = a_i + \sum_{j=i}^{i+k-1} d_j, \text{ for k} \geq 0 \tag{2.4}$$

$$b_{i+1} = a_1 + c_1 + \sum_{j=1}^{i} r_j = a_{i+1} + c_{i+1} = b_i + r_i = a_i + r_i + c_i, \tag{2.5}$$

and

$$c_{\ell+1} = c_1 + \sum_{j=1}^{\ell} (r_j - d_j) = c_\ell + r_\ell - d_\ell, \tag{2.6}$$

where $i, \ell \in \{1, \ldots, m-1\}$.

Example 2.9. Here are some examples to illustrate Definition 2.8.

(a) The spacing of [36, 48] $\to$ [48, 50] is 12/2; 12, 2.

(b) The spacing of [1,2,4] $\to$ [3,4,7] is 1,2/1,3;2,2,3.

(c) The spacing of [100, 101, 102, 103, 104] $\to$ [103, 104, 105, 106, 107] is 1, 1, 1, 1/1, 1, 1, 1; 3, 3, 3, 3, 3.

(d) The spacing of [3,6,7] $\to$ [1,3,7] is 3,1/2,4;$-$2,$-$3,0.

We can rephrase Lemma 2.6 using the spacing notation of Definition 2.8 as follows:

Lemma 2.10. *Let $k \geq 2$ and the spacing of $\sigma = [a_1, a_2, \ldots, a_m] \to [b_1, b_2, \ldots, b_m] \in$ POI(n) be $d_1, d_2, \ldots, d_{m-1}/r_1, r_2, \ldots, r_{m-1}; c_1, c_2, \ldots, c_m$. If $d_i = c_i$ or $d_i = -c_{i+1}$ for some $i \in \{1, 2, \ldots, m-1\}$, then σ does not have a k^{th} root in* POI(n).

Proof of equivalence of Lemmas 2.6 and 2.10: Assume that Lemma 2.6 holds and suppose that $d_i = c_i$ or $d_i = -c_{i+1}$ for some $i \in \{1, 2, \ldots, m-1\}$. If $d_i = c_i$, then, by Definition 2.8,

$$b_i = a_i + c_i = a_i + d_i = a_{i+1}.$$

If $d_i = -c_{i+1}$, then, by Definition 2.8,

$$b_{i+1} = a_{i+1} + c_{i+1} = (a_i + d_i) - d_i = a_i.$$

In either of these cases, we can apply Lemma 2.6 to conclude at once that σ does not have a k^{th} root in POI(n).

Conversely, assume that Lemma 2.10 holds and suppose $a_i = b_{i+1}$ or $a_{i+1} = b_i$. If $a_i = b_{i+1}$, then, by Definition 2.8,

$$d_i = a_{i+1} - a_i = a_{i+1} - b_{i+1} = -c_{i+1}.$$

If $a_{i+1} = b_i$, then, by Definition 2.8,

$$d_i = b_i - a_i = c_i.$$

In either case, Lemma 2.10 can be applied to conclude that σ does not have a k^{th} root in POI(n). □

Example 2.11. By Lemma 2.10, the elements (a) and (d) from Example 2.9 do not have k^{th} roots since $d_1 = c_1 = 12$ for element (a), and $d_1 = -c_2 = 3$ for element(d).

The next two lemmas will only consider classifying elements with a square root, i.e., when $k = 2$.

Lemma 2.12. *If $\sigma \in$ POI(n), has rank(σ) = m and a spacing with $d_{i+1} = r_i = 1$ and $c_{i+1} = 3$ for some $i \in \{1, 2, \ldots, m-2\}$, then σ does not have a square root in* POI(n).

Proof Suppose τ is a square root of σ, i.e., $\tau^2 = \sigma$ for some $\tau \in$ POI(n). By Definition 2.8, we have

$$b_i = a_{i+1} + c_{i+1} - r_i \tag{2.7}$$

and

$$b_{i+1} = a_{i+1} + c_{i+1}. \tag{2.8}$$

Using $r_i = 1$ and $c_{i+1} = 3$, it follows from (2.7) and (2.8) that $b_i = a_{i+1} + 2 > a_i$ and $b_{i+1} = a_{i+1} + 3 > a_{i+1}$, which implies that (2.1) is strictly increasing, for $c = a_i$ and $c = a_{i+1}$. Thus, there exists a positive integer x such that $\tau(a_i) = a_i + x$. It follows that

$$\tau(a_i + x) = \tau^2(a_i) = \sigma(a_i) = b_i = a_{i+1} + 2. \tag{2.9}$$

Let us now consider several cases for the value of x.

If $x < d_i$, then since τ is order-preserving and by using (2.9), we have

$$a_{i+1} + 2 = \tau(a_i + x) < \tau(a_i + d_i) = \tau(a_{i+1}) < \tau^2(a_{i+1}) = b_{i+1} = a_{i+1} + 3,$$

a contradiction since $\tau(a_{i+1})$ is forced to be an integer strictly between consecutive integers $a_{i+1} + 2$ and $a_{i+1} + 3$.

If $x = d_i$, then by using (2.9) and the fact that $a_{i+1} = 1$,

$$a_{i+1} + 2 = \tau(a_i + x) = \tau(a_{i+1}) < \tau(a_{i+2}) = \tau(a_{i+1} + d_{i+1}) < \tau(a_{i+1} + 2) =$$

$$\tau^2(a_{i+1}) = b_{i+1} = a_{i+1} + 3,$$

a contradiction since $\tau(a_{i+1} + 1)$ is an integer strictly between the two consecutive integers $a_{i+1} + 2$ and $a_{i+1} + 3$.

Finally, if $x = d_i$, then by using (2.9) once more,

$$a_{i+1} = a_i + d_i < a_i + x = \tau(a_i) < \tau(a_{i+1}) < \tau(a_i + x) = a_{i+1} + 2.$$

This chain of strict inequalities is a contradiction since the right-most term is only greater than the left-most term by 2, each of the terms in the chain must be an integer, and the chain contains four distinct values. □

Example 2.13. Let us give some examples to illustrate the use of Lemma 2.12.

(a) The element [1, 2, 3] → [4, 5, 7] has the spacing 1,1/1,2;3,3,4. Since $d_2 = r_1 = 1$ and $c_2 = 3$, by Lemma 2.12, [1,2,3] → [4,5,7] does not have a square root in POI(n) for $n \geq 7$.

(b) The element σ = [1, 6, 11, 12, 17] → [3, 4, 7, 9, 10] has the spacing 5,5,1,5/1,3,2,1;2,-2,-4,-3,-7. By switching the domain and the range of this element, we obtain σ^{-1} = [3, 4, 7, 9, 10] → [1, 6, 11, 12, 17], which has spacing 1,3,2,1/5,5,1,5;-2,2,4,3,7. Since $d_4 = r_3 = 1$ and $c_4 = 3$, by Lemma 2.12, σ^{-1} does not have a square root in POI(n) for $n \geq 17$. Hence, σ does not have a square root in POI(n) for $n \geq 17$ by Lemma 2.3.

Note that for both of these examples, $|c_i| \geq 2$, for all i, which implies that Lemma 2.4 does not apply. Furthermore, there does not exist $1 \leq i \leq 4$ such that $a_i = b_{i+1}$ or $a_{i+1} = b_i$ for either element. Thus, Lemma 2.6 does not apply, and, equivalently, neither does Lemma 2.10. Therefore, Example 2.13 demonstrates the necessity of having Lemma 2.12 to help achieve our goal of classifying the elements of POI(n) with square roots.

Lemma 2.14. *If $\sigma \in$ POI(n) has rank $(\sigma) = m$ and spacing such that $d_i = r_{i+1} = 1$, $d_{i+1} + 1 > c_i > 0$, $c_i \in \{2, 3\}$ and $c_i + 2 > 0$ for some $i \in \{1, 2, \ldots, m-2\}$, then σ does not have a square root in* POI(n).

Proof Suppose there exists $\tau \in$ POI(n) such that $\tau^2 = \sigma$. Since $c_i \geq 2 > 0$, $c_{i+2} > 0$, and $b_{i+1} = a_{i+1} + c_{i+1} = a_{i+1} + c_i + r_i - d_i \geq a_{i+1} + r_i + 1 > a_{i+1}$ by (2.5) and (2.6), we have that the sequences (2.1) for $c \in \{a_i, a_{i+1}, a_{i+2}\}$ are strictly increasing. This implies that there exist positive integer x such that $\tau(a_i) = a_i + x$.

If $c_i = 2$, then $x = 1$ since $a_i < \tau(a_i) < \tau^2(a_i) = b_i = a_i + 2$. It follows that $a_{i+1} = a_{i+1} = a_i + x$. Since

$$\tau(a_{i+1}) = \tau(a_i + x) = \tau^2(a_i) = \sigma(a_i) = b_i = a_i + c_i = a_i + 2,$$

it follows that $a_i + 2 \in Domain(\tau)$. Thus, since $a_{i+2} = a_i + d_{i+1} + d_i = a_i + d_{i+1} + 1$ by applying (2.4) with $k = 2$,

$$b_{i+1} = \tau^2(a_{i+1}) = \tau(a_i + 2) < \tau(a_i + d_{i+1} + 1) = \tau(a_{i+2}) < \tau^2(a_{i+2}) = b_{i+2} = b_{i+1} + 1,$$

a contradiction since $\tau(a_{i+2})$ is forced to be an integer strictly between consecutive integers b_{i+1} and b_{i+1} +1. If $c_i = 3$, then $x = 2$ since we will reach a similar contradiction as above if $x = 1$. This implies that $\tau(a_i) = a_i + 2$ and $\tau(a_i + 2) = \tau^2(a_i) = b_i = a_i + c_i = a_i + 3$. It follows that

$$a_i + 2 = \tau(a_i) < \tau(a_{i+1}) < \tau(a_i + 2) = a_i + 3,$$

a contradiction since $\tau(a_{i+1})$ is forced to be an integer strictly between consecutive integers a_i +2 and a_i +3. □

Example 2.15. Let us give some examples to illustrate the use of Lemma 2.14.

(a) The element [1, 2, 5] → [4, 6, 7] has the spacing 1,3/2,1;3,4,2. Since $d_1 = r_2 = 1$ and $c_1 = 3$, by Lemma 2.14, [1,2,5] → [4,6,7] does not have a square root in POI(n) for $n \geq 7$.

(b) The element σ = [4, 5, 9, 13, 14] → [1, 3, 7, 8, 12] has the spacing 1,4,4,1/2,4,1,4;-3,-2,-2,-5,-2. By switching the domain and the range of this element, we obtain σ^{-1} = [1, 3, 7, 8, 12] → [4, 5, 9, 13, 14], which has spacing 2,4,1,4/1,4,4,1;3,2,2,5,2. Since $d_3 = r_4 = 1$ and $c_3 = 2$, by Lemma 2.14, σ^{-1} does not have a square root in POI(n) for $n \geq 17$. Hence, σ does not have a square root in POI(n) for $n \geq 14$ by Lemma 2.3.

Note that for both of these examples, $|c_i| \geq 2$, for all i, which implies that Lemma 2.4 does not apply. Furthermore, there does not exist an integer i with $0 < i < 5$ such that $a_i = b_{i+1}$ or $a_{i+1} = b_i$ for either element. Thus, Lemma 2.6 does not apply, and, equivalently, neither does Lemma 2.10. Moreover, there does not exist an integer i with $0 < i < 4$ such that $d_{i+1} = r_i = 1$ and $c_{i+1} = 3$ for either element. Hence, Lemma 2.12 does not apply. These remarks illustrate that Lemma 2.14 is an important result in the arsenal of results that facilitate our main result.

In the final section, we turn our attention to presenting this main result.

3. Main Theorem

The lemmas presented in Section 2 are sufficient to determine whether elements of POI(n) have a square root in POI(n) with $n \leq 7$. As a result, we have the following:

Theorem 3.1. *Let $\sigma \in$ POI(n) with $n \leq 7$. Then σ has a square root in* POI(n) *if and only if σ fails to satisfy any of the hypotheses of Lemma 2.4, Lemma 2.6, Lemma 2.10, Lemma 2.12, and Lemma 2.14.*

Proof Using GAP, an exhaustive analysis of the elements of POI(n) with $n \leq 7$ verifies that each element either possesses a square root or satisfies the hypothesis of one of the lemmas stated here. □

We suspect that, with further analysis, we can generalize Lemma 2.12 and Lemma 2.14. These results were obtained through studying the 3,432 elements of POI(7). However, note that POI(8) has 12,870 elements. Moreover, analysis of POI(8) is required to be able to conclude whether Theorem 3.1 is sufficient to determine whether the elements of this significantly larger semigroup have square roots, perhaps instead POI(7) does not present an extensive variety of "types" of elements in order to make such a claim.

References

[1] Annin, S., *Hierarchy of efficient generators of the symmetric inverse monoid*, Semigroup Forum 54 (1997), 327-355.

[2] Annin, S., Jansen, T. and Smith, C., *On kth roots in the symmetric and alternating groups*, Pi Mu Epsilon Journal 12:10 (2009), 581-589.

[3] Annin, S., Cannon, T., Hernandez, C. and Torres, L., *On kth roots in the symmetric inverse monoid*, Pi Mu Epsilon Journal 13:6 (2012), 321-331.

[4] Clifford, A.H. and Preston, G., B., "The Algebraic Theory of Semigroups," Vol. 1, American Mathematical Society, Providence, RI, 1961.

[5] GAP 2008, The GAP Group, GAP-Groups, Algorithms, and Programming, Version 4.4.12; 2008. (http://www/gap-systems.org)

[6] Grillet, P.A., "Semigroups: An Introduction to the Structure Theory", Marcel Dekker, Inc., New York, NY, 1995.

[7] Hungerford, T., "Abstract Algebra: An Introduction," 2nd ed., Brooks and Cole, 1996.

The Topology of $\mathbb{BP}^0$

Amy Feaster and Eric Flynn
Advisor: Dr. Alfonso Agnew

Department of Mathematics, California State University, Fullerton

Abstract

The biquaternionic projective point, $\mathbb{BP}^0$, has been shown to contain twistor structure [1]. However the details of the topology and its properties have not been fully explored. In this paper we address this issue by determining an explicit basis for the topology on $\mathbb{BP}^0$ and analyzing some its elements.

1. Introduction

Twistor theory is a subject of great interest in mathematical physics. $\mathbb{BP}^0$ has been shown to contain a twistor structure due to to its topological properties [1]. Although this characteristic has been shown, the complete topology and its properties were unknown. Our goal is to determine a basis for the topology of $\mathbb{BP}^0$ as well as explore stereographic projections and separation properties of this basis. In section II we outline the relevant background needed for the results in section III. We construct $\mathbb{BP}^0$ and then find a basis for the topology in section III. We note that $\mathbb{C}_{2\times 2}$ and $\mathbb{B}$ are isomorphic as algebras, which is the only structure needed this paper. Thus we represent biquaternions as 2×2 complex matrices throughout.

2. Background

2.1 Definitions

For standard results on topological spaces, see [3].

Definition 1. A set X for which a topology τ has been specified is called a **topological space**. The elements of τ are called open subsets of X.

Definition 2. A map $f: X \to Y$ is said to be **continuous** if for each open set $V \subseteq Y$ the set $f^{-1}(V)$ is open in X.

Definition 3. A map $f: X \to Y$ is said to be an **open map** if for each open set U of X, the set $f(U)$ is open in Y.

Definition 4. Let X and Y be topological spaces; let $p: X \to Y$ be a surjective (i.e. onto) map. The map p is said to be a **quotient map**, provided a subset of V of Y is open in Y if and only if $P^{-1}(V)$ is open in X.

Definition 5. If X is a space, A is a set, and $p : X \to A$ is a surjective map, then there exists exactly one topology τ on A relative to which p is a quotient map; it is called the **quotient topology** induced by p. The set A with the quotient topology is called a **quotient space**.

2.2 Theorems

With the previous definitions, we can prove the following general theorems

Theorem 2.1. *Let $f : (X, \tau_X) \to (Y, \tau_Y)$ be invertible and continuous. Then f is open if and only if f^{-1} is continuous.*

Proof. Let f be open. We need to show that f^{-1} is continuous. To show that f^{-1} is continuous, we need to show that $\forall\ U \in \tau_X,\ (f^{-1})^{-1}(U) \in \tau_Y$. Note that since f is invertible, $(f^{-1})^{-1} = f$. Thus, it sufficient to show that $\forall\ U \in \tau_X,\ f(U) \in \tau_Y$. Since f is open, we know by definition that $\forall\ U \in \tau_X,\ f(U) \in \tau_Y$. Therefore, f^{-1} is continuous.

Let f^{-1} be continuous. We need to show that f is open. To show that f is open, we need to show that $\forall\, U \in \tau_X,\ f(U) \in \tau_Y$. Since f^{-1} is continuous, we know by definition that $\forall\ U \in \tau_X,\ (f^{-1})^{-1}(U) \in \tau_Y$. Since f is invertible, $(f^{-1})^{-1} = f$, so $\forall\ U \in \tau_X,\ f(U) \in \tau_Y$. Therefore, f is open. □

Theorem 2.2. *If $f : (X, \tau_X) \longrightarrow (Y, \tau_Y)$ is a continuous, open surjection, and $\mathcal{B}_X$ is a basis for τ_X, then*

$$\{f(B) \mid B \in \mathcal{B}_X\} \tag{1}$$

is a basis for τ_Y.

Proof. Let $V \in \tau_Y$ be arbitrary. Then $f^{-1}(V) \in \tau_X$ since f is continuous Since $\mathcal{B}_X$ is a basis for $\tau_X,\ \exists\ \{B_\alpha : B_\alpha \in \mathcal{B}_X\ \forall\, \alpha\} \subseteq \mathcal{B}_X$ such that $f^{-1}(V) = \bigcup_\alpha B_\alpha$. Since f is a surjection, we have $f(f^{-1}(V)) = V$, so

$$V = f(f^{-1}(V)) = f(\bigcup_\alpha B_\alpha) = \bigcup_\alpha f(B_\alpha). \tag{2}$$

A basis is a subset $\mathcal{B}_Y$ of τ_Y in which all other open sets can be written as unions of the basis elements. Since $V \in \tau_Y$ is arbitrary and $V = \bigcup_\alpha f(B_\alpha)$,

$$\{f(B) \mid B \in \mathcal{B}_X\} \tag{3}$$

is a basis for τ_Y. □

2.3 Stereographic Projection

Stereographic projection (see [2]) is a one-to-one correspondence between complex numbers and the points on the surface of a punctured sphere. Looking at the sphere of radius $\frac{1}{2}$ centered at $(0, 0, \frac{1}{2})$ in Euclidean (ξ, η, ζ) space, the plane $\zeta = 0$ coincides with the complex plane $\mathbb{C}$, and the ξ and η axes correspond to the x and y axes, respectively. We associate each point (ξ, η, ζ) on the sphere with a complex number (x,y) where the ray from the north pole of the sphere (0, 0, 1) through (ξ, η, ζ) intersects $\mathbb{C}$. This correspondence is given by

$$x = \frac{\xi}{1-\zeta},\ y = \frac{\eta}{1-\zeta}, \tag{4}$$

and

$$\xi = \frac{x}{x^2+y^2+1},\ \eta = \frac{y}{x^2+y^2+1},\ \zeta = \frac{x^2+y^2}{x^2+y^2+1}. \tag{5}$$

3. The Projective Point $\mathbb{BP}^0$

3.1 Preliminary: Topology of $\mathbb{B}$

Before we consider the topology of the quotient space, we will provide a brief overview of the topology of $\mathbb{B}$. To find the topology, it is sufficient to find a basis which generates all open sets via arbitrary unions. Consider an arbitrary element A in $\mathbb{B}$

$$A = \begin{pmatrix} z_1 & z_2 \\ z_3 & z_4 \end{pmatrix} \tag{6}$$

Basic open sets in the complex plane are given by open disks $D_\varepsilon(z) = \{\omega \in \mathbb{C} : |z-\omega| < \varepsilon\}$. Define

$$D_\varepsilon(A) = \begin{pmatrix} D_\varepsilon(z_1) & D_\varepsilon(z_2) \\ D_\varepsilon(z_3) & D_\varepsilon(z_4) \end{pmatrix}.$$

Then a basis for $\mathbb{B}$ will be

$$\mathcal{B}_{\mathbb{B}} = \{D_\varepsilon(A) : \varepsilon > 0,\ A \in \mathbb{B}\} \tag{7}$$

For the construction of the projective space, it is necessary to remove the zero vector. From subspace topology, our basis now becomes

$$\mathcal{B}_{\mathbb{B}^0} = \{D_\varepsilon(A) - \{\vec{0}\} : \varepsilon > 0,\ A \in \mathbb{B}\} \tag{8}$$

where $\mathbb{B}^0 = \mathbb{B} - \{\vec{0}\}$.

3.2 Construction of the Matrix Projective Point $\mathbb{B}^0$

To construct the projective point over $\mathbb{B}$, we expand upon the method in [1]. In brief, after forming $\mathbb{B}^0$, we take the quotient modulo the equivalence relation

$$A \sim B \iff A = B\lambda,\ \lambda \in GL(2,\mathbb{C}). \tag{9}$$

We end up getting the equivalence classes of the form

$$\left[\left(\begin{smallmatrix} 1 & 0 \\ 0 & 1 \end{smallmatrix}\right)\right],\ \left[\left(\begin{smallmatrix} 1 & 0 \\ 0 & 0 \end{smallmatrix}\right)\right],\ \left[\left(\begin{smallmatrix} c & 0 \\ 1 & 0 \end{smallmatrix}\right)\right]\ c \in \mathbb{C}. \tag{10}$$

We will refer to these equivalence classes as types I, II, and III, respectively. In more detail we construct $\mathbb{BP}^0$ by considering the quotient space with relation $\sim$, that is $\mathbb{BP}^0 = \mathbb{B}^0/\sim$. Our relation bētwēen the two spaces is then defined by the function

$$p(\alpha) = \Big\{\delta \in \mathbb{B}^0 : \delta = \alpha\Lambda, \alpha \in \mathbb{B}^0, \forall \Lambda \in GL(2,\mathbb{C})\Big\}. \tag{11}$$

Theorem 3.1. *Choosing α appropriately, the space is constructed of the union of three equivalence classes:*

$$\mathbb{BP}^0 = \left[\begin{pmatrix} 1 & 0 \\ 0 & 1 \end{pmatrix} \right] \bigcup \left[\begin{pmatrix} \gamma & 0 \\ 1 & 0 \end{pmatrix} \right] \bigcup \left[\begin{pmatrix} 1 & 0 \\ 0 & 0 \end{pmatrix} \right] \tag{12}$$

where $\gamma \in \mathbb{C}$.

Proof.

Case 1. *Suppose α is a variable.*
We need to find all δ such that $\delta = \alpha\Lambda$ for all arbitrary Λ. But since α is invertible, $\alpha^{-1}\delta = \Lambda$ is true if and only if δ is invertible. Thus, $p(\alpha) = GL(2, \mathbb{C})$ which is the set of all invertible matrices.

Case 1. *Suppose α is a singular.*
The most general singular 2×2 matrix has the form $\alpha = \begin{pmatrix} \mu\vec{u} & \nu\vec{u} \end{pmatrix}$. We can find an invertible matrix in order to replace α with a representative having zeros in the second column. To see this, we need a $\Lambda = \begin{pmatrix} a & b \\ c & d \end{pmatrix} \in GL(2, \mathbb{C})$, that will satisfy

$$\left(\mu \begin{pmatrix} u_1 \\ u_2 \end{pmatrix} \quad \begin{pmatrix} 0 \\ 0 \end{pmatrix} \right) = \left(\mu \begin{pmatrix} u_1 \\ u_2 \end{pmatrix} \quad \nu \begin{pmatrix} u_1 \\ u_2 \end{pmatrix} \right) \begin{pmatrix} a & b \\ c & d \end{pmatrix}. \tag{13}$$

Note that if $\nu = 0$, then there is no issue. If $\mu = 0$, then we can multiply α by a permutation matrix in order to make the second column a zero column. Multiplying and setting the components of the left and right sides equal we have

$$\begin{aligned} \mu u_1 b + \nu u_1 d &= 0 \\ \mu u_2 b + \nu u_2 d &= 0 \\ \mu u_1 a + \nu u_1 c &= \mu u_1 \\ \mu u_2 a + \nu u_2 c &= \mu u_2 \end{aligned} \tag{14}$$

which has solutions $c = \frac{\mu - \mu a}{\nu}$ and $d = \frac{-\mu d}{\nu}$ provided that $u_1, u_2 \neq 0$. So,

$$\begin{pmatrix} a & b \\ c & d \end{pmatrix} = \begin{pmatrix} a & b \\ \frac{\mu - \mu a}{\nu} & \frac{-\mu b}{\nu} \end{pmatrix} \tag{15}$$

where b can be chosen such that $\det(\Lambda) = \frac{-b\mu}{\nu} \neq 0$ Therefore under these assumptions, we may choose our representative α to have the form

$$\alpha = \begin{pmatrix} \gamma & 0 \\ 1 & 0 \end{pmatrix}. \tag{16}$$

It follows that matrices of this form generate the equivalence classes $\left[\begin{pmatrix} \gamma & 0 \\ 1 & 0 \end{pmatrix} \right]$ for $\gamma \in \mathbb{C}$.

Case 1. *Now suppose* $u_2 = 0$, *and* $u_1 \neq 0$.

As above, we can multiply by an invertible matrix to make the second column a zero column. Then α takes the form

$$\alpha = \begin{pmatrix} \mu u_1 & 0 \\ 0 & 0 \end{pmatrix}. \tag{17}$$

We can multiply this matrix by $diag(\frac{1}{\mu u_1}, \frac{1}{\mu u_1})$ to be an element of its own equivalence class represented by $\left[\begin{pmatrix} 1 & 0 \\ 0 & 0 \end{pmatrix} \right]$.

Therefore the space $\mathbb{BP}^0$ must only contain the three equivalence classes and hence

$$\mathbb{BP}^0 = \left\{ \left[\begin{pmatrix} 1 & 0 \\ 0 & 1 \end{pmatrix} \right] \right\} \bigcup \left\{ \left[\begin{pmatrix} \gamma & 0 \\ 1 & 0 \end{pmatrix} : \gamma \in \mathbb{C} \right] \right\} \bigcup \left\{ \left[\begin{pmatrix} 1 & 0 \\ 0 & 0 \end{pmatrix} \right] \right\}. \tag{18}$$

□

3.3 Topology of $\mathbb{BP}^0$

In order to use our quotient map to find a basis, we must first show p is an open map. To do this we consider the simpler case of matrix multiplication.

Theorem 3.2. *Let* $\Lambda \in GL(2, \mathbb{C})$ *be arbitrary. If*

$$\begin{aligned} f_\Lambda : \mathbb{B} &\longrightarrow \mathbb{B} \\ : A &\longmapsto A\Lambda \end{aligned}$$

Then f_Λ *is a continuous, open, bijection.*

Proof. To show that f_Λ is a bijection, we will show that ${f_\Lambda}^{-1} = f_{\Lambda^{-1}}$.

$$f_{\Lambda^{-1}}(f_\Lambda(A)) = f_{\Lambda^{-1}}(A\Lambda) = (A\Lambda)\Lambda^{-1} = A(\Lambda\Lambda^{-1}) = A, \tag{19}$$

$$f_\Lambda(f_{\Lambda^{-1}}(A)) = f_\Lambda(A\Lambda^{-1}) = (A\Lambda^{-1})\Lambda = A(\Lambda^{-1}\Lambda) = A. \tag{20}$$

Therefore, ${f_\Lambda}^{-1} = f_{\Lambda^{-1}}$, and f_Λ is a bijection.

Since multiplication by a fixed matrix is continuous, f_Λ is continuous for an arbitrary fixed $\Lambda \in GL(2, \mathbb{C})$. We need to show that f_Λ is open. From Theorem 2.1, f_Λ is open if and only if $f_{\Lambda^{-1}}$ is continuous. We know that ${f_\Lambda}^{-1} = f_{\Lambda^{-1}}$, and $f_{\Lambda^{-1}}$ is continuous by assumption. Therefore, $f_{\Lambda^{-1}}$ is continuous, so f_Λ is open. □

Now we can use Theorem 3.2 to show p is an open map.

Theorem 3.3. *Let*

$$p : \mathbb{B}^0 \longrightarrow \mathbb{B}^0, \tag{21}$$

where

$$p(A) = \{B \in \mathbb{B}^0 : B = A\Lambda,\ \Lambda \in GL(2,\mathbb{C})\}. \tag{22}$$

Then, $p(A)$ is open.

Proof. To prove P is open, we need to show that

$$\forall\, U \in \tau_{\mathbb{B}^0},\ p(U) \in \tau_{\mathbb{C}^0_{2\times 2}/\sim}. \tag{23}$$

Let $U \in \tau_{\mathbb{B}^0}$ be arbitrary. Then

$$p(U) = \big\{[A] \in \mathbb{BP}^0\ :\ \forall\, A \in U\big\},\ \ [A] = \big\{B \in \mathbb{B}^0\ :\ B = A\Lambda, \forall\, \Lambda \in GL(2,\mathbb{C})\big\}. \tag{24}$$

By the definition of the quotient topology, $p(U) \in \tau_{\mathbb{C}^0_{2\times 2}/\sim}$ if and only if $p^{-1}(p(U)) \in \tau_{\mathbb{C}^0_{2\times 2}}$. By Theorem 2.2 we have,

$$\begin{aligned} p^{-1}(p(U)) &= \big\{B \in \mathbb{B}^0\ :\ B = A\Lambda \quad \forall\, A \in U,\ \forall\, \Lambda \in GL(2,\mathbb{C})\big\} \\ &= \bigcup_{\Lambda \in GL(2,\mathbb{C})} \{f_\Lambda(U)\}. \end{aligned} \tag{25}$$

Since $U \in \tau_{\mathbb{C}^0_{2\times 2}}$ and f_Λ is open, $f_\Lambda(U) \in \tau_{\mathbb{C}^0_{2\times 2}}$ for each $\Lambda \in GL(2,\mathbb{C})$. An arbitrary union of open sets is open, so

$$\bigcup_{\Lambda \in GL(2,\mathbb{C})} \big\{f_\Lambda(U)\big\} \in \tau_{\mathbb{C}^0_{2\times 2}}. \tag{26}$$

Hence $p^{-1}(p(U)) \in \tau_{\mathbb{C}^0_{2\times 2}}$ and $p(U) \in \tau_{\mathbb{C}^0_{2\times 2}/\sim}$. So p maps open sets in the domain to open sets in the codomain, therefore p is open. □

Since our map p is open, we may now use Theorem 2.2 to determine a basis for $\mathbb{BP}^0$.

$$\mathbb{BP}^0 = \{p(D_\varepsilon(A)) : \varepsilon > 0, \forall A \in \mathbb{B}^0\} \tag{27}$$

$$\mathbb{BP}^0 = p\big(\mathcal{B}_\varepsilon(A)\big) = \{*\} \cup \Big\{ \big[\ \begin{pmatrix} \vec{u} & 0 \end{pmatrix}\ \big] : \vec{u} \in \mathcal{B}_\varepsilon \begin{pmatrix} a \\ b \end{pmatrix} \wedge \mathbb{C}\vec{u} \cap \mathcal{B}_\varepsilon \begin{pmatrix} c \\ d \end{pmatrix} \neq \emptyset \tag{28}$$

$$\vee\, \vec{u} \in \mathcal{B}_\varepsilon \begin{pmatrix} c \\ d \end{pmatrix} \wedge \mathbb{C}\vec{u} \cap \mathcal{B}_\varepsilon \begin{pmatrix} a \\ b \end{pmatrix} \neq \emptyset \Big\} \tag{29}$$

Thus we have found a basis for the standard topology of $\mathbb{BP}^0$.

3.4 Separation Properties of $\mathbb{BP}^0$

There are two cases of interest here: the separation of type I from type II and III equivalence classes, and vice-versa.

We first show the type I class is not separable from the type II and III classes, therefore rendering the space non-Hausdorff. Define

$$* = \Big[\begin{pmatrix} 1 & 0 \\ 0 & 1 \end{pmatrix} \Big]. \tag{30}$$

Theorem 3.4. *For all open subsets $V \subseteq \mathbb{BP}^0$, $* \in V$.*

Proof. Suppose we have a general non-invertible matrix $A = \begin{pmatrix} \mu a & 0 \\ \mu b & 0 \end{pmatrix}$ where.$\mu \neq 0$. We need to show that given a basic open set $p(\mathcal{B}_\varepsilon(A)) \subseteq \mathbb{BP}^0, * \in p(\mathcal{B}_\varepsilon(A))$ for all $\varepsilon > 0$. Consider shifting the matrix by some complex matrix $\begin{pmatrix} 0 & \delta \\ 0 & 0 \end{pmatrix}$ where $0 < \delta < \varepsilon$. Then,

$$\begin{pmatrix} \mu a & \delta \\ \mu b & 0 \end{pmatrix} \in \mathcal{B}_\varepsilon(A). \tag{31}$$

We want to find a case where this matrix will be invertible regardless of the choice of a, b or δ. To check this we take a determinant of the shifted matrix and set it equal to 0.

$$\begin{vmatrix} \mu a & \delta \\ \mu b & 0 \end{vmatrix} = \mu b \delta = 0 \tag{32}$$

But $\delta, \mu \neq 0$ if $b \neq 0$. If $b = 0$ then this determinant will be zero. If b = 0, shift instead to

$$\begin{vmatrix} \mu a & 0 \\ 0 & \delta \end{vmatrix} = \mu a \delta \neq 0. \tag{33}$$

There does not exist an $\varepsilon > 0$ such that $* \notin p(\mathcal{B}_\varepsilon(A))$ □

Theorem 3.5. *The ball $\mathcal{B}_{\frac{1}{2}}(I)$ contains no singular matrices.*

Proof. Let $I = \begin{pmatrix} 1 & 0 \\ 0 & 1 \end{pmatrix} \in GL(2, \mathbb{C})$, and consider the ball $\mathcal{B}_{\frac{1}{2}}(I) \subseteq \mathbb{B}^0$. Consider the element

$$\widehat{A} = I + A = \begin{pmatrix} 1 + \alpha & \beta \\ \gamma & 1 + \delta \end{pmatrix} \tag{34}$$

in the ball $\widehat{A}$, where we require $\alpha, \beta, \gamma, \delta \in \mathbb{C}$ subject to $|\alpha|, |\beta|, |\gamma|, |\delta| < \frac{1}{2}$. Taking the determinant of $\widehat{A}$ and setting it equal to zero we have

$$(1+\alpha)(1+\delta) = \beta\gamma \tag{35}$$

We have

$$1/2 < (1+\alpha), (1+\delta) < 3/2$$

and

$$-1/2 < \beta, \gamma < 1/2,$$

so that the left hand side of the equation

$$(1+\alpha)(1+\delta) = \beta\gamma$$

must be greater than the right hand side, and so the equation cannot be satisfied. □

Thus, $p(\mathcal{B}_{\frac{1}{2}}(I)) = \{*\}$ is an open subset of $\mathbb{BP}^0$. As a result the point $*$ can be separated from all other points of $\mathbb{BP}^0$.

3.5 Stereographic Projection and $\mathbb{BP}^0$

To try to have a better understanding of the topology of $\mathbb{BP}^0$, we will use stereographic projection to map the basis elements of $\mathbb{BP}^0$ onto the punctured sphere. We will begin by looking at an epsilon ball of $\frac{1}{2}$ centered at the south pole,
$B_{\frac{1}{2}}\left(\begin{pmatrix} 0 & 0 \\ 1 & 0 \end{pmatrix}\right) = \left\{A = \begin{pmatrix} \alpha & \beta \\ \gamma+1 & \delta \end{pmatrix} : |\alpha|, |\beta|, |\gamma|, |\delta| < \frac{1}{2}\right\}$. We will assume that A is a singular matrix, so $det(A) = \alpha\delta - \beta(\gamma+1) = 0$ or $\beta = \frac{\alpha\delta}{\gamma+1}$. Substituting this value of β into our matrix A, we can see that the second column is a linear combination of the first column,

$$A = \begin{pmatrix} \alpha & \frac{\alpha\delta}{\gamma+1} \\ \gamma+1 & \delta \end{pmatrix} = \begin{pmatrix} \alpha & \frac{\delta}{\gamma+1}(\alpha) \\ \gamma+1 & \frac{\delta}{\gamma+1}(\gamma+1) \end{pmatrix}. \tag{36}$$

We can multiply A by two invertible matrices to get $\begin{pmatrix} \frac{\alpha}{\gamma+1} & 0 \\ 1 & 0 \end{pmatrix}$. This matrix is now similar to our type III equivalence class which in totality represents the complex plane $\mathbb{C}$. Thus, we will analyze the complex number $z = \frac{\alpha}{\gamma+1}$, and use stereographic projection to see what the neighborhood maps to on the punctured sphere.

Note that $|\alpha| < \frac{1}{2}$ and $|\gamma| < \frac{1}{2}$. It follows that $\frac{1}{2} < |1+\gamma| < \frac{3}{2}$, $0 < |\frac{\alpha}{1+\gamma}| < 1$, and so

$$S = \left\{\frac{\alpha}{1+\gamma} : |\alpha|, |\gamma| < \frac{1}{2}\right\} \subseteq D_1(0). \tag{37}$$

If we let $\gamma = 0$, then $\left\{\frac{\alpha}{1+\gamma} : |\alpha| < \frac{1}{2}\right\} = D_{\frac{1}{2}}(0)$. If we fix $\gamma \in (\frac{-1}{2}, \frac{1}{2})$ so that $\frac{2}{3} < \frac{1}{1+\gamma} < 2$, then

$$\left\{z = \frac{\alpha}{1+\gamma} : |\alpha| < \frac{1}{2}\right\} = kD_{\frac{1}{2}}(0), \text{ where } k = \frac{1}{1+\gamma}. \tag{38}$$

Thus,

$$\Big\{\frac{\alpha}{1+\gamma} : |\alpha| < \frac{1}{2} \text{ and } |\gamma| < \frac{1}{2}\Big\} = D_1(0). \tag{39}$$

Doing stereographic projection on all the points of this disk will give us the bottom hemisphere of the sphere.

Now we want to go through the same procedure for the north pole, so we will look at the ball

$$B_{\frac{1}{2}}\Big(\begin{pmatrix}1 & 0\\ 0 & 0\end{pmatrix}\Big) = \Big\{A = \begin{pmatrix}1+\alpha & \beta\\ \gamma & \delta\end{pmatrix} : |\alpha|, |\beta|, |\gamma|, |\delta| < \frac{1}{2}\Big\} \tag{40}$$

If A is non invertible, then we are able to multiply A by invertible matrices to get a matrix of the form

$$\begin{pmatrix}\frac{\alpha+1}{\gamma} & 0\\ 1 & 0\end{pmatrix} \tag{41}$$

Again, the matrix is similar to our type III equivalence class which represents the complex plane $\mathbb{C}$, so we analyze the complex number $w = \frac{\alpha+1}{\gamma}$. Notice that $w = \frac{\alpha+1}{\gamma}$ looks like the reciprocal of $z = \frac{\alpha}{\gamma+1}$. So we will use the reciprocal transformation to see what w looks like on the sphere. Let

$$D_1(0) = \big\{z = \frac{\alpha}{\gamma+1} = x + iy : x^2 + y^2 < 1\big\}. \tag{42}$$

Because

$$z = f^{-1}(w) = \frac{1}{w}, \tag{43}$$

we have

$$\begin{aligned}
u + iv = w \in f\big(D_1(0)\big) &\longleftrightarrow f^{-1}(w) \in D_1(0)\\
&\longleftrightarrow \frac{1}{w} \in D_1(0)\\
&\longleftrightarrow \frac{1}{u+iv} = \frac{u}{u^2+v^2} + i\frac{-v}{u^2+v^2} \in D_1(0)\\
&\longleftrightarrow (\frac{u}{u^2+v^2})^2 + (\frac{-v}{u^2+v^2})^2 < 1\\
&\longleftrightarrow \frac{1}{u^2+v^2} < 1\\
&\longleftrightarrow\ u^2 + v^2 > 1.
\end{aligned} \tag{44}$$

So points of the form $w = \frac{\alpha+1}{\gamma}$ in $\mathbb{C}$ comprise the outside of the open disk of radius one centered at the origin.

Note that the reciprocal transformation and stereographic projection are both continuous bijections onto their images. Also, $\frac{\gamma+1}{\alpha}$ is the complement of $\frac{\alpha}{\gamma+1}$ in $\mathbb{C}$, so rather than use stereographic projection to map $\frac{\gamma+1}{\alpha}$ onto the sphere, we will map $\frac{\alpha}{\gamma+1}$ onto the sphere and consider its complement. As we saw above, $\frac{\alpha}{\gamma+1}$ maps onto the southern hemisphere of the sphere. The complement of the southern hemisphere is the northern hemisphere. Therefore, $\frac{\gamma+1}{\alpha}$ maps to the northern hemisphere of the punctured sphere. So topologically, a basic open neighborhood of $\left(\begin{smallmatrix} 0 & 0 \\ 1 & 0 \end{smallmatrix}\right)$ is locally equivalent to the topology of the southern hemisphere of the sphere. Likewise, a basic open neighborhood of $\left(\begin{smallmatrix} 1 & 0 \\ 0 & 0 \end{smallmatrix}\right)$ is locally equivalent to the northern hemisphere of the sphere.

4. Conclusion

In this article we have determined an explicit basis for the topology of $\mathbb{BP}^0$. By investigating the separation properties of $\mathbb{BP}^0$, we have verified that this space is non-Hausdorff. Through stereographic projection, we discovered that topologically, basic open neighborhoods of points corresponding to the north and south pole are locally equivalent to the basic open neighborhoods of the southern and northern hemisphere of the sphere.

In future work we will provide an explicit homeomorphism between $\mathbb{BP}^0$ and the sphere. Furthermore, we will determine how continuous functions map into and out of $\mathbb{BP}^0$, as well as mappings from $\mathbb{BP}^0$ into itself. We also hope to form a connection between $\mathbb{BP}^0$ and $\mathbb{BP}^1$ to see if there is any relation between the two spaces and their twistor structures.

References

[1] Alfonso F Agnew. The twistor structure of the biquaternionic projective point. *Advances in applied Clifford algebras*, 13(2):231–240, 2003.

[2] J. Bak and D. J. Newman. *Complex Analysis*. Springer, 2010.

[3] James R. Munkres. *Topology of a first course*. Prentice-Hall, Inc., 1975.

What Problems Are Appropriate for Gifted Students in Grades 2-4?

Dulce Fonseca and Vivian Lopez
Advisor: Dr. Bogdan D. Suceavă

Department of Mathematics, California State University, Fullerton

Abstract

In this work we focus on problems explored with gifted math students grades 2–4 during Cal State Fullerton Math Circle, Fall 2015. We examined pedagogical strategies to deliver high quality presentations where students were challenged to think critically and feel encouraged to participate. Problems came from famous problems in mathematics, the 2014–2015 ABACUS International Math Challenge problem sets, and Natasha Rozhkovskaya's *Math Circles for Elementary School Students*. This papers looks at problems that were presented, students' responses to these, and successes and potential improvements for future presentations.

1. Eulerian Trails

The field of graph theory can be quite interactive for young students because of its visual aspects. In one of these graph theory sessions students explored Eulerian Trails. According to Brualdi, author of Introductory Combinatorics, a "trail in a general graph G is called Eulerian, provided that it contains every edge of G." [2]. That is to say, a trail is Eulerian if and only if there exists a continuous way to trace each edge of a graph exactly once.

With tape, a planar, complete graph with four veritices was created on the floor. Two discs were placed on each side of the graph. In the same fashion, a second graph was made in the shape of a rectangle with only one diagonal.

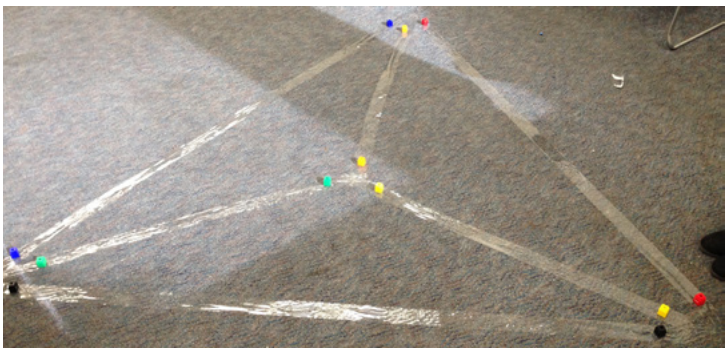

Students were given the following instructions: Stand at any vertex. You must walk through each edge exactly once. As you walk along each edge, pick up the two discs to keep track of where you have been and where you still need to go.

The first graph for which students attempted to find an Eulerian trails was the complete graph. Eventually, they collectively strategized on what vertex to begin and which tape to follow first. The students were unsuccessful at finishing a trial. Their attention was then redirected to the second graph. The Eulerian trail was easily completed as students, randomly but correctly, chose to start at a vertex with odd degree.

Students were then told that an Eulerian Trail was impossible for the first graph. Regardless, they re- fused to accept it and continued to try.

The class came back together to work on the board and investigate when Eulerian trails are possible. Analyzing additional graphs, students arrived to the conjecture that in graphs where each vertex has an even number of ways to walk off of it, Eulerian trails are possible. If there is an odd number of ways to go off of each vertex, then the trail was not possible. However, students then recalled that on the second graph on the carpet, they were able to complete the trail even though they started on a vertex of odd degree. With guidance, they were able to further, and correctly, generalize that a trail can be completed if there are exactly two vertices of odd degree. Students were then asked to draw their own graphs to verify their conjectures.

Such efforts to create these conjectures follow the modern day Common Core Standards. One of the fourth grade Common Core State Standards (CCSS.MATH.CONTENT.4.OA.C.5) states that students should be able to "[g]enerate a number or shape pattern that follows a given rule [and] [i]dentify apparent features of the pattern that were not explicit in the rule itself" [4]. In this activity students were not told of any rules that Eulerian trails follow. Instead, through exploration and inquiry, students were able to develop their own patterns by taking special note of the features of the vertices of the graphs.

One of the bigger demands in this activity was the high vocabulary use. Students were required to use the vocabulary of and understand the concepts of odd and even, concepts not all second graders had been exposed to. Additional vocabulary use include vertex and edge. To ensure successful understanding, time must be spent teaching vocabulary.

Nonetheless, this and other graph theory activities work splendidly for gifted children. Their curiosity and reluctance to accept facts without understanding allow detailed examination. Furthermore, graph theory lends itself to activities that ensure high student engagement, as was the case with the tape activity.

2. Tower of Hanoi

The problem of the Tower of Hanoi is an interesting problem for students to tackle because of the variety of approaches and activities instructors can engage students with. This problem allows for hands-on learning as well as the use of mathematical concepts of exponents.

For this presentation, students were read the legend of the Tower of Hanoi found on the Encyclopedia Britannica website [5]. The set up for this problem has three towers, where the first tower has a specified number of discs. From top to bottom, the discs are in increasing order of radius measure. With the least number of moves and moving one disc at a time, students are to transfer all the discs from the first tower to the third tower. A bigger disc can never go on top of a smaller disc.

We began the activity by considering the first two cases, moving one disc and then two discs from the first to the third tower. The following table was drawn on the board for later purposes:

Discs	Moves
1	1
2	3

Students were then put in groups of two or three. Each group was given the task of solving the Tower of Hanoi problem using three discs. The smallest number of moves for any group was 9. Using the website *Math is Fun*, students were shown that the least number of moves required is 7 [6]. They were then given a chance to try again. Only one group was successful.

This was repeated using four discs. The least number of moves for any group was 16; the smallest number possible is 15.

Students were then asked to return to their seats. Using what they learned during their group collaboration, students were asked if they noticed any patterns on how the problem was to be solved for any given number of discs. This took some effort and a number of visual demonstrations, including the white board, the *Math is Fun* website, and the discs students used. Through discussion and guidance, students were able to see that in the case of four discs, they first had to reconstruct the case of three discs.

Finally, we investigated the numbers. To point students in the right direction, they were told to look at the previous table and the relationship between the numbers on the left hand column and their corresponding number on the right hand column. They were told to think of the numbers on the right hand column in terms of exponents with a base of two. Students were confused, as they correctly noticed that the right hand column had only odd numbers, but what they were asked to do resulted in only even numbers.

Students were then given the next hint to the answer; they were told to subtract a very specific number from each of the exponentiated numbers on the right hand column. After quite some difficulties, someone yelled out, "Subtract one!" Suddenly, the lightbulb went on for many students in the room, and they were able to notice the following pattern in the numbers:

Discs	Moves
1	$1 = 2^1 - 1$
2	$1 = 2^2 - 1$
3	$7 = 2^3 - 1$
4	$15 = 2^4 - 1$

Students were finally able to generalize that for n discs, $2n - 1$ moves were the least number of moves required.

This activity works well for gifted students because it requires long concentration and, at least, a basic understanding of exponents. Additionally, problem of the Tower of Hanoi is helpful with the Common Core Standards for Mathematical Practices (CCSS.Math.Practice.MP8), which states that educators should develop students' abilities to "[l]ook for and express regularity in repeated reasoning" [7]. The essence of this mathematical practice says that students should be able to find patterns and generalize their understanding. Students successfully accomplished this in this problem. They completed the Tower of Hanoi for the first few discs until they were able to correlate the numbers on the board with their own findings. While a future presentation could have students do more number manipulation, students were, nonetheless, able to arrive at a general enough method to find the number of moves required for any given number of discs.

3. ABACUS March 2015, Problem 1018

The following is problem 1018 from the Paul Erdos In- ternational Math Challenge problem set, formerly the ABACUS International Math Challenge, for March 2015:

Four kids are building sand castles. Everybody's castle is a different height. They made the following true statements

Fanny: My castle is not higher than Suzanne's.
Eva: Suzanne's castle is not smaller than Katie's.
Katie: Eva built a smaller castle than Fanny.
Suzanne: Eva's castle is not the smallest.

Put the castles in an increasing order of their heights [1].

In preparing to present this problem, the following, incorrect ordering was made:

Suzanne
Fanny
Katie
Eva

The ordering

Suzanne
Fanny
Katie

was constructed from the first and second statements. However, this is a hasty assumption, as we know Katie's castle size relative to Suzanne's but not rela-tive to Fanny's.

To help students think more critically, they were give the following pre-problem, which they answered correctly: If A and B are friends and A and C are friends, do we know that B and C are friends?

Students were put into groups and given four stacks of blocks, each stack was of different color to represent each castle. Using only the first statement, students were shown one way to use the blocks.

After observing each group, it was apparent that the phrasing of the statements was giving students difficulty. Students were asked to, as a class, rewrite the statements for easier understanding:

Fanny: Suzanne's castle is taller than mine.
Eva: Suzanne's castle is taller than Katie's.
Katie: Fanny built a taller castle than Eva's.
Suzanne: Eva's castle is not the smallest.

More students had success after this rephrasing. A few groups struggled using the blocks; they decided to work on paper. Once students were done working with their group, we had a class discussion where students were required to justify their solutions.

While time would have been saved on this exercise by having students rephrase the statements first, it was very instructive for students to see the importance of rewriting a problem, rather than tackling a problem that is not understood. This exercise also helped students gain a better understanding of methods that work for them individually; some students worked well with pencil and paper whereas other benefiitted from using blocks. Moreover, as the Common Core standards emphasize a more thorough understanding of the logic and reasoning of mathematics, problems such as these tackle the Common Core Standards for Mathematical Practices (CCSS.Math.Practice.MP3) [7]. Through these types of problems, students are learning to construct logical arguments and find evidence to support their conjectures.

4. About Fractals and the Powers of Numbers

Understanding fractals proved to be an engaging focus for our group. The topic of powers of numbers led students to confuse powers with multiplication. The following problem, taken from Natasha Rozhkovskaya's *Math Circles for Elementary School Students*, highlighted the understanding of fractals and power of numbers [8].

The lesson began by having students analyze the following image as it was being drawn on the board:

Students were asked if they noticed any reoccurring patterns as the tree was being drawn. The tree was constructed by first drawing the vertical stem and then two branches parting separate directions. To each branch we added two more branches, just as in the figure above. Then the fractal tree design taken from Koos Verhoeff and his foundation was displayed on the overhead:

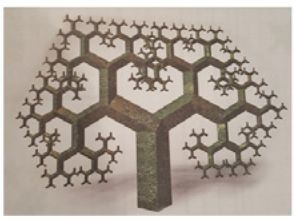

Students were given the following information:

Assume that the tree grows so that the new branches appear at the end of each year. At the end of the first year, two new branches grow on the stem. At the end of the second year, four new branches grow from those two, and so on.

We posed the following question: Would it be possible to determine the age of this tree?

A few students fumbled with the question with an, "I have no idea!", while others mumbled about having to recreate the tree. That is what we did. We divided the class into six groups of two. Four groups garbled with the posed question by using connecting blocks

to build their trees and determine the number of branches after five years, then seven, then ten. The other groups used the white board and dry erase markers to build their trees and, similarly, figure out the number of branches from year to year. We had to remind students to write the number of branches of the tree on their papers or white board as they moved along from year to year, as it was causing students difficulty remembering. Students who used connecting blocks took longer to arrive to their conclusion in comparison to those who used the white board. Interestingly, however, using the technique in the previous figure, all students confidently arrived to the conclusion that there were 30 branches after the fifth year.

2 branches (red) after the first year
4 branches (blue) after the second year
8 branches (green) after the third year
16 branches (orange) after the fourth year . . .

To some groups a simple, "You are very close, try again," was enough to get them to recreate their tree more carefully. Some groups were able to find that there are 32 branches after the fifth year and were quietly told to advance to the next given year. To make sure all groups had figured out the answer on their own, they were asked to explain how they arrived at their conclusion.

A particular female student asked if this activity had any relation to the concept of exponents. It was fascinating to see how this activity stirred this second grader's mind to break outside the borders to relate it to what she had been previously taught. The student's curiosity sparked an interest in other students' minds. The lesson was then led toward a brief explanation on the board to relate fractals to exponents in the following manner:

$$2 = 2$$
$$4 = 2 \cdot 2$$
$$8 = 2 \cdot 2 \cdot 2$$
$$\vdots$$
$$32 = 2 \cdot 2 \cdot 2 \cdot 2 \cdot 2$$

It was explained that $2 \cdot 2 \cdot 2 \cdot 2 \cdot 2$ can also be written as 2^5, where 5 is the exponent. Other cases were shown to give them a better understanding of what exponents are. They were thrilled to find that by using the idea of exponents they could find a method to determine the number of branches of the tree after 100 years without actually drawing the tree. As the Common Core State Standards push forth the importance of recognizing patterns with numbers (CCSS.MATH.CONTENT.3.OA.D.9), our activities enabled our students to make these types of connections. Students are being stimulated to recognize patterns between exponents and the operation of multiplication [3].

A big challenge with the groups that were working with connecting blocks was distinguishing the number of branches that grew from year to year. Because of the lack of quantity of blocks in each color, students were using different colored blocks for one branch. This activity could have proved more useful if students were provided bigger quantities of each color for easier distinctions. Nevertheless, students enjoyed working together to build their

fractal tree and determine the number of branches of the tree after any given year. Students found the activity easier and faster when using the white board but stimulating using the connecting blocks.

5. Logic and Animals

The next problem, taken from Natasha Rozhkoyskaya's *Math Circles for Elementary School Students*, deals with logic and animals.

Problem: Little Squirrel is having a birthday party today. Squirrel's six friends Owl, Deer, Rabbit, Lynx, Mouse, and Fox came to celebrate.

The guests sat around the table so that:

- Owl's neighbors were Fox and Lynx
- Squirrel took chair number four near Rabbit
- Mouse refused to sit next to any predator
- There were two guests seated between Owl and Squirrel.
- Lynx chose chair number two.

Question: Where did Deer sit? [8]

To begin this lesson, the presenter read the problem and then asked, how many animals will be sitting around the table? Immediately students responded "six," but then changed their response to "seven." Indeed, there are seven animals sitting around the table including the host, Squirrel. Seven volunteers were called to stand in a circle in the front of the classroom. Each student was given one of the animals to act out at the pretend birthday party. As only few students knew what a Lynx is, it was explained that it is a wild cat. The presenter may choose to change the animal to something more familiar, but it must be kept in mind that there is a clue that deals with predators of the mouse. The volunteers impersonated their given animal, and then the they sat in a circle in the pretend chairs that were numbered from one to seven as the following figure depicts:

Slowly and clearly, the presenter read the first clue from the problem: Owl's neighbors were Fox and Lynx. The presenter asked the Owl, Fox, and Lynx to raise their hand so that the rest of the class knew who was which animal. This was done for every animal in each round. As the presenter read the clue again and asked for input from the audience, the

volunteers began swapping places. The audience either disagreed or agreed and was asked what movements the volunteers should do instead. The volunteers would then move around the circle accordingly. This pattern was followed after the presenter read each clue.

Another clue read: Mouse refused to sit next to any predator. Most students knew what animals would be considered a predator of the mouse and were quick to eliminate them. However, to ensure all students are follow along, it is suggested that the presenter ask the class what animals are considered predators of the mouse.

This activity took some time as the audience and volunteers gave input on where the animals should be seated. After the volunteers made their switch once the clues were read, the audience either disagreed or agreed with the move. After the audience gave their input the same clue was read again, and many times rearrangements had to be made. None of the clues had said anything about where Deer should sit; how- ever, in the end, the volunteers and clever audience figured out Deer's place on the table – number six.

Students seemed to really enjoy this problem as it brought good humor into the room. All students were active participants whether they had been volunteers or audience members. After this, students were eager to participate in more activities that involved portraying animals or performing skits. Furthermore, the nature of this problem works splendidly in continuing to help students develop the ability to "construct viable arguments and critique the reasoning of others," as specified by the Common Core Standards for Mathematical Practices (CCSS.Math.Practice.MP3) [7].

6. Final Thoughts

Working with gifted children was a privilege and a challenge. Their above average knowledge of mathematics allows for comprehensive exploration. The challenges, then, come in having thorough under- standing of students' abilities.

The problems discussed in this paper are suitable for gifted students because they involve layers of under- standing and logic; they were not mere skill and drill. Additionally, these involved engaging, hands-on activities which ultimately led to higher understanding of mathematical concepts, as is the goal of Common Core. Moreover, the problems presented use logic and critical thinking skills that will be required for success for those who choose to pursue a path in mathematics or other STEM fields.

References

[1] 3rd and 4th Grade – March 2015. *Paul Erdos International Math Challenge*. Byelocorp Scientific, Inc., Picower Foundation, QED Technologies, Begell House. url: http://inside.gcschool.org/abacus/2015/10/02/3rd-and-4th-grade-march-2015.

[2] Brualdi. *Introductory Combinatorics*. 5th ed. Up- per Saddle River, NJ: Pearson/Prentice Hal, 2010.

[3] Operations Grade 3 and Algebraic Thinking. *Common Core State Standards Initiative*. url: http://www.corestandards.org/Math/Content/3/OA/#CCSS.Math.Content.3.OA. D.9.

[4] Operations & Algebraic Thinking Grade 4. *Common Core State Standards Initiative*. url: http://www.core-standards.org/Math/Content/4/ OA/.

[5] Tower of Hanoi. Encyclopedia Britannica Online. url: http://www.britannica.com/topic/ Tower-of-Hanoi.

[6] Tower of Hanoi. *Math Is Fun*. url: http://www.mathsisfun-com/games/towerofhanoi.html.

[7] Standards for Mathematical Practice. *Common Core State Standards Initiative*. url: http:// www.corestandards.org/Math/Practice/.

[8] Natasha Rozhkovskaya. *Math Circles for Ele- mentary School Students*. Berkley: American Mathematical Society, 2014.

Back to Square One

Brian Laverty
Advisor: Dr. Thomas Murphy

Department of Mathematics, California State University, Fullerton

Abstract

For this research, I have found contradictions to the claim made in the article *On Packing of Squares and Cubes* by A. Meir and L. Moser. The claim was that there are exactly two solutions to the equation $1^2 + 2^2 + \ldots + n^2 = m^2$ for integers n and m, namely $(n,m) = \{(1,1), (24,70)\}$. I found multiple (additional) solutions to this equation—the next solution appearing with n in the two millions.

Further, using the solution $1^2 + 2^2 + \ldots + 24^2 = 70^2$, I have been trying to find a perfect squared square. That is, a 70×70 square dissected into squares 1×1, 2×2, $\ldots$, 24×24. There have been claims that such a dissection is not possible, but no proof has been provided. In order to make this problem more approachable, first suppose that there is such a dissection of the 70×70 square. Then the lengths of the squares on the edge must sum to 70. I created a code in MATLAB to provide all possible combinations of 1, 2, $\ldots$, 24 that sum to 70. I have reduced this list considerably and hope to reduce it enough to prove that there is no such dissection, or find the dissection—if it does exist.

(r)-Pancyclic, (r)-Bipancyclic and Oddly (r)-Bipancyclic Graphs*

Lisa Mueller *Department of Mathematics, California State University, Fullerton*
Oliver Sawin *Department of Mathematics, Rensselaer Polytechnic Institute*
WonHyuk "Harry" Choi *Department of Mathematics, Pomona College*
Advisor: Dr. Abdollah Khodkar *Department of Mathematics, University of West Georgia*

Abstract

A graph with v vertices is (r)-pancyclic if it contains precisely r cycles of every length from 3 to v. A bipartite graph with even number of vertices v is said to be (r)-bipancyclic if it contains precisely r cycles of each even length from 4 to v. A bipartite graph with odd number of vertices v and minimum degree at least 2 is said to be oddly (r)- bipancyclic if it contains precisely r cycles of each even length from 4 to $v - 1$. In this paper, using a computer search, we classify all (r)-pancyclic and (r)-bipancyclic graphs, $r \geq 2$, with v vertices and at most $v +$ 5 edges. We also classify all oddly (r)-bipancyclic graphs, $r \geq 1$, with v vertices and at most v + 4 edges.

∗Research supported by NSF REU Grant DMS1262838, University of West Georgia

Edge Magic Total Labelings*

Lisa Mueller *Department of Mathematics, California State University, Fullerton*
Nick Bohall *Department of Mathematics, University of Washington*
Kajal Chokshi *Department of Mathematics, Loyola University Chicago*
Jackie Emrich *Department of Mathematics, Loyola University Maryland*
Advisor: Dr. Abdollah Khodkar *Department of Mathematics, University of West Georgia*

Abstract

A graph with v vertices and e edges has an edge-magic total labeling if the vertices and edges can be labeled with the numbers 1 through $v + e$ such that the sum of any edge and its two adjacent vertices adds up to the same number. The main focus for this research project has been to explore different types of graphs to see which are edge-magic in general or for an entire spectrum of possible sums according to how many vertices and edges a given graph contains.

Edge-Magic Total Labelings

Before we delve into what an edge-magic total labeling is, we first need to establish a few more definitions about magic graphs in general. A connected graph is called *semi-magic* if the edges can be labeled with integers such that the sum of all of the edges incident with each vertex adds up to the same number. [?] A graph is simply called *magic* if all of the edges are labeled with distinct numbers. [?] The property that we focused on for the entirety of our research was finding which graphs are *edge-magic*, meaning that the sum each edge and its two adjacent vertices add up to the same number [?]. In particular, we did research on finding which graphs had an *edge-magic total labelings*. This means that for graphs with v vertices and e edges, the graph turns out to be edge-magic, where only the numbers 1 through $v + e$ are used. [?]

There are many types of graphs that have edge-magic total labelings, such as complete graphs, bipartite graphs, certain types of trees, cycles, paths, and more. [?] However, there are still many different types of graphs that have not had any published material about whether an edge-magic total labeling exists for them or not. Additionally, for graphs that were already known to be edge-magic, there was not much research done determining how many different sums on the possible spectrum of constants that each edge and its adjacent vertices can add up to worked [in this case, they would range from $1 + 2 + v + e$ to $2(v + e)$]. Although we discovered some of these things by hand, we created and perfected a computer pro- gram via Python in which one enters the vertices and edges of a graph, and every possible labeling is outputted into a separate file. This has mainly helped us in finding patterns in the labelings, as well as seeing whether or not certain graphs are edge-magic for all possible sums. For our research, we mainly focused on three different types of graphs: complete tripartite graphs, spiders, and odd-cycle kites.

∗Research supported by NSF REU Grant DMS1262838, University of West Georgia

Edge-Magic Programming via Python

The program that we created uses recursive backtracking to try and find every possible labeling. This program is not as efficient as it could be, especially since it prints out many isomorphic labelings. However, we can make the program more efficient by using a concept similar to a Sidon sequence (a sequence with n terms $0 < a_1 < a_2 < \ldots <$ an such that $a_i + a_j = a_k + a_l$ where i, j, k, l are all different) and restricting the sums [?]. First, as we know that the range of possible magic sums is between $1 + 2 + (v + e)$ and $2(v + e)$, we attempt to find all of the labelings for a given sum, then move on. Next we modify the concept of a Sidon sequence, only imposed that if there is an edge between two vertices, the sum of the vertices is not repeated elsewhere in the graph. Using this concept, we can eliminate many labelings early on. However, this is not a sufficient condition for an edge-magic total labeling, and the program continues on and assigns edge values for the given sum and then checks to see if any label is missing or repeated. If all of these things are satisfied, it then prints out the labelings to a file in an adjacency matrix.

Edge-Magic Complete Tripartite Graphs

For the majority of our research, we sought out to find patterns in complete tripartite graphs of the form $K_{1,m,n}$, with m, $n \geq 1$. There are many different possible magic sums that these graphs could have, ranging from $3 + m +$ n to $2(m + n)$. In the beginning, we conjectured that all complete tripartite graphs are edge-magic, and so we began to try proving this for smaller groups of complete tripartite graphs. First, we wanted to look at graphs of the form $K_{1,m,n}$, and so far, we have been able to prove that all of these graphs are edge-magic for their minimum sums. (The proof is provided below.) After proving this, we changed our pace to figuring out which graphs worked for the spectrum of possible sums that each graph could have.

Conjecture
$K_{1,m,n}$, has an edge-magic total labeling for m, $n \geq 1$, with sum $k = 4 + 2m + 2n + mn$ (its minimum possible sum).

Proof
Consider the complete tripartite graph $K_{1,m,n}$, with m, $n \geq 1$. WLOG, assume $m \geq n$. Note that$K_{1,m,n}$ has $1 + m + n$ vertices and $m + n + mn$ edges. So we need to label the vertices and the edges with the numbers 1 through $1 + 2m + 2n + mn$ such that the sum of the labels of each edge and its two adjacent vertices adds up to $k = 4 + 2m + 2n + mn$. For convenience, we will refer to the solitary vertex with the highest degree as v, the m vertices as $x_1, x_2, \ldots, x_m$, and the n vertices as $y_1, y_2, \ldots, y_n$. Consider the following labeling:

- Label v with the value 1.
- Label $x_1, x_2, \ldots, x_m$ with 2, 3, . . . , $m + 1$, respectively.
- Label $y_1, y_2, \ldots, y_n$ with $m + 2$, $2(m + 2)$, . . . ,$n(m + 2)$, respectively.
- Label each edge with the appropriate number such that each edge and its adjacent vertices add up to the sum k. (For example, the edge connecting 1 and 2 will be $1 + 2m + 2n + mn$; the edge connecting 1 and 3 will be $2m + 2n + mn$; and so on.)

In order to prove that this is an edge-magic total labeling, we need to verify that (1) the vertices and the edges share no common values, and that (2) no two edges have the same label. Note that we do not need to check to see if the vertices are labeled differently since we specifically assigned each vertex a different value.

Let us look at the different values that are assigned to each edge by the way we labeled our vertices:

- The edges connecting v with $x_1, x_2, \ldots, x_m$ are labeled with the values $1 + 2m + 2n + mn$, $2m + 2n + mn, \ldots, 2 + m + 2n + mn$, respectively.
- The edges connecting v with $y_1, y_2, \ldots, y_n$ are labeled with the values $1 + m + 2n + mn$, $-1 + 2n + mn, -3 - m + 2n + mn, \ldots, 3 + 2m$, respectively.
- The edges connecting x_1 with $y_1, y_2, \ldots, y_n$ are labeled with the values $m + 2n + mn, -2 + 2n + mn, -4 - m + 2n + mn, \ldots, 2 + 2m$, respectively.
- The edges connecting x_2 with $y_1, y_2, \ldots, y_n$ are labeled with the values $-1 + m + 2n + mn, -3 + 2n + mn, -5 - m + 2n + mn, \ldots, 1 + 2m$, respectively.

  $\vdots$

- The edges connecting x_m with $y_1, y_2, \ldots, y_n$ are labeled with the values $1 + 2n + mn, -m + 2n + mn, -1 - 2m + 2n + mn, \ldots, 3 + m$, respectively.

As we can see from this list, the numbers 1 through $m + 1$ never appear as an edge value. Similarly, we can see that all multiples of $m + 2$ are not found within the edge values, as well. This proves (1) since all of the vertex values and edge values are distinct.

Now, we need to show that no two edges have the same value. Clearly, focusing on one vertex at a time, all of its adjacent edges will have different values since the vertices to which the edges are connected are all distinct. So, we only have three cases to show. (For convenience, we will say v belongs to the set A; $x_1, x_2, \ldots, x_m$ belong to the set B; and $y_1, y_2, \ldots, y_n$ belong to the set C, where $A \cup B \cup C$ contains all the vertices of $K_{1,m,n}$ and $A \cap B \cap C = \emptyset$.)

Case 1: WNTS all edges connecting A to B are distinct from the edges connecting A to C. From our list of edges above, we are com- paring the following sets of numbers:

- $R_1 = 1 + 2m + 2n + mn, 2m + 2n + mn, \ldots, 2 + m + 2n + mn$, and
- $S_1 = 1 + m + 2n + mn, -1 + 2n + mn, \ldots, 3 + 2m$, where $|R_1| = m$ and $|S_1| = n$.

WNTS $R_1 \cap S_1 = \emptyset$. R_1 consists of m consecutively descending numbers, with $2 + m + 2n + mn$ as its lowest value. S_1 consists of n descending numbers, whose gaps between consecutive terms equal $m + 2$, with $1 + m + 2n + mn$ as its highest value. Since $r \geq 2 + m + 2n + mn$ for all $r \in R$, and $s \leq 1 + m + 2n + mn$ for all $s \in S$, then $r \neq s$ for all possible values of r and s. Thus $R_1 \cap S_1 = \emptyset$, as needed. Therefore all edges connecting A to B are distinct from the edges connecting A to C.

Case 2: WNTS all edges connecting B to A are distinct from the edges connecting B to C. Note that there are m vertices in B, where each vertex is adjacent to $n + 1$ distinct edges. Because the difference between each consecutive vertex in B is 1, then the difference between each edge connecting every consecutive vertex in B to a vertex in C will also differ by 1. WLOG, we will test to make sure all of x_1's edges are distinct. (The proof can then be performed recursively m times with each vertex, subtracting every edge value by 1 with each respective vertex.) From our list of edges above, we are comparing the following sets of numbers:

- $R_2 = 2 + 2m + 2n + mn$, and
- $S_2 = m + 2n + mn, -2 + 2n + mn, \ldots, 2 + 2m$, where $|R_2| = 1$ and $|S_2| = n$

WNTS $R_2 \cap S_2 = \emptyset$. S_2 consists of n descending numbers, whose gaps between consecutive terms equal $m + 2$, with $m + 2n + mn$ as its highest value. Since $r > m + 2n + mn$ for $r \in R_2$ and $s \leq m + 2n + mn$ for all $s \in S_2$, then $r \neq s$ for all possible values of r and s. Thus $R_2 \cap S_2 = \emptyset$, as needed. Therefore, all edges connecting B to A are distinct from the edges connecting B to C.

Case 3: WNTS all edges connecting C to A are distinct from the edges connecting C to B. Note that there are n vertices in C, where each vertex is adjacent to m+1 edges. Because the difference between each consecutive vertex in C is m + 2, then the difference between each edge connecting every consecutive vertex in C to a vertex in B will also differ by m + 2. WLOG, we will test to make sure all of y_1's edges are distinct. (The proof can then be performed recursively n times with each vertex, subtracting every edge value by m + 2 with each respective vertex.) From our list of edges above, we are comparing the following sets of numbers:

- $R_3 = 2 + 2m + 2n + mn$ and
- $S_3 = m + 2n + mn, -1 + m + 2n + mn, \ldots, 1 + 2n + mn$, where $|R_3| = 1$ and $|S_3| = m$

WNTS $R_3 \cap S_3 = \emptyset$. S_3 consists of m descending consecutive numbers, with $m + 2n + mn$ as its highest value. Since $r > m + 2n + mn$ for $r \in R_3$ and $s \leq m + 2n + mn$ for all $s \in S_3$, then $r \neq s$ for all possible values of r and s. Thus $R_3 \cap S_3 = \emptyset$, as needed. Therefore, all edges connecting C to A are distinct from the edges connecting C to B. Note that the set of all edges connecting A to B is equivalent to the set of all edges connecting B to A. (The same can be said for A to C and C to A, and B to C and C to B.) So, these three cases combined have essentially proven that all of the edges between A and B, B and C, and A and C all are assigned distinct values. This proves (2). Since both (1) and (2) have been proven, then the labeling provided for $K_{1,m,n}$ above is in fact an edge-magic total labeling for its minimum possible sum. Thus we have proven the above conjecture.

Regarding graphs of the form $K_{1,1,n}$, with $n \geq 1$, our program discovered that $K_{1,1,1}$ (this is just a standard 3-cycle), $K_{1,1,2}$, $K_{1,1,3}$, and $K_{1,1,4}$ are edge-magic for every possible sum (examples of every possible sum for $K_{1,1,2}$ are provided in Figure 1 on page 7.). Because of this information, we conjecture that all graphs of the form $K_{1,1,n}$ are edge-magic for the entire spectrum of possible magic sums, but we still have yet to provide a proof. Regarding graphs of the form $K_{1,2,n}$, with $n \geq 2$, $K_{1,2,3}$ has been the only graph that our program has determined to be edge-magic for every possible sum. (Examples of each sum are provided in Figure 2 on page 7.) Interestingly, $K_{1,2,2}$ was not edge-magic for its second lowest and highest sums, and $K_{1,2,4}$ was not edge-magic for its second lowest and highest, fourth lowest and highest, and eighth lowest and highest sums. Because of this pattern, we conjectured that no complete tripartite graph of the form $K_{1,2,n}$, with n even, is edge-magic for its second lowest and highest sums, but the proof turned out to be much more difficult that we originally anticipated. We also have the conjecture that the possible sums that will not work for the various graphs of this type will be the $2^k th$ lowest and highest sums, for some integer value(s) k. We originally conjectured that graphs of the form , with n odd, would work for every possible sum, but our program has already discovered that $K_{1,2,5}$'s second lowest and highest sums do not work. Because our program is taking a while to check every possible solution for higher-order graphs, we are holding off on figuring out any other patterns for higher values of m and n (for $K_{1,m,n}$) until we create a more efficient program.

We have also briefly begun testing graphs of the form $K_{2,m,n}$, with m,n ≥ 2, and we have discovered that $K_{2,2,2}$ actually is not edge-magic for any of its possible sums according to our program. Our conjecture that all complete tripartite graphs are edge-magic has thus been disproven with this counterexample (we have yet to provide a proof that $K_{2,2,2}$ is not edge-magic with a method besides brute force); however, we still want to find patterns in higher-order complete tripartite graphs, so we have entered $K_{2,2,3}$ and $K_{2,2,4}$ into our program. Some labelings have already been discovered, but again, because of the inefficiency of our program, we still have yet to figure out if they work for the entire spectrum of possible sums.

Edge-Magic Spiders

With our research, we set out to find a pattern that followed for spiders, a type of tree with a central vertex of degree 3 or higher and spokes extending outward with length ≥ 1. In particular, we focused on spiders with s spoke tails and a longer tail with L edges. We conjecture that all graphs of this type are edge-magic and follow a certain pattern. The edges on the longer-length tail are labeled with $e + v$, $e + v - 1$, $e + v - 2$, . . . , $e + v - L + 2$, $e + v - L + 1$. Whichever number that the highest degree vertex is labeled with, the fol- lowing descending term is labeled the vertex of one of the smaller spoke tails. The numbers then fan out in descending order to all of the other vertices on the outer spoke tails. Once all of the spoke tails are labeled, we begin labeling the inner edge of the spoke tail with the smallest vertex with the next descending number. We then label all the vertices of the inner edges in descending order, fanning back to the spoke tail with the largest vertex. (An example is shown in Figure 3.)

Now, there is another pattern amongst these types of spiders with regards to the vertices on the longer tail. If the tail of length L is even, we label the outer-most vertex of this tail with the number 1. We skip the next vertex and label the third vertex with the number 2. We then skip the next vertex and label the fifth vertex 3, and we continue this pattern until we hit the

central vertex after n times (and thus this vertex will be labeled with the number n). Now, we go back to the vertices that were originally skipped on the longer tail and label them with $n + 1$, $n + 2$, . . . (starting with the vertex between the vertices labeled 1 and 2, and moving upward towards the central vertex) until all of the vertices on the longer tail have been labeled. (An example is shown in Figure 4.) If the longer tail of length L edges is odd, we skip the outer most vertex and label the second-to-last vertex with the number 1. We skip the next vertex and label the next vertex with the number 2. We continue this pattern n times until we hit the central vertex, which we will label with the number n. From here, we go back to the outermost vertex and label it with the number $n + 1$. We then ascend up the tail and label the remaining vertices consecutively with $n + 2$, $n + 3$,... until all of the vertices on the longer tail have been labeled. (An example of this is shown in Figure 4.) Note that the number of spokes does not matter, as one would just continue the fanning pattern until all spokes are dealt with as explained in the previous paragraph. Also, as the speaker mentioned, all trees with < 15 vertices have been discovered to be edge-magic; this pattern still works for all spiders of this kind, though. We have attempted to form a proof to extend these patterns to all spiders of this type, but we have not been successful so far; we are leaving the proof-making to our advisor, Dr. Khodkar.

Edge-Magic Kites

The majority of the research with regards to odd-cycle kites has been finding patterns for labelings of 3-cycle kites with either odd or even tails. Figure 5 shows the pattern for even-length and odd-length tails. We have begun to conduct proofs to extend these kites to kites of higher cycles - such as 5-cycle and 7-cycle kites - but so far we have not had any success being able to generalize these patterns.

Future Research

Our research is far from being over, and we will continue our research individually for an extended period of time; that being said, we still have many questions to address, and the following are some of the questions that we will be continuing to try to answer but can be researched by anyone who has an interest for it:

Complete Tripartite-Graphs

1) Which graphs apart from $K_{1,1,n}$, with $n \geq 1$, are edge-magic for every possible magic sum?
2) Are all graphs of the form $K_{1,2,n}$, with $n \geq 2$ and $n \neq 3$, not edge-magic for their second lowest and highest possible magic sums?
3) Can any patterns be generalized to magic sums apart from the minimum possible sum for $K_{1,m,n}$, with m, $n \geq 1$?
3) Are any other graphs of the form $K_{2,m,n}$, with m, $n \geq 2$, not edge-magic for any possible sum, like $K_{2,2,2}$?
4) Can any patterns be made about graphs of the form $K_{2,m,n}$, with m, $n \geq 2$ and m, n not both 2?
5) Which graphs are edge-magic for $K_{k,m,n}$, with k, m, $n \geq 3$? $K_{1,m,n}$, with m, $n \geq 1$?

Complete Tripartite-Graphs

1) Prove the given patterns in Figure 4 can be generalized to all spiders of the given form.
2) Which types of trees are edge-magic for every possible magic sum?
3) Prove or disprove the minimum sum for all trees is $v + e + 4$, where v is the number of vertices and e is the number of edges.
4) Prove or disprove that all possible spiders are always edge-magic.

Kites

1) Prove all 3-cycle kites are edge-magic.
2) Do any patterns exist amongst all 5-cycle kites? 7-cycle kites? Higher odd-cycle kites?
3) Do any patterns exist for odd-cycle kites in general?

References

[1] Marr, A.M., and Wallis, W.D. (2013). Magic Graphs. New York: Spring Science+Business Media. DOI: 10.1007/978-0-8176-8391-7_2.

[2] Gallian, J. A. (2011). A Dynamic Survey of Graph Labeling. The Elec- tronic Journal of Combinatorics, 18, p. 70-101.

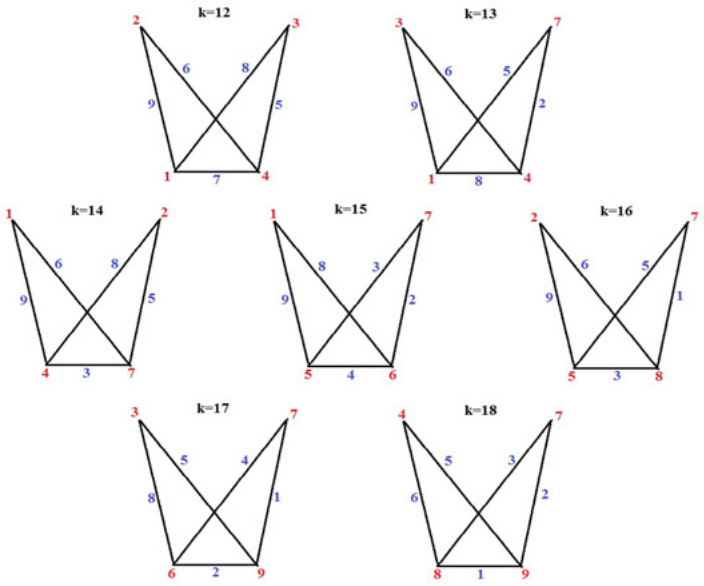

Figure 1: *Examples of edge-magic total labelings of* $K_{1,2,2}$ *for every possible sum from 12 to 18*

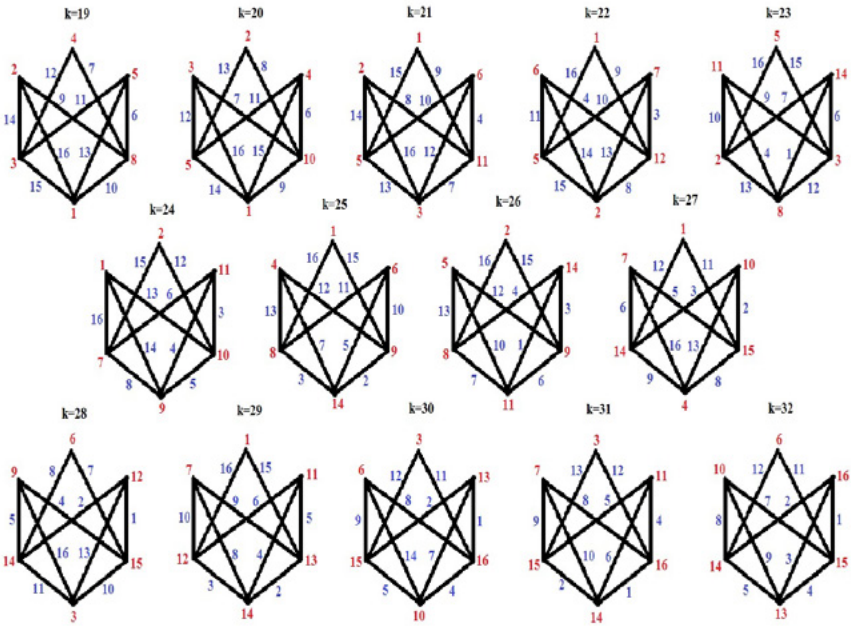

Figure 2: *Examples of edge-magic total labelings of* $K_{1,2,3}$ *for every possible sum from 19 to 32*

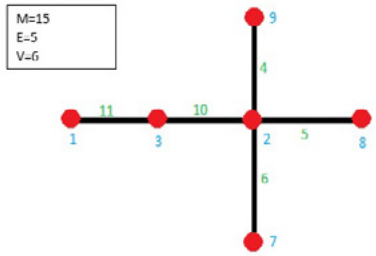

Figure 3: *Blue numbers = vertex labels; green numbers = edge labels; M = magic sum; E = number of edges; V = number of vertices*

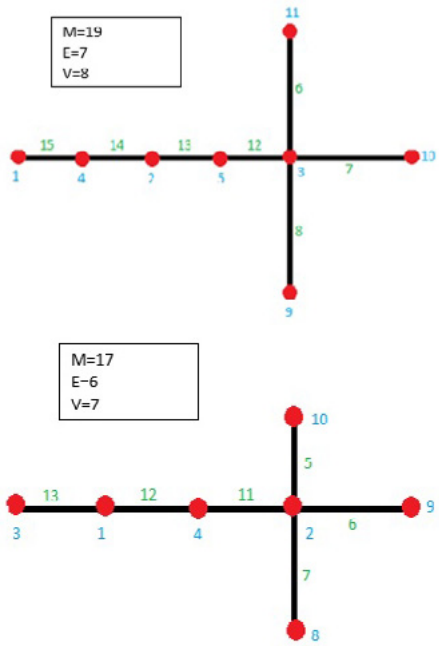

Figure 4: *(From left to right) Examples of spiders with its longest tail of even and odd length.*

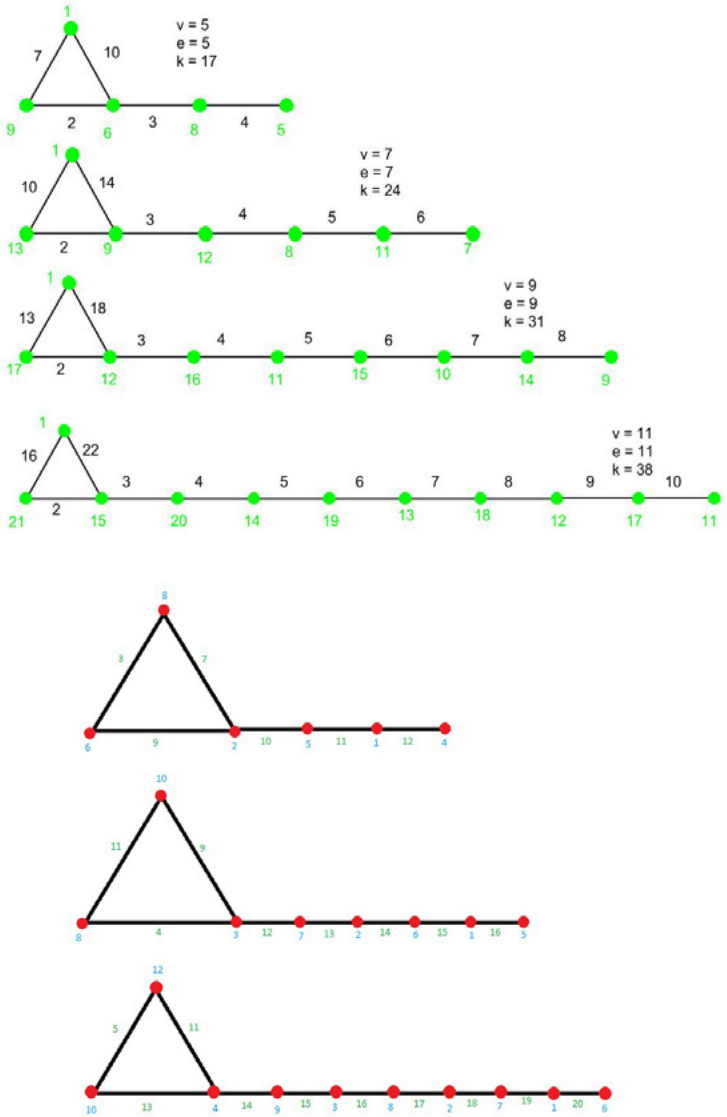

Figure 5: *(From left to right) Examples of 3-cycle kites with even and odd-length tails.*

Picard Numbers Of Certain K3 Surfaces

Bora Olcken
Advisor: Dr. Christopher Lyons

Department of Mathematics, California State University, Fullerton

1. Introduction

The purpose of this research is to study polynomials $F_A = F_A(x, y, z, w)$ of BHK-*type* (see Definition 2.1). The zero-sets of these polynomials give rise to special examples of geometric objects known as K3 surfaces. The Picard number of a K3 surface, roughly speaking, measures the size of the collection of all curves lying on the surface that are defined by polynomial equations. Our interest is in the calculation of this Picard number for the K3 surface arising from F_A. In [1], Kelly provides a concrete method for this calculation, which can be carried out by a computer, but the formula is still fairly complicated. This paper yields a simpler way to calculate the Picard number when F_A satisfies an additional condition (labeled as ($\star$) below).

2. Preliminaries

Definition 2.1. *Let F_A be a polynomial of the form*

$$F_A = \sum_{i=0}^{3} \prod_{j=0}^{3} x_j^{a_{ij}}.$$

Then we will say F_A is a polynomial of BHK-*type if the following hold:*

(i) *The 4×4 matrix $A = (aij)$ is invertible.*

(ii) *Each column of A has at least one zero.*

(iii) *Let $e = (1,1,1,1)^{tr}$. Then the (unique) solution v to $Av = e$ is, up to permutation of the coordinates, one of the 95 vectors in the left column of Table 2.2 of* [2].

Definition 2.2. *A polynomial $f(x_0, \ldots, x_r) \in \mathbb{C}[x_0, \ldots, x_r]$ is* quasi-homogeneous *of degree h and weights $(q_0, \ldots, q_r)$ if and only if*

$$f(\lambda^{q_0} x_0, \ldots, \lambda^{q_r} x_r) = \lambda^h f(x_0, \ldots, x_r)$$

for all $\lambda \in \mathbb{C}^*$.

As a result of part (iii) of Definition 2.1, a polynomial F_A of BHK-type is quasi-homogeneous, and its degree and weight system can be determined as follows. The solution to $Av = e$ is a vector v with rational coordinates, and can be written with least common denominator as

$v = (\frac{q_0}{h}, \frac{q_1}{h}, \frac{q_2}{h}, \frac{q_3}{h})^{tr}$. Then F_A is quasi-homogeneous of degree h and weights $(q_0,\ q_1,\ q_2,\ q_3)$ of F_A.

Note that by assumption the weights $(q_0,\ q_1,\ q_2,\ q_3)$ are relatively prime. The requirement that the vector v belongs to Yonemura's Table 2.2 in [2] guarantees that the weight system belongs to one of the "95 families" that give rise to all K3 surfaces which can be realized as hypersurfaces in weighted projective spaces. It moreover implies that $q_0 + q_1 + q_2 + q_3 = h$.

Polynomials and their mirrors. Let $F_A = F_A(x_0,\ x_1,\ x_2,\ x_3)$ be a polynomial of BHK-type of degree h with weights $(q_0,\ q_1,\ q_2,\ q_3)$. As in part (i) of Definition 2.1, let A be the 4×4 associated exponent matrix of F_A, which is formed by placing the exponent of x_j from the i-th term in the position $(i,\ j)$. (Note that we are indexing nontraditionally with $0 \leq i,\ j \leq 3$.) Now using A^T , the transpose of A, we can reverse this process and form the *mirror polynomial* $F_{A^T} = F_{A^T}(x_0,\ x_1,\ x_2,\ x_3)$. This polynomial will also be of BHK-type, with some degree h_T and weights $(q_0^T, q_1^T, q_2^T, q_3^T)$. Note that the mirror polynomial of F_{A^T} is the original polynomial F_A.

In general it is true that $h \cdot h_T \mid \det(A)$, but $\det(A)$ (which we can assume to be positive without loss of generality) can be greater than $h \cdot h_T$. In this paper we will be studying polynomials that satisfy the additional condition

$$(\star) \qquad \det(A) = h \cdot h_T.$$

Note that this restriction still includes many polynomials, such as the following example.

Example. Let $F_A = x_0^2 + x_1^3 + x_2^7 x_3 + x_3^{36}$. This polynomial is of BHK-type with degree $h = 36$ and weights $(q_0,\ q_1,\ q_2,\ q_3) = (18,\ 12,\ 5,\ 1)$.

Using the exponents of each monomial of F_A, we form the 4×4 matrix

$$A = \begin{bmatrix} 2 & 0 & 0 & 0 \\ 0 & 3 & 0 & 0 \\ 0 & 0 & 7 & 1 \\ 0 & 0 & 0 & 36 \end{bmatrix}.$$

Taking the transpose of matrix A, we have

$$A^T = \begin{bmatrix} 2 & 0 & 0 & 0 \\ 0 & 3 & 0 & 0 \\ 0 & 0 & 7 & 0 \\ 0 & 0 & 1 & 36 \end{bmatrix}.$$

Now using matrix A^T, we can reverse the process above to form the polynomial

$$F_{A^T} = x_0^2 + x_1^3 + x_2^7 + x_2 x_3^{36}.$$

This is the mirror polynomial of F_A. Notice F_{A^T} is also of BHK-type, but with degree $h_T = 42$ and weights $(q_{0^T}, q_{1^T}, q_{2^T}, q_{3^T}) = (21, 14, 6, 1)$.

Finally, we let d be the least common denominator of all nonzero entries of A^{-1}, which will play an important role in the calculation of the Picard number below.

Lemma 2.3. *Let h be the degree of a polynomial F_A of BHK-type and d be as above. Then $h \mid d$.*

Proof. From part (iii) of Definition 2.1 we know that $Av = e$ where $v = (\frac{q_0}{h}, \frac{q_1}{h}, \frac{q_2}{h}, \frac{q_3}{h})^{tr}$ and $e = (1, 1, 1, 1)^{tr}$. Since A is invertible, then we can write $v = A^{-1}e$. Now multiplying both sides by d, we have $dv = dA^{-1}e$. By definition of d the right hand side is a vector with integer entries. Since the weights do not have any common factors, then for dv to have integer entries, $h \mid d$ must be true. □

Calculating the Picard number. Consider 4-tuples of the form $(a_0, a_1, a_2, a_3) \in (\mathbb{Z}/d)^4$. Define

$$\mathfrak{A}_d = \{(a_0, a_1, a_2, a_3) \in (\mathbb{Z}/d)^4 \mid a_0 + a_1 + a_2 + a_3 \equiv 0 \pmod{d} \text{ and } a_i \not\equiv 0 \pmod{d} \text{ for all } i\}$$

Define

$$\mathfrak{B}_d(0) = \left\{(a_0, a_1, a_2, a_3) \in \mathfrak{A}_d \;\middle|\; \sum_{i=0}^{3} \left\langle \frac{ta_i}{d} \right\rangle = 2 \text{ for all } t \in \mathbb{Z} \text{ such that } (t, d) = 1 \right\}.$$

Here $\langle \frac{m}{n} \rangle$ is the fractional part of the rational number $\frac{m}{n} \in \mathbb{Q}$, and hence lies in [0,1). For any $b \in \mathbb{Z}$ such that $(b,\ d) = 1$, let f be the order of b in and $(\mathbb{Z}/d)^*$ define.

$$\mathfrak{B}_d(b) = \left\{(a_0, a_1, a_2, a_3) \in \mathfrak{A}_d \;\middle|\; \sum_{i=0}^{3} \sum_{j=0}^{f-1} \left\langle \frac{ta_i b^j}{d} \right\rangle = 2f \text{ for all } t \in \mathbb{Z} \text{ such that } (t, d) = 1 \right\}.$$

It is important to note that $\mathfrak{B}_d(b)$ only depends upon b modulo d, and therefore we will often assume $0 < b < d$. Finally, define $\mathfrak{I}_d(b) = \mathfrak{A}_d - \mathfrak{B}_d(b)$.

Now define the following cyclic subgroups of $(\mathbb{Z}/d)^4$:

$$G = \langle \alpha \rangle, \text{ where } \alpha = \left(\frac{q_0 d}{h}, \frac{q_1 d}{h}, \frac{q_2 d}{h}, \frac{q_3 d}{h} \right), \tag{1}$$

$$G_T = \langle \alpha_T \rangle, \text{ where } \alpha_T = \left(\frac{q_{0^T} d}{h_T}, \frac{q_{1^T} d}{h_T}, \frac{q_{2^T} d}{h_T}, \frac{q_{3^T} d}{h_T} \right). \tag{2}$$

Note that for $i \in \{0, 1, 2, 3\}$, $\dfrac{q_i d}{h} \in \mathbb{Z}$ by Lemma 2.3.

Now let X be the complex K3 surface defined by F_A. Since F_A has integer coefficients, it can be reduced modulo p, for any prime $p \nmid d$, to give a K3 surface X_p defined over $\mathbb{F}_p$. Then in Corollary 1.4 of [1], Kelly has shown the following:

Theorem 2.4 (Kelly)**.** *The geometric Picard numbers $\rho(X)$ and $\rho(X_p)$ are given by*

$$\begin{aligned}\rho(X) &= 22 - \#(\mathfrak{I}_d(0) \cap G_T)\\ \rho(X_p) &= 22 - \#(\mathfrak{I}_d(p) \cap G_T).\end{aligned}$$

3. Findings

So as to simplify notation, let $A_d \coloneqq \mathfrak{A}_d \cap G, B_d(b) \coloneqq \mathfrak{B}_d(b) \cap G$, and $I_d(b) \coloneqq \mathfrak{I}_d(b) \cap G$.

Calculation of $I_d(0)$. In this section, we focus on producing a simplified formula for computing the Picard number $\rho(X)$ when the condition $\det(A) = h \cdot h_T$ is satisfied.

Proposition 3.1. $\mathrm{Ord}(G) = h$.

Proof. Since $G = \langle\alpha\rangle$ where $\alpha = (\frac{q_0 d}{h}, \frac{q_1 d}{h}, \frac{q_2 d}{h}, \frac{q_3 d}{h})$ as in equation (1), then $h\alpha = (0,0,0,0)$. This means $\mathrm{Ord}(G) \mid h$. Now let $j \coloneqq \mathrm{Ord}(G)$. Then $j\alpha = (0,0,0,0)$ with $j \mid h$. Let $h = jk$ and by Lemma 2.3, write $d = hh'$ for some $k, h' \in \mathbb{Z}$. Then $j\alpha = (0,0,0,0)$ implies $j\frac{q_i a}{h} = jh'q_i \equiv 0 \pmod{d}$ for all i. This means that $d \mid jh'q_i$ for all i. Substituting for d, we have $jkh' \mid jh'q_i$ for all i. Thus, $k \mid q_i$ for all i. Since the greatest common divisor of $q_0,\ q_1,\ q_2,\ q_3$ is 1, then $k = 1$. Hence $h = j$ and the order of G is h. □

Lemma 2.3. *If $(k,\ h) = 1$, then there exists a $K \in \mathbb{Z}$ such that $K \equiv k \pmod{h}$ and $(K,\ d) = 1$.*

Proof. Let $q_1,\ q_2, \ldots,\ q_n$ be the distinct primes that divide d but not h. Then by the Chinese Remainder Theorem, the system

$$\begin{aligned}K &\equiv k \pmod{h}\\ K &\equiv 1 \pmod{q_1 q_2 \cdots q_n}\end{aligned}$$

has a solution modulo $hq_1q_2 \cdots q_n$. In fact, we may take K to lie between 1 and $hq_1q_2 \cdots q_n$. Thus we have found a $K \in \mathbb{Z}$ such that $K \equiv k \pmod{h}$ and $(K, d) = 1$. □

Theorem 3.3. *Let F_A be a polynomial of BHK-type of degree h and weights $(q_0,\ q_1,\ q_2,\ q_3)$, and let A be its associated exponent matrix. Suppose as in $(\star)$ that $\det(A) = h \cdot h_T$. Then we have $I_d(0) = \{k\alpha \mid (k,h) = 1\}$, where $\alpha = (\frac{q_0 d}{h}, \frac{q_1 d}{h}, \frac{q_2 d}{h}, \frac{q_3 d}{h})$ as in equation (1).*

Proof. Let $(a_0, a_1, a_2, a_3) \in A_d$. First suppose $(a_0, a_1, a_2, a_3) = k\alpha$ for some $(k,h) = 1$. Then we have

$$\sum_{i=0}^{3} \left\langle \frac{ta_i}{d} \right\rangle = \sum_{i=0}^{3} \left\langle \frac{tkq_i}{h} \right\rangle$$

By Lemma 3.2, there exists $K \in \mathbb{Z}$ such that $K \equiv k \pmod{h}$ and $(K,d) = 1$. Choose t such that $tK \equiv 1 \pmod{h}$. Then $(t,d) = 1$ and

$$\sum_{i=0}^{3}\left\langle\frac{tkq_i}{h}\right\rangle=\sum_{i=0}^{3}\left\langle\frac{tKq_i}{h}\right\rangle=\sum_{i=0}^{3}\left\langle\frac{q_i}{h}\right\rangle.$$

Since $q_0+q_1+q_2+q_3=h$, then this sum equals 1. Thus $(a_0,a_1,a_2,a_3)\in I_d(0)$.

Now suppose $(a_0,a_1,a_2,a_3)=k\alpha$ for some $k\in\mathbb{Z}$ such that $(k,h)=r>1$. Then we have

$$\sum_{i=0}^{3}\left\langle\frac{ta_i}{d}\right\rangle=\sum_{i=0}^{3}\left\langle\frac{tkq_i}{h}\right\rangle.$$

Since $(k,h)=r$ and $(t,h)=1$ implies $(tk,h)=r$, then for all t relatively prime to h, we have in particular that $tk\not\equiv\pm1 \pmod h$. A key consequence of part (iii) of Definition 2.1 (which we will not prove here) is that,

$$\sum_{i=0}^{3}\left\langle\frac{t'q_i}{h}\right\rangle=2$$

for all t' such that $(t',h)=1$ and $t'\not\equiv\pm1 \pmod h$. (Note that the sum is not equal to 2 when $t\equiv\pm1 \pmod h$.) So with $t'=tk$ we have

$$\sum_{i=0}^{3}\left\langle\frac{tkq_i}{h}\right\rangle=2.$$

This implies $(a_0,a_1,a_2,a_3)\notin I_d(0)$. □

Corollary 3.4. *Let F_A be as in Theorem 3.3 and let X be the K3 surface arising from F_A. Then the Picard number $\rho(X)$ is given by*

$$\rho(X)=22-\phi(h_T),$$

where ϕ is Euler's phi function.

Proof. Using Kelly's formula in Theorem 2.4, we need to compute $\#(\mathfrak{I}_d(0)\cap G_T)$. By Theorem 3.3 we can conclude that $\mathfrak{I}_d(0)\cap G_T=\{k\alpha_T\mid(k,h_T)=1\}$ where $\alpha_T=(\frac{q_0{}_Td}{h_T},\frac{q_1{}_Td}{h_T},\frac{q_2{}_Td}{h_T},\frac{q_3{}_Td}{h_T})$ as in equation (2). Hence $\#(\mathfrak{I}_d(0)\cap G_T)=\phi(h_T)$. □

Calculation of $I_d(b)$ for $(b,d)=1$. The focus of this section is to prove results about $I_d(b)$ in order to produce a simplified formula (when $\det(A)=h\cdot h_T$) for $\rho(X_p)$, the Picard number of the K3 surface defined over $\mathbb{F}_p$.

Proposition 3.5. *For all $(b,\ d)=1$, we have $I_d(b)\subseteq I_d(0)$.*

Proof. Let $(a_0,\ a_1,\ a_2,\ a_3)$ be an element of A_d but not of $I_d(0)$. This implies that $(a_0,\ a_1,\ a_2,\ a_3)$ $\in B_d(0)$. Thus,

$$\sum_{i=0}^{3}\left\langle \frac{ta_i}{d}\right\rangle = 2 \text{ for all } t\in\mathbb{Z} \text{ such that } (t,d)=1 \tag{3}$$

We now examine the double sum

$$\sum_{i=0}^{3}\sum_{j=0}^{f-1}\left\langle \frac{t'a_ib^j}{d}\right\rangle$$

for a fixed t' such that $(t',d)=1$. We can rearrange the sum as

$$\sum_{j=0}^{f-1}\sum_{i=0}^{3}\left\langle \frac{t'a_ib^j}{d}\right\rangle.$$

Since $(b,d)=1$, then $(t'b^j,d)=1$. Thus by (1) above with $t=t'b^j$,

$$\sum_{i=0}^{3}\left\langle \frac{(t'b^j)a_i}{d}\right\rangle = 2$$

for all b. So, the double sum equals

$$\sum_{j=0}^{f-1}\sum_{i=0}^{3}\left\langle \frac{t'a_ib^j}{d}\right\rangle = \sum_{j=0}^{f-1}2 = 2f.$$

Thus $(a_0,a_1,a_2,a_3)\in B_d(b)$, showing $(a_0,a_1,a_2,a_3)\notin I_d(b)$ for any b. □

Proposition 3.6. *We have either $I_d(b)=I_d(0)$ or $I_d(b)=\{\}$.*

Proof. By Theorem 3.3 we know $I_d(0)=\{k\alpha \mid (k,h)=1\}$. First suppose $\alpha=(a_0,a_1,a_2,a_3)\notin I_d(b)$ for some b. This implies

$$\sum_{i=0}^{3}\sum_{j=0}^{f-1}\left\langle \frac{ta_ib^j}{d}\right\rangle = 2f \text{ for all } (t,d)=1.$$

Substituting for a_i we have

$$\sum_{i=0}^{3}\sum_{j=0}^{f-1}\left\langle \frac{tq_ib^j}{h}\right\rangle = 2f \text{ for all } (t,h)=1.$$

Let $k \in \mathbb{Z}$ such that $(k,h)=1$. Then we know $k\alpha \in I_d(0)$. Let t' be coprime to d. Since $(t',d)=1$, then $(t',h)=1$. Also $(t',h)=1$ and $(k,h)=1$ implies $(t'k,h)=1$. Thus the double sum above with $t=t'k$ is

$$\sum_{i=0}^{3}\sum_{j=0}^{f-1}\left\langle \frac{t'ka_ib^j}{d}\right\rangle = \sum_{i=0}^{3}\sum_{j=0}^{f-1}\left\langle \frac{(t'k)q_ib^j}{h}\right\rangle = 2f,$$

which implies $k\alpha \in B_d(b)$. Therefore $k\alpha \notin I_d(b)$. This proves that if $\alpha \notin I_d(b)$, then $I_d(b)=\{\}$.

Now suppose $\alpha=(a_0,a_1,a_2,a_3)\in I_d(b)$. Then there exists $(t,\ d)=1$ such that

$$\sum_{i=0}^{3}\sum_{j=0}^{f-1}\left\langle \frac{ta_ib^j}{d}\right\rangle \neq 2f. \tag{4}$$

Let $k\in\mathbb{Z}$ such that $(k,h)=1$. This implies $k\alpha\in I_d(0)$. By Lemma 3.2, there exists $K\in\mathbb{Z}$ such that $K\equiv k \pmod h$ and $(K,d)=1$. Let $K'\in\mathbb{Z}$ be a solution to $K'K\equiv 1 \pmod d$. Now we examine the double sum

$$\sum_{i=0}^{3}\sum_{j=0}^{f-1}\left\langle \frac{t'ka_ib^j}{d}\right\rangle$$

where $t'=K't$. Then this sum will be

$$\sum_{i=0}^{3}\sum_{j=0}^{f-1}\left\langle \frac{tK'ka_ib^j}{d}\right\rangle = \sum_{i=0}^{3}\sum_{j=0}^{f-1}\left\langle \frac{ta_ib^j}{d}\right\rangle.$$

By equation (2) above, this sum does not equal $2f$. Therefore $k\alpha\in I_d(b)$, as required. This proves that if $\alpha\in I_d(b)$, then $I_d(b)=I_d(0)$. □

Lemma 3.7. *Let $G=\langle\alpha\rangle$ with $\alpha=(a_0,a_1,a_2,a_3)$. Then we have*

$$\sum_{i=0}^{3}\sum_{j=0}^{f-1}\left\langle \frac{ta_ip^j}{d}\right\rangle = 2f-1, 2f, \text{ or } 2f+1. \tag{5}$$

Proof. Using the fact that $(q_0,\ q_1,\ q_2,\ q_3)$ belongs to the 95 weight systems, one may show that

$$\sum_{i=0}^{3}\left\langle \frac{t'a_i}{d}\right\rangle = 1,2, \text{ or } 3 \text{ for all } (t',d)=1.$$

In fact, it is known that this sum equals 1 only when $t' \equiv 1 \pmod{h}$ and equals 3 only when $t' \equiv -1 \pmod{h}$. Since p has order f in $(\mathbb{Z}/d)^*$, then the powers p^j are distinct modulo d for all $0 < j < f - 1$. This implies that for a fixed t, the products tp^j will be distinct for all $0 < j < f - 1$. Thus the double sum on the right hand side of equation (5) contains f sums, which include some that equal 2, at most one that equals 1, and at most one that equals 3. If one of these sums equals 1 but none equal 3, then the double sum will equal $2f - 1$. If the one of these sums equals 3 but none equal 1, then the double sum will equal $2f + 1$. If the one of the sums equals 1 and another equals 3, then the double sum will equal $2f$. And finally if the sums all equal 2, then the double sum will equal $2f$. □

Theorem 3.8. *Let F_A be a polynomial of BHK-type of degree h and weights (q_0, q_1, q_2, q_3), and let A be its associated exponent matrix. Suppose as in $(\star)$ that $det(A) = h \cdot h_T$. Then $I_d(b) = \{\}$ if and only if $b^k \equiv -1 \pmod{h}$ for some $k \in \mathbb{Z}$.*

Proof. Note that $b^k \equiv -1 \pmod{h}$ for some $k \in \mathbb{Z}$ if and only if the equivalence class of -1 modulo h, written $[-1]$, is an element of the subgroup of $(\mathbb{Z}/d)^*$ generated by powers of b modulo h, written $\langle [b] \rangle$. Hence it is sufficient to prove $I_d(b) = \{\}$ if and only if $[-1] \in \langle [b] \rangle$. First suppose $[-1] \notin \langle [b] \rangle$. Then the double sum for $\alpha = (\frac{q_0 d}{h}, \frac{q_1 d}{h}, \frac{q_2 d}{h}, \frac{q_3 d}{h})$ as the generator of G and some $(t,d) = 1$ is

$$\sum_{i=0}^{3} \sum_{j=0}^{f-1} \left\langle \frac{t a_i b^j}{d} \right\rangle = \sum_{j=0}^{f-1} \sum_{i=0}^{3} \left\langle \frac{t q_i b^j}{h} \right\rangle.$$

With $t = 1$ we have

$$\sum_{i=0}^{3} \left\langle \frac{q_i}{h} \right\rangle + \sum_{i=0}^{3} \left\langle \frac{q_i b}{h} \right\rangle + \cdots + \sum_{i=0}^{3} \left\langle \frac{q_i b^{f-1}}{h} \right\rangle.$$

Note that the first sum equals 1 as shown in the proof of Theorem 3.3. In the rest of the sums, $b^j \not\equiv -1 \pmod{h}$, thus each sum must equal 2. Hence the double sum is equal to $2f - 1$, and not 2f. Therefore $\alpha \in I_d(b)$, so $I_d(b) \neq \{\}$.

Now suppose $[-1] \in \langle [b] \rangle$. Also suppose for contradiction $I_d(b) \neq \{\}$. This implies that there exists $(t,\ d) = 1$ such that

$$\sum_{i=0}^{3} \sum_{j=0}^{f-1} \left\langle \frac{t a_i b^j}{d} \right\rangle \neq 2f.$$

By Lemma 3.7, this implies that the double sum equals either $2f - 1$ or $2f + 1$.

Case 1: Suppose the sum is $2f - 1$. Then $tb^j \equiv 1 (\mathrm{mod}\ h)$ for some j, but $tb^k \not\equiv -1 \pmod{h}$ for all k. So $t \equiv b^{-j} \pmod{h}$. Thus $b^{k-j} \not\equiv -1 \pmod{h}$ for all k, which implies that $[-1] \notin \langle [b] \rangle$. This is a contradiction, hence the sum cannot equal $2f - 1$.

Case 2: Suppose the sum is $2f+1$. Then $tb^j \equiv -1 \pmod{h}$ for some j, but $tb^k \not\equiv 1 \pmod{h}$ for all k. So $t \equiv -b^{-j} \pmod{h}$. Thus $-b^{k-j} \not\equiv 1 \pmod{h}$ implies $b^{k-j} \not\equiv -1 \pmod{h}$ for all k. As above, this is a contradiction. Thus, the sum is not $2f+1$.

Therefore, the sum must equal $2f$, and hence $I_d(b) = \{\}$. □

$$\rho(X_p) = \begin{cases} 22 & \text{if } p^{f_T/2} \equiv -1 \pmod{h_T} \\ 22 - \phi(h_T) & \text{if } f \text{ is odd or } p^{f_T/2} \not\equiv -1 \pmod{h_T} \end{cases}$$

Proof. If $p^{f_T/2} \equiv -1 \pmod{h)_T}$, then by Theorem 3.8 we know that $I_d(p) = \{\}$. Hence $\#(I_d(p) \cap G_T) = 0$. On the other hand, if f_T is odd or $p^{f_T/2} \not\equiv -1 \pmod{h_T}$, then we know that $I_d(p) \neq \{\}$. Hence by Proposition 3.6 it must be that $I_d(p) = I_d(0)$. Thus by Corollary 3.4 we have $\#(\mathfrak{I}_d(p) \cap G_T) = \#(\mathfrak{I}_d(0) \cap G_T) = \phi(h_T)$. □

Acknowledgements

This research was conducted at California State University, Fullerton, under the direction of Dr. Christopher Lyons. We are grateful to acknowledge the support of the CSUF Math Summer Research Program.

References

[1] T. Kelly. Picard Ranks of K3 Surfaces of BHK Type. *Preprint.*

[2] T. Yonemura. Hypersurface Simple K3 Singularities. *Tôhoku Math.* J. 42 (1990), 351-380.

A Demonstration of the Application of Geometric Series to Certain Inequalities

James Shade
Advisor: Dr. Bogdan D. Suceavă

Department of Mathematics, California State University, Fullerton

Abstract

In a paper published in 2012 in the *American Mathematical Monthly*, C. Mortici used a classical technique to solve some inequalities by converting terms to geometric series. In this paper, we apply the same method on an inequality relating properties of a polygon. The result uses geometric series convergence and the generalized means inequality.

I. Introduction

We demonstrate here a method of solving certain inequalities by representing terms as the sums of convergent geometric series. This method can make otherwise complex proofs much simpler and, for applicable inequalities, is a viable alternative to standard algebraic and induction proofs. To demonstrate, consider the following theorem:

Theorem 1. *Let a_1, a_2, ... , a_n be the lengths of the sides of a given n-gon, $n \geq 3$. Let*

$$s = a_1 + a_2 + ... + a_n. \tag{1}$$

Then

$$\frac{a_1}{s-2a_1} + \frac{a_2}{s-2a_2} + ... + \frac{a_n}{s-2a_n} \geq \frac{n}{n-2}. \tag{2}$$

A typical proof might consist of using mathematical induction on n, and complicated algebra. Here we demonstrate an alternative approach using geometric series.

First, it is important to note that if this theorem holds in the case of $s = 1$, then it holds in general. To show this, first divide both sides of (1) by s, which yields:

$$1 = \frac{a_1}{s} + \frac{a_2}{s} + ... + \frac{a_n}{s}.$$

Denote $\frac{a_i}{s}$ by a_i', for $i = 1, 2, ..., n$ so that $1 = a_1' + a_2' + ... + a_n'$.
Multiplying each term on the left side of (2) by $\frac{\frac{1}{s}}{\frac{1}{s}}$ gives:

$$\frac{a_1'}{1-2a_1'} + \frac{a_2'}{1-2a_2'} + ... + \frac{a_n'}{1-2a_n'} \geq \frac{n}{n-2}.$$

If this inequality holds, then (2) also holds. Note that this is (2) in the case $s = 1$. In geometric terms, the polygon has been scaled down to have a perimeter of 1. Because this technique can be applied regardless of the value of s, we need only prove the case where $s = 1$.

Proof. Assume without loss of generality that $s = 1$. Then $a_1, a_2, ..., a_n \in (0, 0.5)$.

Then we need to show:

$$\frac{a_1}{1-2a_1} + \frac{a_2}{1-2a_2} + ... + \frac{a_n}{1-2a_n} \geq \frac{n}{n-2}.$$

Multiplying both sides by 2, we have:

$$\frac{2a_1}{1-2a_1} + \frac{2a_2}{1-2a_2} + ... + \frac{2a_n}{1-2a_n} \geq \frac{2n}{n-2}.$$

Since all $a_i \in (0, 0.5)$, then $2a_i < 1$ for $i = 1, 2, ..., n$. Then each term on the left side of the inequality is the sum of a geometric series. Specifically,

$$\begin{aligned}\frac{2a_1}{1-2a_1} + \frac{2a_2}{1-2a_2} + ... + \frac{2a_n}{1-2a_n} &= \sum_{i=1}^{\infty}(2a_1)^i + \sum_{i=1}^{\infty}(2a_2)^i + ... + \sum_{i=1}^{\infty}(2a_n)^i \\ &= \sum_{i=1}^{\infty} 2^i \left(a_1^i + a_2^i + ... + a_n^i\right) \\ &= n\sum_{i=1}^{\infty} 2^i \left(\frac{a_1^i + a_2^i + ... + a_n^i}{n}\right).\end{aligned}$$

According to the generalized means inequality [1], since $i \geq 1$:

$$\left(\frac{a_1^i + a_2^i + ... + a_n^i}{n}\right)^{\frac{1}{i}} \geq \left(\frac{a_1 + a_2 + ... + a_n}{n}\right)$$

Therefore,

$$\left(\frac{a_1^i + a_2^i + ... + a_n^i}{n}\right) \geq \left(\frac{a_1 + a_2 + ... + a_n}{n}\right)^i$$

and hence,

$$n\sum_{i=1}^{\infty} 2^i \left(\frac{a_1^i + a_2^i + ... + a_n^i}{n}\right) \geq n\sum_{i=1}^{\infty} 2^i \left(\frac{a_1 + a_2 + ... + a_n}{n}\right)^i.$$

Since $a_1 + a_2 + ... + a_n = 1$, this gives:

$$n\sum_{i=1}^{\infty} 2^i \left(\frac{a_1 + a_2 + ... + a_n}{n}\right)^i = n\sum_{i=1}^{\infty} 2^i \left(\frac{1}{n}\right)^i$$
$$= n\sum_{i=1}^{\infty} \left(\frac{2}{n}\right)^i.$$

Since $n \geq 3$, then $\frac{2}{n} < 1$. Thus, this is a convergent geometric series. Hence,

$$n\sum_{i=1}^{\infty} \left(\frac{2}{n}\right)^i = n\left(\frac{\frac{2}{n}}{1 - \frac{2}{n}}\right)$$
$$= \frac{2}{1 - \frac{2}{n}}$$
$$= \frac{2n}{n-2},$$

as needed.

Thus, by convergent geometric series and the generalized means inequality, we have shown that

$$\frac{a_1}{s - 2a_1} + \frac{a_2}{s - 2a_2} + ... + \frac{a_n}{s - 2a_n} \geq \frac{n}{n-2}.$$

□

References

[1] J. M. Steele- *The Cauchy-Schwarz Master Class: An Introduction to the Art of Mathematical Inequalities*, Cambridge: Cambridge University Press, 2004.

[2] C. Mortici- A Power Series Approach to Some Inequalities, *The American Mathematical Monthly*, Vol. 119, No. 2 (February 2012), pp. 147-151.

Comparison of False Discovery Rate and p-value in Microarray Experiments

Adam Walder
Advisor: Dr. Gulhan Bourget

Department of Mathematics, California State University, Fullerton

Abstract

The high dimensional structure of Microarray data complicates several aspects of statistical inference. Since current statistical methods are generally for "small p (number of columns), and large n (number of obervations)", these methods can be insufficient to draw valid conclusions for microarray data. Nevertheless, some of these methods, such as Analysis of Variance (ANOVA) are still widely used. F test is used in ANOVA. One of the assumptions of F test is that populations (genes) are assumed to be independent. This assumption is obviously violated in microarray experiments because gene-gene interactions can naturally occur. In this paper, we use an effective "column" size idea to take correlations (interactions) among genes into account to modify the F test. We consider various magnitudes of correlation among genes in Monte Carlo simulation studies. We compare the proposed test (F-MOD) with the classical F test through p-value and False Discovery Rate (FDR). We also discuss the use of FDR in comparison with p-value.

I. Introduction

Microarray data is used to measure gene expression levels of a genome. Problems arising in biological and medical studies have required the need to explore genes through gene expression data. However, many standard statistical procedures are unreliable due to the structure of the microarray data. The issue lies in the dimensionality of the microarray. In general, the data is stored in an $n \times p$ matrix, where n is the sample size and p is the number of variables, and n is much bigger compared to p. For example, we might want to compare three treatments ($p = 3$) using $n = 10$ observations for each treatment. However, in microarray data, the sample size n (e.g., number of arrays) is much smaller than the number of genes p (e.g., 23,000). This kind of data structure is known as "cursed dimensionality" because most of the current statistical methods cannot be used to make inference about this data.

The F test determines whether or not the means of three or more populations are equal. The F test is valid if (1) all populations of interest are normally distributed, (2) samples are randomly and independently selected from each population, and (3) populations have equal standard deviations (or variances). The F test is robust against normality as long as the number of sample sizes are large, but it is not robust if populations have unequal variances with unequal sample sizes. Failure to meet these assumptions changes the Type I error rate. That means the actual Type I error may be greater or less than significance level α, depending on which assumptions are violated.

If the independence of samples are violated, then the F test shouldn't be used to

analyze the data. In nature, gene-gene interactions exist. F-MOD, proposed by [3, 4, 5], takes correlation among genes into account in F test. It uses an effective sample size idea. The effective sample size formula was originally proposed by Clifford et al. [7], and was improved for small sample sizes by Dutilleul (1993) [8]. Also, the same effective sample size formula was used in modified F tests to assess multiple correlation between one spatial process and several others [9], and to assess correlation between two time series [1]. In this paper, we compare the F - MOD test proposed in [6] with F test. Actually, F - MOD in [6] implemented the same effective sample size formula described in [8] to compute effective column size not effective sample size.

2. Materials and Methods

2.1 Comparing Mean Vectors from Two Populations

A single multivariate observation is the collection of measurements on p different variables (genes) taken from the same trial (array). If n observations have been obtained, the entire data set can be represented in an $n \times p$ matrix

$$= \begin{bmatrix} X_{11} & X_{12} & \cdots & X_{1p} \\ X_{21} & X_{22} & \cdots & X_{2p} \\ \vdots & \vdots & \ddots & \vdots \\ X_{n1} & X_{n2} & \cdots & X_{np} \end{bmatrix} = \begin{bmatrix} \mathbf{X}_1' \\ \mathbf{X}_2' \\ \vdots \\ \mathbf{X}_n' \end{bmatrix} \tag{1}$$

The row vector $\mathbf{X}_j'$ represents the jth multivariate observation. The matrix $\mathbf{X}$ represents p genes each having n observations.

Now, consider a microarray experiment of n_1 and n_2 samples from populations 1 and 2, respectively. For example, population 1 can represent the disease group, while population 2 can represent the healthy group. Suppose that the expression levels of p genes are measured and matrix representations of populations 1 and 2 are defined in (1) as $\mathbf{X}$ and $\mathbf{Y}$.

The observations on p variables can be arranged as follows:

$$\text{Population 1:} \quad \mathbf{X}_1', \mathbf{X}_2', \ldots, \mathbf{X}_{n_1}' \text{Population 2:} \quad \mathbf{Y}_1', \mathbf{Y}_2', \ldots, \mathbf{Y}_{n_2}' \tag{2}$$

Our goal in this paper is to only make inferences about the differences of the vector mean of the populations. That is, we want to know if $\boldsymbol{\mu}_1 = \boldsymbol{\mu}_2$, or equivalently if $\boldsymbol{\mu}_1 - \boldsymbol{\mu}_2 = \mathbf{0}$. However, one further can investigate which means are different if the hypothesis of $\boldsymbol{\mu}_1 - \boldsymbol{\mu}_2 \neq \mathbf{0}$ is concluded. We need to make some assumptions to provide answers to these questions. The assumptions are:

1. The sample $\mathbf{X}_1', \mathbf{X}_2', \ldots, \mathbf{X}_{n_1}'$ is a random sample of n_1 from a p-variate population with mean vector $\boldsymbol{\mu}_1$ and covariance matrix $\boldsymbol{\Sigma}_1$.

2. The sample $\mathbf{Y}_1', \mathbf{Y}_2', \ldots, \mathbf{Y}_{n_2}'$ is a random sample of n from a p-variate population with 12n2 2 mean vector $\boldsymbol{\mu}_2$ and covariance matrix $\boldsymbol{\Sigma}_2$.

3. The samples $\mathbf{X}_1', \mathbf{X}_2', \ldots, \mathbf{X}_{n_1}'$ are independent of the samples $\mathbf{Y}_1', \mathbf{Y}_2', \ldots, \mathbf{Y}_{n_2}'$.

For large samples, these assumptions are enough to make an inference about $\boldsymbol{\mu}_1 - \boldsymbol{\mu}_2$. However, when the sample sizes n_1 and n_2 are small we need to have the following assumptions as well.

1. Both populations are multivariate normal, and

2. $\boldsymbol{\Sigma}_1 = \boldsymbol{\Sigma}_2$.

The null (H_0) and alternative (H_a) hypotheses we are interested are:

$$H_0 : \boldsymbol{\mu}_1 - \boldsymbol{\mu}_2 = \mathbf{0} \qquad \text{versus} \qquad H_a : \boldsymbol{\mu}_1 - \boldsymbol{\mu}_2 \neq \mathbf{0} \tag{3}$$

where $\boldsymbol{\mu}_1 = (\mu_{11}, \mu_{12}, \ldots, \mu_{1p})'$ is the vector mean expression level of population 1, and $\boldsymbol{\mu}_2 = (\mu_{21}, \mu_{22}, \ldots, \mu_{2p})'$ is the vector mean expression level of population 2. The null and alternative hypothesis can also be written as

$$\begin{aligned} H_0 &: (\mu_{11} - \mu_{21}, \mu_{12} - \mu_{22}, \ldots, \mu_{1p} - \mu_{2p})' = (0, 0, \ldots, 0)' \\ H_a &: (\mu_{11} - \mu_{21}, \mu_{12} - \mu_{22}, \ldots, \mu_{1p} - \mu_{2p})' \neq (0, 0, \ldots, 0)' \end{aligned} \tag{4}$$

or equivalently

$$\begin{aligned} H_0 &: \mu_{11} = \mu_{21}, \mu_{12} = \mu_{22}, \ldots, \mu_{1p} = \mu_{2p} \\ H_a &: \text{at least one } \mu_{1i} \neq \mu_{2i}, \ (i = 1, 2, \ldots, p) \end{aligned} \tag{5}$$

Note that, we test the mean expression of p genes all together not the individual mean expressions in (3) - (5). That is, we consider a global test not an individual test.

2.2 *F* Test

The classical F test compares the means of the columns of $\mathbf{X}$, and assumes that these columns are independent (univariate case). In microarray experiment, we want to compare the differences of the p means of $\mathbf{X}$ and $\mathbf{Y}$. We have multivariate data structure but univariate F and F-MOD tests. Therefore, we need to adopt the data structure from the multivariate to univariate case by considering the factor observations as the *differences* of the data matrices $\mathbf{X}$ and $\mathbf{Y}$. That is, we compute $X_{ij} - Y_{ij}$, and apply the univariate F test on these observations. The F test is defined as

$$F_{\text{obs}} = \frac{\text{MST}}{\text{MSE}} \tag{6}$$

where MST is the mean square for treatments (genes), and MSE is the mean square for errors. The F_{obs} in (6) follows an F distribution with $p - 1$ degrees of freedom for the numerator and $p(n - 1)$ degrees of freedom for the denominator, where $n_1 = n_2 = n$.

2.3 F - MOD

When the assumptions are not satisfied by sample data, there are two general remedies: (1) to transform the data so that the assumptions are satisfied, or (2) to develop a modified inferential method in which the assumptions are relaxed at the estimation stage, or deviations from the assumptions are taken into account at the testing stage.

In linear models, the autocorrelation of errors has an impact on the inefficiency of slope estimators and the invalidity of significance levels. When regressors have fixed structure, the only source of autocorrelation comes from errors. However, when regressors also have random structures, their autocorrelations along with correlations of errors have an impact on estimation and testing [2, 3, 4, 5]. Since the autocovariances of stochastic processes bias the variance of sample correlation coefficients [10], the incorporation of effective sample size into modified t-tests were proposed [7, 8]. The effective sample size $\hat{n}$ in [7] was defined as

$$\hat{n} = \hat{\sigma}^{-2} + 1 \quad \text{with} \quad \hat{\sigma}^2 = \text{tr}(\hat{\mathbf{\Sigma}}_{\mathbf{X}}\hat{\mathbf{\Sigma}}_{\mathbf{Y}})/[\text{tr}(\hat{\mathbf{\Sigma}}_{\mathbf{X}})\text{tr}(\hat{\mathbf{\Sigma}}_{\mathbf{Y}})] \tag{7}$$

where $\hat{\mathbf{\Sigma}}_{\mathbf{X}}$ and $\hat{\mathbf{\Sigma}}_{\mathbf{Y}}$were the estimated covariance matrices of $\mathbf{X}$ and $\mathbf{Y}$, respectively. Dutilleul (1993) proposed an improved effective sample size for small sample sizes [8]. However, the effective sample sizes prosed in [7] and [8] behave similarly for large sample sizes. The effective sample size in [8] was defined as

$$\hat{n} = \hat{\sigma}^{-2} + 1 \quad \text{with} \quad \hat{\sigma}^2 = \text{tr}(\mathbf{B}\hat{\mathbf{\Sigma}}_{\mathbf{X}}\mathbf{B}\hat{\mathbf{\Sigma}}_{\mathbf{Y}})/[\text{tr}(\mathbf{B}\hat{\mathbf{\Sigma}}_{\mathbf{X}})\text{tr}(\mathbf{B}\hat{\mathbf{\Sigma}}_{\mathbf{Y}})] \tag{8}$$

where $\mathbf{B} = n^{-1}(\mathbf{I} - n^{-1}\mathbf{J})$, $\mathbf{J}$ is the $n \times n$ matrix of ones, and $\mathbf{I}$ is the identity matrix.

In this paper, we implement the F-MOD test considered in [6] that used equation (8) defined in [8] to compute effective column size to identify differentially expressed genes in microarray data. We considered the following steps for F -MOD test in the simulation runs: first, we computed the effective column size, $\hat{p}$, as in equation (8). The estimated covariance matrices $\hat{\mathbf{\Sigma}}_{\mathbf{X}}$ and $\hat{\mathbf{\Sigma}}_{\mathbf{Y}}$ were computed using the raw data of $\mathbf{X}$ and $\mathbf{Y}$, respectively. Second, we replaced p by $\hat{p}$ in the degrees of freedoms of the classical F test defined in (6). Finally, we computed the p-value of the global F test in (6) with $\hat{p} - 1$ and $\hat{p}(n - 1)$ degrees of freedoms for the numerator and denominator degrees of freedoms, respectively. Note that, the sample size is $n_1 = n_2 = n$.

2.4 False Discovery Rate

In statistical significance and multiple comparisons, we want to know what is the chance of getting "statistically significant" results when the null hypothesis is true. The answer is given by computing p-value. However, in genomics studies we have a lot of data, and hence a lot of hypotheses to test. For example, in a typical microarray experiment, we might perform 10,000 separate hypothesis tests. If we use a standard p-value with a significance level of $\alpha = 0.05$, we would expect $10,000 \times 0.05 = 500$ genes to be declared "significant" by chance. To control false positives, we can adjust p-values for the number of hypothesis tests performed, i.e., controlling Type I error rate. Many different methods have been proposed, such as Family Wise Error Rate (FWER), which is the probability of at least one Type I error occurring. However, when multiple testing is performed, the most natural question is to ask what is the chance that the null hypothesis is true when a comparison is "statistically significant". The answer leads to the new multiple testing method called False Discovery Rate (FDR).

Assume that we test m hypotheses of $H_1, H_2, \ldots, H_m$ with m_0 be the number of true null hypothesis, R be the number of rejected hypotheses, and V be the number of Type I errors (false positives).

Table 1: FDR.

	Null True	Alternative True	Total
Not Called Significant	U	T	$m-R$
Called Significant	V	S	R
	m_0	$m-m_0$	m

The FDR is defined as the expected value of the ratio of the number of false positive features, V, and the number of significant features, S. That is,

$$\text{FDR} = \text{E}\left(\frac{V}{V+S}\right) = \text{E}\left(\frac{V}{R}\right) \tag{9}$$

3. Results and Discussion

We generated two multivariate normal distributions: MVN(μ1, Σ1) and MVN(μ2, Σ2), each with dimension p (genes). The variance covariance matrices are defined as

$$\boldsymbol{\Sigma}_1 = \boldsymbol{\Sigma}_2 = \begin{pmatrix} \boldsymbol{\Sigma}_\rho & 0 & 0 & \ldots & \ldots & \ldots \\ 0 & \boldsymbol{\Sigma}_{(-\rho)} & 0 & 0 & \ldots & \vdots \\ 0 & 0 & \boldsymbol{\Sigma}_\rho & 0 & \ldots & \vdots \\ \vdots & 0 & 0 & \boldsymbol{\Sigma}_{(-\rho)} & 0 & \vdots \\ \vdots & \vdots & \vdots & 0 & \ddots & \vdots \\ \ldots & \ldots & \ldots & \ldots & \ldots & \ddots \end{pmatrix}_{p\times p} \tag{10}$$

where

$$\boldsymbol{\Sigma}_\rho = l \begin{pmatrix} 1 & \rho & \ldots & \rho^{g-2} & \rho^{g-1} \\ \rho & 1 & \ldots & \ldots & \rho^{g-2} \\ \vdots & \ddots & \ddots & \ddots & \vdots \\ \rho^{g-2} & \ldots & \vdots & \vdots & \rho \\ \rho^{g-1} & \rho^{g-2} & \ldots & \rho & 1 \end{pmatrix}_{g\times g} \tag{11}$$

where $l = \sigma^2/\sqrt{1-\rho^2}$. We can similarly define $\boldsymbol{\Sigma}_{(-\rho)}$ by replacing ρ by $(-\rho)$ in (11).
The simulation set up for $\boldsymbol{\Sigma}_1$ and $\boldsymbol{\Sigma}_2$ has actually sound basis in real microarray data: (1) weak connections between groups may exist, hence independence between groups is a reasonable

assumption (i.e., off diagonals are 0 matrices); (2) genes are either positively or negatively correlated within each group (i.e., correlations among genes are either ρ or $-\rho$); and (3) the further apart two genes, the less correlation between them (i.e., covariance matrix in (11)).

We assumed that both populations have equal sample sizes (i.e., $n_1 = n_2$), and there are 10 matrices on the diagonals of $\mathbf{\Sigma}_1$ and $\mathbf{\Sigma}_2$. For example, if $p = 100$ then there are 10 matrices on the diagonal of $\mathbf{\Sigma}_1$ and $\mathbf{\Sigma}_2$ with 10 genes in each matrix (i.e., $g = 10$). To assess the effects of correlation among genes, we took $\rho = 0, 0.1, 0.2, \ldots, 0.9$ as various magnitudes of correlations. We also set the variances of each gene at 0.01 (i.e., $\sigma^2 = 0.1$). We considered two different significance levels, $\alpha = 0.01$ and 0.05. The null hypothesis was set to $\boldsymbol{\mu}_1 = \boldsymbol{\mu}_2 = (0, 0, 0, \ldots, 0)'_{(p\times p)}$, and alternative hypothesis was set to $\boldsymbol{\mu}_1 \neq \boldsymbol{\mu}_2$ with $\boldsymbol{\mu}_1 = (0, 0, \ldots, 0)'_{(p\times 1)}$ and $\boldsymbol{\mu}_2 = (\underbrace{0.5, \ldots, 0.5}_{0.02\star p}, \underbrace{0, 0, \ldots, 0}_{0.98\star p})'_{(p\times 1)}$. More precisely, the first 2% of the means of the genes were set to 0.5, and the rest were set to 0 in $\boldsymbol{\mu}_2$. If $0.02\star$p was not an integer value, then we used ceiling function in R that takes a single numeric argument a and returns a numeric value containing the smallest integers not less than the corresponding elements of a.

We wrote and ran multiple simulations in R, which is a free software. We ran 10,000 data sets to compute p-values, and 10,000 data sets to compute FDR values for each values of ρ. We then drew conclusions about the testing procedures using p-values and FDR.

3.1 Comparison of Methods

The *strict validity* of a testing procedure is that the actual p-value, which is the probability of rejecting the null hypothesis when in fact the null hypothesis is true, is less than or equal to α. However, in simulations there are variability among generated data sets. Hence, strict validity is not a reasonable measure. To take variability into account, we can consider the upper limit of the approximate 95% confidence interval for the actual p-value. Under binomial distribution model, for α and m simulation runs, the approximate 95% confidence interval is $\alpha \pm 2\sqrt{\alpha(1-\alpha)/m}$. In simulation runs, we took $\alpha = 0.01$ and 0.05, and $m = 10,000$. The upper limits are

$$\alpha = 0.01 \Longleftrightarrow 0.01 + 2\sqrt{(0.01 \cdot 0.99)/10,000} = 0.012 \tag{12}$$

$$\alpha = 0.05 \Longleftrightarrow 0.05 + 2\sqrt{(0.05 \cdot 0.95)/10,000} = 0.054 \tag{13}$$

Table 2 shows results of FDR for F test and F -MOD test. In Table 2, the F test performs well when correlations among genes are negligible or very small. However, F test fails to control significance levels as correlation among genes increases. Also, the FDR values rapidly increase as the number of genes rise. F-MOD outperforms F test for any combinations of correlation among genes, ρ, number of genes p, and sample size n at any α. F-MOD fails to control significance level when p is small (i.e., $p = 20$). Comparing α values, we see F -MOD behaving better for larger α values. Overall, F-MOD controls FDR values by providing values that are smaller than α values.

Table 3 shows results of p-values for F test and F -MOD test. The results of p-values are very similar to FDR. Hence, we suggest F-MOD to be used when correlations among genes are suspected. In such cases, we strongly advise against the use of classical F test. The F -MOD test is a univariate test that is easy to compute. In practice, the researchers prefer to use tests that are straightforward and robust against violations of assumptions. Hence, F-MOD test is recommended.

4. Conclusion

Microarray data has a high dimensional data structure. Therefore, it is challenging to make statistical inferences from this type of data. The most widely used statistical methods for finding differentially expressed genes from microarray data are univariate, such as ANOVA. While univariate methods do not take correlations among genes into account, we should not ignore gene-gene interactions in testings.

In this paper, we have compared the F-MOD test proposed in [6] with the classical F test. We used FDR and p-values as measures to assess the performance of the tests. Overall, the F-MOD outperforms the F test in the presence of mild to strong correlations among genes. Also, the number of genes does not affect the performance of the F-MOD. Hence, we recommend researchers to use F-MOD test in microarray experiments.

In future work, we shall investigate the performance of the classical t-test with the degrees of freedom adjusted using the effective column size idea.

5. Tables

Table 2: FDR when $n_1 = n_2 = n$.

					$p = 20,\ n = 5$						
						ρ					
α	Test	0	0.1	0.2	0.3	0.4	0.5	0.6	0.7	0.8	0.9
0.01	F	0.010	0.013	0.012	0.012	0.018	0.015	0.022	0.026	0.032	0.037
	F-MOD	0.014	0.016	0.015	0.015	0.019	0.013	0.018	0.017	0.016	0.018
0.05	F	0.046	0.049	0.047	0.053	0.061	0.062	0.071	0.078	0.088	0.092
	F-MOD	0.052	0.054	0.052	0.053	0.062	0.051	0.060	0.059	0.059	0.057
					p=50, n=10						
0.01	F	0.008	0.011	0.012	0.014	0.018	0.024	0.033	0.049	0.065	0.077
	F-MOD	0.009	0.011	0.011	0.012	0.011	0.014	0.010	0.012	0.013	0.013
0.05	F	0.046	0.052	0.052	0.052	0.065	0.076	0.089	0.101	0.123	0.133
	F-MOD	0.048	0.054	0.050	0.049	0.047	0.049	0.050	0.049	0.050	0.046
					p=100, n=10						
0.01	F	0.009	0.009	0.013	0.017	0.025	0.030	0.040	0.059	0.082	0.109
	F-MOD	0.009	0.010	0.011	0.011	0.015	0.013	0.010	0.012	0.013	0.011
0.05	F	0.047	0.046	0.053	0.066	0.073	0.079	0.099	0.119	0.136	0.161
	F-MOD	0.049	0.047	0.049	0.056	0.052	0.048	0.049	0.050	0.048	0.045

Table 3: p-value when $n_1 = n_2 = n$.

					$p = 20,\ n = 5$						
						ρ					
α	Test	0	0.1	0.2	0.3	0.4	0.5	0.6	0.7	0.8	0.9
0.01	F	0.009	0.010	0.012	0.012	0.016	0.017	0.022	0.028	0.032	0.038
	F-MOD	0.012	0.014	0.015	0.017	0.017	0.015	0.016	0.017	0.018	0.016
0.05	F	0.044	0.049	0.051	0.058	0.061	0.068	0.075	0.088	0.093	0.104
	F-MOD	0.053	0.056	0.055	0.064	0.059	0.060	0.060	0.064	0.064	0.063
					p=50, n=10						
0.01	F	0.010	0.010	0.013	0.015	0.019	0.029	0.036	0.048	0.065	0.088
	F-MOD	0.011	0.011	0.011	0.011	0.012	0.013	0.013	0.012	0.011	0.010
0.05	F	0.050	0.048	0.059	0.060	0.072	0.084	0.095	0.113	0.133	0.156
	F-MOD	0.052	0.048	0.056	0.053	0.053	0.056	0.049	0.050	0.046	0.048
					p=100, n=10						
0.01	F	0.009	0.011	0.014	0.015	0.022	0.030	0.040	0.058	0.090	0.125
	F-MOD	0.010	0.012	0.014	0.012	0.012	0.013	0.011	0.012	0.012	0.012
0.05	F	0.048	0.054	0.056	0.064	0.075	0.090	0.101	0.128	0.154	0.192
	F-MOD	0.049	0.053	0.052	0.052	0.053	0.050	0.048	0.048	0.050	0.049

References

[1] G. Alpargu and J. P. Buonaccorsi. A model free test for assessing dependence between times series. *J. Agricultural, Biological, and Environmental Statistics*, 14(1):115–132, 2009.

[2] G. Alpargu and P. Dutilleul. Efficiency analysis of ten estimation procedures for quantitative linear models with autocorrelated errors. *J. Statist. Comput. Simulation*, 69:257–275., 2001.

[3] G. Alpargu and P. Dutilleul. Efficiency and validity analyses of two-stage estimation procedures and derived testing procedures in quantitative linear models with ar(1) errors. *Comm. Statist. Simulation Comput.*, 32:799–833, 2003a.

[4] G. Alpargu and P. Dutilleul. To be or not to be valid in testing the significance of the slope in simple quantitative linear models with autocorrelated errors. *J. Statist. Comput. Simulation*, 73:165–180., 2003b.

[5] G. Alpargu and P. Dutilleul. Stepwise regression in mixed quantitative linear models with autocorrelated errors. *Comm. Statist. Simulation Comput.*, 35:79–104, 2006.

[6] G. Bourget. Modifying the classical f test for microarray experiments. *J. of Biometrics and Its Applications*, 1(1):105:1–15, 2016.

[7] P. Clifford, S. Richardson, and D. H´emon. Assessing the significance of the correlation between two spatial processes. *Biometrics*, 45:123–134, 1989.

[8] P. Dutilleul. Modifying the t test for assessing the correlation between two spatial processes. *Biometrics*, 49:305–314, 1993.

[9] P. Dutilleul, B. Pelletier, and G. Alpargu. Modified f tests for assessing the multiple correlation between one spatial process and several others. *Journal of Statistical Planning and Inference*, 138(5):1402–1415, 2008.

[10] G. M. Jenkins and D. G. Watts. *Spectral Analysis and its Applications*. Holden-Day, San Francisco, CA, 1968.

Modeling the Chain Fountain

Adam Walder
Advisor: Dr. Tyler McMillen

Department of Mathematics, California State University, Fullerton

Abstract

The chain fountain can simply be described as a looping chain that seemingly defies the laws of gravity. A chain fountain arises when a chain is released from the side of a container. As the chain falls from the container to the floor, the chain begins to levitate out of its container and forms a loop at its peak. We have constructed a realistic model of the chain fountain composed of rigid mass-less links connected by circular beaded masses. Simulations of this model, implemented in Matlab, allow us to investigate the behavior of the chain in a controllable setting.

This natural phenomenon is a result of collisions causing a lift in the chain. Modeling the collisions of the masses became the most difficult aspect of our work. The failure of our initial collision detection techniques will be discussed, as well as the proper way to realistically represent the elastic chain collisions.

The results of our simulations will help make sense of the chain fountain formation. We shall provide evidence to demonstrate cases in which a chain fountain fails to occur. We also provide intuition for future works in non-conservative chain fountain experiments.

I. Introduction

A chain falling from a pot exhibits an interesting course of motion. As the chain slides out of the pot towards the floor, a portion of the chain begins to levitate above the side of the pot, forming a loop at its peak. We refer to this counter-intuitive phenomenon as a chain fountain. This gravity defying feat was introduced in a YouTube video created by physicist Steve Mould. After millions had viewed the video, several physicists sought a physical explanation for this phenomenon. This inspired several papers [5, 6, 1, 2].

One explanation was offered in a paper written by Biggnins and Warner of Cambridge University [1, 2]. They observed that as the chain left the pot, each link of the chain was coming into contact with other beads coiled within the cup. They concluded that each collision resulted in a kicking motion, or reaction force, causing the chain to experience a lift. It was concluded that a certain amount of bending stiffness was needed to experience a proper kick that would result in a chain fountain. Biggins and Warner also found, through both quantitative and physical experiment, that the height of the chain fountain depends on the initial height of the cup.

1.1 Purpose of Work

We aim to create and implement a mathematical model of the chain fountain that captures the many physical features associated with this phenomenon. By providing animations of our numerical simulations, we hope to discover the significance of each included physical feature.

2. The Chain Model

2.1 The Lagrange formalism

In mechanics, Newton's laws of motion can be used to form a mathematical representation of an objects path. However, the Euler-Lagrange equations are often better suited to extend an object's equations of motion to a set of generalized coordinates. To calculate the Euler-Lagrange equations we first define the Lagrangian (L) to be the difference between the kinetic and potential energy in the system [3]. The Euler-Lagrange equations are then given by the following equation:

$$\frac{\partial^2 L}{\partial t \partial \dot{q}_i} - \frac{\partial L}{\partial q_i} = 0 \tag{1}$$

where each q_i represents generalized coordinate i.

2.2 The Single Pendulum

To provide some intuition for the use of the Lagrange formalism, we shall briefly discuss the single pendulum. We begin by considering the position and velocity of mass m1. We denote this position $\vec{r}$.

$$\vec{r} = l_1(\sin\theta_1, -\cos\theta_1) \tag{2}$$
$$\dot{\vec{r}}_1 = l_1\dot{\theta}_1(\cos\theta_1, \sin\theta_1) \tag{3}$$

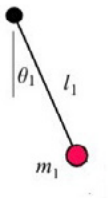

Figure 2: *A Single Pendulum*

Using the position and velocities above we can define the kinetic energy (T) and potential energy (U). Recall that the Lagrangian (L) is taken to be the difference in KE and PE in a given system.

$$T = \frac{1}{2}m_1\dot{\vec{r}}^2 = \frac{1}{2}m_1 l_1^2 \dot{\theta_1}^2 \tag{4}$$
$$U = -gm_1 l_1 \cos\theta_1 \tag{5}$$
$$L = T - U = \frac{1}{2}m_1 l_1^2 \dot{\theta_1}^2 + gm_1 l_1 \cos\theta_1 \tag{6}$$

We consider $q_1 = \theta_1$ as the generalized coordinate of this system. Using the Lagrangian (6), we compute the equations governing the motion of the pendulum as follows:

$$\frac{\partial L}{\partial \dot{\theta_1}} = m_1 l_1^2 \dot{\theta_1} \tag{7}$$

$$\frac{\partial^2 L}{\partial t \partial \dot{\theta_1}} = m_1 l_1^2 \ddot{\theta_1} \tag{8}$$

$$\frac{\partial L}{\partial \theta_1} = -g m_1 l_1 \sin\theta_1 \tag{9}$$

By substituting into equation (1) and dividing by m_1 and l_1, we obtain the equation governing the pendulums course of motion.

$$l_1 \ddot{\theta}_1 = -g \sin\theta_1 \tag{10}$$

This brief exercise should demonstrate the elegance of the Lagrange formalism. In the following sections we discuss how this formalism was used to construct the chain's equations of motion.

2.3 Motivation for the Model

Our chain model is an extension of the double pendulum (Figure 3) to the case of N links. We briefly illustrate the derivation of the double pendulum's equations of motion.

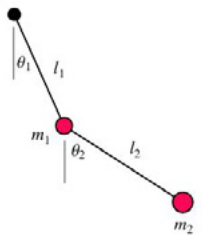

Figure 3: A Double Pendulum

Positions	**Velocities**
$\vec{r_1} = l_1(\sin\theta_1, -\cos\theta_1))$	$\dot{\vec{r}_1} = l_1\dot{\theta}_1(\cos\theta_1, \sin\theta_1)$
$\vec{r_2} = \vec{r_1} + l_2(\sin\theta_2, -\cos\theta_2))$	$\dot{\vec{r_2}} = \dot{\vec{r}_1} + l_2\dot{\theta}_2(\cos\theta_2, \sin\theta_2)$

We can obtain the Lagrangian by computing the difference in KE and PE in the system.

$$\begin{aligned} T &= \frac{1}{2}m_1\dot{\vec{r}_1}^2 + \frac{1}{2}m_2\dot{\vec{r}_2}^2 && (11)\\ U &= -2gm_1l_1\cos\theta_1 - gm_2l_2\cos\theta_2 && (12)\\ L &= T - U && (13) \end{aligned}$$

We consider $q_1 = \theta_1$ and $q_2 = \theta_2$ to be our generalized coordinates. We can then use (1) to obtain the following two equations:

$$\begin{aligned} (m_1+m_2)l_1^2\ddot{\theta}_1 &+ m_2l_2^2\ddot{\theta}_2\cos(\theta_1-\theta_2) && (14)\\ &= -m_2l_2\dot{\theta_1}^2\sin(\theta_1-\theta_2) - g(m_1+m_2)\sin\theta_1 \\ m_2l_1\ddot{\theta}_1\cos(\theta_1-\theta_2) + m_2l_2\ddot{\theta}_2 &= m_2l_1\dot{\theta_1}^2\sin(\theta_1-\theta_2) - gm_2\sin\theta_2 && (15) \end{aligned}$$

We consider equations (14) and (15) to be the equations of motion for a double pendulum. It is not hard to imagine that one may attempt extending the pendulum to the case of an N-pendulum. We use this idea to create a chain of N links. To obtain our chain model, we need only detach the N-pendulum, adding an extra mass to the top.

2.4 Description of the Model

As discussed in the prior section, our chain is an extension of the double pendulum. The chain shall be composed of N massless rigid links of length l_i, and N+1 beaded masses of mass m_i. The chain is defined recursively, with each mass' position, velocity, and acceleration dependent on those prior to it. Beaded mass mi is connected to beaded mass m_{i+1} by a rigid rod of length l_i. Beneath mass m_{i+1} is positively oriented angle θ_{i+1}. Thus, we can recursively define our chain with N angles as follows:

Positions	**Velocities**
$\vec{r}_1 = (x_1, y_1)$	$\dot{r_1} = (\dot{x_1}, \dot{y_1})$
$\vec{r}_{i+1} = \vec{r}_i + l_i(\sin(\theta_i), -\cos(\theta_i)))$	$\dot{r}_{i+1} = \dot{\vec{r}}_i + l_i\dot{\theta}_i(\cos(\theta_i), \sin(\theta_i))$

for i = 1,2,...,N.

2.5 Collisions

Detecting and handling collisions proved to be the most interesting aspect of this model's development. We believe that our failed first attempt at modeling the collisions provides the most intriguing illustration of the difficulties associated with this problem.

2.5.1 Manual Detection

Our first attempt at handling the collisions began with an intuitive approach. If a beaded mass, m_i, collides with a barrier, we reverse this mass' velocity component wise. This is the intuitive approach associated with modeling a bouncing ball's collisions with a wall. The idea to implement this approach stemmed from our view of the chain as N+1 bouncing balls attached by N rigid rods.

Much to our surprise, this method failed. The issue seemed resolvable at first, due to the correct behavior of mass m_{N+1}. However, for any mass $m_1 - m_N$, collisions resulted in an immediate simulation crash. The issue with this intuitive approach lies in the recursive nature of the chain's equations. We see that each mass' velocity is dependent on the prior mass' velocity. In turn, the j^{th} mass is dependent upon masses' $m_1 - m_{j-1}$ velocities. In order to implement such a method, each time a collision is detected, we must exit our numerical solver, then restart the simulation with the algebraically adjusted velocities.

2.5.2 Detection Zones

Manually detecting collisions quickly became both tedious and computationally expensive. In order to improve upon our simulation complexity, we sought a method that would automatically detect and handle collisions simultaneously. To combine these two tasks, we implemented collision detection zones. The detection zones are portions of the coordinate plane in which a collision must occur. We now need only use the masses' coordinates to determine if a mass is within a detection zone. If a mass is found to be within the detection zone, we note that a collision has occurred during the given iteration.

To handle the collisions, we incorporate the use of "anti-gravity" in each detection zone. This method of "anti-gravity" forces the chain to reverse its velocity upon entering a detection zone. When a mass enters a detection zone, standard gravity is replaced by a large constant (k), with the sign(k) = sign(v_{y_j}). We note that the same method is used to handle collisions with vertical barriers, we instead determine the sign of the constant from sign(v_{y_j}).

Our new method allows for a significantly less complex simulation. We no longer require any breaks in our simulation and are able to automatically detect collisions. The result requires only a small alteration of our original equations of motion, as described in the Equations of Motion section. This alteration accounts for a change in potential energy within each detection zone. By augmenting the potential energy, we do not need to account for the chain's recursive velocity dependence.

2.6 Equations of Motion

The equations of motion shall be derived using the Lagrangian formalism, similar to what is done in [4]. We take T to be total kinetic energy in the system, and U to be the potential energy.

$$T = \frac{1}{2}\sum_{i=1}^{N+1} m_i \dot{r}_i^2 \tag{16}$$

$$U = \sum_{i=1}^{N+1}(c_i y_i + d_i x_i) + \sum_{i=1}^{N-1} R_i(\theta_{i+1} - \theta_i)^2 \tag{17}$$

The Lagrangian is then given by,rigid rods.

$$L = T - U.$$

The equations of motion shall be derived using the Lagrangian formalism, similar to what is done in [4]. We take T to be total kinetic energy in the system, and U to be the potential energy.

$$\frac{\partial}{\partial t}\frac{\partial L}{\partial \dot{q}_i} - \frac{\partial L}{\partial q_i} = 0 \tag{18}$$

where we take $q_1 = x_1$, $q_2 = y_1$, and $q_{i+2} = \theta_i$ for i = 1,2,...,N.

$$\ddot{x}_1\bar{m}_0 + \sum_{i}^{N} l_i\ddot{\theta}_i\bar{m}_i\cos\theta_i = \sum_{i=1}^{N} l_i\dot{\theta_i}^2\bar{m}_i\sin\theta_i - \bar{d}_0 \tag{19}$$

$$\ddot{y}_1\bar{m}_0 + \sum_{i}^{N} l_i\ddot{\theta}_i\bar{m}_i\sin\theta_i = -\sum_{i=1}^{N} l_i\dot{\theta_i}^2\bar{m}_i\cos\theta_i - \bar{c}_0 \tag{20}$$

$$\begin{aligned}\ddot{x}_1\bar{m}_i\cos\theta_i &+ \ddot{y}_1\bar{m}_i\sin\theta_i + \sum_{j<i} l_j\ddot{\theta}_i\bar{m}_i\cos(\theta_j-\theta_i) + \ddot{\theta}_i l_i\bar{m}_i + \sum_{j>i}^{N}\ddot{\theta}_j l_j\bar{m}_j\cos(\theta_j-\theta_i) \\ &= \sum_{j<i} l_j\dot{\theta}_j^2\bar{m}_i\sin(\theta_j-\theta_i) - \sum_{j>i}^{N} l_j\dot{\theta}_j^2\bar{m}_j\sin(\theta_i-\theta_j) - \bar{c}_i\sin\theta_i - \bar{d}_i\cos\theta_i + \bar{R}_i\end{aligned} \tag{21}$$

The constants defined are given by:

$$\bar{c}_i = \sum_{j=i+1}^{N+1} c_j, \qquad \bar{d}_i = \sum_{j=i+1}^{N+1} d_j, \qquad \bar{m}_i = \sum_{j=i+1}^{N+1} m_j$$

The terms $\bar{R}_i$ control the angular restrictions between each link. For each $R_i > 0$, an bending stiffness is introduced between the links l_i and l_{i+1}.

$$\bar{R}_i = \begin{cases} 2R_1(\theta_1-\theta_2) & \text{for } i = 1 \\ -2R_{i-1}(\theta_{i-1}-\theta_i) + 2R_i(\theta_i-\theta_{i+1}) & \text{for } 1 < i < N-1 \\ -2R_{N-1}(\theta_{N-1}-\theta_N) & \text{for } i = N-1 \end{cases}$$

We introduce linear viscous damping in the angles by the equivalence of virtual work drawn from Schagerl et al [4]. These terms are accounted for by the adding term Q_i to the right hand side of each equation of generalized coordinates θ_i.

$$Q_i = \begin{cases} 2\dot{\theta}_1 - \dot{\theta}_2 & \text{for } i = 1 \\ -\dot{\theta}_{i-1} + 2\dot{\theta}_i - \dot{\theta}_{i+1} & \text{for } 1 < i < N \\ \dot{\theta}_N - \dot{\theta}_{N-1} & \text{for } i = N \end{cases}$$

3. Results and Discussion

Our model is able to capture many physical features including friction, viscous damping, and bending stiffness. By considering systems with varying imposed physical features, we are able to inspect the chain's behavior in several distinct cases.

3.1 Conservative System

We begin by creating a chain simulation with perfectly elastic collisions. We also allow for free rotation about each mass (i.e. no bending stiffness). We observe no fountain in this case. We observe that the links within the cup are unable to come to a full rest. The links are also free to rotate about each mass, thus the chain in this state lacks a moment of inertia. These coupled issues are what we believe prevents the formation of a chain fountain.

In the following trial, we only allow every fifth link to rotate about every fifth mass. The purpose of doing so is to help ensure that the chain is capable of exhibiting the "kicking-motion" described by Biggins and Warner[2]. We still maintain elastic collisions in this simulation. We again fail to observe any chain fountain in this case. As in the prior simulation, the links never come to rest at the bottom of the cup. This appears to be a significant issue.

It appears that the presence of friction in the system is essential to the formation of the fountain. This result is somewhat counter intuitive, as we are still able to see the chain exert a "kicking" motion as each link leaves the floor of the cup. We note that it was previously found, by Biggins and Warner, that a floating chain exhibits no chain fountain [1]. Our findings add to this previous result, as the floating chain did not account for contact with the floor of the cup.

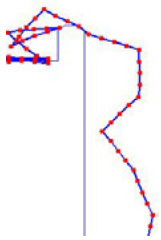

Figure 4: Conservative System Simulation

3.2 Non-Conservative Simulations

We now inspect the systems behavior with the inclusion of additional parameters. Lateral and vertical friction are implemented within the cup. The addition of friction within the cup allows for the chains' links to settle down. As the chain begins to fall, the connected links begin exhibiting this described "kicking motion". The links that are allowed to rotate do so quite chaotically. To help control the chaotic motion of the freely rotating links, we include a viscous damping term. The chain now follows a more settled path over the side of the cup.

To our surprise, we still see no profound chain. Previous findings have lead us to believe that the height of the chain fountain should be proportional to the distance of the cup from the floor [1]. We see the chain is tending towards fountain formation, however the height of the fountain is not as expected. The cup is set 300 meters above the ground in simulation, thus we suspect the fountain should be much larger.

The beginnings of the fountain formation suggests that we have found a model that can experience a chain fountain, thus we suspect the issue lies with our chosen friction and damping parameters. A more extensive coverage of damping coefficients should produce our desired result.

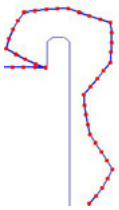

Figure 4: Conservative System Simulation

References

[1] J.S. Biggins. Growth and shape of a chain fountain. *Europhysics Letters*, 106(4), 2014.

[2] J.S. Biggins and M. Warner. Understanding the chain fountain. *Proc. Roy. Soc. A: Math, Phys. and Eng. Sci*, 470(2163), 2014.

[3] Reinhardt M. Rosenberg. *Analytical dynamics of discrete systems, volume 4 of Mathematical Concepts and Methods in Science and Engineering*. Plenum Press, New York-London, 1977.

[4] M. Schagerl, A. Steindl, W. Steiner, and H. Troger. On the paradox of the free falling folded chain. *Acta Mech.*, 125(1-4):155–168, 1997.

[5] Epifanio G. Virga. Dissipative shocks in a chain fountain. *Physical Review E*, 89(5), 2014.

[6] Epifanio G. Virga. Chain paradoxes. *Proc.* A., 471(2173):20140657, 24, 2015.

Comparing Numerical And Analytic Approximate Gravitational Waveforms

Nousha Afshari and Dr. Geoffrey Lovelace

Department of Physics, California State University, Fullerton

Abstract

A direct observation of gravitational waves will test Einstein's theory of general relativity under the most extreme conditions. The Laser Interferometer Gravitational-Wave Observatory, or LIGO, began searching for gravitational waves in September 2015 with three times the sensitivity of initial LIGO. To help Advanced LIGO detect as many gravitational waves as possible, a major research effort is underway to accurately predict the expected waves. In this poster, I will explore how the gravitational waveform produced by a long binary-black-hole inspiral, merger, and ringdown is affected by how fast the larger black hole spins. In particular, I will present results from simulations of merging black holes, completed using the Spectral Einstein Code (black-holes.org/SpEC.html), including some new, long simulations designed to mimic black hole-neutron star mergers. I will present comparisons of the numerical waveforms with analytic approximations.

Low-Energy Electron Scattering From Ethylene: Elastic And Vibrational Excitation

Borna A. Hlousek
Advisor: Dr. Murtadha Khakoo

Department of Physics, California State University, Fullerton

1. Abstract

We have measured normalized differential and integral cross sections for elastic and vibrationally inelastic scattering of low-energy electrons from ethylene (C_2H_4) over a large range of incident electron energies and angles. The Differential cross sections(DCS) were measured over a large number of electron incident energies (E_0) and scattering angles ranging from 0.5 to 100 eV and 5° to 130°. These measurements are found to be sensitive to the role of resonances in the scattering dynamics. We also found an unusual feature in our 90° data (excitation function) at ≈ 3.5 eV and tentatively associated it with the onset of the $\tilde{a}^3B_1u$ triplet electronic state. In addition, DCSs for the vibrational excitation of four composite features in ethylene electron energy loss spectrum in the range of 0 to 0.8 eV energy loss are also presented. These DCSs are taken at incident electron energies of 1.25 eV to 15 eV and for scattering angles (θ) in the range of 0° to 180°. These results are compared to previous measurements regarding the behavior of these features in the scattering dynamics.

2. Introduction

The theoretical and experimental electron interactions of ethylene or ethene C_2H_4 have been extensively studied, especially with regard to resonant elastic scattering and vibrational excitation. The C=C double bond in ethylene is a region of high electron density and of great interest as it allows for the occurrence of vibrational resonances. Ethylene is the most fundamental molecule that comprises the C=C double bond and thus the simplest to look at resonances associated with this bond. Low-energy electron collisions with ethylene have also been of interest in modeling low-temperature plasmas as well as for their role in basic combustion of a primary hydrocarbon. Differential cross sections, are essentially scattering probabilities for the deflection of electron of energy E_0 through any scattering angle.

3. Experiment

The experimental apparatus is a low energy electron spectrometer located in Dan Black Hall which produces a collimated, highly mono-energetic electron beam that collides with a gas target emitted through a collimated aperture. The incident electrons are deflected off the gas and detected by a scattered electron detector.

Both the gun and the detector were constructed from titanium and employed a set of cylindrical transport lenses with a double hemispherical energy selectors. The entire apparatus was housed in a magnetically shielded high-vacuum chamber.

Electrons were detected by a discrete dynode electron multiplier with a background rate of <0.01 Hz, capable of linearly detecting >105 Hz without saturating [1]. The typical electron cur- rents hovered in the range of 15–25 nA, with a total system energy resolution of between 38 and 50 meV, full width at half the maximum. Lower currents were chosen for lower E_0 values to minimize the effect of space charge broadening of the incident electron beam. The beam was easily focused to 1 eV and extremely stable, with variation of less than a maximum of 10% during the days data taking. The energy of the beam was regularly checked via measuring the dip in the elastic scattering caused by

the 2 ^{2}S He resonance at 19.366 eV [2] at $\theta = 90°$ during an experimental run. The energy loss spectra of the elastic peaks were collected at fixed E_0 values and by repetitive, multichannel scaling techniques.

The gas target was formed by the flow of gas through a small 0.3mm aperture, which was carbon coated (sooted, acetylene flame) to reduce the secondary electron emission off of other components. The aperture was attached to a movable source arrangement. This is important because when low-energy electron-scattering rates are to be accurately determined, the background scattering can be significant (>20%) at small scattering angles. The measured DCSs were normalized using the relative flow method with helium as the reference gas, using DCSs from the well-established work of Nesbet [3] for E_0 below 20 eV and of Register et al. [4] and Boesten and Tanaka [5] for E0 above 20 eV. The aperture pressure ranged from 1.2 to 2 torr for Helium and 0.12 to 0.25 torr for ethylene, corresponding to chamber pressures in the range of 1.2 10^6 to 2 10^6 torr. For each E_0 value the set of DCS was taken a minimum of two times to check the measurements reproducibility. A weighted average was made of multiple data sets to obtain the final DCSs.

The DCSs are given along with 1 standard deviation error bars in Table I. For the vibrational excitation experiment, electron energy loss spectra on the energy-loss range of 0.15 to 0.65 eV were taken at 1.25, 1.5, 1.75, 2, 3, 4, 5, 8, and 15 eV for the same angles as the elastic-scattering data. A sample spectrum is given in Fig. 1. These spectra were unfolded using the energies of vibrational modes given in Table II obtained from NIST [6]. Each spectrum was taken multiple times to ensure reproducibility. The DCSs for vibrational excitation were obtained by normalizing, to the elastic DCS of this work, the intensity ratios of the vibrational features to the elastic feature taken in the same energy-loss spectrum. In the unfolding algorithm, because of our restricted energy resolution of 38–45 meV, it was necessary to group energy-loss features, to obtain reproducible DCSs with reasonable statistics. This reduces the detail that could be obtained on the excitation of individual vibrations, compared with the higher-resolution data of Walker et al. [7] (resolution 22 meV) and Allan et al. [8] (20 meV).

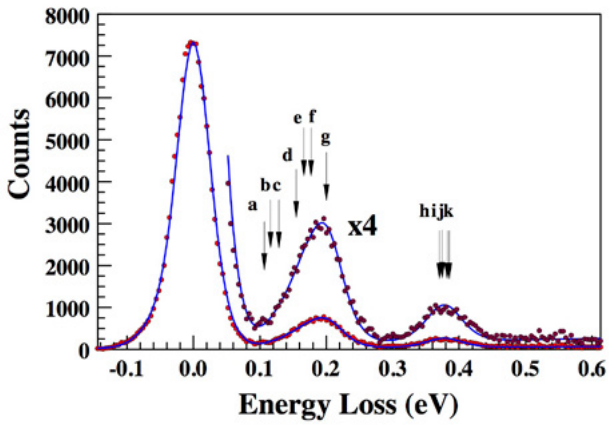

Figure 1: *Background subtracted electron energy-loss spectrum of ethylene at $E_0 = 2$eV and $\theta = 90°$. The Black dots are the experimental data and the blue line is the fit to the data.*

4. Results and Discussion

4.1 Elastic

Our experimental were especially used to determine the elastic Integral Cross Section and Multi-Channel Schwinger Methods (MTCS). We measured many elastic DCSs from E0 values in the region of 1.25 - 2.5 eV; where the π^* $^2B_{2g}$ resonance is located. Figure 2 shows the trend of the angular distribution for E_0 from 0.5 to 2.5 eV. At $E_0 = 0.5$ eV the scattering shows basic polarization potential scattering, i.e., a forward peak merging into a backward peak without any midangle structure. At higher energies, we see in Fig. 3(a) that the $d\pi$ distribution due to π^* $^2B_{2g}$ resonance sets in around E0 = 1 eV and persists until 3 eV. This E0 range was also observed by [6,7], except that our results track it in the elastic scattering channel only whereas [8] tracks it in both elastic and vibrational excitation channels and [10] only in the vibrational excitation channels. The present elastic DCSs at 1.5 and 5 eV (Fig. 45) show excellent agreement with Allan et al. [8] at both E0 values where they have published their DCSs, and they are in good agreement with the results of Panajotovic et al. [9] at large θ, but at small θ the data of Ref. [9] do not display the forward scattering observed in the present work and in Ref. [8] below 5 eV.

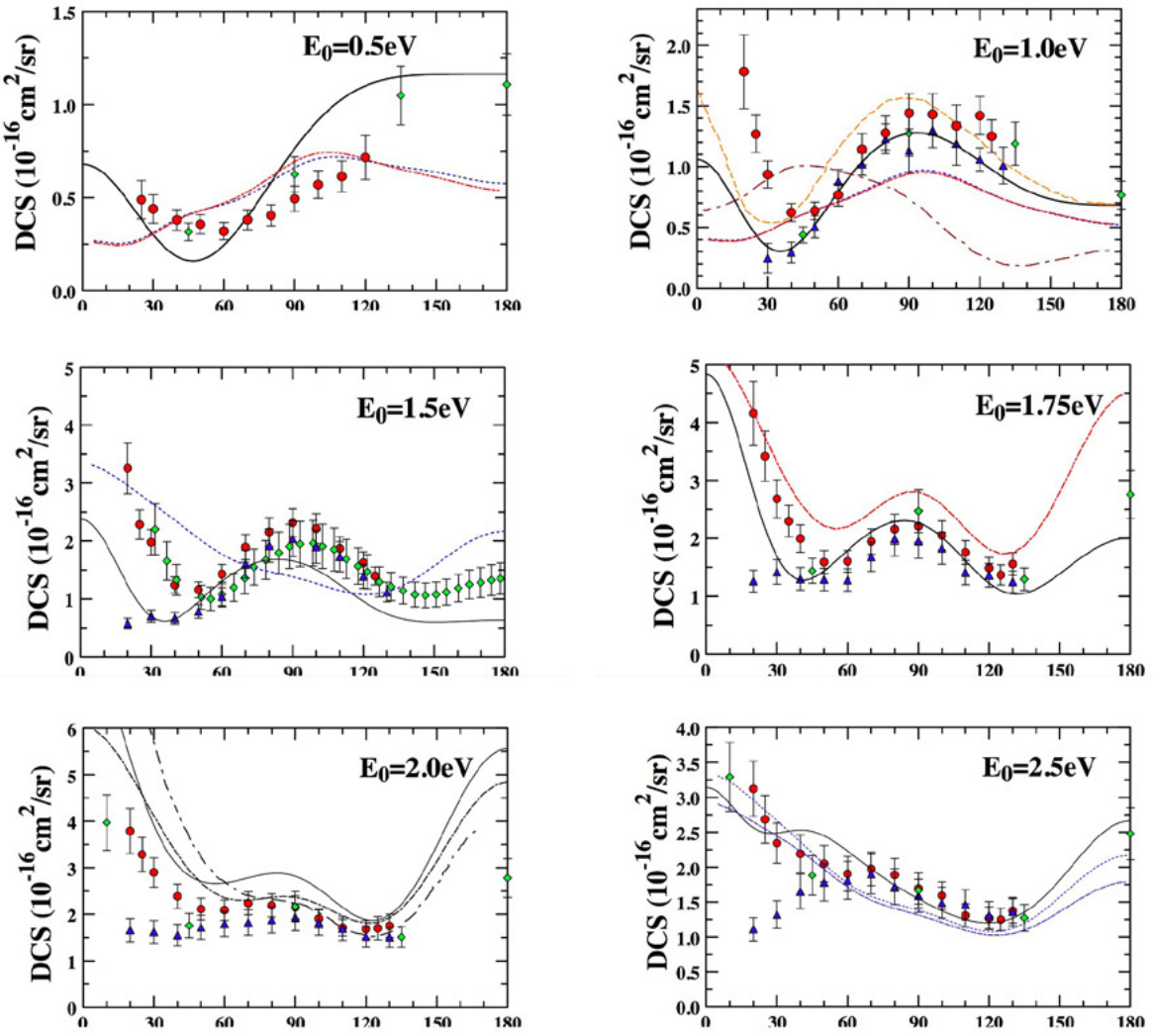

Figure 2: *DCSs for low-energy elastic electron-ethylene scattering. Experiments: The red circle represents present results, the green diamond represents Allan et al. [8] digitized from their paper, and the blue triangle Panajotovic et al. [8].*

At most scattering angles θ the forward scattering is more pronounced in our measurements than any theoretical DCS. As our E0 values rise above 5 eV, the agreement with theory typically improves, with greatest confirmation in the 8-15 eV range. At energies greater than 15 eV the neglect of ionization and other open channels makes Schwinger Multichannel methods less accurate and creates disagreements between theory and experiment.

The effect of the dominant π^* $^2B_{2g}$ is seen in figure 2 where the elastic scattering at θ=90° is measured as a function of E0. There is also a feature that extends from E0 = 3.0 to 5.2 eV, coinciding with the a ^{3} B_{1u} triplet electronic state which extends in the Franck-Condon region of 3.2 to 5.9 eV as observed by Allan et al. [8], and could possibly suggest the decay of a near-threshold core-excited resonance into the elastic channel.

4.2 Vibrational

Our vibrational excitation DCSs were taken at E_0 values of 1.25–15 eV and for from 15° to 130°. These DCSs were integrated using numerical methods to obtain integral cross sections (ICSs). Figure 4 shows E_0 = 8 eV and 15 eV DCSs for the sum of the first two features a,b,c,d in figure 1 and the last feature. The error bars range in 20% levels for 5 eV and above 25% levels at 8 eV. The distributions are nominally flat, showing the major influence of the ^2A_g shape resonance according to the assignment of [7] in the region around E0 = 7.5 eV, which has a width of ≈5 eV as shown in figure 3 for the 0.379 eV excitation function. However, a molecular orbital calculation using a minimal basis set suggests the 7.5 eV peak results from overlapping CH σ^*resonances of $^2B_{2u}$, B_{1u}, and ^2A_g symmetries.

A different figure (not included here) also shows "excitation functions" for other applicable energy losses to compare with [6,7]. These are obtained by fixing the energy loss at the given value on the spectrometer and monitoring the scattered counts at the fixed $\theta = 90°$ as a function of E0. These relative counts are normalized to our elastic DCSs for features 1–4, respectively, at the resonance peak around E_0 = 2 eV. Our results excluding feature 4 h,i,j,k in figure 1 are higher at E0 above 3eV than Ref. [10]'s because of our experiments broader resolution which includes excitations outside of the nominal energy loss for exciting a single vibrational mode at the energy-loss setting.

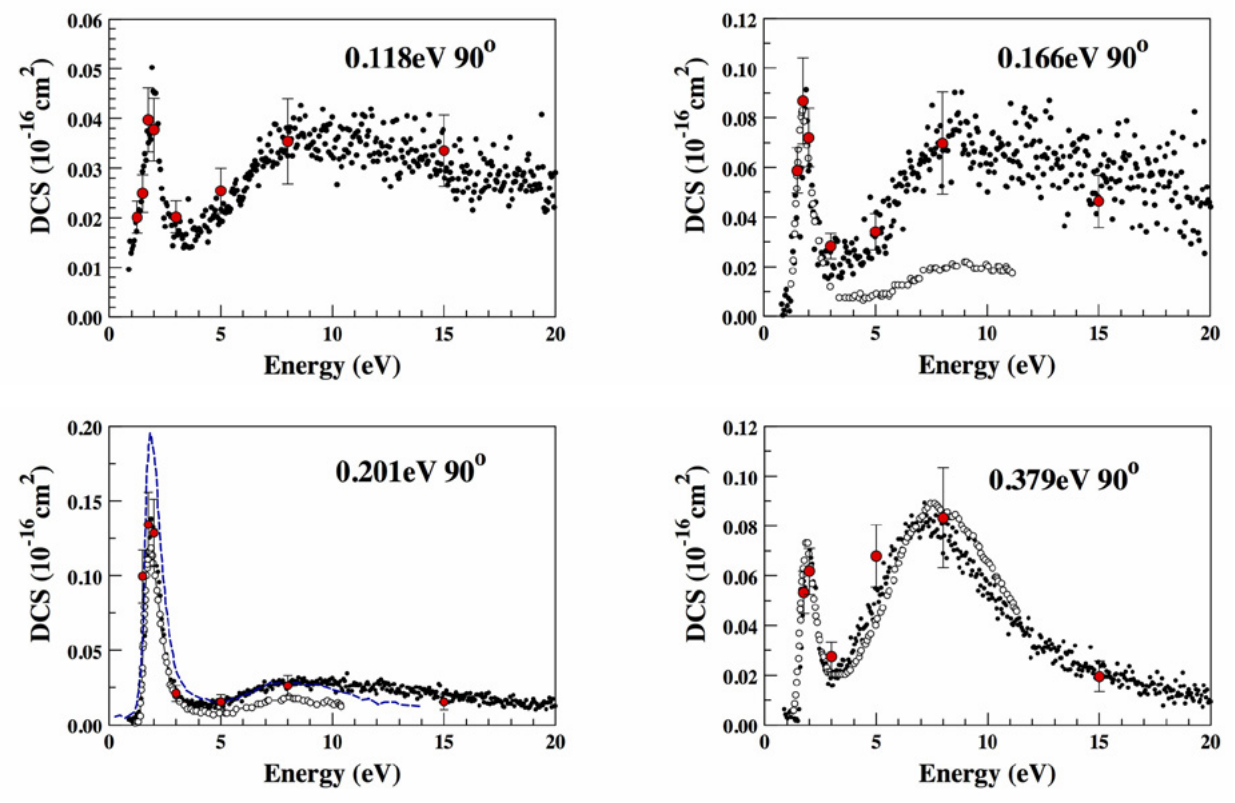

Figure 3: *Experimental DCSs for vibrational excitation of ethylene for features at the energy loss specified, at the fixed θ of 90°, as a function of energy E_0. Red dots represent Present DCS points at θ = 90°, for regions 1, 2, 3, and 4, respectively. Black dots represent Present results normalized to the present regional DCSs; Triple dash represents Walker et al. [7] digitized data at θ = 90°; Allan et al. [8] digitized data at θ = 180°.*

We can still observe all modes affected by the longer-lived $^2B_{2g}$ and short-lived 7.5 eV shape resonances across their E_0 ranges. Feature 4 sums several C-H stretch modes is far more excited in the 7.5 eV energy range. In figure 3 the DCSs of the four features are displayed. For the first feature, the d-wave distribution due to the π^* $^2B_{2g}$ resonance at 2 eV does not affect this feature as strongly as it does the others, but it nevertheless excites these modes. Feature 2–4 are all enhanced by resonant scattering, especially the C=C double bond excitation at low E_0 values.In fact the DCS for feature 3 (the C-C stretch) is increased in size by a factor of 2 at E0 = 1.75 eV or 2 eV when comparing to E_0 = 8 eV which is the next highest in magnitude. This mode shows a persistent d-wave angular distribution even at E_0 = 5 eV.

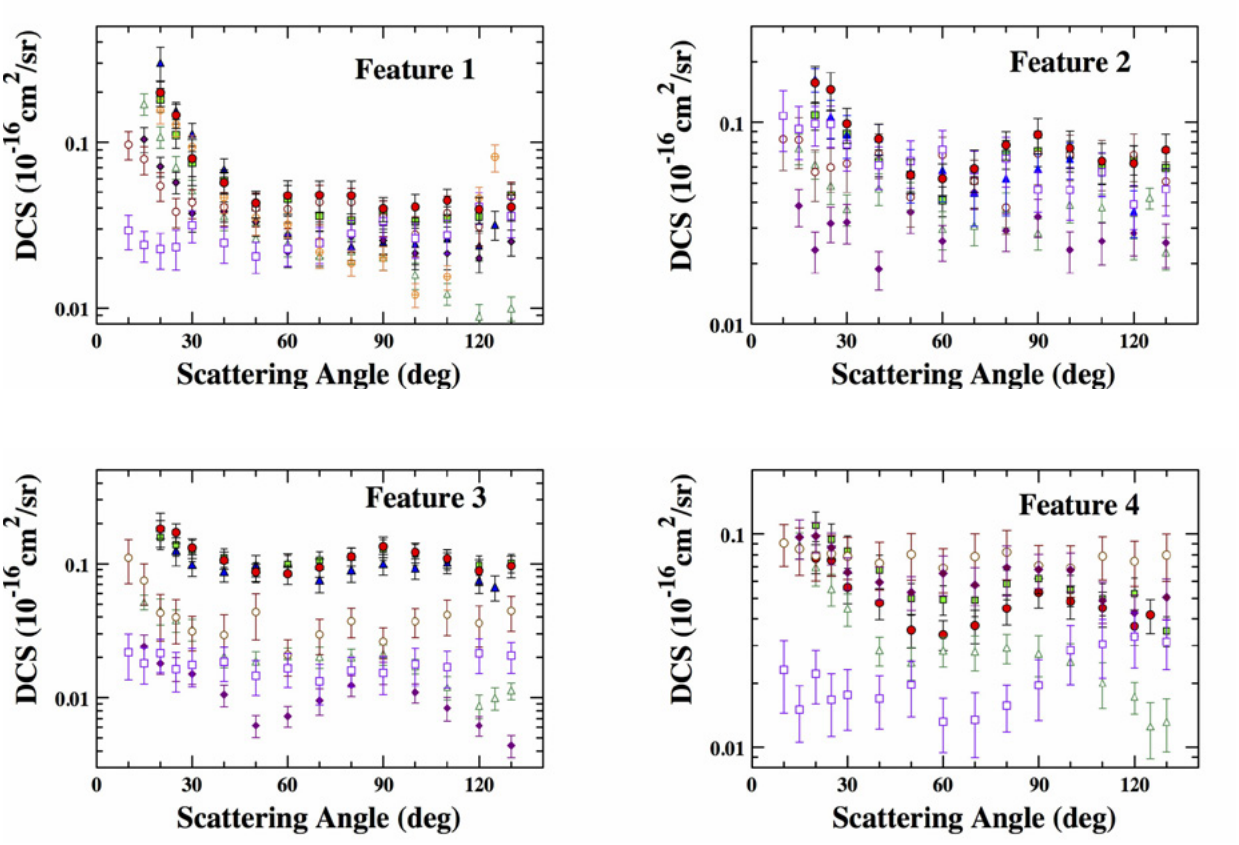

Figure 4: *Experimental DCSs for vibrational excitation of features. Legend for E_0 values: yellow circle for 1.25, blue triangle for 1.5, red dot for 1.75, green square for 2.0, green triangle for 3.0,purple diamond for 5.0 eV, black circle for 8.0, and red square for 15 eV.*

5. Conclusion

The present work has presented DCSs for elastic scattering from C_2H_4 over a large range of energies from 0.5 to 100 eV. Our results are in very good agreement with previously measured DCSs, especially those of Allan et al. [8] where agreement is excellent. The cross section displays clear for- ward scattering at low energies, clarifying the low-energy elastic DCS picture for theoretical models to reproduce. Forward scattering, and in some cases backward scattering, in the elastic channel at low energies is not completely accounted for by theory, possibly indicating the need for larger calculations that better address polarization and/or long-range (or equivalently high partial-wave) scattering. An interesting feature in our 90° scattering elastic excitation function coincides in energy with the excitation energy of the a ^{3} B_{1u} triplet electronic state which extends in the excitation Franck-Condon region of 3.2–5.9 eV as observed by Allan et al. [8], and we tentatively assign this to a threshold coupling between elastic and electronic excitation channels. Further, independent, work to confirm this assignment would be desirable. Our lower-resolution vibrational excitation DCSs also provide angular distributions and magnitudes for groups of vibrational excitations that point to enhancement via C-C π^* ($^2B_{2g}$) and C-H σ^* ($^2B_{2u}$, $^2B_{1u}$, and 2Ag) shape resonances, showing regions of $d\pi$ and $s\sigma$ angular distributions, respectively, and complement the work of Walker et al. [7] and Allan et al. [8]. However, theoretical work on the vibrational excitation of the C-H and C=C modes of ethylene is needed to fully understand the observed resonant behavior.

6. Acknowledgements

This work was funded by the National Science Foundation research Grants No. NSF-RUI-AMO 1306742 and No. NSF-RUI-AMO 0968874. Important discussions with, and supporting data from, Carl Winstead on this work (especially concerning the symmetry and role of shape resonances) are very gratefully acknowledged. We also thank Carl Winstead and Vince McKoy from Caltech for pro- viding tabulations of their elastic-scattering Schwinger multichannel calculations, Cynthia Trevisan and Ann Orel for providing tabulations of their variational complex Kohn (VCK) calculations, and Romarly F. da Costa for sending us tabulations of their Schwinger multichannel with pseudopo- tentials (SMCPP) results. High school students Justin Lee and Ryan Murase worked under a Troy Tech High School summer internship program in our laboratory

References

[1] Ashton F. Embry III, and Klovan, J. E., 1971, A Late Devonian Reef Tract on Northeastern Banks Island, N.W.T.: Bulletin of Canadian Petroleum Geology, v. 19, no. 4, p. 730-781.

[2] J. H. Brunt, G. C. King, and F. H. Read, J. Phys. B: At. Mol. Phys. 10, 1289 (1977).

[3] R. K. Nesbet, Phys. Rev. A 20, 58 (1979).

[4] D. F. Register, S. Trajmar, and S. K. Srivastava, Phys. Rev. A 21, 1134 (1980).

[5] L. Boesten and H. Tanaka, At. Data Nucl. Data Tables 52, 25 (1992).

[6] T. Shimanouchi, Tables of Molecular Vibrational Frequencies Consolidated, Vol. 1 (NSRDS- NBS, Washington, DC, 1972), pp. 1–64.

[7] I. C. Walker, A. Stamatovic, and S. F. Wong, J. Chem. Phys. 69, 5532 (1978).

[8] M. Allan, C. Winstead, and V. McKoy, Phys. Rev. A 77, 042715 (2008).

[9] T. P. T. Do, K. L. Nixon, M. Fuss, G. García, F. Blanco, and M. J. Brunger, J. Chem. Phys. 136, 184313 (2012).

[10] B. Mapstone, M. J. Brunger, and W. R. Newell, J. Phys. B: At. Mol. Phys. 33, 23 (2000).

Modeling Binary Neutron Stars

Conner Park
Advisor: Dr. Jocelyn Read

Department of Physics, California State University, Fullerton

1. Background

Neutron Stars
When a star dies the remnants create a black hole, white dwarf, or neutron star. A black hole is a celestial body where all of the matter has collapsed into a singularity. A neutron star is a "cold" star with a gravitational force strong enough that quantum pressure of degenerate neutrons is needed to keep it stable. The focus of the paper will be on two neutron stars orbiting each other.

A neutron star has greater mass than the sun in our solar system but is smaller in radius. The Equation Of State (EOS) of the star tells us the relationship between physical properties e.g. density and pressure. Depending on the EOS of the neutron star the radius of the celestial body will be approximately 10 to 13 km. This becomes important in determining how deformed a star becomes due to tidal effects. An EOS with a smaller radius will have smaller deformations whereas an EOS with a larger radius will have larger deformations. This research focuses on the different EOSs and how they affect the gravitational waves emitted binary neutron star systems.

Gravitational Waves
As two neutron stars orbit each other there will be orbital decay due to gravitational radiation. This gravitational radiation, or gravitational waves, stretches and squeezes the space- time as it travels and is predicted to modify the space-time on Earth.

Laser Interferometer Gravitational wave Observatory (LIGO) has been designed to catch these gravitational signals that are predicted. For LIGO to most accurately extract gravitational wave signals from all the possible fluctuations in the detector, we need to create an accurate prediction. To create a prediction, we need to consider all the factors that can contribute to gravitational waves. The focus of this research will be on the effects of Tides and Resonance Frequencies on the gravitational waves emitted from the coalescence of binary neutron stars.

2. Methods

Different Post-Newtonian Models
There are many different ways to mathematical represent two masses orbiting each other. These are not to be confused with Newtonian models because the PN models will take into account Einstein's theory of General Relativity.

The first PN model examined in this paper is the Taylor T4. Taylor T4 will have parameters containing the masses of the two neutron stars and a post Newtonian expansion parameter, x. This representation models the inspiral of two point masses. Modeling the binary system in the aforementioned way we get an ordinary differential equation that we can be solved without the use of a supercomputer. I will refer to this model as Point Particles because that is assumption we are using for the first model.

The second PN model will take Point Particle and add a correction factor. This correction factor will contain information about the tides (Λ) and resonances of the neutron stars. The model will then be parameterized by additional factors but the equation will still be an ordinary differential equation. Most tidal models in the literature assume that the system has gravitational wave frequency well below the resonance frequency (f -> infinity is assumed in

our equations). In our implementation we don't take that limit, but for comparison we reproduce that assumption by setting the resonance frequencies to large values. Doing this I will get a result that is only affected by the Post-Newtonian piece and the tides; I will call this model Particles with Tides.

The third model will take the second model and include estimates of the actual fundamental mode frequency of the neutron star predicted by Chan et al. [Phys.Rev.D90, 124023 (2014)]. This model requires the same information as the second model but has a predicted frequency instead of an arbitrarily large value; therefore this representation is still an ordinary differential equation. I will refer to this model as Particles with Tides and Resonances since it requires tides and a calculated resonance frequency.

After creating the three different models a code to solve the ordinary differential equation will be created. I will use a starting frequency of and a starting phase angle of 0 radians. Then all of this information will be put into the numpy function, odeint, to solve and output an array of data. The data points will then be put into Veronica Lockett-Ruiz's truncate function1 which will read in all the data points and keep the frequencies that are below a certain threshold. This is to ensure that the models end at a fixed point that is within the limits of the differential equation solver. Then to change the orbital waveform data into gravitational waveform data, the orbital data is multiplied by a factor of $e^{2i\varphi}$. After the data has been modified appropriately another function from Lockett-Ruiz's code, export1, will be used to create an excel spreadsheet with all of the information about the gravitational waveforms.

Numerical Matching

Using Eric Flynn's hybrid matching code[2] the 3 Post-Newtonian models were matched with the data from our Japanese collaborators. The hybrid code reads in PN waveform and a numerical waveform to find the best match. The scipy function, correlate, slides the numerical waveform onto the PN until a match is found. It should be noted that the numerical waveform is truncated to exclude the sporadic beginning and any parts after merger. In previous work, the numerical waveform matched onto the PN waveform before the predicted merger, which innately caused some error. To account for the end of the numerical wave not matching the end of the PN, all of the values after the merger for both the waves are replaced with zeros.

Calculating Errors

To test the accuracy of the Post-Newtonian models, I will use two methods: one is the quantified match and the second is the root mean square of the phase.

The first method is an extension of the hybrid code that I will use to match the PN and the numerical. The hybrid code determines the match of the numerical region on the PN and I will take the quantified match value and then normalize it. To normalize the match value I will take the match value and then dividing by the PN match with itself and the numerical match with itself.

$$\text{HybridMatch} = \frac{\max\left(\int_0^{t^*} PN(t)Num(t-\tau)dt\right)}{\max\left(\int_0^{t^*} PN(t)PN(t-\tau)dt\right) * \max\left(\int_0^{t^*} Num(t)Num(t-\tau)dt\right)}$$

The second method is to use the numpy function unwrap to obtain the phase angles and compute a root mean square. This requires the waveforms to be in its complex form and then an inverse tangent will be computed to get the phase. The unwrap function automatically keeps adding the phase angles so that the result is a one-to-one function. We then match the values accordingly and do a root mean square, and it should be noted that the concatenation of zeros also affects the RMS values so that we expect a trend much like that of the first method.

3. Results

Hybrid Error and RMS Error

There were a total of 99 Post-Newtonian waveforms, 3 different methods, and 33 different Numerical waveforms. An example with the best match is shown below:

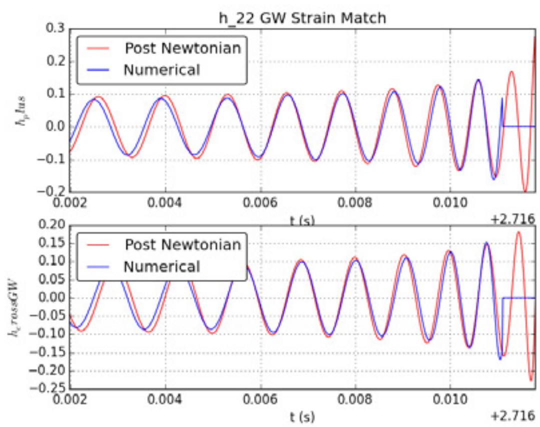

Point Particles
EOS: APR4
Mass 1: 1.30
Mass 2: 1.50

Λ 1: 392.303
Λ 2: 158.003
f01: 2705.83 hz
f02: 2739.178 hz
match value: .8596586

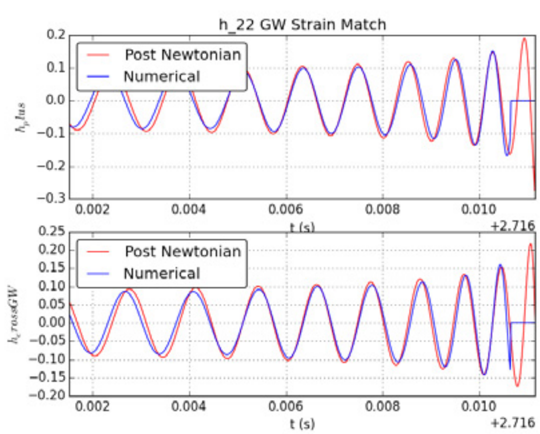

Point Particles
EOS: APR4
Mass 1: 1.30
Mass 2: 1.50

Λ 1: 392.303
Λ 2: 158.003
f01: 2705.83 hz
f02: 2739.178 hz
match value: .8596586

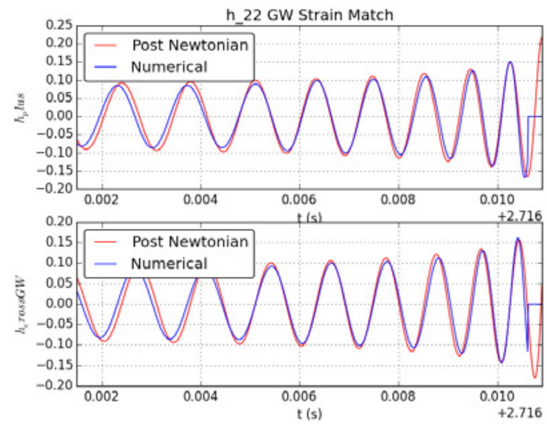

Point Particles
EOS: APR4
Mass 1: 1.30
Mass 2: 1.50

Λ 1: 392.303
Λ 2: 158.003
f01: 2705.83 hz
f02: 2739.178 hz
match value: .8596586

The match above represents the matching done with Eric's code. The code matches the two waveforms for a certain region of the numerical, which is shown in the graphs. The outside of the graphs that are not shown are either the buildup of the PN or zero.

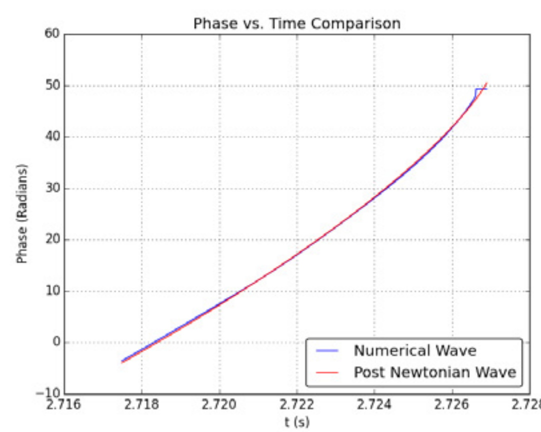

Point Particles
EOS: APR4
Mass 1: 1.30
Mass 2: 1.50

Λ 1: 392.303
Λ 2: 158.003
f01: 2705.83 hz
f02: 2739.178 hz
match value: .8596586

This graph represents the phase angles associated with the above hybrid match.

Collection of Errors

A combined lambda is created using a combined tidal parameter term derived by Wade et al. [Phys. Rev. D 89, 103012 (2014)]. This method takes the two Λ parameters and creates a new lambda that can be thought of as an average lambda of the system.

$$\Lambda = \frac{8}{13}\left[(1+7\eta-31\eta^2)(\Lambda_1+\Lambda_2)+\sqrt{1-4\eta}(1+9\eta-11\eta^2)(\Lambda_1-\Lambda_2)\right]$$

Using this new parameter η we plot the two errors against the new lambda:

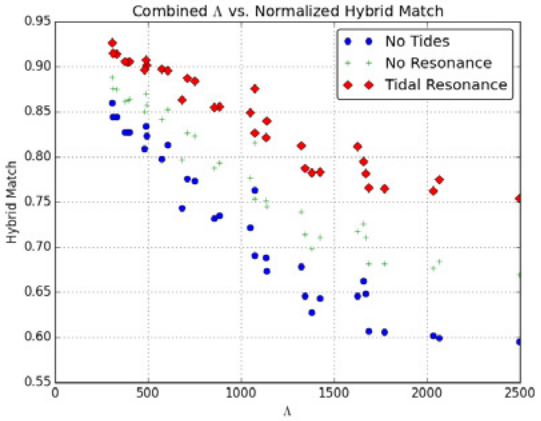

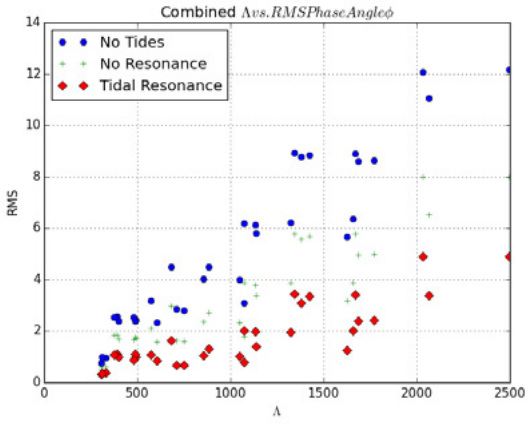

Interpretation of Data

The first thing that is brought to my attention with these graphs is the width of the Particles with Tides and Resonance model and the Point Particles model. The graphs show that for every numerical match the Particles with Tides and Resonance was a better fit. An example is shown below with Point Particles, Particles with Tides, and Particles with Tides and Resonance respectively. I used the worst hybrid match as an example to be able to see the difference because it is more apparent.

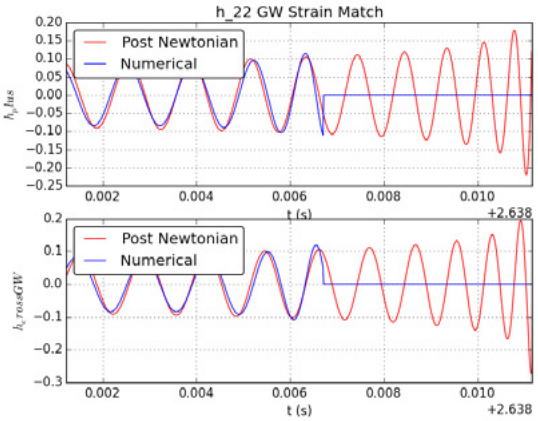

Point Particles
EOS: APR4
Mass 1: 1.30
Mass 2: 1.50

Λ 1: 392.303
Λ 2: 158.003
f01: 2705.83 hz
f02: 2739.178 hz
match value: .8596586

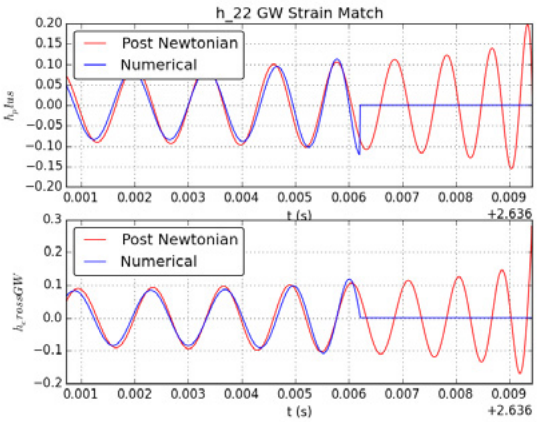

Point Particles
EOS: APR4
Mass 1: 1.30
Mass 2: 1.50

Λ 1: 392.303
Λ 2: 158.003
f01: 2705.83 hz
f02: 2739.178 hz
match value: .8596586

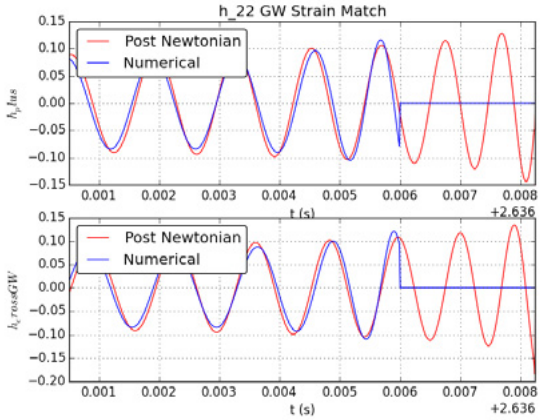

Point Particles
EOS: APR4
Mass 1: 1.30
Mass 2: 1.50

Λ 1: 392.303
Λ 2: 158.003
f01: 2705.83 hz
f02: 2739.178 hz
match value: .8596586

The graphs of the match show that each PN model ends at different times and the Particles with Tides and Resonance with the best match ends closest to the end of the Numerical data. Also the width between the two data points grows as a function of lambda. The Particles with Tides and Resonance model increases in fit, compared to the Point Particles model, as lambda increases.

The data still show that the matches tend to get worse as lambda increase. That seems to suggest that although the Particles with Tides and Resonance is a better match than Point Particles or Particles with Tides, it is still not sufficient to match the numerical data at higher lambdas

Cutoff of Frequency

From here there are a few ways to change the Particles with Tides and Resonance model to have a frequency cutoff that matches the numerical wave. First is to analytically derive a representation of the quadruple moment during the last orbits of the system. Second is to use a fit that matches the cutoff frequency mathematically and maybe has a useful physical interpretation. Third is to use the frequency at the merger for the numerical as the resonance frequency for the PN models. Lastly, work comparing the effectiveness of these three models is required to determine the best model to use.

Different Models

This work used a particular Post-Newtonian model. To verify results, we should compare the effect in other Post-Newtonian-based models, like the Effective One Body (EOB) model. We can then determine how different PN models behave at higher frequencies where resonance affects the inspiral of the neutron stars.

An Analysis of Defense Innovation Unit Experimental in Silicon Valley Tech Innovation

Phillipe Diego Rodriguez
Advisor: Mr. John Bradley Jackson

Department of Physics, California State University, Fullerton

Abstract

On July 2, 2015, Defense Innovation Unit Experimental (DIUx) was created by the Department of Defense (DoD) as part of the Defense Innovation Initiative efforts to acquire new technological innovations in Silicon Valley. Although the Department of Defense already works with major industry contractors, DIUx provides a new source for technological innovations and entrepreneurial business processes that may ultimately serve to improve the national security of the United States of America. However, many startups avoid contact with the government by serving as subcontractors to existing organizations. DIUx has plans to bolster relationships with entrepreneurs and startups to obtain breakthrough technological capabilities despite a history of the decline of governmental contracts because of their bureaucratic nature. Improvements ranging from the better sharing of acquisition information to implementing easier sales processes are necessary for acquiring Silicon Valley technologies. While many barriers to Silicon Valley defense acquisition exist, this analysis aims to address the concerns of Silicon Valley tech firms by providing recommendations to DIUx and the DoD in order to improve their chances for acquiring breakthrough technologies that may prove essential in the national security efforts of the United States of America.

Student Understanding of Non-Cartesian Coordinate Systems in Upper-division Physics*

Marlene Vega
Advisor: Dr. Michael Loverude

Department of Physics, California State University, Fullerton

Abstract

Understanding of Electricity & Magnetism in the upper division requires a considerable amount of integration of mathematical concepts with abstract physics concepts. So the ability to incorporate the use of vectors in several different coordinate systems is an essential skill in an E&M course. This study aims to understand how students think about coordinate systems and vectors in non-Cartesian coordinate systems (plane polar and spherical). Data were collected in a math methods course for physics majors over several semesters, using free response written questions posed on ungraded quizzes and graded course assessments given after instruction. Student responses were coded and assigned to categories. Based on the analysis of the written responses it was not clear to determine whether if student were obtaining corrects responses because they had correct reasoning, or if they had correct reasoning and just happened to answer incorrectly. Because of this, the written questions were revised in a way that would limit this ambiguity. The revised questions were then given to a couple of students in an interview type setting. Overall, students appear to be overgeneralizing from Cartesian coordinate systems in ways that are not productive and appear to have difficulty understanding what unit vectors are and what they represent.

Acknowledgements:

I would like to thank Michael Loverude and Warren Christensen for helping me and guiding me throughout this research experience, and Gina Passante and Brian Forlow for contributing to our research as well.

Supported in part by NSF DRL #1156974

Authors and Editors

Nousha Afshari

Nousha Afshari is earning a Bachelor of Science Degree in Physics. She performs research with Dr. Geoffrey Lovelace in the Gravitational Wave Physics and Astronomy Center at CSUF as the Undergraduate System Administrator and a research assistant. The research focuses on aiding the efforts to directly detecting gravitational waves. Next fall, Nousha will be applying to Medical Physics and Bio-Medical Engineering graduate schools.

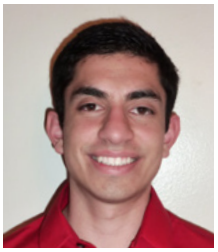

Allen Alvarez

Allen Alvarez is a senior Mathematics major set to graduate in the spring 2017 from California State University, Fullerton. In addition to his undergraduate research in collaboration with Dr. Tyler Mcmillen, Allen has also participated in the 2015 PUMP program at Cal Poly Pomona, and will be attending the Mathematical Biosciences Institute summer undergraduate research experience in the summer of 2016. Post-graduation, Allen hopes to continue pursuing his goal of attaining a Ph.D. in applied mathematics.

Ulysses Alvarez

Ulysses Alvarez completed his BA in Mathematics, including this project, in August of 2015. In addition to his undergraduate research collaboration with Dr. Scott Annin, Ulysses has also participated in the 2013 PUMP program at CSU Northridge as well as the undergraduate research experience SCCUR 2014 at CSUF. Post-graduation, Ulysses is pursuing his goal of attaining a Ph.D. in pure mathematics at Binghamton University.

Alexander Arita

As a fourth year, Alexander Arita is working towards a Bachelor of Science in geology. He works in Dr. Valbone Memeti's lab as he examines the geochemical relationships between the Twentynine Palms and Queen Mountain plutons in Joshua Tree National Park. His research will be presented at the Geological Society of America, Cordilleran section meeting. He hopes to encourage other first generation students get involved in STEM research.

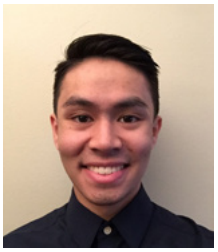

Jake Bergara

Jake Bergara is a senior pursuing a degree in Biology with a concentration in Cell and Developmental Biology at California State University, Fullerton. He currently works in Dr. Merri Lynn Casem's research lab, studying the differences in lipid content and metabolic activity in black and brown widow spider eggs. He is an aspiring dentist and is applying to dental school following graduation this spring. In addition, regarding dentistry, he is on the executive board for the CSUF Pre-Dental Society and is in charge of coordinating fundraising events.

Kaitlyn Berry

Kaitlyn Berry is a senior pursuing a Bachelor of Science Degree in Biological Science with a concentration in Marine Biology and a Minor in Chemistry. She has been apart of Dr. Stapp's Vertebrate Ecology and Conservation laboratory for two years where she has been conducting independent field research examining desert cottontail activity in the aftermaths of a fire. Kaitlyn plans on continuing her education to pursue a Master's Degree in Biological Science in Fall 2016. She hopes to have a career in wildlife conservation with an emphasis on conservation and management of mammals and endangered species.

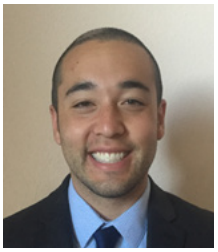

Brandon Betancourt

Brandon Betancourt is a senior who is completing a Bachelor of Science Degree in Kinesiology, and a minor in Biology. He is involved in Dr. Tracy's Herpetology Physiology Lab, and Dr. Abraham's Plant Ecology Lab, and is apart of the Urban Agriculture Community-based Research Experience (U-ACRE). His research focuses on sustainable food production practices that incorporate agriculture ecology, and was conducted at the Saint Andrews Seeds of Hope Community Garden. He will be applying to the Peace Corps. upon graduation where he can utilize his education to give back to the less fortunate.

Gloria Camacho

Gloria Camacho is a fourth year Biological Science major concentrating in Cell and Developmental biology. She works in Dr. Merri Lynn Casem's spider research lab looking at different aspects that can influence brown and black widow development. She is also a Supplemental Instruction leader for Biology 151 and 152. She interns at two different children's hospitals and takes great interest in being apart of medical trips around the world. She will be applying to medical school next year and aspires to be a pediatrician specializing in endocrinology.

Nancy Chen (Geological Sciences Section Editor)

Nancy Chen is a graduate student pursuing a Master of Science degree in Geology. She is currently a teaching associate instructing Physical Geology labs, a graduate research assistant for Dr. Diane Clemens-Knott, and a CSU Sally Casanova scholar. Her thesis is a detrital zircon provenance study of metamorphic pendants in the western Sierra Nevada foothills, which focuses on using U-Pb zircon geochronology. In the future, she will be applying to Ph.D. programs for volcanology or igneous petrology in hopes of using geochronology as a method to understand the generation and evolution of magmas in subduction zones.

Precious Daileg

Precious Daileg is a senior pursuing a Bachelor of Science Degree in Biology with a concentration in Cell and Developmental Biology. She works in Dr. Merri Lynn Casem's education lab, looking at different aspects that influence students' learning and how to help students perform better in biology courses. She also conducts spider research, exploring the proteins that consist the shell of a spider's egg. She is a Supplemental Instruction Leader for the Biology Department with her specialty being Biol 151: Cellular Basis of Life. She also is a part of the Teaching as a Primary Profession (TaPP) program. She will be applying to the teaching credential program at CSU Fullerton upon graduation to continue her path to attaining a teaching career in secondary education.

Jessica Duron (Physics Section Editor)

Jessica Duron is a current physics undergraduate student at California State University, Fullerton (CSUF). At the moment, she is contributing to research with Prof. Leigh Hargreaves that aspires to help improve the safety of radiation therapy treatments for cancer patients. She was the first student in her research lab to give an invited talk for Undergraduate Women in the Physical Sciences, held at the University of Nebraska, Lincoln. Her talk designed a new electron scattering spectrometer that will enable the first measurements of electron interactions with DNA bases. She plans to attend the physics and counseling masters' program at CSUF before she applies to PhD programs in physics. Under the guidance of her mentor Allen Curry, her plan is to teach at a university level and perform pro bono work in counseling.

Amy Feaster

Amy Feaster is a senior pursuing a Bachelor of Arts Degree in Mathematics with a concentration in Applied Mathematics. She works with Dr. Alfonso Agnew studying topological properties of the biquaternionic projective point. She has applied to several graduate programs in mathematics and hopes to continue her education next fall.

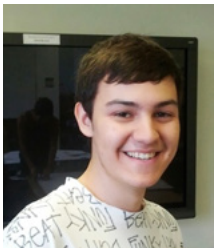

Eric Flynn

Eric Flynn is a fourth year mathematical physics student currently working on various problems in mathematics and physics. He began gravitational wave research with Dr. Jocelyn Read in 2013. This work includes developing methods for the construction and characterization of hybrid gravitational waves which has possible uses for parameter estimation relevant to LIGO. Recent mathematical work with Dr. Agnew involves investigating the twistor structure of matrix projective spaces and explorations of split-quaternionic gauge theory. Eric has many interests in mathematics, physics and many other fields although he is most interested in problems found in nuclear and gravitational wave physics and twistor and representation theory.

Dulce Fonseca

Dulce Fonseca graduated from California State University Fullerton in the Fall of 2015 with a Bachelor of Arts degree in mathematics with a teaching concentration. She is currently enrolled in the Single Subject Credential Program at Cal State Fullerton as she pursues her dream of becoming a secondary school teacher. During her undergraduate career, she worked with Cal State Fullerton's Math Circle alongside colleague Vivian Lopez and program coordinator Dr. Bogdan Suceava. She also worked as a math tutor for the university's Mathematics Intensive Summer Session, where tutors and instructors supported female students in their mathematical endeavors to ensure success for their upcoming school year. As she makes her way through the credential program, she continues to work as a tennis coach for K-8 students in the hopes of becoming the tennis coach at her future place of teaching.

Niv Ginat (Layout Editor)

Niv Ginat is a graphic designer based in Los Angeles, with a focus in branding and packaging. Niv strives to create clean, sophisticated, and functional design. He spends much of his time educating himself about the latest trends in graphic design in order to stay up-to-date and able to communicate with clients effectively. He graduated from Califronia State Universty of Fullerton with a BFA in Graphic Design.
Niv is very passionate about music and thinks Paul McCartney is the best musician of all time.

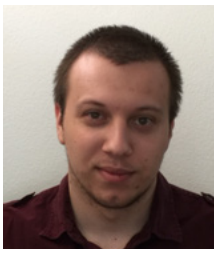

Borna Hlousek

Borna Hlousek is a third-year undergraduate student majoring in physics and mathematics. He spends most of his time working with Dr. Murtadha Khakoo, running and collecting data on the inelastic and elastic electron scattering experiments. In addition to this, he has also built several circuits and devices which have been incorporated into other projects within the lab. After his undergraduate education, Borna plans to continue onward and attain a PhD in physics.

Desiree Jacoby

Desiree Jacoby is a recent graduate from CSU Fullerton with a Bachelor of Science Degree in Biology with a concentration in Cell and Developmental Biology. She worked in Dr. Joel K. Abraham's education lab, looking at the relationship between food safety and handling knowledge and practice in elementary aged children. She was a part of The Urban Agriculture Community-based Research Experience (U-ACRE) program at CSU Fullerton for two years, reaching out to the community while gaining experience in research on community-based projects. She is in the process of applying to the microbiology Master's program at San Jose State University and the Stem Cell Internships in Laboratory Based Learning (SCILL) there as well.

Saumya Jani (Biological Science Section Editor)

Saumya Jani, biology section editor, is a President's Scholar and a third-year Biology major, with a concentration in Cellular and Developmental Biology. She works in Dr. Tolmasky's microbiology lab, testing the capacity of different molecules and oligonucleotides to combat antibiotic resistance. She is also the student assistant for the MARC program and a health scholar at St. Francis Medical Center. Upon graduation, she plans to apply to MD/PhD programs.

Jarrett Jones

Jarrett Jones is an alumnus with a Bachelor of Science Degree in Biology with a concentration in Ecology and Conservation Biology. He performed research under Dr. Joel K. Abraham looking at the effects of different biochar feedstocks. He worked as a greenhouse assistant in the Biology Greenhouse Complex and as a Supplemental Instruction Leader for Biology 171. He is currently looking for a career as an environmental scientist with the State of California.

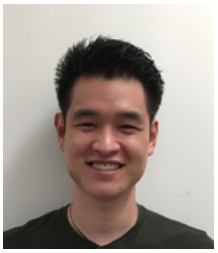

Jacob Kato

Jacob Kato is a graduate of CSUF with a Bachelor of Science Degree in Geology and has a background in cellular biology. He worked in research labs at City of Hope, in addition to undergraduate research in Jeff Knott's lab. He is a member of professional associations such as South Coast Geological Society and Geological Society of America. He presented his research at various Cordilleran Section Geological Society of America meetings. For Jacob graduate school is a goal, but he would like to find a career where he can incorporate cellular biology, chemistry and geology in remediation processes.

Brian Laverty

Brian Laverty is a senior pursuing a Bachelor of Science Degree in Mathematics with a concentration in Classical Applications. He is a tutor at CSU Fullerton's Mathematics Tutoring Center as well as a private tutor. He will be applying to graduate school in pursuit of his Master's Degree in Mathematics, once graduating.

Ashley Le-Pham

Ashley Le-Pham is a fifth year biochemistry major and music minor. She is currently researching with Dr. Christopher Meyer in the Department of Chemistry and Biochemistry, where she studies an enzyme that is crucial to starch and glycogen biosynthesis. Ashley was elected by NSM students to serve on the ASI Board of Directors representing the students of the College of Natural Sciences and Mathematics. She represents and voices the opinions and ideas of all NSM students. Additionally, she is an SI leader for CHEM 315: Theory of Quantitative Chemistry and has been working and loving it for 2 years.. After getting her undergraduate degree, she hopes to pursue either a medical degree or go into policy.

Phyllis Liang

Phyllis Liang is a recent graduate with a Bachelor of Science Degree in Biology with a concentration in Biodiversity, Ecology, and Conservation. She joined the Urban Agriculture Community-based Research Experience (U-ACRE) program and worked in Dr. Joel K. Abraham's lab looking at how CSUF students handle their produce. As an undergraduate at CSUF, she was a Supplemental Instruction Leader for the Biology Department, the co-president of the SUCCESS club, and a peer mentor for students in different programs such as STEM^2, PUMP, and CNSM.

Vivian Lopez

Vivian Lopez is a senior Mathematics major set to graduate in the Fall 2016 from California State University, Fullerton. She will be applying to the single-subject math credential program for the Spring 2016 to fulfill her passion in becoming a secondary school teacher. In addition to her undergraduate research in collaboration with Dr. Bogdan Suceava and colleague Dulce Fonseca, Vivian has worked as a fourth grade instructor at an after school program called ASES in the Buena Park School District that is partnered with CSUF. She also worked with the Upward Bound program at CSUF in providing tutoring in math and academic counseling to prepare high school scholars for college success and was a peer mentor to first-year college students of the Freshman Programs at CSUF.

Anthony Macias

Anthony A Macias is a senior pursuing a Bachelor of Science in Geology with a concentration in Sedimentary Geochemistry. He works with Dr. Adam Woods in the Inductively Coupled Plasma (ICP) optical emission spectrometry lab, researching planetary recovery rates post- Permian Triassic extinction approximately 250 million years ago. Anthony has also worked as a Supplemental Instruction Leader for the Geology Department at CSUF and as an Instructional Assistant at Santa Ana College for the Department of Earth Science and Geology. He will be applying to the Master of Science in Geology programs at CSU Fullerton and at the University of Montana upon graduation to continue his path in the Geosciences.

Dr. Colleen McDonough (CNSM Assistant Dean for Student Affairs)

Dr. McDonough has served as the Assistant Dean for Student Affairs in the College of Natural Sciences and Mathematics since September 2015. Her research interests focus on STEM students' perceptions of educational climate and their formal and informal relationships with faculty. McDonough earned a Ph.D. in Higher, Adult, and Lifelong Education from Michigan State University, a master's degree in public administration from the University of Southern California, and a bachelor's degree in sociology from Hobart and William Smith Colleges.

Ryan McKay

Ryan McKay is a senior pursuing a B.Sc. in Geology. For over a year, he has worked with Vali Memeti on his senior thesis searching for the source rock which ancient Native Americans used to create cogged stones. Through geologic methods such as petrography and geochemical analysis Ryan compared the results of cogged stones to that of collected samples within Southern California in an attempt to locate the outcrop Native Americans used to collect from. He also works at the J.D. Cooper Center curating, cataloging and researching fossils in the Orange County Paleontology Collection.

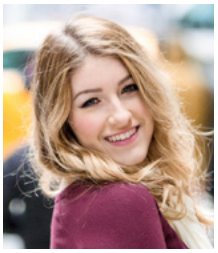

Lauren Michelle (Chemistry & Biochemistry Section Editor)

Lauren Michelle is a second-year post-baccalaureate pre-med student in CSU Fullerton's Pre-Health Post-Baccalaureate Program (PHPBP). She graduated from her alma mater, Benedictine College, in 2012, with a degree in Journalism. She currently sits on the PHPBP admissions committee, and is a member of the NSM-Interclub Council. She plans to take the MCAT in May as she completes her prerequisite courses before applying to medical school this summer.

Lisa Mueller (Mathematics Section Editor)

Lisa Mueller is a fourth-year pure mathematics major with a psychology minor who strives to get her Ph.D to become a university-level math professor after receiving her Bachelor's. Lisa has been consistently taking on jobs and leadership roles over her college career that have kept her interest in mathematics high, including being a Supplemental Instruction Leader, a tutor, a grader, an officer for both S.M.A.R.T. Girls and Math Club (including President), and, of course, the Math Section Editor for DIMENSIONS. She also has participated in unique summer programs over the past two years that have prepared her for graduate schools (P.U.M.P. in 2014) and gave her the opportunity to conduct research with students from across the country (REU at University of West Georgia in 2015) for which she is now sharing in this journal.

Bora Olcken

Bora Olcken is a senior pursuing a Bachelor of Arts in Mathematics with a concentration in Pure Mathematics and a Minor in Computer Science. He works as a private math tutor for high school and college students and is currently working on research projects with Dr. Christopher Lyons on calculating Picard ranks of certain K3 surfaces. He will be attending a PhD. program upon graduation from CSU Fullerton and hopes to become a professor at a 4-year university in the future.

Jennifer Palermo (Graduate Assistant)

Jennifer is a Master's of Geological Sciences student who intends to defend her graduate thesis this summer. Her research is focused on hydrological changes in Southern California over the past 1300 years. In addition to her research, she currently works as a Graduate Assistant for the College of NSM as well as teaches introductory geology labs. After her Master's, Jennifer aims to pursue her PhD. in the geological sciences and to continue to promote the transformation of STEM to STEAM.

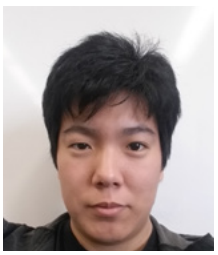

Conner Park

Conner Park will be graduating in Spring 2016 after transferring from Irvine Valley College in Fall 2014. Working under Dr. Jocelyn Read, Conner is working on semi-analytic modeling of the coalescence of binary neutron star systems. He takes previous and current student's work and expands on their ideas and methods. With the recent detection of gravitational waves, he believes that his work has become more important in the grand scheme for Laser Interferometer Gravitational-wave Observatory (LIGO) and future detections. In the future, Conner Park plans to go to Law School to pursue a Juris Doctor Degree with a specialization in patent law with the advent of new technologies. Conner Park aspires to have a pivotal role in patents and patent law.

Velvet L. Park

Velvet L. Park is a senior pursuing a Bachelor of Science degree with a concentration in Marine Biology at California State University, Fullerton. She is also a Southern California Ecosystems Research Program (SCERP) scholar and works in Dr. Kristy Forsgren's reproductive physiology laboratory. Currently, she is investigating the potential effect of wastewater effluent on the reproductive health of Pacific sand-dab (*Citharichthys sordidus*). Velvet has presented her work at several conferences and symposia. Most recently she won a best presentation in marine biology award while presenting at the Society for the Advancement of Chicanos and Native Americans in Science (SACNAS) conference in Washington D.C. After graduation, she intends to pursue a graduate degree where she can explore her interests in evolutionary ecology, fisheries biology, and conservation of marine biodiversity.

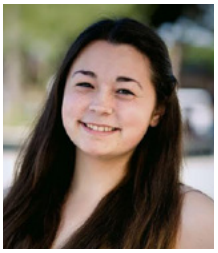

Sierra Patterson

Sierra Patterson is a senior pursuing a Bachelor of Science Degree in Geological Sciences. She is currently working with Valbone Memeti for her undergraduate research thesis. Sierra will be applying to different graduate programs upon graduation to continue her path to become a geologist.

Phillipe Diego Rodriguez (Editor-in-Chief)

Phillipe Diego Rodriguez will graduate Summa Cum Laude with a Bachelor of Science in Physics, an emphasis in Business, and an independent concentration in Intelligence and National Security. Phillipe is a Dan Black Physics/Business Scholar, a University Honors Program Scholar, and a Cal State D.C. Scholar. Phillipe was a DIMENSIONS Physics Section Editor for two years prior to assuming the role of DIMENSIONS Editor-in-Chief. Phillipe's research interests involve the how the Department of Defense interacts with entrepreneurs in Silicon Valley and which geographical locations the Department of Defense will target next in its search for innovation. Subsequent to graduation, Phillipe will attend the Stanford Graduate School of Business to pursue a Master of Business Administration.

Evelyn Ruelas

Evelyn Ruelas is a senior pursuing a Bachelor of Science Degree with a concentration in Marine Biology. She is a Southern California Ecosystems Research Program (SCERP) Scholar, and conducts research in Dr. Kristy L. Forsgren's reproductive physiology lab. Evelyn is interested in researching the reproductive morphology of male and female black perch, *Embiotoca jacksoni*. She will be applying to the CSUF Master of Science (M.S.) in Biology degree, to continue and expand her current research on black perch.

James Shade

James Shade is a junior pursuing a Bachelor of Arts Degree in Mathematics with a concentration in Classical Applied Mathematics, and a Bachelor of Science in Computer Science. He works at the Department of Mathematics Tutoring Center. Upon graduation, he plans to pursue a graduate degree in classical mathematics.

Prarthana Shankar

Prarthana Shankar is a senior at CSUF pursuing a Bachelor of Science Degree in Biology with a concentration in Molecular Biology and Biotechnology. She is a Southern California Ecosystems Research Program (SCERP) scholar and through the NSF-funded program, she works under the guidance of Dr. Kristy Forsgren and Dr. Jennifer Burnaford to understand the reproductive physiology of the California mussel in southern California. After graduating in May 2016, she plans to attend graduate school and ultimately become a college professor.

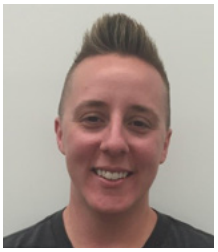

Amanda Shellhorn

Amanda Shellhorn is a senior working for her Bachelor of Science in Geology. She has spent the past two semesters spending her free weekends in the Eastern Sierra Nevada Mountains mapping and collecting data for her undergraduate thesis. Amanda has also been treasurer for the Geology Club for two straight years. She is set to graduate in the summer after attending field camp in Montana. Post-graduation, she hopes to make a career with a geotechnical company either local or out of state.

Sophia Shimamura (Cover Designer)

Sophia Shimamura is a graphic design student from Anaheim, California. She is a senior at California State University, Fullerton and plans to graduate in the spring of 2017. She is a 2015 Jerry Samuelson Scholarship winner for her leadership and commitment to the College of the Arts. Aside from art and design Sophia spends her free time volunteering at the OC Zoo. Her job there is to educate people about animals, bring out live animals for the public, and lead tours.

Emily Silveira

Emily Silveira is currently working towards a Master's of Science in Geology, specializing in paleoclimatology. She works as a Teaching Associate in the Geological Sciences department and leads Physical Geology lab classes. Following completion of her degree, Emily will be pursuing a career in Earth Science education.

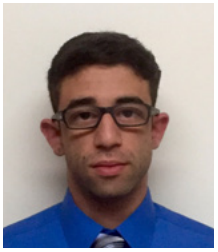

Salim Soubra

Salim Soubra has pursued his Bachelor of Science Degree in Chemistry. He worked in Dr. Scott Hewitt's lab performing studies on the kinetics, reaction mechanisms, and spectroscopy of atmospheric species using gas chromatography. The research was preliminary results to demonstrate the computational results for Dr. Fu-Ming Tao's calculations. Salim has recently started working as a Laboratory Technologist with NAMSA, a Medical Research Organization. He work in the Analytical Services department, performing USP Monograph testing on medical devices, ensuring that they are sterile before put on the market.

Rebecca Steever

Rebecca Steever is graduating Summer 2016 with a B.S. in Geological Sciences. Her undergraduate research was completed under the guidance of Dr. Diane Clemens-Knott and focused on igneous rock relationships in the Southern Sierra Nevada. She hopes to transition into environmental geology after graduation.

Christine Tong

Christine Tong has recently graduated from CSUF this Fall 2015 with a Bachelor of Science in Geological Sciences. She worked with Dr. Nicole Bonuso, exploring the recovery of the Permian to Middle Triassic Extinction in the northern Nevada region in Favert Canyon. Her goal
is to work in an environmental or energy company.

Marlene Vega

Marlene Vega is an undergraduate senior majoring in physics. At the moment, she conducts research with Dr. Michael Loverude by observing how students understand and think about vectors and coordinate systems in higher division physics courses. In addition, she also conducts research with Dr. Leigh Hargreaves by simulating the design of the electron spectrometer under the software program SIMION. Aside from research, she works as a supplemental instructional leader for the physics department. Upon graduation, she plans to attend the physics master's program at California State University, Fullerton. She is exploring her options in her physics career, but is certain she wants a career that can make a difference.

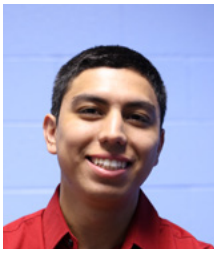

Ignacio Vera

Ignacio Vera is a Biology major with a concentration in Ecology and Evolutionary Biology expecting to graduate in spring 2016. Ignacio has been a Southern California Ecosystems Research Program (SCERP) Scholar since the summer of 2012. Heavily interested in conservation biology he chose to work with Dr. Sandquist on the federally endangered plant *Eriastrum densifolium* ssp. *sanctorum*. SCERP has further developed his skills not only as a scientist, but as a public speaker with numerous oral and poster presentations culminating in a Best Poster Award at the Botanical Society of America's 2014 Botany Conference in Boise, ID.

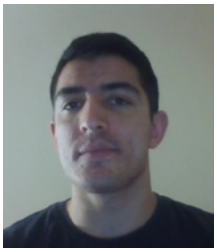

Adam Walder

Adam is a senior finishing his last semester at CSUF. He is an Applied Mathematics Major with a minor in Computer Science. His projects have involved mathematical modeling, statistical simulation, and scientific computing. In the summer of 2015, Adam was selected to participate in MBI's summer REU at Virginia Tech. He will be attending graduate school pursuing a Ph.D. in Statistics this coming Fall.

Daniel Weiherer

Daniel Weiherer is perusing a B.S. in Biological Science with a concentration in Ecology and Evolutionary Biology. He has a strong interest in Ecology and Botany. Daniel has received three years of experience preparing, curating, and researching fossils at The Cooper Center by participation in internships, volunteering, and working to reconstruct the Eocene paleoenvironment of Orange County. He also is conducting research on the seed germination of the Santa Ana river woolly star in a physiological plant ecology lab. Additionally, Daniel went to Thailand last summer through the SMRT program to research medicinal plants used by Buddhist monks. Daniel will continue on to obtain a graduate education in Biology. Ultimately, through his passion for the outdoors, Daniel wants to conduct biological research in the field.